Interrogating Mechanisms of *SLC6A1*-Associated Epilepsy Using Human Medial Ganglionic Eminence Organoids

by

Maria Carmen Varela

A dissertation submitted in partial fulfillment
of the requirements for the degree of
Doctor of Philosophy
(Neuroscience)
in the University of Michigan
2026

Doctoral Committee:

Professor Jack M. Parent, Co-Chair
Professor Emeritus Michael D. Uhler, Co-Chair
Associate Professor Sami J. Barmada
Professor Lori L. Isom
Professor Geoffrey G. Murphy

Maria Carmen Varela

mcvarela@umich.edu

ORCID iD: 0000-0001-7229-3285

© Maria Carmen Varela 2026

Dedication

This dissertation is dedicated to my mom, Maggie, from whom I learned my strength and determination; my husband, Marcus, who remained my source of stability and peace throughout everything; and my children, Ariana and Bryson, who have been my endless sunshine even on cloudy days.

I also dedicate this to my grandparents, Arturo and Janie Varela, whose sacrifices in life gave their children and grandchildren access to educational opportunities that they themselves were not afforded.

With all my love and gratitude, this accomplishment belongs to you all as much as it does to me.

Acknowledgements

I would like to express my deepest gratitude to my mentors Jack and Mike for their unwavering support, patience, and guidance throughout my graduate training. Your encouragement, faith in me, and commitment to my development as a scientist have shaped the way I approach mentoring the next generation of scientists. Thank you for giving me the freedom (and the funds 😊) to explore my own scientific ideas and avenues of research. I am incredibly fortunate to have learned under both of your mentorship!

I would also like to extend my thanks to my thesis committee members, Lori, Geoff, and Sami, for their kindness, patience, expertise, and valuable guidance. Your advice and perspectives have strengthened this project and pushed me to think more critically and broadly about my research.

To the mentor who taught me everything I know about stem cells, Asif. Your continued support, guidance, and advice throughout my graduate career has meant more to me than you know. I am grateful to have you as a mentor and friend.

I am also sincerely thankful for my lab colleagues and mentees, whose collaboration, generosity, and camaraderie made this journey both productive and enjoyable. Whether through troubleshooting experiments, sharing ideas, or simply offering encouragement during challenging moments, you have all contributed meaningfully to this work and to my growth as a scientist. Special thanks to Andrew, Louis, Julie, Kyle, and Sanaa for answering my endless amount of questions and for giving me a sounding board to bounce my ideas off of, and to Sandra, Rouku, Miranda, and Sheetal for being amazing coworkers and always willing to help with troubleshooting. To my undergraduate mentees, Juan, Tyler, Leah, and Reeya, your contributions to this research have been invaluable and I am so happy to have watched you grow as scientists over the years.

Thank you to my friends and cohort mates who have kept me going throughout this experience. Kaisha, September, Sophie, and Muyu, you have all brought joy and laughter into my

life and I am honored to call you friends. Special thanks to Muyu for always bringing me yummy snacks!

Finally, to my family, thank you for your constant support, patience, and belief in me. Mom, thank you for your endless encouragement and belief in me. Your unconditional love and strength have tremendously helped me reach this finish line. To my husband, Marcus, thank you for being the best husband and partner anyone could ask for and for being my rock throughout this whole experience. I wouldn't have been able to do this without you. Thank you to my kids, Ariana and Bryson for giving me their love and encouragement, and for helping Dad to hold down the fort these past few years. To my mother-in-law, Eloisa, thank you for all your help and support over the years.

Table of Contents

Dedication ii

Acknowledgements iii

List of Figures vii

Abstract ix

Chapter 1 Introduction 1

1.1 The Role of GABAergic Cells in Early Brain Development 1

1.2 Epilepsy and the role of GABA 7

1.3 The *SLC6A1* gene and GAT1 Transporter 9

1.4 Modeling Neurodevelopmental Disorders with Human iPSC-derived Brain Organoids . 15

Chapter 2 Robust Production of Parvalbumin Interneurons and Fast-Spiking Neurons from Human Medial Ganglionic Eminence Organoids 26

2.1 Summary 26

2.2 Introduction 27

2.3 Materials and methods 29

2.4 Results 38

2.5 Discussion 58

Chapter 3 *SLC6A1* Haploinsufficiency Alters Cortical Interneuron Migration, Maturation and Subtype Specification in Human Medial Ganglionic Eminence Organoids 62

3.1 Summary 62

3.2 Introduction 63

3.3 Materials and methods 64

3.4 Results 70

3.5 Discussion 87

Chapter 4 Dissertation Summary and Future Directions 93

4.1 Summary of results 93

4.2 Progressing onward 108

References 113

List of Figures

Figure 1.1: Inhibitory innervation patters of MGE lineage interneuron subtypes. 5

Figure 1.2: Mechanism of action of GAT1 in GABA reuptake at the synapse. 11

Figure 1.3: Localization of loss of function variants in the GAT1 protein topology. 14

Figure 1.4: Avenues of pluripotent stem cell generation and downstream applications..... 16

Figure 1.5: Comparison of single rosettes vs. multi-rosette organoid models...... 23

Figure 2.1: Generation of human subpallial brain organoids with MGE regional specificity. 39

Figure 2.2 MGE regional specificity of MGEOs 42

Figure 2.3: Single-Cell RNA sequencing of 1-month and 3-month MGEOs..... 44

Figure 2.4: MGEO interneuron subtypes..... 46

Figure 2.5: MGEOs generate human MGE-derived cell-types 48

Figure 2.6: Comparison of MGEO and developing human subpallium transcriptomes..... 50

Figure 2.7: MGEO-derived interneuron progenitors are highly migratory 53

Figure 2.8: MGEO-CO assembloids form functional synapses, display increasingly complex network activity and exhibit fast-spiking units..... 55

Figure 3.1: Generation and GAT1 CRISPR edited and patient derived iPSCs and validation of GAT1 expression in MGEOs...... 72

Figure 3.2: Migratory deficits of GAT1 MGEOs on ECM. 74

Figure 3.3: Genetic rescue of migratory deficits in GAT1 MGEOs...... 75

Figure 3.4: SLC6A1 migratory deficits are cell autonomous in MGEO-CO assembloids... 77

Figure 3.5: Pharmacological rescue of migratory deficits on MGEO-CO assembloids...... 79

Figure 3.6: Multielectrode array recordings from SC79 treated and untreated assembloids. 81

Figure 3.7: Bulk RNAseq analysis of DIV 21 SLC6A1 KO and iCont MGEOs 83

Figure 3.8: Time course of MGE lineage marker expression in control and het MGEOs... 84

Figure 3.9: Time course of expression of GABAergic neuron subtypes in control and het MGEOs 86

Figure 4.1: SLC6A1 Cortical organoids display increased intermediate progenitor population expansion and increased organoid size. 102

Figure 4.2: Dysregulated numbers and positioning of cortical neurons and ectopic expression of somatostatin in SLC6A1 KO cortical organoids. 104

Figure 4.3: Species conservation of VXPX ciliary targeting motifs on the c-terminus of GAT1 106

Figure 4.4: Evaluation of patient variants reported in the Silva et al., 2024 dataset with no loss of GAT1 function and their associated clinical diagnoses. 110

Abstract

Genetic factors are estimated to contribute to 70-80% of all epileptic disorders, with an especially high prevalence in pediatric epilepsies. Myoclonic–atonic epilepsy (MAE) is a severe developmental and epileptic encephalopathy (DEE) with frequent seizures and intellectual disability that typically emerge between 8 months and 5 years of age. Pathogenic variants in the *SLC6A1* gene, which encodes the GABA transporter 1 (GAT1), are a leading genetic cause of MAE and have been linked to other neurodevelopmental disorders including autism spectrum disorder and schizophrenia. GAT1 is highly expressed in cortical interneurons and mediates the reuptake of γ-aminobutyric acid (GABA) from the synaptic cleft where it regulates inhibitory neurotransmission and maintains the balance of cortical networks. *SLC6A1* variants often reduce transporter function, leading to disrupted GABA homeostasis. Existing human cellular models do not endogenously express sufficient levels of *SLC6A1* to interrogate disease mechanisms and access to developing human brain tissue is extremely limited. Although animal models have provided insight into synaptic GAT1 dysfunction and behavioral phenotypes, they fail to fully recapitulate key aspects of the human disorder, including spontaneous seizures and complex developmental features, indicating that there may be human-specific alterations not seen in animal models. Whether *SLC6A1* regulates cortical interneuron development in humans, and how its disruption contributes to epilepsy remains unknown.

This dissertation investigates how *SLC6A1* variants affect human cortical interneuron development and explores mechanisms that may contribute to seizure generation using human induced pluripotent stem cell (iPSC)–derived brain organoid models. Cortical interneurons that express high levels of GAT1, particularly parvalbumin expressing (PV+) interneurons, originate in the medial ganglionic eminence (MGE) and migrate tangentially to the cortex, where they provide precise inhibitory control over excitatory networks. Existing organoid models fail to fully recapitulate human MGE lineages or generate robust numbers of PV+ interneurons, thus limiting the study of disorders linked to their dysfunction in human systems. Herein, I describe our development and characterization of a highly specific human MGE organoid (MGEO) model that

reproducibly generates MGE lineages with transcriptomic profiles similar to the human fetal MGE, including substantial numbers of PV+ GABAergic interneurons with immunohistological features of fast-spiking interneurons. Upon fusion with cortical organoids, MGEO-derived interneurons migrate and integrate into circuits, resulting in network activity that contains fast-spiking units, establishing a robust human platform to study MGE-derived interneurons, including those expressing high levels of GAT1

To examine the impact of *SLC6A1* variants on MGE-derived interneurons, I derived *SLC6A1*-DEE patient and CRISPR edited iPSCs and generated MGEOs and assembloids. I discovered a cell-autonomous migration deficit in *SLC6A1*-mutant interneurons and demonstrated rescue of this phenotype through both genetic correction and pharmacological activation of AKT pathway signaling. I further revealed disruptions in MGE lineage competence, maturation, and interneuron subtype specification. Using multi-electrode array recordings, I uncovered network hyperexcitability in *SLC6A1* mutant assembloids and demonstrated that enhancement of interneuron migration through pharmacological AKT pathway activation mitigated this hyperexcitability, directly linking early developmental defects to later network dysfunction. Together, this work establishes a human MGE organoid model capable of generating disease-relevant interneuron subtypes and reveals a previously unrecognized developmental mechanism by which *SLC6A1* variants disrupt inhibitory circuit assembly. By identifying early, targetable developmental defects that contribute to network hyperexcitability, this study provides new mechanistic insight into *SLC6A1*-DEE and lays the groundwork for therapeutic strategies aimed at restoring inhibitory circuit formation during critical developmental windows.

.

Chapter 1 Introduction

Notes on Chapter 1

Portions of this chapter were published in modified form as:

Varela, M. C., Samarasinghe, R., & Parent, J. M. (2024). Functional Exploration of Epilepsy Genes in Patient-Derived Cells. Jasper's Basic Mechanisms of the Epilepsies, 841–860. https://doi.org/10.1093/med/9780197549469.003.0042

1.1 The Role of GABAergic Cells in Early Brain Development

Overview of Cortical and Subpallial Development

Human brain development follows a series of highly coordinated stages beginning with neural induction, followed by neural tube formation, regional patterning, neurogenesis, migration, and circuit formation. Neural induction occurs with the formation of the neural plate, which folds inwards to form a single neural tube (Hamburger & Hamilton, 1951; Shepard et al., 2002). The neural tube serves as the precursor structure for the entire central nervous system and establishes the dorso-ventral and rostro-caudal axes which enable the emergence of distinct brain regions through gradients of morphogen signaling (Briscoe et al., 2000; Ericson et al., 1995; Hongo et al., 1999). Minute disruptions during these early patterning events can have profound downstream consequences for neuronal identity and circuit organization (Chiang et al., 1996; Sussel et al., 1999).

As the forebrain develops, regionalization factors allow for the distinction of the pallium, which gives rise to the cerebral cortex, and subpallium, which includes the medial, lateral, and caudal ganglionic eminences (MGE, LGE and CGE, respectively) (Shimamura & Rubenstein, 1997). Excitatory glutamatergic neurons are born locally within the dorsal pallium and migrate radially to populate the cortical strata (Rakic, 1972). Cortical inhibitory interneurons arise from the ventral subpallium, largely originating from the MGE and CGE, and migrate tangentially into the cortex (Anderson et al., 1997, 2001; Sussel et al., 1999; Q. Xu, Cobos, De La Cruz, et al., 2004). This spatial segregation of excitatory and inhibitory neuron origins is a defining feature of

mammalian cortical development and requires precise coordination among proliferative zones, migratory pathways, and target cortical regions (Gao et al., 2013).

The Medial Ganglionic Eminence

The MGE is a transient embryonic structure within the ventral telencephalon that emerges shortly after neural tube closure and dorsal-ventral telencephalon regionalization at gestational week (GW) 5-6 (Boitor-Borza et al., 2021). The distinct anatomical structural of the MGE persists until the late second trimester (GW 18-22) at which point it becomes incorporated into developing basal ganglia and adjacent ventral forebrain structures (Boitor-Borza et al., 2021). The MGE functions as a specialized developmental niche that generates the majority of somatostatin (SST) and parvalbumin (PV) interneurons that populate the neocortex and hippocampus (Rudy et al., 2011).

At the molecular and cellular levels, the MGE is defined by a distinct transcriptional profile that determines interneuron identity and fate specification. MGE progenitors are characterized by the expression of key transcription factors including NK2 homeobox 1 (NKX2.1), which is necessary for MGE identity, as well as downstream effectors such as LIM homeobox 6 and 8 (LHX6, LHX8), which promote GABAergic neuron differentiation and maturation (Du et al., 2008; Liodis et al., 2007). The precise temporal and spatial regulation of these transcription factors is essential for determining MGE-derived GABAergic neuron subtype, laminar positioning, and functional properties (Asgarian et al., 2022; Du et al., 2008).

The specification of MGE identity and interneuron fate is orchestrated by the synergistic interaction of key signaling pathways, most prominently, the Sonic hedgehog (SHH) and WNT signaling pathways. SHH signaling, initially emanating from the notochord, is the dominant ventralizing cue that induces NKX2.1 expression, while WNT signaling promotes dorsalization, and its suppression is necessary to maintain ventral telencephalic identity (Avilés et al., 2013; Ericson et al., 1995; Liem et al., 2000). The balanced integration of these pathways ensures proper progenitor patterning and regulates the relative production of PV and SST interneuron subtypes (Tyson et al., 2015).

Following their generation, postmitotic MGE progenitors initiate a series of temporally and fate-restricted migratory waves that populate several cortical and subpallial regions. The earliest migratory wave occurs in humans between GW 6-9 and contains neurons that migrate to adjacent

subpallial regions, and those that tangentially migrate to the cortex (Hansen et al., 2013; Ma et al., 2013). The first neurons to exit the MGE preferentially populate the globus pallidus, generating both GABAergic projection neurons and local pallidal interneurons (Flandin et al., 2010; Nóbrega-Pereira et al., 2010). (Munguba et al., 2023; Tuncdemir et al., 2016; Wu et al., 2023). Shortly after, between GW 9-16, a second and larger wave produces both SST and PV cortical interneurons as well as subpallial populations that target the striatum, contributing GABAergic interneurons that display PV lineage as well as cholinergic identities(Butt et al., 2005; Fazzari et al., 2020; Fragkouli et al., 2009; Marín et al., 2000; Miyoshi et al., 2007). The last and most prolonged migratory phase occurs after GW 16-20 and persists through late gestation with some neurons continuing to migrate well after birth (Paredes et al., 2016). These late-born neurons consist primarily of PV lineage interneurons destined for the cortex, while some interneurons continue to populate basal ganglia regions (Paredes et al., 2016). The extended timeline of MGE-derived interneuron migration in humans highlights a prolonged developmental window during which these cells are vulnerable to disruptions that affect their specification, migration, or maturation. The timing of insults can differentially alter inhibitory circuit assembly in the cortex and basal ganglia and increase vulnerability to neurodevelopmental disorders such as epilepsy.

While the role of GABA is most commonly associated with synaptic inhibition, it also serves several other important functions during early brain development. Prior to the formation and maturation of synapses, GABA acts as a signaling molecule that influences key neurodevelopmental processes including progenitor proliferation, neuronal differentiation, migration, and neurite outgrowth (Behar et al., 1996; LoTurco et al., 1995). At E13.5 in mice, ambient GABA is detectable at similar levels in the neocortex along tangential migratory streams and in the MGE (Cuzon et al., 2006). This ambient GABA is released from the growth cones of migrating neurons, astrocytes, and endothelial cells through non-vesicular, calcium-independent mechanisms including GABA transporter reversal (Demarque et al., 2002). Through activation of concomitantly expressed GABA receptors on neural progenitors and immature neurons, ambient GABA modulates intracellular calcium dynamics and gene expression patterns critical for early cortical patterning (Cuzon Carlson & Yeh, 2011).

GABAergic signaling is involved in guiding subpallial-born interneurons as they migrate along tangential migratory routes towards the cortex. Experimental disruption of early GABA

signaling alters migration speed and directionality, leading to aberrant positioning of inhibitory neurons and long-term circuit defects (López-Bendito et al., 2003). While ambient GABA is detected in the MGE, it is important to note that cells within the MGE, and those beginning to exit the MGE, display little to no sensitivity to GABA and acquire increased responsiveness as they near the cortical boundary (Cuzon et al., 2006). This is believed to be due to changes in $GABA_A$ receptor subunit assembly as the cells traverse their migratory journey to the neocortex (Cuzon et al., 2006). In organotypic cultures of developing mouse brain slices, application of bicuculine, a $GABA_A$ receptor blocker, resulted in the accumulation of MGE-derived neurons at the corticostriate junction and inhibited cortical entry (Cuzon et al., 2006). Interestingly, blockade of GABA transporters GAT1 and GAT3 during these early migratory stages did not impair migration from the MGE to the cortex, indicating that the role of GABA transporters in early migration may not be linked to GABA reuptake mechanisms or reversal of transporter function (Cuzon et al., 2006).

Inhibitory-excitatory balance in cortical circuit formation

Upon completion of their migratory journeys, excitatory and inhibitory neurons continue to mature and form and refine their connectivity to establish functional networks. A defining feature of GABAergic system maturation is the developmental shift in GABA receptor signaling polarity, transitioning from a depolarizing response in immature neurons to a hyperpolarizing response in mature neurons. High intracellular chloride concentrations in immature neurons are maintained by high expression of the inward-directed chloride co-transporter NKCC1 and low expression of the outward-directed chloride cotransporter KCC2 (Ben-Ari, 2002). At this immature stage, activation of $GABA_A$ receptors allows for the outward flow of chloride ions, thus depolarizing the membrane and leading to spontaneous network activity that facilitates activity-dependent maturation of neural circuits.

As neuronal maturation proceeds, increased expression of KCC2 lowers intracellular chloride levels, resulting in a hyperpolarizing and inhibitory effect with the activation of $GABA_A$ receptors (Vanhatalo et al., 2005). This maturation-linked chloride gradient switch is essential for establishing inhibitory control of neural networks and preventing excessive synchronization. Disruptions in the timing of this transition have been linked to neurodevelopmental disorders and

heightened seizure susceptibility (Huberfeld et al., 2007; Muñoz et al., 2007). Thus, the maturation of GABAergic signaling polarity represents an important developmental checkpoint that enables the emergence of mature inhibitory networks necessary for long-term circuit stability.

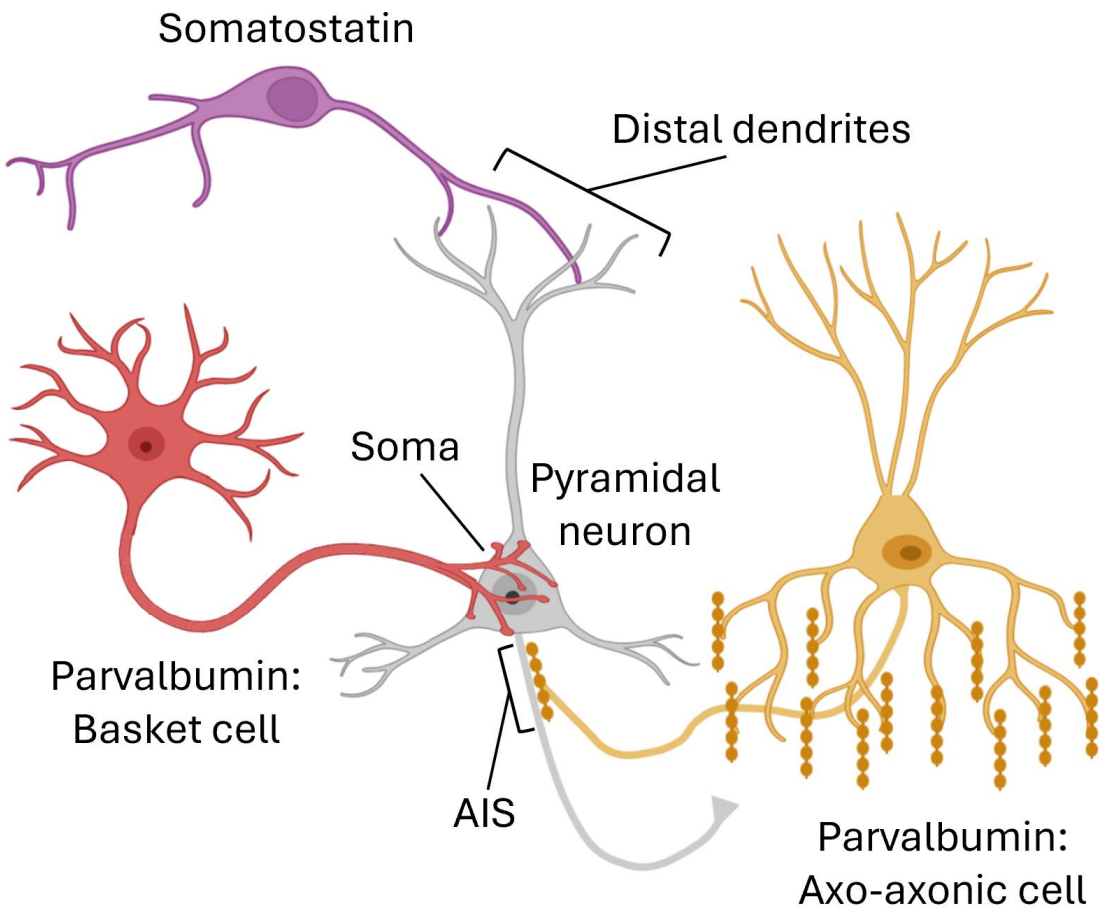

Figure 1.1: Inhibitory innervation patters of MGE lineage interneuron subtypes.

Schematic showing the patterns of inhibitory synapses of medial ganglionic eminence (MGE) interneuron subtypes, somatostatin (SST) and two distinct types of parvalbumin (PV) expressing interneurons onto an excitatory pyramidal neuron. SST interneurons target the distal dendrites of pyramidal neurons while PV interneurons synapse onto the soma and the axon initial segment. PV Basket cells preferentially target the soma and perisomatic regions and PV axo-axonic cells, also known as chandelier cells, provide strong inhibitory control to the axon initial segment (AIS) of the target neuron.

With the acquisition of interneuron subtype specificity, unique subtype-specific attributes allow interneurons to contribute in variable ways to the formation and stabilization of cortical circuits. Among the interneuron subtypes, PV+ and SST+ interneurons have been most strongly implicated in seizure susceptibility and epilepsy pathogenesis (**Figure 1.1**) (Jiang et al., 2016). PV

interneurons, a subtype derived predominantly from the MGE, mature into fast-spiking cells that provide powerful perisomatic inhibition to pyramidal neurons, enabling precise control over excitatory neuron outputs by regulating action potential initiation, spike timing, and firing synchrony (Lazarus & Huang, 2011; Lu et al., 2014). Fast-spiking PV interneurons are particularly important for generating and stabilizing gamma-frequency oscillations (30–80 Hz), which are important for cognition and information processing and depend on tightly coordinated inhibitory feedback loops (Antonoudiou et al., 2020; Bartos et al., 2002; Sohal et al., 2009). Reduced PV interneuron function or density has been observed across multiple genetic and acquired epilepsy models, emphasizing their critical role in network stability (Kaneko et al., 2022; Miralles et al., 2024; Yu et al., 2020).

SST interneurons, another largely MGE-derived subtype, preferentially target the distal dendrites of pyramidal neurons and modulate the integration of excitatory synaptic inputs (Lazarus & Josh Huang, 2011). By controlling dendritic excitability through the filtering and contextualizing of incoming information, SST interneurons influence synaptic plasticity and the propagation of excitatory signals to the soma (Lazarus & Josh Huang, 2011). This type of inhibition is particularly important for preventing excessive summation of excitatory inputs that could otherwise trigger aberrant firing. Loss or dysfunction of SST interneurons has also been linked to developmental disorders and heightened seizure susceptibility (Chen et al., 2019; Wengert et al., 2021).

PV and SST interneuron populations integrate into cortical circuits at different times during development and their subtype-specific connectivity patterns shape excitatory neuron maturation and plasticity. Disruption of inhibitory neuron migration, specification, or maturation can lead to reduced interneuron density, improper laminar positioning, or dysregulated functional maturation (Subramanian et al., 2025). Even subtle shifts in interneuron maturation timing or connectivity can produce lasting circuit pathology, as inhibitory neuron integration with excitatory circuits must occur during precise critical windows of development (Lybrand et al., 2021). Perturbations that occur long before seizure onset can establish maladaptive network architectures that predispose the brain to epilepsy and comorbid neurodevelopmental disorders (Powell et al., 2003).

1.2 Epilepsy and the role of GABA

Overview of Epilepsy

Epilepsy is a chronic neurological disorder defined by the presence of recurrent, unprovoked seizures, resulting from abnormal, excessive, or synchronous neuronal activity in the brain (Fisher et al., 2014). Epilepsy affects approximately 50–70 million individuals worldwide, making it one of the most common serious neurological disorders (Thijs et al., 2019). The incidence of epilepsy is high in early childhood, with 1.2-1.5 million new pediatric epilepsy diagnoses occurring globally each year (Xu et al., 2025). The disease burden of epilepsy in childhood and adolescence has risen over the years, partially due to improved survival of high-risk infants, and enhanced diagnostic capabilities, and is expected to continue to increase in the future with global incidence and prevalence predicted to increase by 37.3% and 32.2%, respectively, by the year 2050 (Su et al., 2025).

Seizures are broadly classified as either focal or generalized based on their anatomical onset and propagation patterns. Focal seizures arise from a localized region of the brain or are constrained to a single hemisphere and may occur with or without altered awareness (Scheffer et al., 2016). Generalized seizures initiate and propagate bilaterally and are typically associated with impaired consciousness (Scheffer et al., 2016). Beyond seizures, epilepsy is often associated with neurodevelopmental comorbidities, including intellectual disability, developmental delays, autism spectrum disorder (ASD), attention-deficit/hyperactivity disorder, and other psychiatric conditions (Johannesen et al., 2018; Reilly et al., 2014). These comorbidities often emerge in early development and can have a greater long-term impact on quality of life compared to seizure burden alone (Berg, 2010). The high prevalence of developmental impairments in childhood epilepsies, which are often diagnosed prior to seizure onset, suggests a disruption of normal brain development, particularly in genetically mediated forms of the disease.

E/I Balance and Seizure Generation

Seizures are widely understood to emerge from pathological network hyperexcitability and hypersynchrony. At the cellular level, neuronal hyperexcitability can reflect altered membrane properties, ion channel function, or synaptic transmission, while at the network level it manifests as runaway excitation, impaired inhibitory control, and aberrant oscillatory dynamics. When mechanisms that normally constrain neuronal firing fail, epileptiform activity can arise and

propagate uncontrollably across local and long-range circuits (Schevon et al., 2012; Trevelyan et al., 2007). Disruption of inhibitory strength, timing, or spatial targeting can lead to excessive synchronization, which is a hallmark of epileptic activity (Cardin, 2018; Miri et al., 2018). This perspective positions epilepsy as a disorder of neural networks, rather than solely a consequence of single-cell dysfunction.

A well-established central framework for understanding seizure generation is the excitation/inhibition (E/I) balance model, which asserts that stable brain function is dependent on a fine-tuned balance of excitatory glutamatergic and inhibitory GABAergic signaling. Excitatory pyramidal neurons serve as the primary drivers of information processing, while inhibitory interneurons adaptively modulate the timing and synchrony of network activity (Cardin, 2018). GABAergic inhibition plays a critical role in shaping cortical oscillations and preventing hypersynchronous activity, with inhibitory neurons coordinating neuronal ensembles through both phasic synaptic inhibition and tonic extrasynaptic signaling (Mann & Mody, 2009).

While the E/I balance model is broadly accepted as a fundamental principle of cortical circuits, the argument that it represents an oversimplification of seizure pathology is becoming increasingly recognized. Studies have shown that seizures can arise even in the presence of intact or increased inhibition, and that inhibitory circuits may even contribute to seizure initiation or propagation under certain conditions. For example, excessive synchronous inhibition can lead to post-inhibitory rebound excitation (Lévesque et al., 2022), while depolarizing GABA responses in immature or pathologically altered neurons may enhance rather than suppress network activity (Huberfeld et al., 2007; Muñoz et al., 2007). Additionally, seizures are often not a manifestation of a static E/I imbalance, but rather reflect dynamic, state-dependent changes in network function, involving alterations in neuromodulation, chloride homeostasis, glial signaling, and circuit connectivity (Dzhala et al., 2010; Kékesi et al., 2015; Tian et al., 2005). Thus, epilepsy is increasingly understood as a disorder of impaired inhibitory control and disrupted network coordination, rather than a simple imbalance of excitation to inhibition.

Limitations of existing models in studying the GABAergic contributions to epilepsy

Due to limited access to human brain tissue during crucial developmental stages and through epileptogenesis, animal and in vitro models have been used broadly to investigate epilepsy disease pathogenesis. While these models have been fundamental in laying a foundational

understanding of the central nervous system, they are not without limitations. Many mouse models of monogenic epilepsies do not fully recapitulate human phenotypes, including spontaneous seizures, making it difficult to draw parallels between rodent and human pathogenic hallmarks (Marshall et al., 2021).

In vitro cellular models, including heterologous HEK and Hela pathogenic variant overexpression models, have likewise been useful in understanding the function of disease related proteins of interest in a controlled system. However, these heterologous models may lack endogenous interacting partners, thus limiting mechanistic insight into protein interactions, cell signaling, and cell-cell interactions. A human based model that can recapitulate endogenous interactions is therefore needed to further our understanding of mechanisms behind the development of human brain disorders.

1.3 The *SLC6A1* gene and GAT1 Transporter

Genetic Epilepsies

As discussed previously, epilepsy is a broad categorization of neurological disorders characterized by the occurrence of spontaneous recurrent seizures (Fisher et al., 2014). Although seizures can arise spontaneously from various structural, immune, metabolic, and environmental factors, genetic influences play a central role in many forms of epilepsy (Helbig et al., 2016; Hildebrand et al., 2013). Recently, an increasing number of epilepsies previously deemed to have idiopathic causes have been linked to underlying genetic contributions that arise from inherited or de novo variants that ultimately affect neuronal excitability and network function (Thomas & Berkovic, 2014). This linkage has led to genetic causes being recognized as a primary etiologic category in current epilepsy classifications.

Within the umbrella of genetic epilepsies lies development and epileptic encephalopathies (DEEs), which represent an especially severe subgroup with symptoms typically presenting in infancy or early childhood (Baer et al., 2025; Johannesen et al., 2018). DEEs not only present with frequent seizures, which are often intractable, but also significant cognitive impairments and developmental delays (Devries et al., 2020; Johannesen et al., 2018). Through the rise of next generation sequencing efforts, many severe DEEs have now been identified as having monogenic causes. These monogenic epilepsies are linked to a pathogenic variant in a single gene, which is sufficient to cause seizures and associated phenotypes. Variants in hundreds of genes encoding ion

channels, transporters, receptors, and proteins critical for neuronal development and synapse formation have been discovered and implicated in epilepsy syndromes of diverse severity. About 17 of these genes identified thus far are directly involved in the GABAergic system including GABA receptor subunit genes (*GABRA1-6, GABRB1-3, GABRG1-3*, and *GABRD*), GABA transporter genes (*SLC6A1, SLC6A11*) and genes involved in the metabolism and breakdown of GABA (*ABAT, ALDH5A1*) (Chung et al., 2025; Feng et al., 2022; Hu et al., 2023; Macdonald et al., 2012; Mohammadi et al., 2024). The limited number of GABA-related gene variants observed in patient populations further emphasizes the importance of the GABAergic system in the proper development of the human central nervous system and, ultimately, fetal viability.

GAT1 structure and function

Variants in the solute carrier family 6 member 1 (*SLC6A1*), the gene encoding the sodium- and chloride-dependent, membrane bound, GABA transporter type 1 (GAT1), are particularly interesting as GAT1 is the most abundant GABA transporter in the brain and has been linked to a broad spectrum of neurodevelopmental disorders (Carvill et al., 2015; Johannesen et al., 2018; Rauch et al., 2012; Sanders et al., 2012). The *SLC6A1* gene, containing 15 exons and located on human chromosome 3, is one of approximately 20 members of the solute carrier family 6 set of genes, many of which share high sequence homology and similar transport mechanisms (Bröer, 2006). The predominant isoform of GAT1 contains 12 transmembrane domains (TMs) connected by intracellular and extracellular loops that mediate the transport of GABA coupled with sodium and chloride ions across the plasma membrane. These transmembrane domains participate directly in creating the binding sites for GABA and the co-transported ions, with TMs 1, 3, 6, and 8 being particularly important for substrate binding and conformational changes during the transport cycle (Yamashita et al., 2005).

The primary physiological role of GAT1 is to mediate the reuptake of GABA from the extracellular space back into neurons and glia following synaptic release (Scimemi, 2014). GABA is not enzymatically degraded in the extracellular space, and therefore it is entirely reliant on diffusion and uptake by transporters to clear it from the synaptic cleft. GAT1 harnesses the electrochemical gradients of sodium and chloride to drive the uptake of one GABA molecule coupled with two sodium and one chloride ion (Lester et al., 1994) (**Figure 1.2A**).

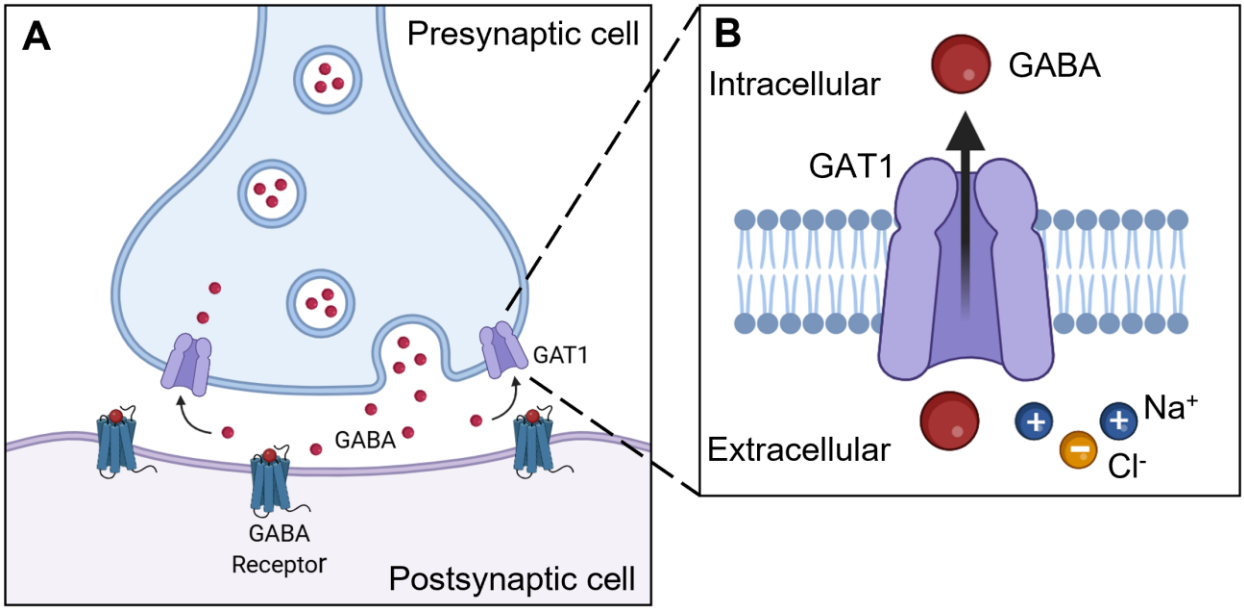

Figure 1.2: Mechanism of action of GAT1 in GABA reuptake at the synapse.

(**A**) Schematic showing the localization of GAT1 on the presynaptic terminal of a GABAergic neuron. The presynaptic neuron releases vesicles containing the inhibitory neurotransmitter, GABA, into the synaptic cleft. Membrane bound GABA receptors on the postsynaptic neuron bind GABA, initiating inhibition to the postsynaptic neuron. Excess GABA is transported back into the neuron via GAT1. (**B**) A magnified schematic of the GAT1 transporter showing that it is a trans-membrane protein that transports one molecule of GABA from the extracellular space into the intracellular space by coupling to two sodium ions (NA+) and one chloride ion (Cl-), transporting GABA in the direction of these ions' concentration gradients.

This process both terminates synaptic GABAergic signaling and replenishes presynaptic stores for repackaging and reuse. By rapidly clearing GABA from the synaptic cleft, GAT1 temporally and spatially regulates inhibitory signaling by limiting spillover to adjacent synapses and prevents aberrant activation of extrasynaptic receptors (Isaacson et al., 1993). Loss of GAT1 function through pharmacological blockade or genetic deletion leads to enhanced tonic $GABA_A$ receptor currents and prolonged inhibitory postsynaptic current decay (Bragina et al., 2008; Chiu et al., 2005; Cope et al., 2009; Jensen et al., 2003), demonstrating its critical role in regulating inhibitory synaptic dynamics.

Beyond its core function of GABA transport, GAT1 exhibits additional electrophysiological properties that are not dependent on the inward transport of GABA. GAT1 can behave as an ion channel via generation of an inward sodium current with the binding of GABA to the transporter (MacAulay et al., 2002; Risso et al., 1996). Even in the absence of

substrate, GAT1 can support a leak current mediated by alkali ions or a sodium-dependent capacitive current (MacAulay et al., 2002; Mager et al., 1993; Risso et al., 1996). These currents can influence local membrane potential and shunt membrane resistance, suggesting that GAT1 may modulate neuronal excitability in ways not strictly limited to GABA clearance (MacAulay et al., 2002; Mager et al., 1993; Risso et al., 1996). Regulation of GAT1 activity can also occur through interactions with other proteins including actin and syntaxin-1A. Syntaxin-1A, an important component of synaptic machinery, has been shown to interact with GAT1 to influence its trafficking and transport kinetics, while disruption of actin can increase GABA uptake activity (Imoukhuede et al., 2009; Jahodova et al., 2023; Lin et al., 2024) indicating that GAT1 transporter function can be modulated by mechanisms associated with direct protein-protein interactions.

GAT1 developmental expression timeline

Expression of *SLC6A1* is enriched in the mammalian brain, particularly within the adult frontal cortex, but expression emerges much earlier during neurodevelopment (Hawrylycz et al., 2012; Kang et al., 2011). GAT1 mRNA and protein are detectable in embryonic GABAergic neurons prior to the onset of glutamatergic excitatory neurotransmission and is present in MGE cells as they begin their migratory journey, around GW 8-10 in humans (Anderson et al., 2001; Conti et al., 2004). The maturation of the GABAergic system, and correspondingly *SLC6A1* expression, continues through adolescence, mirroring the protracted development of inhibitory networks in humans (Caballero & Tseng, 2016; Kilb, 2012).

While traditionally considered a neuronal transporter, GAT1 is also expressed in astrocytes, oligodendrocytes, and microglia, where it may contribute to regional and cell-type-specific modulation of GABA tone and metabolic support (Conti et al., 1998; Fattorini et al., 2017, 2020; Minelli et al., 1995), although the role of GAT1 in these cell types during development is largely unexplored. This broad expression pattern contrasts with other GABA transporters such as GAT2 and GAT3 whose expression is predominantly limited to non-neuronal cell types including leptomeningeal cells and astrocytes (Conti et al., 2004; Minelli et al., 1996). Despite the presence of other GABA transporters in non-neuronal cells, the loss of GABA uptake due to GAT1 loss of function (LOF) in neurons cannot be fully compensated by other transporters. There is no detecatable compensatory upregulation of GAT2 or GAT3 in GAT1 knock out animals, but instead an increase in GAD 65/67 positive cells has been reported (Chiu et al., 2005; Jensen et al., 2003),

suggesting that there is an upregulation in GABA synthesis to sustain depleted levels in the axon terminals.

An alternative role for GAT1 in development

Although the defining function of GAT1 is GABA transport, emerging evidence suggests that GAT1 may play a role in neurodevelopmental processes that extends beyond its known canonical synaptic function. Mouse models of a pathogenic *Slc6a1* missense variant S295L, which impairs transporter trafficking and GABA uptake, show not only perturbed inhibitory signaling in the hippocampal dentate gyrus, but also impaired neurogenesis, with reductions in neural progenitor populations, neuroblasts, and immature neurons. Abnormalities in neuronal morphology and dendritic complexity were also observed (Liu et al., 2025). These phenotypes coincided with altered GABA homeostasis and disrupted neurotrophin signaling. Specifically, reduced brain-derived neurotrophic factor (BDNF) expression was observed across all mutant mice (Liu et al., 2025), implying that GAT1 influences developmental programs that govern cell proliferation and network assembly, not only via mechanisms linked to sustained alteration of GABAergic tone but also through interactions with important neurotrophic pathways and signaling molecules.

SLC6A1variant spectrum and Clinical Phenotypes

SLC6A1-related DEEs are typically diagnosed in early childhood (Goodspeed et al., 2020; Johannesen et al., 2018). Patients with *SLC6A1* haploinsufficiency often present with epilepsy, particularly childhood absence and myoclonic-atonic seizure syndromes (Carvill et al., 2015; Johannesen et al., 2018). A large cohort study of over 100 individuals has shown that developmental delay and intellectual disability occur in the majority of patients, often alongside epilepsy and additional features such as hypotonia, speech delay, sleep disturbances, and behavioral disorders resembling ASD (Stefanski et al., 2023).

Pathogenic variants in *SLC6A1*, including splice-site altering, missense, and truncating variants, are distributed broadly along the GAT1 protein sequence, with missense variants particularly clustered within structural regions that are essential for transporter function, including transmembrane domains and extracellular loops (**Figure 1.3**) (Silva et al., 2024).

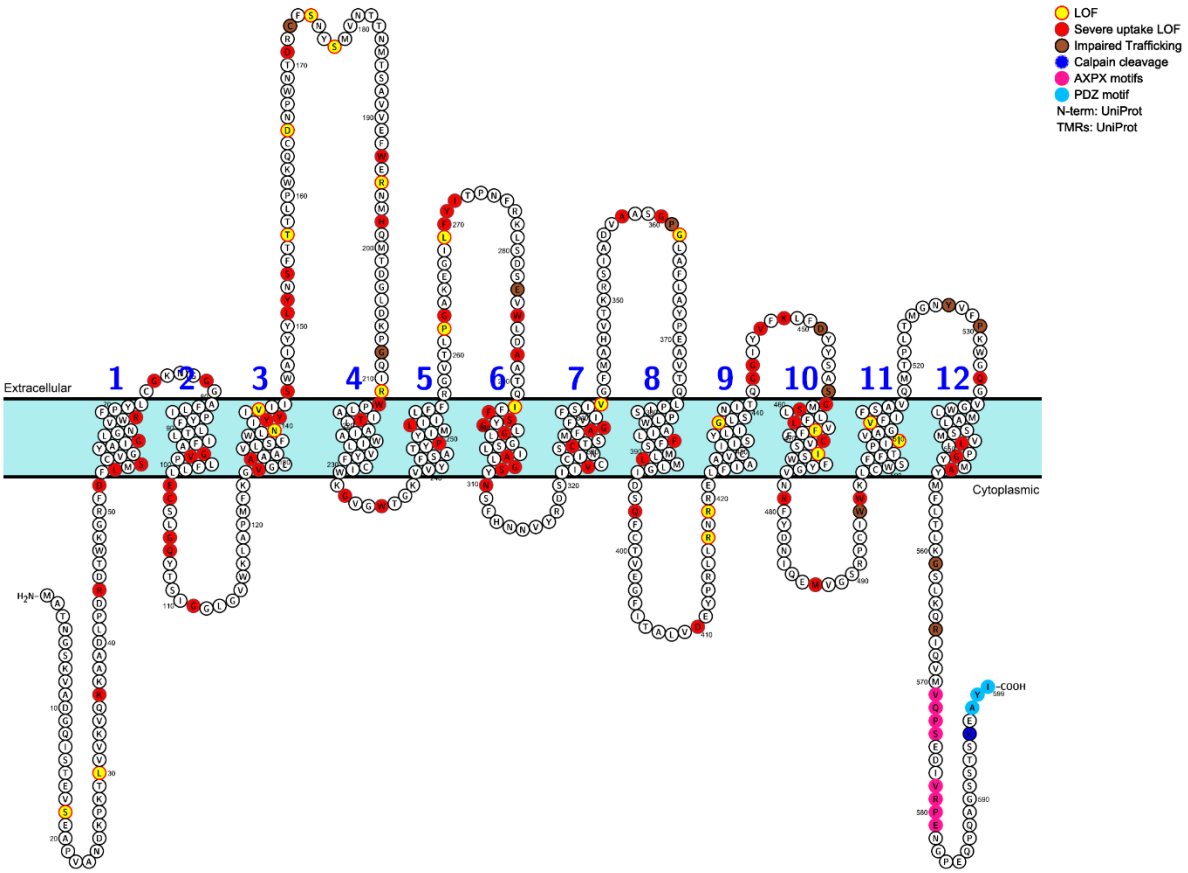

Figure 1.3: Localization of loss of function variants in the GAT1 protein topology.

Schematic showing the protein topology map of the GAT1 protein which is bound to the plasma membrane and contains 12 transmembrane domains, 6 extracellular loops, 5 intracellular loops and intracellular N and C terminus. Loss of function variants (LOF) are depicted in yellow while severe LOF variants are depicted in red. Many LOF and severe LOF variants are clustered within transmembrane domains, specifically transmembrane domain 3 and 6 which form the GABA binding pocket. Variants that result in impaired trafficking to the membrane are depicted in brown. These variants largely occur in the extracellular loops of the protein. Patient data used to generate this plot was made available by the Sliva et al., 2024 large cohort study. The Protter platform was used to generate the plot.

Recent high-throughput functional assays across hundreds of *SLC6A1* patient-associated variants reinforce that partial or complete loss of transporter function is a central molecular consequence of pathogenic variants. In a comprehensive study of 213 unique variants, de *novo* missense changes reduced GABA uptake relative to wild type in the majority of cases, supporting a haploinsufficiency model in which one functional allele is not able to maintain sufficient GABA uptake activity (Silva et al., 2024). Analysis of variant surface localization shows that about two-thirds of functionally significant missense mutations disrupt membrane targeting, largely due to

misfolding of the GAT1 protein, resulting in endoplasmic reticulum (ER) retention, reduced total and surface expression, and subsequent degradation of the mutant protein (Silva et al., 2024). Other missense variants allow the protein to reach the membrane but with reduced transport activity (Silva et al., 2024; Stefanski et al., 2023). Missense variants are enriched among patients and are more likely to result in severe loss-of-function and associated severe epilepsy, intellectual disability, or ASD phenotypes (Silva et al., 2024; Stefanski et al., 2023). In contrast, variants located farther from key functional domains tend to retain more residual transporter activity and are associated with more variable clinical expressivity (Silva et al., 2024). These findings support a model in which proximity to the ligand binding and transport pathway is a determinant of variant impact, providing a structural framework for interpreting genotype–phenotype correlations in *SLC6A1*-related disorders.

1.4 Modeling Neurodevelopmental Disorders with Human iPSC-derived Brain Organoids

Recent years have seen a surge in the discovery of epilepsy related genes and, with it, a blooming of mechanistic studies. Because of the inaccessibility of human epileptic tissue, the lack of adequate control tissue, and the fact that only late-stage specimens are acquired when available, model systems are necessary for the study of epilepsy mechanisms and the development of novel therapies. Moreover, as epilepsies typically are associated with comorbidities involving diverse and widespread brain networks, a useful strategy is to incorporate multifaceted approaches that encompass structural, functional, and developmental features to model epilepsies and their associated comorbidities.

The mainstay of genetic epilepsy models over the past five decades has been spontaneous or genetically engineered rodent models harboring genetic abnormalities similar to those identified in human genetic epilepsies. Such models have contributed a wealth of knowledge to the epilepsy field, specifically surrounding the function of neural networks in epilepsy and the underlying in vivo pathophysiological processes. Zebrafish represent a more recent addition to the armamentarium of genetic epilepsy models and are particularly useful for high-throughput drug screening (Baraban, 2021). However, several limitations arise in the use of animal models of epilepsy. Fish and even mice possess important genetic, structural, and neurodevelopmental differences from humans. And while some rodent models exhibit a seizure phenotype that closely resembles those seen in humans, most do not completely recapitulate the complex pathophysiology

of human epilepsies. Moreover, animal models for many genetic epilepsies do not exhibit spontaneous seizures. Despite extensive research using animal models, understanding of the cellular and molecular mechanisms surrounding monogenic epilepsies remains elusive, and disease modifying treatments are lacking.

To overcome some of these obstacles and expand the tools available to model epilepsies, human pluripotent stem cells (hPSCs), a term that encompasses both human embryonic stem cells (hESCs) and induced pluripotent stem cells (iPSCs), have become increasingly used. In 1998, the Thomson laboratory discovered that they could derive hESCs from blastocysts and that these cells could then be used to generate many different cell types in vitro (**Figure 1.4**) (Thomson, 1998).

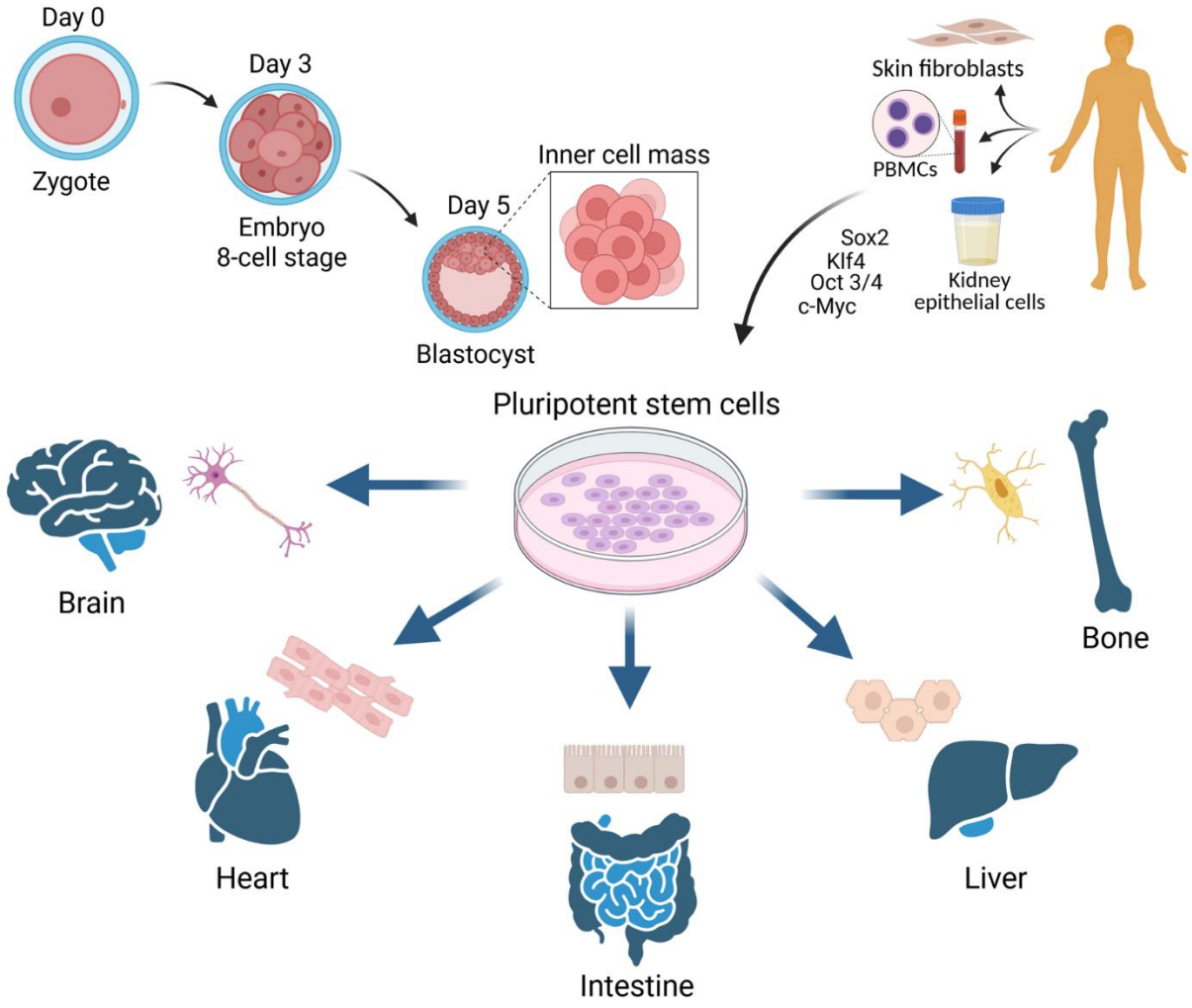

Figure 1.4: Avenues of pluripotent stem cell generation and downstream applications

Schematic demonstrating the two main avenues of generating pluripotent stem cells (PSCs). The top left of the figure shows the progressive stages of development from a zygote on Day 0 to a

blastocyst on 5 days post conception. The inner cell mass in the blastocyst is the source of pluripotent embryonic stem cells. The top right of the image shows methods of generating induced pluripotent stem cells from human skin fibroblasts, peripheral blood mononuclear cells (PBMCs) obtained from blood, or kidney epithelial cells from urine. The "Yamanaka factors" Sox2, Klf4, Oct3/4, and c-Myc are used to reprogram these cells into induced pluripotent stem cells. Human PSCs can then be used downstream to generate many different cell types including brain, heart, intestine, liver, and bone among many others.

The breadth of stem cell research was further enhanced in 2006 when Yamanaka and colleagues(Takahashi & Yamanaka, 2006) demonstrated that mouse somatic cells could be reprogrammed to generate iPSCs. This discovery was quickly followed by the generation of human iPSCs in 2007 (Meissner et al., 2007; Takahashi et al., 2007), and the use of human iPSCs in translational research, drug discovery, and therapeutic development has since become increasingly widespread. Skin or blood cells taken from a patient can be reprogrammed to iPSCs and used to model a genetic disease by generating the affected cell type. Germline genetic variants found in a given patient are carried on in their somatic cell-derived iPSCs and in any subsequent progeny that are generated from these iPSCs. Since samples of the affected tissue cannot easily be taken from patients suffering from CNS diseases, brain cells generated from patient iPSCs provide a useful tool to study and model the development of brain diseases, particularly neurodevelopmental disorders. In the next few sections, I review the current techniques and applications of hPSC models for studying genetic epilepsies using both 2D and 3D neural culture approaches. Additionally, I highlight potential limitations and avenues for future research using hPSC model systems.

Generating iPSCs

The ability to generate patient-specific iPSC lines provides the opportunity to model a wide range of genetic epilepsies in an in vitro system. The forced expression of specific transcription factors reverts somatic cells to a pluripotent epigenetic state and silences lineage-specific genes. This process, called "reprogramming," is typically carried out by introducing four transcription factors, Sox2, Oct3/4, Klf4, and c-Myc, into somatic cells (Takahashi et al., 2007; Takahashi & Yamanaka, 2006). These four factors are commonly referred to as the "Yamanaka factors." Typically, reprogramming involves the use of dermal fibroblasts obtained by a skin biopsy. More recently, peripheral blood mononuclear cells derived from patient blood samples are increasingly

used as a less invasive source of somatic cells for reprogramming, and kidney epithelial cells extracted from urine are another option (Okita et al., 2013; Zhou et al., 2011). These advances have broadened the source of iPSCs and have contributed to the ease and accessibility of iPSC research.

Gene editing of iPSCs

Genome editing technologies have greatly expanded the utility of hPSCs for studying neurological disorders, including genetic epilepsies. The CRISPR/Cas9 system enables highly precise modification of genomic sequences (Cong et al., 2013; Ran et al., 2013), making it a powerful tool for generating disease-relevant cellular models. One major advantage of this approach is the ability to minimize variability between patient-derived iPSC lines that arises from differences in genetic background. Using CRISPR-mediated homology-directed repair, pathogenic variants can be corrected in patient iPSCs to generate isogenic control lines, allowing direct comparison between genetically matched cells that differ only at the mutation of interest. Conversely, when patient-derived samples are unavailable, epilepsy-associated variants can be engineered into a control iPSC line to create paired "virtual patient" and isogenic control lines for mechanistic studies.

CRISPR-based genome editing also enables additional experimental strategies for investigating disease mechanisms. Homology-directed repair can be used to insert exogenous DNA sequences into defined genomic loci, allowing endogenous genes to be tagged with fluorescent reporters and facilitating studies of protein localization, expression dynamics, or mutant protein behavior in living cells (Roberts et al., 2017). In addition, CRISPR-mediated gene knockout, typically generated through non-homologous end joining that produces frameshift insertions or deletions, can be used to model loss-of-function conditions, including autosomal recessive epilepsies or disorders caused by haploinsufficiency. Recent advances have further improved the efficiency of this strategy by integrating CRISPR editing with somatic cell reprogramming, enabling rapid generation of iPSC-based loss of function (LOF) models of genetic epilepsy (Tidball et al., 2017).

Brain Organoid models

Although human stem cell–derived 2D cultures have provided useful insights for modeling epilepsy, these systems have important limitations, including physiological, functional, and molecular differences compared with native human brain tissue (Bershteyn & Kriegstein, 2013). A major challenge is the difficulty of establishing complex neural circuits in two-dimensional environments. Several factors contribute to this limitation, including restricted neuronal diversity (particularly among interneuron subtypes), relatively short culture durations that typically do not exceed three months, and the absence of a three-dimensional tissue cytoarchitecture. Because epilepsy is fundamentally a disorder of neural circuit dysfunction, these constraints represent a substantial drawback for 2D culture models. Brain organoids are self-organizing 3D cellular structures containing multiple neuronal and glial cell types, and are capable of reproducing certain aspects of brain cytoarchitecture, including cortical layering and the generation of coordinated neural network activity (Lancaster et al., 2013; Samarasinghe et al., 2021; Sun et al., 2019; Trujillo et al., 2019; Watanabe et al., 2017). Although organoids do not fully replicate the structural and cellular complexity of the developing brain in vivo, they possess several features that distinguish them from commonly used rodent models. For instance, hPSC–derived organoids develop an expanded subventricular zone (SVZ), including an outer subventricular zone (oSVZ), a structure that is largely absent in the rodent brain. Importantly, these organoids also contain substantial numbers of outer radial glial cells (oRGs), also referred to as basal radial glia, which are progenitor cells predominantly associated with the oSVZ. oRGs are believed to be responsible for the evolutionary expansion of the human cortex and are abundant in gyrencephalic species such as humans and nonhuman primates but are largely lacking in lissencephalic species such as mice (Hansen et al., 2010; Martínez-Cerdeño et al., 2012). Given the significant contribution of genetic variation to epilepsy, organoid systems provide a valuable platform for investigating how disease-associated variants influence human cortical development and expansion.

In order to generate brain organoids, hPSCs are aggregated in suspension using a number of different approaches such that they differentiate and self-organize into 3D brain-like structures. While the available protocols for organoid generation continue to expand in this highly dynamic field (and are reviewed in detail elsewhere; (Mayhew & Singhania, 2023)), the general approaches can be divided into two broad categories. In one set of so-called intrinsic protocols, stem cells are allowed to differentiate in the absence of specific patterning factors. The resulting organoids typically contain a wide assortment of cell types, including forebrain cortex, hindbrain, and retinal

cells (Lancaster et al., 2013). In the second category of approaches are protocols that utilize the timed application of patterning factors to direct differentiation into specific brain-like regions. For example, SMAD inhibition is used in multiple protocols to limit mesoderm and endoderm formation in favor of ectoderm (Kadoshima et al., 2013; Pasca et al., 2015; Qian et al., 2016). Often, SMAD inhibition is combined with other morphogens or small molecules to generate dorsal forebrain-like brain organoids that consist primarily of glutamatergic (excitatory) neurons (Bagley et al., 2017b; Kadoshima et al., 2013; Pasca et al., 2015). These dorsal cortical organoids notably lack inhibitory interneurons. Similarly, SHH pathway agonists both in the presence and absence of WNT inhibition have been used to generate ventralized ganglionic eminence-like organoids with a large population of inhibitory interneurons (Bagley et al., 2017; Watanabe et al., 2017). In addition to dorsal and ventral forebrain organoids, this approach of directed differentiation has been used to generate a growing list of additional regional specificities, including hypothalamus, cerebellum, hippocampus, and others (Atamian et al., 2024; Muguruma et al., 2015; Qian et al., 2016; Rao et al., 2025; Sakaguchi et al., 2015); and reviewed in (Mayhew & Singhania, 2023)).

Modeling genetic epilepsies using brain organoids

A number of studies, primarily using directed differentiation of human forebrain cortex-like organoids, have utilized 3D culture approaches to determine the effects of epilepsy-associated genetic variants on various anatomical measures, including organoid cytoarchitecture and organization, cell expression patterns, and neuronal migration. This work has been reviewed elsewhere (Baldassari et al., 2020; Nieto-Estévez & Hsieh, 2020). Recent studies have additionally examined neural circuit activities generated by organoids. One of the first to do so utilized microelectrode arrays to document the generation of neural oscillations that increased in complexity with age (Trujillo et al., 2019). Measurements were performed in cortical organoids that were retained in culture from 2 to 10 months. In a more direct study of epilepsy, Sun and colleagues generated a cortical organoid model of Angelman syndrome resulting from a mutation in the ubiquitin ligase *UBE3A* gene (Sun et al., 2019). Angelman syndrome is associated with intellectual disability and lifelong seizures. Cortical organoids examined after 120–150 days in vitro demonstrated evidence of neuronal hyperexcitability by patch-clamp recording, and calcium indicator imaging revealed hypersynchronous discharges in the mutant organoids that were not observed in isogenic controls.

Both of these studies involved directed differentiation of forebrain cortex-like organoids, which would not be expected to contain a significant number of inhibitory interneurons. Interestingly, transcriptomic analyses by Trujillo and colleagues did reveal the spontaneous expression of an inhibitory interneuron population by 8-10 months in culture (Trujillo et al., 2019), which may partly explain the increased complexity of oscillatory activity observed by these authors at later time points. In contrast, and as expected, Sun et al. observed sparse inhibitory interneurons in their culture conditions (Sun et al., 2019). Given the importance of interneurons and excitatory-inhibitory connectivity in neural circuit activity in general and the pathophysiology of epilepsy in particular, recently developed approaches to integrate these populations within a single organoid are of particular relevance to organoid modeling of epilepsy. Birey and colleagues pioneered an innovative and elegant approach to achieve this integration by generating "assembloids" (also referred to as organoid "fusions") in which glutamatergic neuron-rich dorsal and interneuron-rich ventral organoids are separately generated and then combined by placing the two structures adjacent to each other such that they physically fuse together (Birey et al., 2017). This protocol appears to recapitulate in fused organoids the in vivo process of tangential migration of interneurons, whereby ventrally born interneurons and interneuron progenitors migrate and integrate into dorsal cortex. The assembloid approach has since been used to model circuit activity in an organoid model of Rett syndrome resulting from mutations in the *MECP2* gene (Samarasinghe et al., 2021). In this study, *MECP2* mutations were shown to result in hypersynchrony by calcium indicator imaging as well as both a loss of gamma oscillations and increased, putatively pathogenic high-frequency activity (previously known as high-frequency oscillations [HFOs]) by extracellular recording of local field potentials. These authors also leveraged the assembloid approach to specifically identify ventral organoid derived interneurons, as opposed to dorsal excitatory neurons, as the primary drivers of the hyperexcitable phenotype.

Modeling MGE-derived cells using organoids

Existing protocols for generating interneuron-enriched subpallial brain organoids typically rely on early ventralization with SHH agonists and, in some cases, FGF signaling, followed by prolonged culture to facilitate neuronal differentiation and maturation (Bagley et al., 2017; Birey et al., 2017; Xiang et al., 2017; Yu et al., 2025; and reviewed by Pavon et al., 2024). These approaches robustly induce general GABAergic markers such as GAD1/2 and DLX1/2, but yield

mixed populations resembling LGE, CGE, and other ventral forebrain identities. Many such models show inconsistent or incomplete expression of canonical MGE-defining markers, including NKX2.1, LHX6, and OLIG2, and frequently lack authentic MGE progenitor specification. As a result, these organoids more accurately represent broad subpallial tissue rather than a bona fide MGE developmental niche, limiting their utility for studying MGE-specific interneuron lineages.

While the majority of subpallial organoid protocols generate multi-rosette structures, single-rosette organoid models are increasing in popularity as they offer key structural advantages over multi-rosette systems (Kim et al., 2025; Rao et al., 2025; Tidball et al., 2023; Y. Wang et al., 2022). A single rosette, analogous to the neural tube, more closely recapitulates the early organization of the ventral telencephalon, which consists of a single neural tube with a unified ventricular zone, consistent apical–basal polarity, and more synchronized progenitor patterning. In contrast, multi-rosette organoids are structurally heterogeneous and often exhibit asynchronous differentiation, which complicates the interpretation of developmental timing and lineage relationships (**Figure 1.5**). Considering these advantages, the development of a single-rosette, MGE-specified organoid model would be particularly useful for investigating MGE interneuron development and their disease-associated phenotypes.

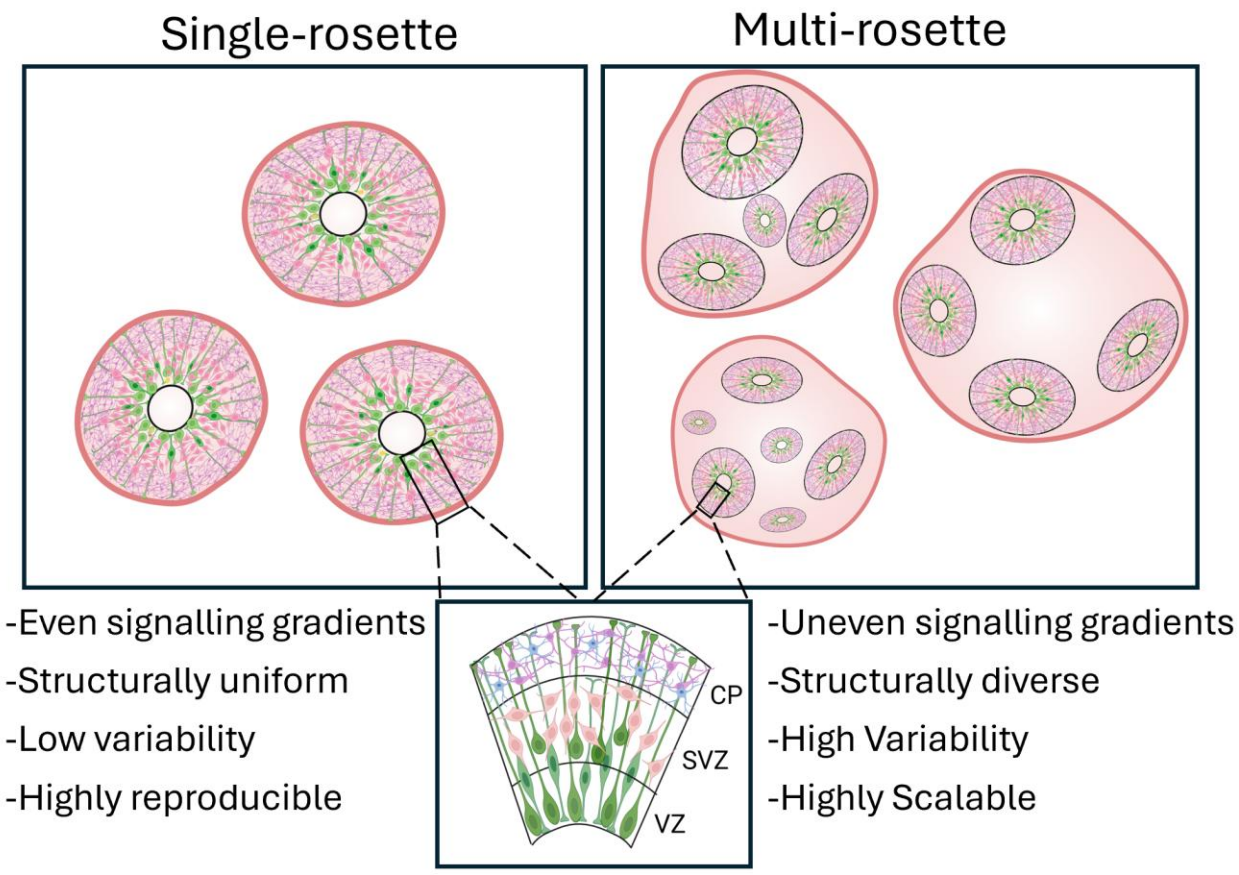

Figure 1.5: Comparison of single rosettes vs. multi-rosette organoid models.

Schematic showing the cellular structure of single rosette organoids on the left and multi-rosette organoids on the right. A single rosette structure, analogous to the single neural tube in early brain development, better models the developing nervous system compared to multi-rosette structures. Zoomed in insert shows the structural and cellular components of the developing brain that are recapitulated by both organoid models including dividing progenitors populating a ventricular zone (VZ)-like region on the bottom, apical side followed by intermediate progenitors and outer radial glia in a subventricular zone (SVZ)-like region in the middle and a cortical plate (CP)-like zone populated by maturing neurons at the top of the image representing the basal side. The structural uniformity of single rosette organoids provide advantages such as even dispersion of endogenous morphogen gradients, high reproducibility and low variability, although these protocols tend to be less scalable than multi-rosette systems. I contrast, multi rosette organoids are highly scalable but are structurally diverse leading to high variability between organoids and batches. The variability in structure can lead to uneven signaling gradients which increases variability in cell type composition and maturation stages of cell within the organoid

Challenges in generating PV+ fast spiking interneurons

Along with the difficulty in generating MGE lineages in vitro comes the notorious challenge of generating mature PV+ fast-spiking interneurons. Recent two-dimensional and three-

dimensional studies have made progress in improving the specification of MGE-like progenitor cells with many of them able to produce LHX6 expressing cells, a hallmark identifier of MGE lineage that prior studies have failed to produce in meaningful numbers (Bershteyn et al., 2023a; Walsh et al., 2025a). However, despite being enriched in these cell lineages, both 2D and 3D models continue to yield relatively few, if any, PV+ cells, and those that do arise, frequently display incomplete maturation and lack the hallmark fast-spiking electrophysiological properties observed in vivo.

Several factors contribute to the difficulty of generating PV+ interneurons in human stem cell–derived systems. PV+ interneurons in vivo are among the last interneuron subtypes to mature during development, requiring extended time periods and environmental cues to acquire their molecular identity and functional properties. In vitro systems often fail to fully replicate the signaling gradients, cell–cell interactions, and activity-dependent mechanisms present in the developing brain that guide interneuron specification and maturation. Additionally, the long developmental timeline of human interneurons, often requiring many months of culture, poses practical challenges for culture-based systems. As a result, current organoid and 2D differentiation protocols tend to preferentially produce earlier-born interneuron subtypes, such as SST-expressing neurons, while PV+ interneurons remain vastly underrepresented. These limitations have hindered the study of diseases in which PV+ interneuron dysfunction is thought to play a central role and highlight the need for improved human models capable of reliably generating mature, fast-spiking PV+ interneurons.

1.5 Questions addressed in this Dissertation

This dissertation aims to evaluate how alterations in interneuron developmental processes during early human cortical development can lead to cellular and functional changes that may contribute to epileptogenesis and other neurodevelopmental disorders. In Chapter 2 the question of how MGE-derived interneuron development can be reliably assessed in a human in-vitro model is addressed. We conduct a thorough morphogen screen to determine the precise cocktail that produces MGE-like interneurons in vitro using a hPSC-derived single-rosette organoid model. We further evaluate the migratory characteristics, maturation timelines, and the development of functional properties of these interneurons and reveal the emergence of important interneuron

subtype populations, specifically PV+ cortical interneurons, which are frequently implicated in epilepsy.

Chapter 3 expands this line of investigation in the context of epilepsy by assessing the developmental consequences of genetic variants in the epilepsy-associated gene, *SLC6A1*. I utilize the MGE organoid model developed in Chapter 2 to evaluate the impact of *SLC6A1* variants on interneuron migration, maturation, and subtype specification. Finally, I investigate the downstream effects of interneuron developmental alterations on neural network activity and explore mechanistic insights. In the concluding chapter, I summarize findings and frame them in the context of their broader impact to the scientific community. I discuss potential future directions of investigation including identifying and characterizing the molecular signatures of early PV progenitors and using the knowledge gained to increase yields for potential cell transplant therapies. Additionally, I propose methods to further dissect the mechanisms and protein interactions that contribute to the observed phenotypes in *SLC6A1* mutant organoids and present the possibility that GAT1 may also play an unexpected role in the development of excitatory cortical neuron populations through modulation of key developmental pathways.

Chapter 2 Robust Production of Parvalbumin Interneurons and Fast-Spiking Neurons from Human Medial Ganglionic Eminence Organoids

2.1 Summary

The medial ganglionic eminence (MGE) gives rise to PV- and SST-expressing cortical interneurons essential for regulating cortical excitability. Although PV interneurons are linked to various neurodevelopmental and neurodegenerative disorders, reliably generating them from human pluripotent stem cells (hPSCs) has been extremely challenging. We present a robust, reproducible protocol for generating single-rosette MGE organoids (MGEOs) from hPSCs.

Transcriptomic analyses reveal that MGEOs exhibit MGE regional identity and faithfully model the developing human fetal MGE. As MGEOs mature, they generate abundant PV-expressing cortical interneurons, including putative basket and axoaxonic cells, at a scale not previously achieved *in vitro*. When fused with hPSC-derived cortical organoids, these interneurons rapidly migrate into cortical regions, integrate into excitatory networks, and contribute to complex electrophysiological patterns and the emergence of large numbers of fast-spiking neurons. MGEOs thus offer a powerful *in vitro* approach for probing human MGE-lineage cortical and subcortical GABAergic neuron development, modeling various neuropsychiatric disorders, and advancing cell-based therapies for neurodevelopmental and neurodegenerative disorders

2.2 Introduction

The human cortex is largely populated by two divergent classes of neurons: glutamatergic excitatory neurons and gamma-aminobutyric acid (GABA)-containing inhibitory interneurons. During development, glutamatergic neurons are generated in the dorsal telencephalon and migrate radially as they form the cortical layers. In contrast, the majority of cortical GABAergic interneurons are generated in the ganglionic eminences (GEs) before migrating tangentially from the basal telencephalon to the cortex. These neurons are essential for maintaining the balance of excitation and inhibition within neural circuits, which is fundamental for proper neural circuit function and cortical information processing (Buzsáki & Chrobak, 1995). GABAergic neurons modulate brain network activity by regulating the timing and synchrony of neuronal firing, leading to the formation of neuronal oscillations critical for information transfer in the brain (Bartos et al., 2002; Hájos et al., 2004; Jacobs et al., 2007). Disruptions in the migration, maturation, synaptogenesis or function of these interneurons have been linked to various neurologic and psychiatric disorders. These disorders include neurodevelopmental conditions (Marín, 2012), such as autism (Amegandjin et al., 2021; Q. Chen et al., 2020; Juarez & Martínez Cerdeño, 2022; Nomura, 2021; Smith et al., 2020; Vogt et al., 2018), attention deficit disorder and intellectual disability (Ferguson et al., 2023; Lupien-Meilleur et al., 2021), epilepsy (Gertler et al., 2022; Jiang et al., 2016, 2018; Rossignol et al., 2013; Ryner et al., 2023), and schizophrenia (Lewis, 2014; Shen et al., 2021; Sohal & Rubenstein, 2019), as well as neurodegenerative diseases (Gabitto et al., 2024), highlighting the critical nature of these cells in maintaining neural homeostasis.

The GEs are transient structures in the developing brain comprised of three distinct regions: medial ganglionic eminence (MGE), caudal ganglionic eminence (CGE) and lateral ganglionic eminence (LGE). The MGE and CGE, along with the preoptic area (POA), generate the majority of interneurons in the cortex and hippocampus. The MGE serves as the origin of approximately 60% of cortical interneurons and produces several interneuron subtypes crucial for cortical function (Anderson et al., 2001, 2002; Flames et al., 2007; Wonders & Anderson, 2006; Xu, Cobos, De, et al., 2004; Xu et al., 2008). The MGE is characterized by the expression of the forebrain marker FOXG1, as well as homeobox transcription factors NKX2.1 and LHX6, with no expression of the dorsal cortical marker PAX6 or the more ventral hypothalamic marker RAX (Keefe et al., 2023; Maroof et al., 2013; Nicholas et al., 2013; Shi et al., 2021; Z. Zhao et al., 2022).

NKX2.1 is also expressed in the rostral pallidum, ventral septum, preoptic area, and ventral hypothalamic regions. In contrast, *LHX6* is largely restricted to MGE-derived lineages. In MGE-derived GABAergic lineages, upregulation of *LHX6* is induced by *NKX2.1* expression at approximately gestational week 8 (GW8) in humans or embryonic day 11.5 in mice and is essential for the proper positioning and maturation of cortical SST and PV interneurons (Flames et al., 2007; Fogarty et al., 2007; Jakovcevski et al., 2010; Lim et al., 2018; Liodis et al., 2007; Neves et al., 2013; Sussel et al., 1999; Vogt et al., 2014; Xu et al., 2008; Zhao et al., 2008). In addition to SST and PV cortical interneurons, the MGE also produces GABAergic and cholinergic striatal interneurons, subpallial GABAergic projection neurons, astrocytes, and oligodendrocytes (Sussel et al., 1999; Wichterle et al., 1999; Zhao et al., 2003).

Recent transcriptomic studies of human fetal brain tissues have provided significant insights into the gene expression profiles of the developing human GEs (Alzu'bi et al., 2017; Keefe et al., 2023; Shi et al., 2021, Yu et al., 2021; Zhao et al., 2022). However, the availability of human brain tissues from a broad range of fetal development is limited. To address this limitation, human pluripotent stem cell (hPSC)-derived 2D and brain organoid models have emerged as promising tools for recapitulating neural development *in vitro*. In particular, brain organoids are 3D structures that recapitulate key aspects of brain cytoarchitecture, cellular diversity, and complex network connectivity. These models simulate key features of the native brain environment and offer the potential for generating unique insights into human neurodevelopment and associated disorders. Several pioneering groups have generated GABAergic neurons from hPSCs in both 2D cultures (Bershteyn et al., 2023; Maroof et al., 2013; Nicholas et al., 2013) and 3D brain organoid models (Bagley et al., 2017; Birey et al., 2017; Sloan et al., 2018; Xiang et al., 2017). These methods produce NKX2.1+ progenitors and generate primarily GABAergic SST+ neurons and neurons that arise from other subpallial regions but little to no PV+ cortical interneurons in culture. PV+ interneurons are the largest class of interneurons in the human cortex, comprising approximately 30-40% of all cortical interneurons, and play a critical role in regulating cortical excitability. PV interneuron fast-spiking properties allow them to tightly regulate and synchronize cortical network activity through gamma oscillations. These oscillations facilitate rapid information transfer across brain circuits and thus are critical for cognition, sensory processing, and working memory. Dysregulation of PV interneuron development and function is implicated in epilepsy, schizophrenia, and autism spectrum disorders, making them a highly desirable cell type to generate

for *in vitro* disease modeling (Gonzalez-Burgos & Lewis, 2012; Jiang et al., 2016; Juarez & Martínez Cerdeño, 2022; Sohal et al., 2009). To date, however, no hPSC-derived *in vitro* model has been reported that consistently and robustly generates PV cortical interneurons or fast-spiking neurons.

Recent studies have made progress in generating PV-expressing cortical basket interneurons and fast-spiking neurons from hPSCs using organoid assembloid approaches (Walsh et al., 2025) or xenotransplant strategies (Bershteyn et al., 2025). However, the efficiency in PV interneuron generation remains low, with PV interneuron clusters identified indirectly through predictive identity algorithms (Bershteyn et al., 2025), or via immunostaining that shows limited PV expression (Walsh et al., 2025). To date, no hPSC-derived in vitro model has shown robust, quantified expression of PV at the protein level. Furthermore, to our knowledge, PV-expressing axoaxonic cells have not been shown in any published human subpallial organoid or assembloid models.

Here we describe a human MGE-specific organoid (MGEO) model that exhibits MGE lineage marker expression and cell type specificity. The model exhibits transcriptomic similarities to human fetal MGE, generates highly migratory pallial interneuron progenitors, and displays robust development of MGE lineage interneuron subtypes that include SST and PV interneurons. When fused to human cortical organoids (hCOs) to generate assembloids, MGEO-derived interneurons migrate into hCOs where they integrate with excitatory cortical neurons, leading to complex network activity and the development of fast-spiking neurons. Our model offers a powerful platform for studying human-specific MGE interneuron development and disorders related to MGE interneuron dysfunction and provides a potential source of MGE interneuron progenitors for therapeutic grafting.

2.3 Materials and methods

MGEO generation

Self-organizing single rosette MGEOs were generated from a hPSC monolayer by modifying our SOSR-CO protocol (Tidball et al., 2023). For the initial formation of the monolayer, iPSC lines were dissociated using Accutase (Innovative cell) and plated onto Geltrex-coated (1:50 dilution in DMEM/F12) 12-well plates at 3–4 × 10^5 cells/mL in mTeSR1 with 10 μM Rho-kinase inhibitor (Y-27632; Tocris, 1254). Media without the inhibitor was replaced daily until the cells

reached 80%–100% confluency. The medium was then changed to 3N (50:50 DMEM/F12:Neurobasal with N2 and B27 supplements) without vitamin A with 2 μM DMH1 (Tocris, 4126), 2 μM XAV939 (Cayman Chemical, 13596), and 10 μM SB431542 (Cayman Chemical, 13031) (2 mL of media per well). On DIV 4, media was removed, and the monolayer was incubated for 1 min with L7 hPSC passaging solution (Lonza). After aspirating the L7 solution, the monolayer was cut into squares using a StemPro EZ passage tool. The squares were sprayed off the bottom of the culture plate with 1 mL of pre-prepared culture media with a P1000 micropipette. Approximately 200 μL of resuspended squares were then transferred into each well of a 96-well plate preincubated at 37°C for 30 min with 40 μL of 100% Geltrex solution/well. Each monolayer will seed up to 16 wells containing approximately 20-40 organoids per well. Additional media was added to each well the day after plating without media change. Half-media changes were performed daily beginning 48 hrs post plating. On day 6 (2 days after cutting), human FGF2 (20 ng/ml, Gibco, PHG0261) was added to the culture media to support cell survival. On day 10, a 100% media change was performed with 3N media plus 100 nM SAG (Selleckchem, S7779) and FGF2, without DMH1, XAV939 and SB431542. Between days 10 and 12, the organoids were individually removed using a STRIPPER Micropipetter (Cooper Surgical) with 275 μm tips and placed in suspension individually in the wells of a low-adherence U-bottom 96-well plate with 200 μL of 3N medium without vitamin A. The ideal diameter for picking the MGEOs is ~250 μM. Larger sizes may produce additional rosettes, and smaller sizes tend to have suboptimal survival. Starting on day 12, half-media changes (100 μL/well) of 3N with vitamin A, 100 nM SAG, BDNF (20 ng/mL), and NT3 (20 ng/mL) without FGF2 were repeated every other day until day 18 when SAG was removed from the culture medium. After 35 days of differentiation, 3N media with vitamin A (but without BDNF and NT3) was used for half-media changes every other day. At this time, MGEOs were transferred to low-adherence 24-well plates for a necessary increase in media volume due to expanded organoid size. Beginning day 90, MGEOs were cultured in BrainPhys media (Stemcell technologies, 05790) containing N2 supplement, NeuroCult™ SM1 Neuronal Supplement (Stemcell technologies, 05711), BDNF (20 ng/mL), GDNF (20 ng/mL), and Ascorbic acid (200nM). Self-organizing single rosette cortical organoids (SOSR-COs) were generated as described (Tidball et al., 2023).

Cryopreservation, sectioning and immunocytochemistry

Organoids were collected, washed with phosphate-buffered saline (PBS), and incubated in 4% paraformaldehyde (PFA) diluted in PBS at 4°C for 30 min (for 1-month organoids) or an hour (for older organoids). After three 10-min PBS washes, organoids were incubated overnight at 4°C in a 30% sucrose (in PBS) solution, embedded in cryomolds (Tissue-Tek 4566) using O.C.T compound (Fisher Healthcare 4585), frozen on dry ice, and stored at -80°C. Frozen organoid blocks were sectioned onto Superfrost Plus glass slides (ThermoFisher 12-550-15) at a thickness of 20µM using a Leica CM1850 cryostat. After drying at room temperature (RT) for at least 2 h, slides were stored at -20°C until use. For immunostaining, organoid sections were washed three times with PBS, permeabilized for 20 min in PBS with 0.2% Triton-X100 at RT, and incubated in blocking buffer (PBS with 0.05% Tween- 20, 5% normal goat serum, and 1% bovine serum albumin (BSA)) for 1 h at RT. Normal horse serum was used in blocking buffer for immunostaining using goat primary antibodies. Fixed and permeabilized sections were incubated overnight at 4°C in a humidified chamber with primary antibodies diluted in blocking buffer. Sections were then washed 3 times in PBST (PBS with 0.05% Tween-20) and incubated for 2 hours at RT with Alexa-Flour secondary antibodies diluted 1:500 in blocking buffer. Sections were washed once with PBST for 10 minutes and incubated with bisbenzimide for 5 min to label nuclei. After 3x-10 min washes of PBST, coverslips were mounted onto slides using Glycergel mounting medium (Agilent Dako C0563). Once set, the edges of the slides were sealed using clear nail polish. Slides containing immunolabeled organoid sections were imaged using an Andor BC43 benchtop spinning disc confocal microscope (Oxford Instruments). Acquired images were analyzed in Fiji.

RT-qPCR

For reverse transcriptase quantitative PCR (RT-qPCR), total RNA was extracted using the miRNeasy Mini Kit (Qiagen 217004) as per manufacturer's protocols (with optional DNase1 digestion step), with at least four organoids pooled per sample. Template RNA (100 ng) was used to synthesize cDNA using the SuperScript™ III First-Strand Synthesis SuperMix kit (Invitrogen 11752-050). RT-qPCR was performed as per manufacturer protocols, using 2 ng of cDNA and Power SYBR Green PCR Master Mix (Thermofisher 4367659) with an AppliedBiosystems QuantStudio3 thermocycler. Fold changes were calculated using the $2^{-\Delta\Delta Ct}$ method, normalizing to the average undifferentiated 2E iPSC levels from n=3-4 experiments. Samples were run in

triplicate and GAPDH was used as an internal control. Undetectable levels of mRNA were set to a CT value of 40 for analysis, which was performed in Microsoft Excel and graphed using GraphPad Prism.[58]

Fixation of whole MGE organoids

For the MGEO protocol, whole organoid fixation for downstream scRNA-seq analysis of MGEOs was conducted using the 10X Genomics Chromium Next GEM Single Cell Fixed RNA Sample Preparation Kit (10X Genomics, 1000414). All reagents described below were supplied with the kit and the protocol was carried out as described on the 10X Genomics website. In brief, 4-8 organoids (depending on age/size) were collected using a P1000 micropipette with a cut pipette tip and transferred to a 1.5 mL Eppendorf tube. Organoids were allowed to sink to the bottom of the tube, and the supernatant media was carefully aspirated from the tube without disturbing the organoids. Organoids were rinsed once with 1 ml of PBS, the PBS was removed from the tube and 500 ml of Fixation Buffer was added and incubated for 24 h. at 4°C. The next day, the Fixation Buffer was removed without disturbing the organoids and the organoids were washed with 1 mL of chilled PBS. PBS was removed and 500 µL of Quenching Buffer was added to the tube containing the fixed organoids. Enhancer (50 µL) was added and pipette mixed. Glycerol (137.5 µL of a 50% solution) was then added and pipette mixed for a final concertation of 10% glycerol. Samples were stored in -80°C until they were sent to the University of Michigan's Advanced Genomics core for further processing and analysis.

MGEO tissue dissociation, library prep, and sequencing

Tissue dissociation, library prep and next-generation sequencing was carried out in the Advanced Genomics Core at the University of Michigan. Fixed organoid tissue samples were dissociated, then individual samples were barcoded, and pooled together for sequencing. Cells were processed through the 10x Genomics Chromium system (10x Genomics). 10x Genomics v.3 libraries were prepared according to the manufacturer's instructions. Libraries were then sequenced using paired-end sequencing with a mean coverage ranging from 15,000 to 39,000 raw reads per cell using an Illumina NovaSeqXPlus. Day 90 pooled samples were subjected to 28x90bp of sequencing according to the manufacturer's protocol (Illumina NovaSeqXPlus). scRNA-seq data were aligned and quantified using Cell Ranger Single-Cell software suite (v.7.1.0, 10x

Genomics) against Homo sapiens (human) genome assembly GRCh38.p13 from ENSEMBL. BCL Convert Conversion Software v4.0 (Illumina) was used to generate de-multiplexed Fastq files.

Analysis of scRNAseq data

Analysis of scRNA-seq data was done as previously reported(Xue et al., 2024). Briefly, the data were analyzed using the R package Seurat (v.4.2.3, https://satijalab.org/seurat/)). Datasets were filtered, normalized, and scaled. Differences between G2/M phase and S phase scores were regressed out during the scaling process. The dataset further went through PCA analysis and was embedded into low-dimensional space using UMAP algorithm for visualization. Clusters were identified using shared nearest neighbor modularity optimization-based clustering algorithm. The clusters were annotated based on expression of known marker genes and genes found to identify specific cell types in human fetal MGE data sets (Shi et al., 2021;Yu et al., 2021; Zhao et al., 2022).

To compare our day 90 MGEO scRNA-seq data to human fetal GE expression, we used the Shi *et al.* dataset (Shi et al., 2021), which includes scRNA-seq data from MGE, LGE, and CGE human fetal tissue at GW 9, 12, 16, and 18. A PCA plot was used to determine how closely related the gene expression profile of our MGEO samples were to the GW9-19 human dataset's regional and cell type clusters, and to determine the GW age to which the MGEOs were most similar. A Pearson correlation was used to compare day 90 MGEO neuronal clusters 1-7 to human fetal MGE subclusters. To assess regional specificity and determine the extent to which MGEOs more closely recapitulate MGE-like expression markers, we compared the percentage of cells expressing key regional and interneuron gene markers between our MGEO scRNA-seq dataset, established subpallial organoid protocols (Birey et al., 2017; Xiang et al., 2017), and the Shi *et al*. human MGE cluster.

The number and percentage of cells expressing key regional and interneuron gene markers in each dataset was calculated and plotted using a custom R function. In brief, gene expression percentages were calculated across different Seurat objects, combined into a data frame, transformed using the melt() function, and visualized for comparison across datasets using ggplot2. To visualize the number of neurons expressing one or more interneuron subtype-specific markers, neuronal clusters (clusters 1-7) were extracted from the day 90 MGEO data set and the top five subtype specific gene markers (based on the percentage of neurons expressing each marker) were

selected for multi gene expression analysis. All valid gene combinations were identified using a custom R function and the number of neurons with single or multi gene expression profiles was plotted using ggplot2.

Viral labeling and generation of cortical-MGEO assembloids

To visualize migrating neurons in assembloids, cortical organoids (SOSR-COs) were labeled with codon diversified AAV1-CAG-tdTomato (Addgene # 59462), while interneuron progenitors and interneurons were labeled in MGEOs using AAV1-mDlx-GFP (Addgene # 83900) virus prior to fusion, as previously described(Sloan et al., 2018). Briefly, 46 DIV organoids were transferred into 1.5 mL Eppendorf tubes and incubated overnight (37°C, 5% CO2) in 250 µL of 3N with vitamin A organoid culture media containing diluted virus (1:50). Fresh 3N media with Vitamin A (750 µL) was added the next day. The following day, organoids were washed with PBS to remove residual virus, then transferred to ultra-low attachment plates with fresh culture media for maintenance until fusion into assembloids approximately one week later. To generate MGEO-cortical assembloids, SOSR-CO and MGEO regions with the brightest viral reporter expression were placed in contact with each other along the bottom edge of a 48- or 24-well plate. Plates were tilted at an angle to ensure the organoids maintained contact with each other and left undisturbed for at least 24 hours. At later stages, PV basket cells were labeled in assembloids with AAV1-BiPVe3-dTomato_nls-dTomato (Addgene # 213940) virus using the same methods as above.

2D assay of MGEO neuronal migration

To interrogate the migration of interneurons from 3D MGEOs onto 2D extra-cellular matrix, 21 DIV organoids were plated into individual wells of a 1:50 Geltrex-coated, thin-bottom, black-walled 96-well culture plate (PerkinElmer 6055300) containing 3N+A media. Organoids were gently moved to the center of each well using a pipette tip and allowed to settle to the bottom of the well. Automated live imaging of migration in phase or brightfield was performed using an Incucyte S3 Live Cell Analysis System or Andor BC43 benchtop spinning disc confocal microscope. Using the Incucyte, multiple 10x images were acquired per well at 15-min intervals over 48 h, starting immediately after plating. Andor confocal microscope images were collected at 5-10 min intervals over 15 h, beginning at least 2 h post plating. For both imaging methods,

cultures were maintained at 37°C and 5% CO2. Plates were fixed with 4% PFA at 48 h post-plating for immunostaining, which was performed as described above.

To block CXCR4, a receptor that regulates the migration of interneurons in the developing neocortex(Stumm et al., 2003; Y. Wang et al., 2011), the CXCR4 antagonist AMD3100 (100 nM) was added to organoid media(Birey et al., 2017a). For the "chronic" exposure condition, AMD3100 was added beginning 6 days prior to the migration assay (24 DIV), with a half media change containing fresh 100 nM drug performed every 2-3 d. For the "acute" groups, 100 nM of drug was added at the time of plating for the migration assay (30 DIV). Incucyte images were taken as described above and Fiji ImageJ was used to quantify the area of cell migration (onto ECM) between control, acute, and chronic conditions at 48-h post plating. The organoid area and spots of debris were excluded prior to quantification. Experiments were performed using 8 MGEOs per condition from 2 differentiations derived from the 79B hPSC line. Graphpad Prism was used to graph the migrated neuron area of each replicate organoid and for statistical analysis (see below).

Live imaging of assembloids, 3D migration, and quantification

To assess interneuron migration in a 3D environment, SOSR-COs and MGEOs were virally labeled and fused at 56 DIV as described above. Live imaging of GFP+, migrating cells was conducted using the Andor BC43 benchtop spinning disk confocal microscope. Migration in assembloids was imaged every 5 min for 15 h. Static confocal images of live assembloids were also collected at multiple timepoints between 24 h to 15 d post fusion to assess migration over time. mDLX-GFP labeled cells that migrated into the cortical organoid area were quantified in Fiji as the percent of GFP area in the CAG-TdTom area and plotted using Graphpad Prism.

Complementing our 2D neuronal migration experiments above, we exposed 79B- derived assembloids to the CXCR4 antagonist AMD3100 (or no drug control) 1 day post MGEO-CO fusion. We imaged and quantified the area of mDLX-GFP MGEO interneurons that migrated into CO organoid 24 h later, as described above.

Multi-electrode array (MEA) recordings

Assembloids (at 20-34 wk differentiation) were plated individually in each well of a 6-well cytoview MEA plate (Axion Biosystems, Atlanta, GA, USA) coated with ploy-L- ornithine (PLO)

(100 µg/mL) and Geltrex (1:100). As opposed to the conventional method of organoid MEA recording, wherein organoids grow chronically on the MEA plate, which alters their 3D cytoarchitecture over time, we transferred each organoid to the MEA plate immediately before recording and carefully removed the majority of the media after positioning the organoid on top of the electrodes. This method takes advantage of the adhesion properties of liquid, allowing the organoid to firmly contact the electrodes as the media is removed. After a 5-min recording, media was added back into the MEA plate, and the organoid was gently removed from the MEA plate and maintained in suspension culture. The reproducibility of MEA recordings was verified by removing, replating, and then re-recording from the same organoid several times over a short time window and across multiple MEA wells to ensure consistency of signal (data not shown).

All recordings were performed using a Maestro MEA system and AxIS Software in Spontaneous Neural Configuration (Axion Biosystems). MEA signals were sampled at 12.5 kHz and bandpass filtered at 200-3000 Hz with Butterworth filtering to detect APs. APs were detected using a threshold of 5.5 times the standard deviation of the noise. Single electrode bursts were detected as a minimum of five APs occurring with a maximum interval of 100 ms. Network bursts were detected as a minimum of 50 APs with 100 ms maximum inter-AP interval observed on a minimum of 25% of active electrodes. Mean firing rate estimation was determined within a 10 s window and synchrony parameters were detected using a window size of 20 ms.

Patch-clamp recording of organoid slices

Procedures for cutting organoid slices were similar to those used for acute mouse brain slices. The slicing solution contained (in mM): 110 sucrose; 62.5 NaCl; 2.5 KCl; 7.5 $MgCl_2$; 1.25 $KH2PO_4$; 26 $NaHCO_3$; 0.5 $CaCl_2$ and 20 D-glucose (pH 7.35-7.4 when saturated with 95% O2 /5% CO2 at room temperature of 22-25° C). To prepare fresh organoid slices, one assembloid (1-2 mm) was manually cut into 4-6 slices (~300 µm) in ice-cold, oxygenated "slicing" solution saturated with 95% O_2 /5% CO_2. Slices were incubated in slicing solution for 15-20 min at RT and then in a mixture (1:1) of slicing solution and artificial cerebrospinal fluid (ACSF), the latter containing (in mM): 125 NaCl; 2.5 KCl; 1 $MgCl_2$; 1.25 $KH2PO_4$; 26 $NaHCO_3$; 2 $CaCl_2$ and 20 D-glucose, (pH 7.35-7.4), in a holding chamber aerated continuously with 95% O_2 /5% CO_2 at 35° C for 30 min before transfer to ACSF at RT.

Procedures for electrophysiological recordings in assembloid slices were similar to those used previously for acute mouse brain slices or for cultured iPSC-derived neurons (Lopez-Santiago et al., 2017; Tidball et al., 2020; Yuan et al., 2019, 2024). An assembloid slice was transferred to a recording chamber where it was perfused (2-3 ml/min) with ACSF bubbled continuously with 95% O_2 /5% CO_2. The mDLX-GFP-labeled interneurons and CAG-tdTom labeled pyramidal cells were visually selected using a NIKON E600FN upright microscope equipped with Nomarski optics (x 40 water immersion objective). For recording of AP firing, recording electrodes had resistances of 4-7 MΩ when filled with a potassium gluconate (K-gluconate)-based pipette solution consisting of (in mM): 140, K-gluconate; 4, NaCl; 0.5, $CaCl_2$; 10, HEPES; 5, EGTA, 5 phophocreatine; 2, Mg-ATP and 0.4, GTP (pH 7.2-7.3 adjusted with KOH). Repetitive firing and AP frequencies from individual neurons were examined using the whole cell current-clamp recording technique. Repetitive AP firing was evoked by injection of a series of 1500 ms depolarizing currents varying from -60 pA to 200 pA at 10 pA-step from resting membrane potentials. Spontaneous AP firing was recorded in the gap-free model from resting membrane potentials. The pipette solution for spontaneous inhibitory synaptic current (sIPSC) recordings consisted of (in mM): 140, CsCl; 4, NaCl; 0.5, CaCl2; 10, HEPES; 5, EGTA, 5 phosphocreatine; 2, Mg-ATP and 0.4, GTP (pH 7.3 adjusted with CsOH). Signals were amplified with a Multiclamp 700B amplifier (Molecular Devices, Sunnyvale, CA), filtered at 2-4 kHz and digitized at 20 kHz for off-line analysis. Data were acquired with a Digidata 1440A interface and analyzed using pClamp11 offline. All experiments were carried out at RT (22-25^{o}C).

Statistics

GraphPad Prism 10.2.2 was used for all statistical analyses. In Figures 1 and 3, RT-qPCR data are presented as mean ± SEM, with each dot representing a single experimental replicate sample, which is composed of data from 4-8 pooled organoids. Migration data is graphed as mean ± SD with each dot being a datapoint from a single organoid. One-way ANOVA with Tukey multiple comparisons correction analysis was used to determine the statistical significance in migrated neuron area between control, acute, and chronic AMD3100 treatments 48 h post plating for 2D migration assays. Student T-test statistical comparison was used to compare the effects of control vs AMD3100 treatment on the area of mDLX-GFP MGEO interneuron migration into the CO organoid area of MGEO-CO fusion 48 h post-fusion. Experimental conditions were blinded

during analysis. In all graphs, dot shapes denote the hPSC lines from which organoids were derived (circle for 79B, triangle for 2E, diamond for H9). For comparisons of MEA firing patterns (Figure 7), cumulative distribution of maximum firing rates and burst counts were compared via two-tailed Kolmogorov-Smirnov test. Firing rate per burst before and after bicuculline exposure was compared using two-tailed Mann-Whitney test.

2.4 Results

Timing and concentration of patterning molecules influence MGE specificity of subpallial organoids

Regional specification of the MGE is mediated by precisely controlled spatiotemporal signals, including gradients of Wingless-related Integration Site (WNT) and Sonic Hedgehog (SHH), during forebrain development (**Figure 2.1A**) (Avilés et al., 2013; Stoeckli, 2009). In addition to the notochord, SHH is also expressed at high levels in the preoptic area (POA) and floor plate, while its expression is present to a lesser extent in the MGE (Flandin et al., 2011; Kohtz et al., 1998; Liem et al., 2000). Conversely, WNT expression is highest in the cortex with a graduated decrease in expression in ventral telencephalic regions (Avilés et al., 2013; Stoeckli, 2009). Established protocols for generating ventral telencephalic (subpallial) organoids rely on SHH pathway agonists and WNT pathway antagonists to guide organoids towards a ventral brain region identity (Bagley et al., 2017; Sloan et al., 2018; Xiang et al., 2017).

Recently, the Parent lab developed a method for generating dorsal forebrain patterned self-organizing single-rosette cortical organoids, termed SOSR-COs (Tidball et al., 2023). Given the robust cell-type specificity, reproducibility, and improved structural organization of the single-rosette organoids for modeling early neurodevelopmental disorders (Niu et al., 2024; Takla et al., 2023; Tidball et al., 2023), we used this approach as a foundation for developing self-organizing single rosette MGEOs, with the aim of achieving MGE regional specificity with a high yield of PV+ cortical interneurons. Unlike multi-rosette protocols that begin with aggregation of hPSCs into embryoid bodies, the MGEO protocol starts from modeling the formation of the neural plate by first culturing a 2D monolayer of hPSCs and exposing them to dual SMAD inhibition. The monolayer is then cut into evenly sized squares and plated onto thick extracellular matrix (100% Geltrex), allowing each piece to self-organize into a single rosette structure which is subsequently removed from the matrix and grown in suspension (Tidball et al., 2023).

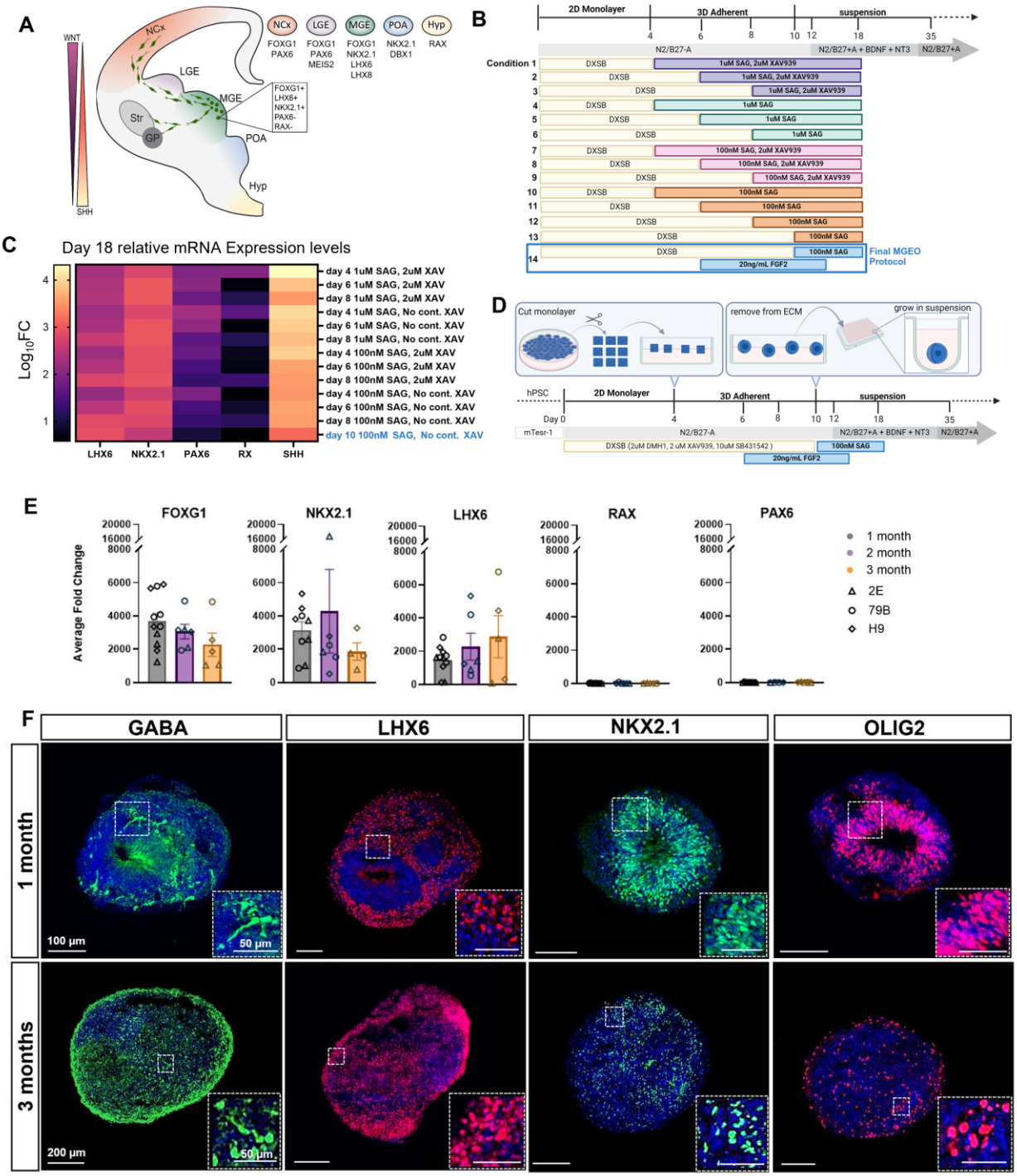

Figure 2.1: Generation of human subpallial brain organoids with MGE regional specificity.

(**A**) Schematic of MGE-derived interneuron tangential migration, key markers differentiating MGE from nearby regions, and the distribution of SHH and WNT patterning molecules. (**B**) Protocol variations tested for generating organoids with MGE specificity. DXSB condition: 2uM DMH1, 2uM XAV939, 10uM SB431542. (**C**) Heat map of relative mRNA levels measured by qRT-PCR in 18 DIV organoids exposed to various timings and concentrations of SAG with or

without continued (cont.) XAV939 after DXSB. n=1-2 differentiations/condition of 2E iPSCs. Graphed as $Log_{10}FC$ relative to GAPDH and iPSC baseline. Blue text indicates the optimal conditions (high *LHX6*, low *PAX6* and *RX*). (**D**) Final MGEO protocol. Boxes in blue above the timeline illustrate the key steps at days 4 (monolayer cutting) and 10 (transition from 3D adherent to suspension culture). (**E**) Relative mRNA expression of 1-, 2- and 3-month MGEOs for key markers. n≥5 differentiations. Graphed as average ΔΔCT fold change ± SEM, normalized to GAPDH and relative to average iPSC baseline. Shapes denote hPSC line and colors indicate age (triangle: 2E, circle: 79B, diamond: H9; gray: 1 month, purple: 2 month, orange: 3 month). (**F**) MGEO immunostaining at 1-month (top) and 3-months (bottom) shows strong expression of GABA (green), LHX6 (red), NKX2-1 (green), and Olig2 (red). Bisbenzimide nuclear stain (DNA) in blue. Higher magnification views shown in insets. Abbreviations: NCx: Neocortex; LGE: Lateral Ganglionic Eminence; Str: Striatum; GP: Globus pallidus; MGE: medial ganglionic eminence; POA: preoptic area; Hyp: Hypothalamus; ECM: extracellular matrix.

To achieve MGE specificity of our model, we systematically altered the timing of dual SMAD inhibition, as well as the timing and concentrations of SAG and XAV939 (**Figure 2.1B**). As a readout, we quantified expression of region-specific mRNAs at 18 DIV using RT-qPCR (**Figure 2.1C**) and found that *PAX6*, a dorsal telencephalic marker with some expression in LGE and CGE, but not MGE (Mo & Zecevic, 2008), was more highly expressed in conditions with earlier SAG exposure. In contrast, *LHX6* expression was higher with later SAG exposure. Conditions with higher SAG concentrations resulted in higher levels of *SHH* mRNA expression, suggesting subpallial organoids with a regional identity associated with deeper ventral telencephalic regions including the preoptic area (POA) and hypothalamus (Avilés et al., 2013). In contrast, *NKX2.1* was expressed at relatively similar levels across all conditions, demonstrating that *NKX2.1* expression alone cannot be used as a sole marker to establish MGE identity. A combination of 100 nM SAG exposure from 10-18 DIV, brief XAV939 exposure during SMAD inhibition, and FGF2 treatment from 6-12 DIV showed the greatest MGE-like specificity as defined by high *LHX6* expression, moderate *NKX2.1* expression, and negligible levels of *PAX6* and *RAX* expression (**Figure 2.1C,** bottom row). We therefore selected this specific patterning protocol for generating MGEOs for the rest of this study (**Figure 2.1D**).

MGEOs display high MGE regional specificity

To ensure the robustness of our protocol across different cell lines, we conducted our experiments using human foreskin fibroblast- and blood-derived iPSC lines, denoted as 2E and 79B, respectively, as well as a human embryonic stem cell (hESC) line (H9). Continuing WNT

inhibition until 10 DIV followed by SHH pathway activation from days 10 to 18 consistently produced MGEOs with robust expression of key forebrain-specific (*FOXG1*), ganglionic eminence progenitor (*NKX2.1*), and MGE-specific (*LHX6*) markers for all the hPSC lines, as measured by RT-qPCR at one, two, and three months (**Figure 2.1 E, F**) (Du et al., 2008; Nóbrega-Pereira et al., 2010). LHX6 mRNA and protein remained highly expressed in MGEOs from 1 to 3 months **(Figure 2.1 E, F)**. Immunostaining of MGEOs at 1 and 3 months also showed the expected expression patterns for GABA, and OLIG2 (**Figure 2.1 F**). Negligible mRNA expression levels of the hypothalamic marker RAX and the dorsal telencephalic marker *PAX6* were observed **(Figure 2.1 E)**, with no protein detectable via immunostaining at 1 month (**Figure 2.2 A-C**) and only miniscule amounts in glial clusters of our scRNA-seq analyses **(Figures 2.3 C, F**).

To further validate the MGE specificity of our organoids, colocalized expression of OLIG2 and NKX2.1 was quantified through immunofluorescence analysis. In early developmental timepoints of the human brain (GW 8-12), OLIG2 is almost exclusively co-expressed with NKX2.1 in the MGE but not in surrounding brain regions including the LGE, CGE, hypothalamus, and POA (Alzu'bi et al., 2017; Maroof et al., 2013). At mid to late gestational weeks (GW 24+), NKX2.1 and OLIG2 segregate in their expression patterns and do not co-express in mature MGE-derived cells. Our analysis of 1-month MGEOs shows a 98.5% colocalization of OLIG2+ cells with NKX2.1 (**Figure 2.2 D, E**). In 3-month MGEOs, in contrast, most OLIG2+ cells did not colocalize with NKX2.1 (**Figure 2.2 D, E**). These results further support the MGE specificity of our model.

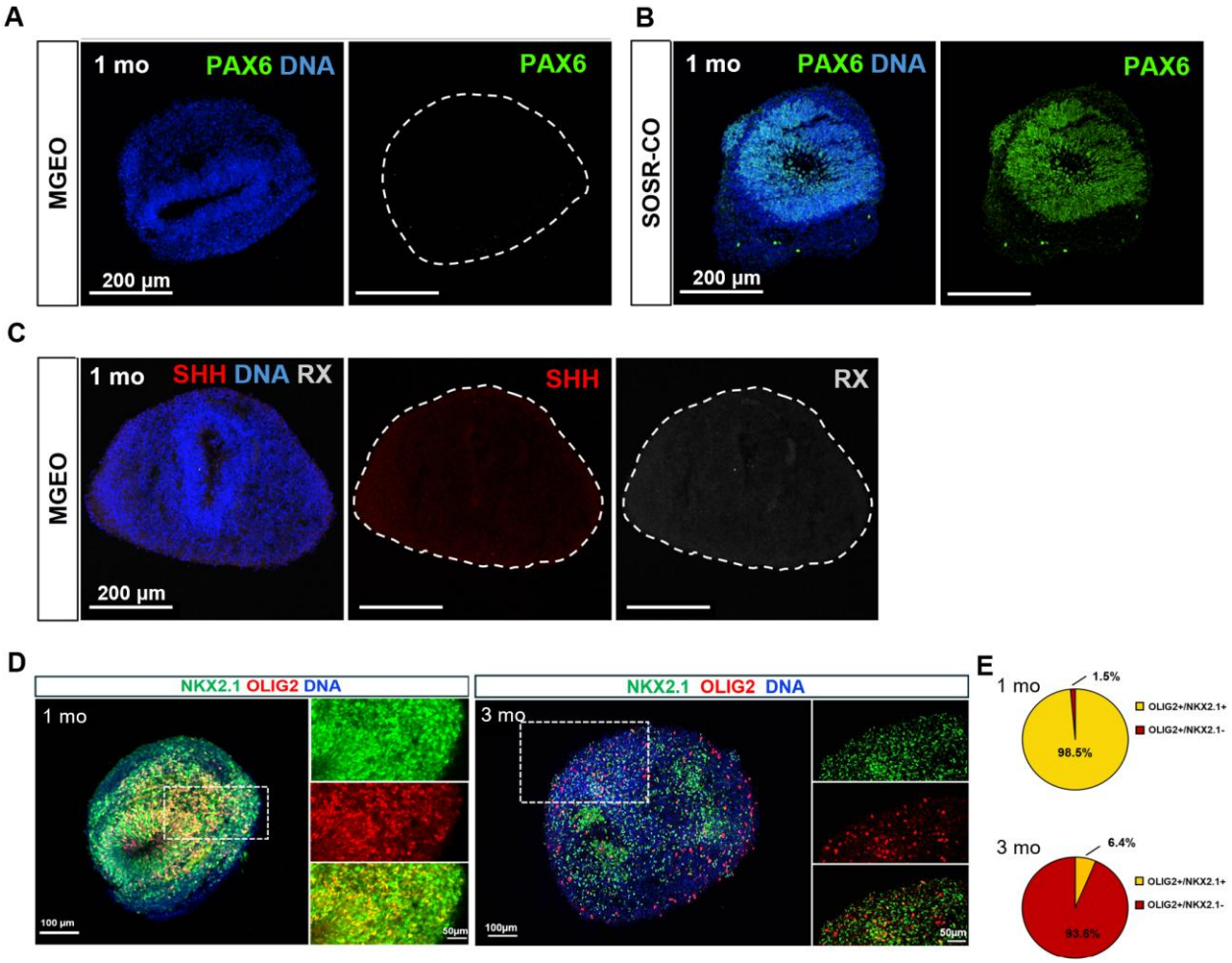

Figure 2.2 MGE regional specificity of MGEOs

((**A, B**) Immunostaining of PAX6 in 1-month (mo) MGEOs (**A**) and SOSR-COs (**B**). (**C**) 1-month MGEOs immunostained with SHH and RAX. (**D**) Immunostaining for NKX2.1 (green) and OLIG2 (red) at 1 month (left) and 3 months (right) shows co-expression at early timepoint, but not the latter. Boxed region indicates areas of magnification displayed on the right of each image. Bisbenzimide nuclear stain (DNA) is in blue for images in **A-D**. (**E**) Pie charts showing the percent of OLIG2 area that co-localizes with NKX2-1 (yellow) vs does not co-localize (red) in 1- and 3-month MGEOs.

Newborn cortical interneurons express ERBB4, which is required for their tangential migration (Rakić et al., 2015). Migratory MGE cortical interneurons are distinguished from other GABAergic lineages by the co-expression of *LHX6*, *MAF*, and *MAFB*, alongside downregulated *NKX2.1* and *LHX8*. In contrast, subpallial lineages (GABAergic and cholinergic neurons) maintain the expression of *LHX8* and *NKX2.1* and do not express *MAF* genes(Shi et al., 2021a; Z. Zhao et al., 2022). We next performed single-cell RNA-sequencing (scRNA-seq) analysis of 1-month MGEOs to assess their regional identity and cell type composition. Uniform Manifold

Approximation and Projections (UMAP) plots revealed five distinct cell clusters annotated as radial glia (*VIM, NES, HES1*), inhibitory neuron progenitors (*ASCL1, HES6, DLX2*), and populations of GABAergic neurons that resemble tangentially migrating somatostatin (*SST*)+ cortical interneurons (*SST, LHX6, CXCR4, ERBB4, ZEB2, PLS3, ARX, MAF*), PV neuron precursors (*MAFB, MEF2C, ETV1, ST18, CRABP1*), and MGE subpallial destined neurons (*LHX8, GBX2*) (Keefe et al., 2023; Shi et al., 2021a; Y. Yu et al., 2021; Z. Zhao et al., 2022) (**Figure 2.2A**). Importantly, the percent distribution of each of these cell types in MGEOs was consistent within each sample replicate and between hPSC lines (**Figure 2.2B**). We confirmed the presence of cells in MGEOs expressing the MGE-specific marker LHX6, as well as the absence of cells expressing off target markers that would indicate non-MGE identities, including CGE (*SP8, COUPTF2(NR2F2)*), LGE (*EBF1, ZFHX3*), hypothalamus (*NKX2-2, RAX*), POA (*HMX3, DBH*) and dorsal telencephalon (*PAX6*) (**Figure 2.2C, D**). Together these data strongly support the MGE specificity of MGEOs.

MGEOs produce human MGE-derived cell types

The MGE primarily generates SST and PV GABAergic neuron subtypes, although there is evidence that to a lesser extent it generates neurons that express calretinin (*CALB2*), TH, and CHAT (Flandin et al., 2010; Fragkouli et al., 2009; Nóbrega-Pereira et al., 2010; Xu et al., 2008). The MGE also gives rise to astrocytes and oligodendrocytes (Kessaris et al., 2006; Minocha et al., 2015). To further characterize the cell types produced in MGEOs, we conducted scRNAseq analysis for MGEOs at 3 months, RT-qPCR at 1-3 months, and immunostaining from 3-8 months. scRNA-seq data analysis of 3-month MGEOs generated from the three hPSC lines revealed distinct MGE-like cell lineages including: cortical PV precursors with or without CRAPBP1, SST+ cortical-destined cells, and MGE subpallial/striatal/globus pallidus-destined cells with or without LHX8 expression (**Figure 2.3D**). We also identified astrocytes/pre-astrocytes and pre-oligodendrocyte precursor cells (pre-OPCs)/OPCs in the MGEOs. While there was some variation in the cellular composition between experimental replicates and MGEOs generated from different hPSC lines (**Figure 2.3D**), the average percentages of GABAergic precursors/neurons, pre-astrocytes/astrocytes, pre-OPCs/OPCs, and dividing cells were highly consistent between cell lines and replicates (**Figure 2.3E**).

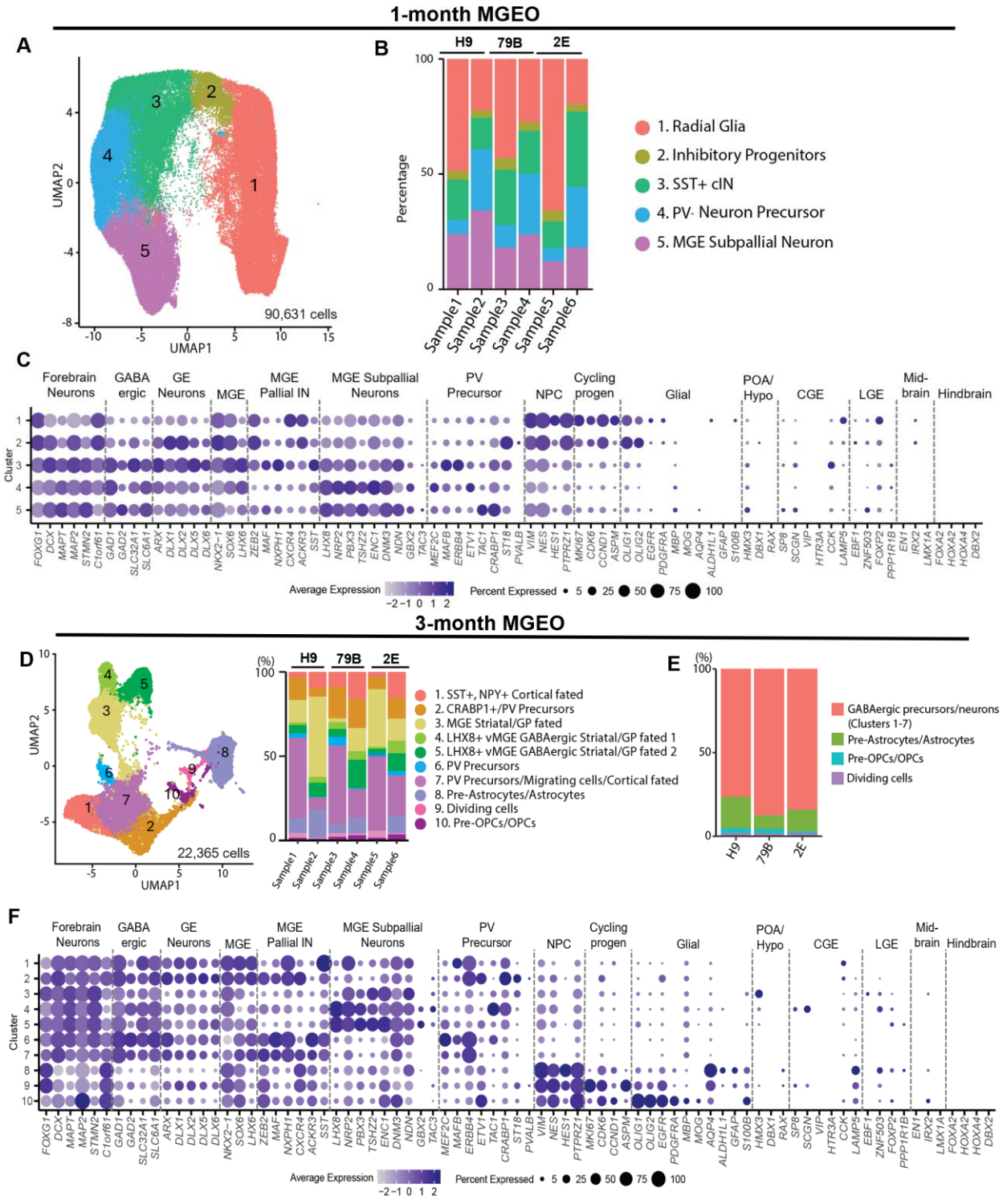

Figure 2.3: Single-Cell RNA sequencing of 1-month and 3-month MGEOs

(**A**) UMAP plot of 1-month-old MGEOs with color coded and numbered clusters. n= 90,631 total cells from 6 samples (2 experimental replicates per hPSC line, 6-8 organoids pooled per sample). (**B**) Left: Stacked bar graphs denoting the cluster percent composition for each individual sample included in the UMAP in panel A. Right: Cluster name and color key. (**C**) Dot plot showing

expression of markers of interest by cell cluster. Circle size denotes percent of cells within clusters expressing the gene of interest. Dot color indicates average expression level relative to other clusters. Dots were included for genes that contained > 1 percent of cells in a cluster. All cells with >0 expression levels were included. (**D**) UMAP plot shows 10 clusters from six 3-month-old MGEO samples, 2 differentiations/cell line, with clusters color-coded and numbered. Middle: bar graphs denote percentages of cells within each sample corresponding to clusters on the UMAP. Cells from 4-6 pooled organoids/sample from H9 (samples 1 & 2), 79B (samples 3 & 4), and 2E (samples 5 & 6) hPSC lines. Right: Cluster identities by number and color. (**E**) Average percentage of cells in each cluster by cell line. (**F**) Dot plots showing expression of markers of interest by 3-month MGEO cluster. Key and analysis as in C. Abbreviations: GE: Ganglionic Eminences; MGE: Medial Ganglionic Eminence; IN: Interneurons; POA: Preoptic area; CGE: Caudal Ganglionic Eminence; LGE: Lateral Ganglionic Eminence; NPC: Neural Progenitor Cell; Cycling Projen: Cycling Progenitors.

As expected, there was negligible expression of the CGE lineage VIP or CCK GABAergic neuron subtypes in 3-month MGEOs (**Figure 2.4 A, C**). Expression of NPY in 3-month MGEOs was limited to SST+/NPY+ cortical-destined neurons (**Figures 2.4 A**). CALB2+ cells that co-expressed NKX2.1 were found in the striatal/GP-destined clusters, and those that co-expressed LHX6 appeared in cortical-destined clusters (data not shown). Neither of these populations substantially expressed the CGE markers SP8 or NR2F2 (COUPTFII) (**Figures 2.4 B**), supporting non-CGE origins. Minimal expression of other off-target region-specific markers, such as POA/hypothalamus, midbrain and hindbrain, was observed **(Figure 2.3 C, F**). To confirm selected scRNA-seq findings, we next performed RT-qPCR for specific transcripts. Analysis of MGEOs revealed that the GABAergic neuronal markers VGAT and SST were expressed in MGEOs generated from all three hPSC lines at one, two, and three months (**Figure 2.5A**).

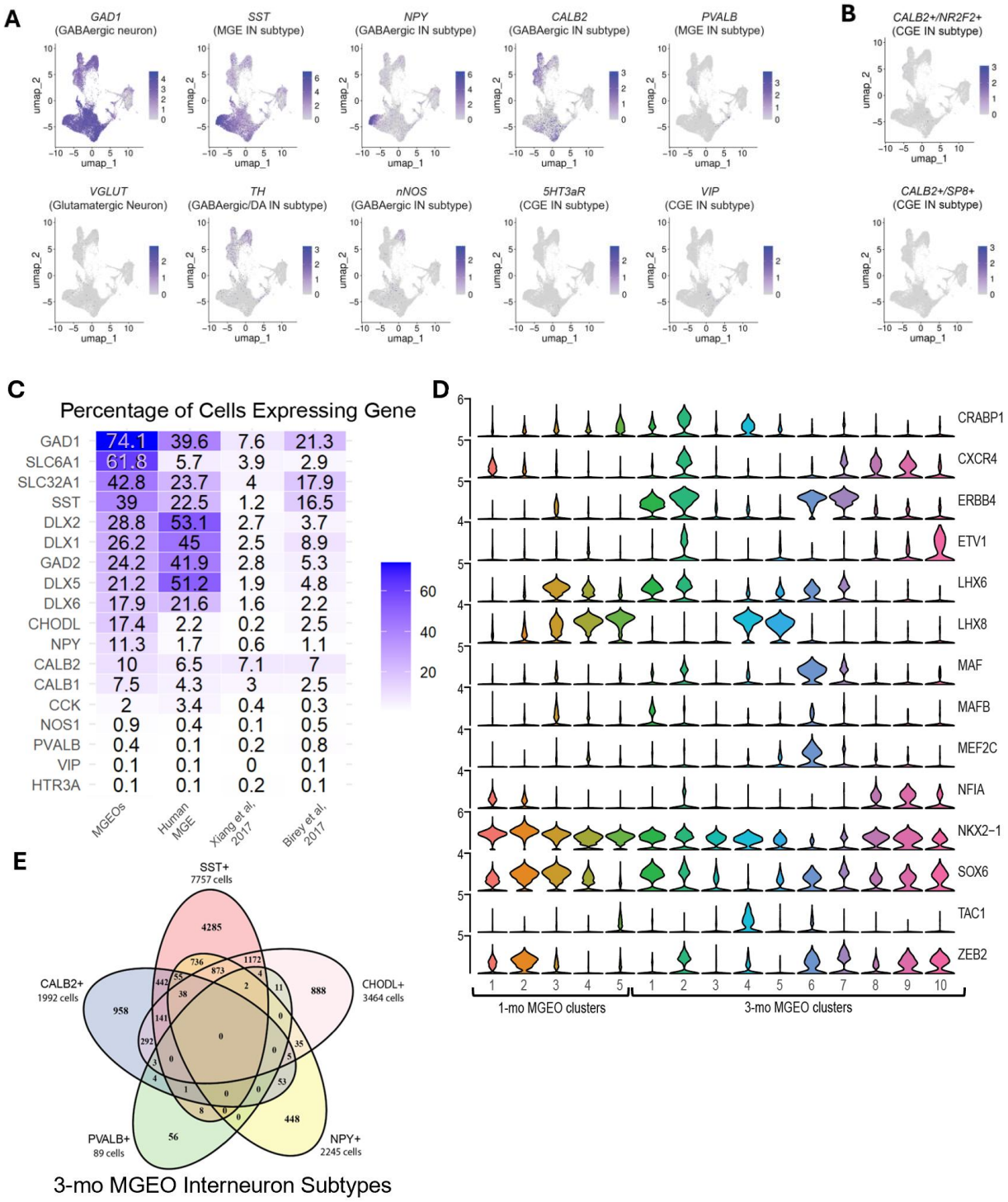

Figure 2.4: MGEO interneuron subtypes

(**A**) UMAP feature plots showing expression of key GABAergic interneuron markers and lack of Glutamatergic and CGE cell types in 3-month MGEOs. (**B**) UMAP feature plots show minimal or no CALB2+ cells that co-express known CGE markers NR2F2 (top) or SP8 (bottom). (**C**) Heat map comparing the average percentage of cells expressing key GABAergic cell markers across scRNA-seq datasets from 3-month MGEOs, human fetal MGE (Shi et al., 2021; gestational weeks

9–18), and other subpallial organoids at similar timepoints (Xiang et al., 2017; Birey et al., 2017). (**D**) Stacked violin plots of MGE lineage markers grouped by MGEO age and cluster. (**E**) Venn diagram of scRNA-seq transcript co-expression between interneuron subtypes in 3-month MGEOs

Expression of SLC12A5 (KCC2) relative to SLC32A2 (NKCC1) progressively increased from one month to three months, consistent with neuronal maturation. As expected, *LHX8* expression was highly upregulated in MGEOs at 1 month and decreased thereafter. While calretinin (CR; CALB2)-expressing interneurons primarily originate from the CGE, a subpopulation is known to arise from the dorsal MGE (Butt et al., 2005; Fogarty et al., 2007; Xu, Cobos, De, et al., 2004; Xu et al., 2008). We identified populations of CR and SST expressing neurons, both of which also expressed *LHX6*, indicating that both populations were derived from an MGE-like lineage (**Figure 2.5 B, C**). Immunostaining of MGEOs at 3 months also revealed expression of GFAP in putative astrocytes, and sparse oligodendrocytes expressing both myelin basic protein (MBP) and OLIG2 (**Figure 2.5 D**).

MGEOs at 1 and 3 months exhibited robust expression of MEF2C (**Figure 2.5 A, G, H)**, an early marker of PV-fated cortical interneurons (Allaway et al., 2021; Pai et al., 2020). Immunostaining of 3-month MGEOs further revealed a small number of PV-immunoreactive cells (2.2% ± 0.63 of DAPI area, **Figure 2.5 E, F**). At 4 months, however, PV immunolabeling robustly increased (32.8% ±7.52) and was maintained at 6 (31.3% ± 7.06) and 8 months (32.5% ± 5.75) (**Figure 2.5 E, F**). PV fast-spiking cortical interneurons express K_v3 family potassium channels, predominantly $K_v3.1$ and $K_v3.2$ (Kaczmarek & Zhang, 2017). Although mRNA expression of *KCNC1*, which encodes $K_v3.1$, was already present in 1-month MGEOs (**Figure 2.5 A**), there was minimal $K_v3.1$ immunolabeling in 3-month MGEOs **(Figure 2.5 H**), similar to PV immunoreactivity at this time point. However, $K_v3.1$ immunolabeling increased markedly in 8-month MGEOs and was seen predominantly in MEF2C+ cells (**Figure 2.5 H**).

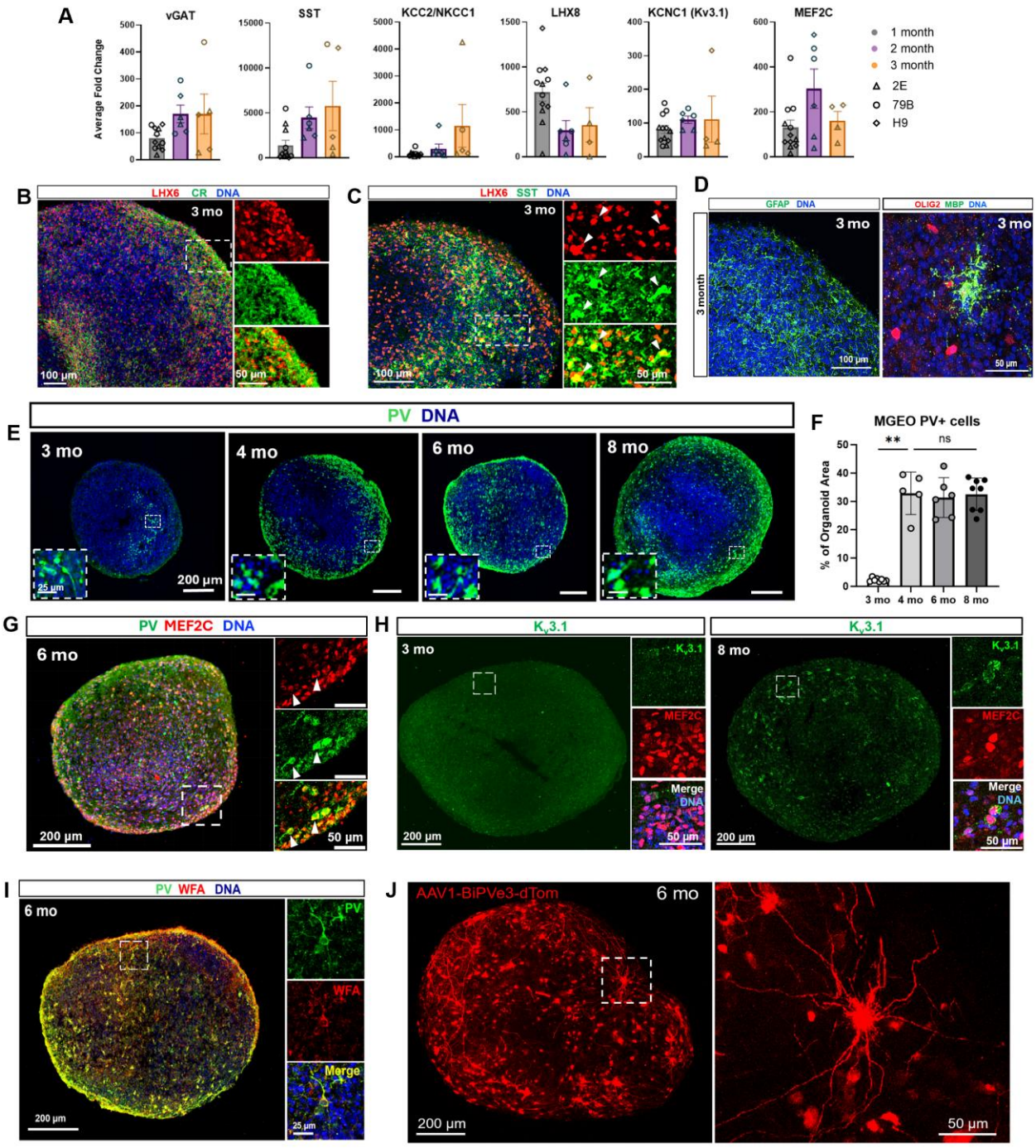

Figure 2.5: MGEOs generate human MGE-derived cell-types

(**A**) RT-qPCR of 1-, 2- and 3-month MGEOs shows expression of GABAergic, chloride transporter, potassium channel, and MGE transcripts. n≥5 differentiations between 3 cell lines, graphed as average fold change (ΔΔCT) ± SEM, normalization to GAPDH and relative to average iPSC baseline. Shapes denote cell line and color indicates time point (triangle: 2E, circle: 79B, diamond: H9; gray: 1-month, purple: 2-month, orange: 3-month). (**B-D**) Representative confocal images of cell type-specific marker immunolabeling in 3-month (mo) MGEOs. Dashed boxes in B and C are shown in higher magnification on the right. DNA is bisbenzimide nuclear stain. (**E**)

Representative confocal images of parvalbumin (PV, green) immunostaining at 3, 4, 6 and 8 months shows robust PV expression in MGEOs from 4 months onwards. Dashed boxes shown at higher magnification in lower left insets. (**F**) PV expression as percentage (%) of organoid area ± SD. n=5-8 organoids per timepoint and 2-3 differentiations/line. One way ANOVA with Dunnett's T3 multiple comparisons post hoc test. **, P= 0.0036. ns, non-significant. (**G**) Immunostaining of 6-month organoids shows colocalization of PV (green) and MEF2C (red). Dashed box enlarged at right. (**H**) Immunostaining of 3-month (left) and 8-month (right) MGEOs shows voltage-gated potassium channel $K_v3.1$ (green) co-expression with MEF2C+ (red) at 8 months. Dashed boxes shown at higher magnification on the right. (**I**) Confocal images of immunostaining shows PV (green) co-expressed with the perineuronal net marker WFA (red) in 6-month MGEOs. Dashed boxed area shown in higher magnification on the right. (**J**) Confocal imaging of PV basket cell-specific AAV1-BiPVe3-dTom virus expression in live-imaged 6-month MGEOs reveals complex morphologies of putative PV basket cells.

In 6-month MGEOs, we observed PV-immunoreactive cells co-expressing Wisteria floribunda agglutinin (WFA), a marker for perineuronal nets that surround fast-spiking interneurons (**Figure 2.5 I**) (Favuzzi et al., 2017; Härtig et al., 1992). Viral labeling using an AAV1 PV basket cell-specific enhancer-driven tdTomato virus (AAV1-BiPVe3-dTom) (Furlanis et al., 2025a) confirmed the presence of putative PV basket cells with complex morphologies in 6-month MGEOs (**Figure 2.5 J**). Together, these data indicate that MGEOs robustly produce PV+ cortical interneurons within 4 months in culture that exhibit molecular and structural features consistent with fast-spiking activity.

MGEO transcriptome closely resembles that of the developing human MGE

To assess the fidelity of the MGEO model in recapitulating the transcriptomic features of the developing human MGE, we compared the scRNAseq data of 3-month MGEOs to a human fetal GE scRNA-seq dataset published by Shi and colleagues (Shi et al., 2021a). The human fetal GE dataset was visualized by UMAP plot using cell cluster annotations originally assigned in the dataset and then integrated with our MGEO dataset, and the relationships analyzed using UMAP and PCA plots (**Figure 2.6A-D**). The analysis shows a close overlap of MGEOs with the human fetal MGE cluster, suggesting that the transcriptome of the organoids closely mirrors that of the human fetal MGE. We next conducted Pearson correlation analysis to compare the neuronal clusters in the MGEOs with the human MGE cell lineage clusters from the human fetal GE dataset. A high degree of similarity between the corresponding neuronal subtypes in both datasets was revealed (**Figure 2.6E**), reinforcing the fidelity of the MGEO model to the human MGE.

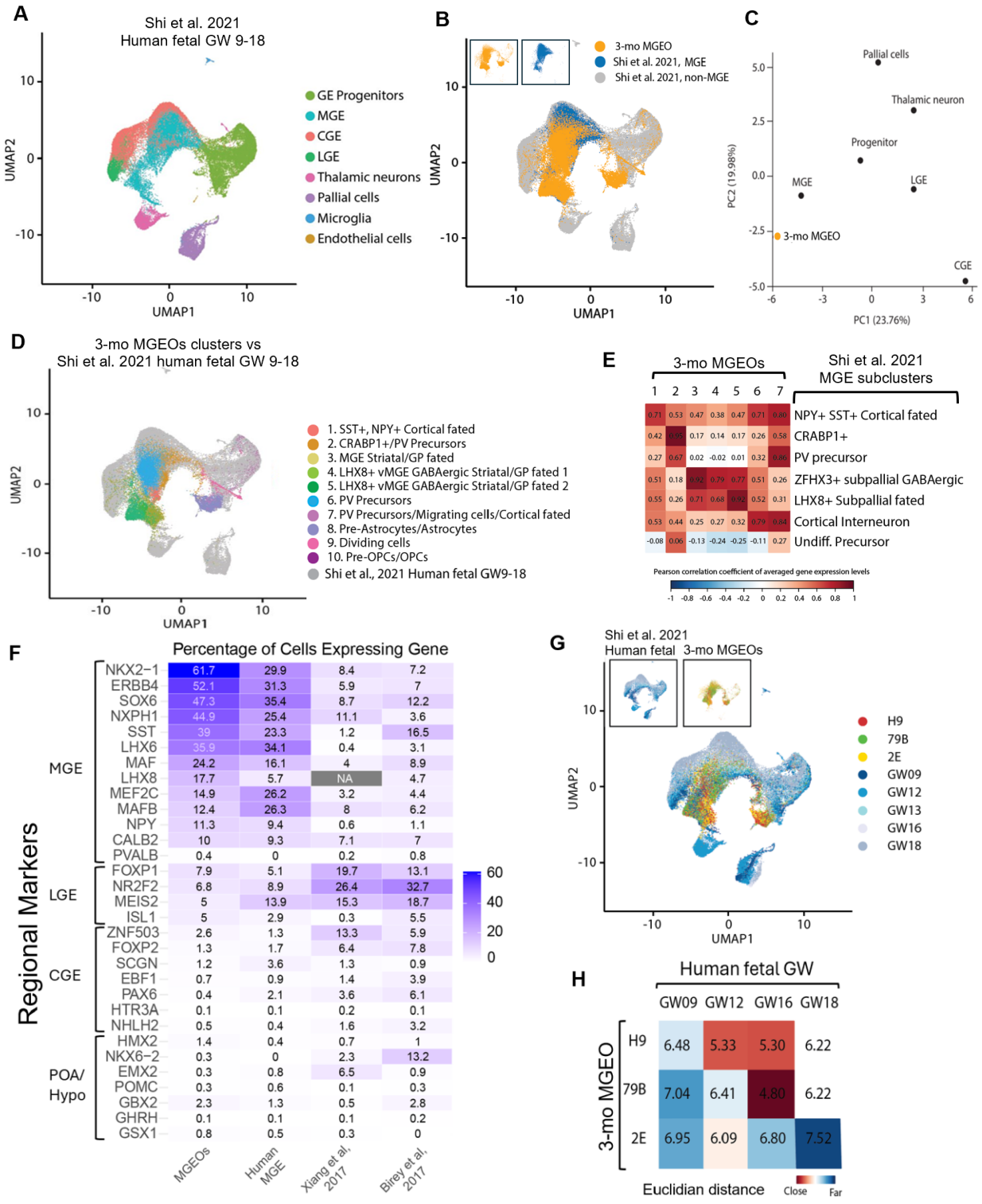

Figure 2.6: Comparison of MGEO and developing human subpallium transcriptomes

(A) UMAP plot of human GW9-18 scRNA-seq data from Shi et al., 2021, with color-coded regional and cell type clustering. (**B**) Integrated UMAP plot of scRNAseq data from 3-month MGEOs (orange) compared with data from panel (A). Human fetal MGE cluster: Blue; non-MGE

clusters: grey. Insets show the MGEO and human MGE clusters individually. (**C**) Principal component analysis (PCA) of 3-month MGEO scRNA-seq data (orange dot) versus human fetal data from (A) shows that MGEOs map closest to the human MGE cluster. (**D**) UMAP showing 3-month MGEO cell type clusters integrated with human GW9-18 fetal GEs (Shi et al., 2021; in gray). MGEO cell clustering and colors as in Figure 2D. (**E**) Heat map of Pearson correlation coefficients comparing 3-month MGEO clusters 1-7 (columns, numbered as in panel D) with Shi et al. 2021 human fetal MGE subclusters (rows). (**F**) Heat map comparing the average percentage of cells expressing selected gene markers for MGE, LGE, CGE, and preoptic area/hypothalamus (POA/Hypo) across scRNA-seq datasets from 3-month MGEOs, human fetal MGE (Shi et al., 2021; gestational weeks 9–18), and other subpallial organoids of similar timepoints (Xiang et al., 2017; Birey et al., 2017). (**G**) Integrated UMAP of 3-month MGEO and human fetal GE scRNA-seq data, as shown in panels B and D. Developmental age clusters from Shi et al. are depicted in shades of blue, while 3-month MGEO cells are colored by cell line (red: H9; green: 79B; yellow: 2E). Insets display human fetal cells (left) and MGEO cells (right) separately. (**H**) Heatmap of PCA Euclidean distances comparing each 3-month MGEO cell line to human fetal gestational developmental ages (GW 9, 12, 16, and 18) shows 3-month MGEOs are, on average, closest to human developmental GW12-16.

We then compared gene expression between the MGEOs, human MGE, and two published subpallial organoid models (Birey et al., 2017; Shi et al., 2021; Xiang et al., 2017) by analyzing the percentage of cells expressing genes specific to various regions of the developing subpallium (**Figure 2.6F**). The results demonstrated that MGEOs exhibit strong expression of MGE-specific markers, with minimal off-target expression of genes associated with other brain regions including LGE, CGE, POA, and hypothalamus. In contrast, other subpallial organoids (Birey et al., 2017; Xiang et al., 2017) showed a broader distribution of gene expression, with regionally mixed expression patterns and limited MGE specificity. Furthermore, we found that the MGEOs produced much larger percentages of GABAergic neurons and MGE-specific GABAergic neuron subtypes (**Figure 2.4 C, 2.6 F**). Several cell populations in 3-month MGEOs expressed markers of cortical PV precursors, including *LHX6, MEF2C, MAFB, ERBB4, ETV1*, or markers of subpallial destined PV precursors, with co-expression of LHX8, TAC1, and CRABP1(**Figure 2.4 D**). Detailed analyses of gene expression patterns of GABAergic neuron subtypes in the MGEOs further revealed that many cells co-expressed *SST*, including *SST+/CHODL+*, *SST+/CALB2+*, and *SST+/NPY+* combinations, known *SST* subtypes generated in the MGE (Munguba et al., 2023; Wu et al., 2023). Notably, *SST, CHODL, CALB2*, and *NPY* were largely not co-expressed in PV+ (*PVALB*) cells, consistent with prior studies showing that PV^+ and SST^+ interneurons, though both derived from the MGE, represent virtually non-overlapping cell populations (Zhang et al., 2025) (**Figure 2.4 E)**. Together these results suggest that MGEOs produce cell types that are

predominantly specific to an *in vivo* MGE regional identity. Integration of MGEO data from multiple cell lines with human data across various gestational weeks showed that MGEOs consistently clustered within the MGE region across all datasets, demonstrating that the model is robust across different cell lines (**Figure 2.6 B, G**). A UMAP plot of the 3-month MGEO clusters mapped onto the integrated human dataset revealed that the cell types within the MGEOs closely align with those of the human MGE at similar stages of development (**Figure 2.6 G**). To further investigate the developmental trajectory of the MGEOs, we computed Euclidean distances between MGEOs and the human dataset (Shi et al., 2021) at different gestational weeks (**Figure 2.6 H**). The heatmap revealed that the 3-month MGEOs most closely resemble human MGE tissue from gestational weeks 12-16. Together, these data show that the MGEO model captures key features of MGE cellular diversity and accurately recapitulates the transcriptomic signature of the developing human MGE.

MGEOs recapitulate cortical interneuron migration and structural integration in assembloids

Given that MGE-derived cortical interneurons are highly migratory and possess specific migratory characteristics that differentiate them from radially migrating cortical neurons (Nadarajah et al., 2003; Valiente et al., 2009), we next characterized migratory properties of interneuron progenitors in MGEOs alone and in assembloids after fusion with COs. MGEOs at different time points were first plated on extracellular matrix (ECM)-coated plates (**Figure 2.7 A**). Day 21 was the earliest time in which neuron-specific migration could be observed without the spread of proliferative cells (**Figure 2.7 B-C**). Neuronal migration was robust and rapid, as seen by comparing images at 0-, 12- and 24-hours post-plating of the MGEOs (**Figure 2.7 B'**). Cells that migrated away from the MGEOs co-expressed MAP2ab and LHX6, supporting their neuronal and MGE lineage identity (**Figure 2.7 C**).

To examine migration using an assay that more faithfully recapitulates *in vivo* cortical interneuron migration, we fused MGEOs with dorsally patterned SOSR-COs (hereafter referred to as "CO")(Tidball et al., 2023) at 56-58 DIV to generate assembloids. Prior to fusion, MGEOs and COs were virally labeled with mDLX-GFP (Dimidschstein et al., 2016), and CAG-tdTomato, respectively (**Figure 2.7 D**). We observed robust migration of mDLX-GFP+ interneurons that began several hours after fusion and continued rapidly throughout the first two weeks post-fusion (**Figure 2.7 E-G)**. The rapid migration of mDLX-GFP+ interneurons was consistent across cell

lines and experimental replicates (**Figure 2.7 G**). Migrating interneurons displayed properties indicative of cortical interneuron migration, including somal translocation and leading-edge branching in MGEO-CO assembloids **(Figure 2.7 H**).

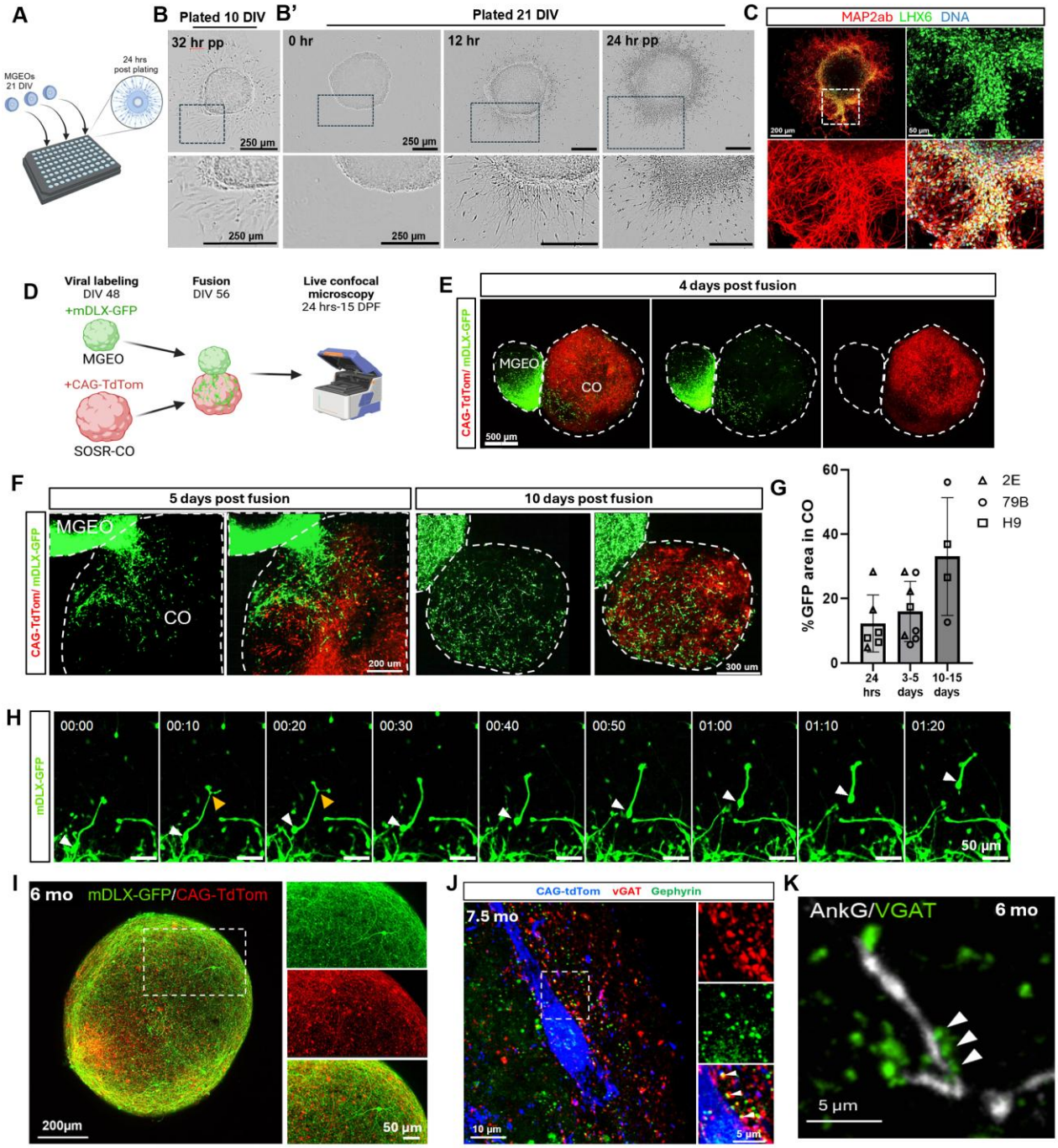

Figure 2.7: MGEO-derived interneuron progenitors are highly migratory

(**A**) Diagram of 2D migration assay. (**B**) Images of MGEOs at 32 hours post-plating (hr pp) at 10 DIV, and (B') 0, 12, and 24 hr pp at 21 DIV on Geltrex. (**C**) Confocal images of a MGEO at 3

days pp immunolabeled for MAP2ab (red) and LHX6 (green) showing co-expression in MGE-derived neurons. Bisbenzimide (DNA) in blue. Boxed region of upper left image is shown at higher magnification in the other panels. (**D**) Schematic of assembloid protocol, involving viral labeling at 48 DIV, fusion at 56 DIV, and subsequent live confocal microscopy from 1-15 days post fusion (DPF). (**E-F**) Images from representative MGEO-CO assembloids at 4 (E) or 5 and 10 (F) DPF. mDLX-GFP (green) virus labels GABAergic cells originating from the MGEO, whereas tdTomato (red) labels CO progenitors and putative excitatory neurons. (**G**) Quantification of mDLx-GFP+ virally labeled MGEO interneuron migration into COs at 1, 3-5, and 10-15 DPF. Percentage area of GFP expression in the CO organoid ± standard deviation (SD) is shown. Points represent single organoid replicates (n≥4), with the point shape denoting the cell line used (triangle: 2E, circle: 79B, diamond: H9). (**H**) Timelapse live imaging of a mDLX-GFP-labeled MGEO interneuron within the CO region of a MGEO-CO assembloid shows characteristic interneuron leading edge branching movement patterns. Time is listed as hr:min. The white arrow denotes the neuronal soma, and the yellow arrowhead points to branching of the leading process. (**I**) Confocal image of an MGEO-CO assembloid at 6 months, immunolabeled with mDLX-GFP (green) and tdTomato (red) as in D-F, shows full fusion into a single spherical structure. The boxed area at left is expanded in the right panels. (**J**) Confocal image of a 7.5-month MGEO:CO assembloid immunolabeled for GABAergic post- and pre-synaptic markers Gephyrin (green) and vGAT (red), respectively, on a CAG-tdTom CO neuron (pseudocolored blue). Boxed area in the left panel is shown at higher magnification at right, with white arrowheads in the merged image showing closely apposed vGAT+ and Gephyrin+ puncta. (**K**) Immunolabeling of a 6-month MGEO:CO assembloid shows VGAT puncta (green) localized along an Ankyrin G (AnkG)-positive axon initial segment (white).

After ~5 months post fusion, MGEOs fully merged with COs and the entire assembloid became a single spherical structure (**Figure 2.7 I**). Immunostaining of assembloids at 7.5 months revealed the formation of inhibitory synapses, with vGAT+ puncta closely apposed to Gephyrin+ puncta, onto the somas of putative cortical excitatory neurons marked by CAG-tdTomato (**Figure 2.7 J**). vGAT+ puncta were also identified along Ankyrin G immunolabeled axon initial segments (**Figure 2.7 K**), indicative of inhibitory axo-axonic synapses. These data provide structural evidence for the maturation of MGEO-derived interneurons and their synaptic integration with excitatory neurons in assembloids.

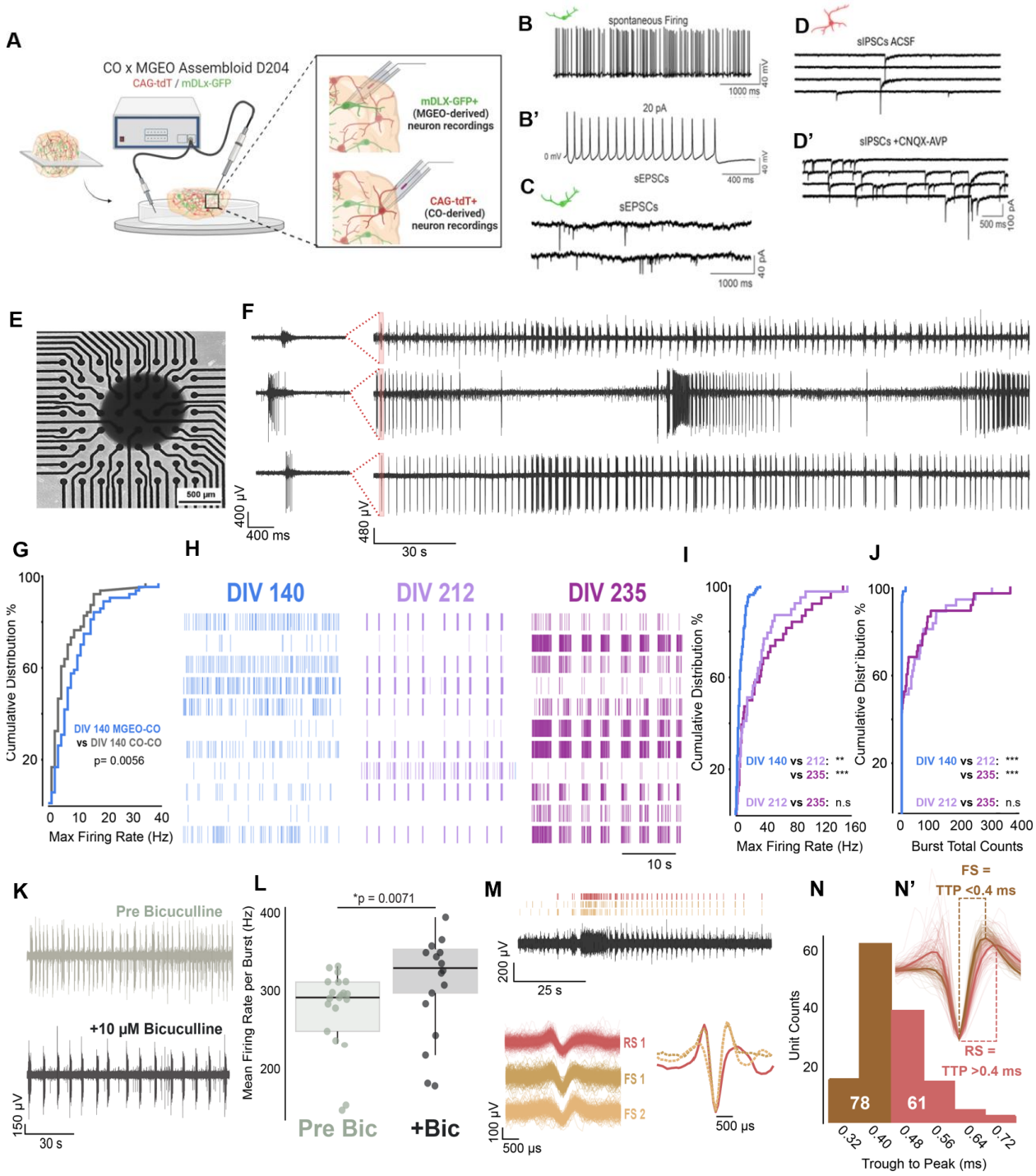

Figure 2.8: MGEO-CO assembloids form functional synapses, display increasingly complex network activity and exhibit fast-spiking units

(**A**) Diagram of assembloid acute slice whole-cell patch clamp recordings. (**B**) Representative traces showing spontaneous (B) and evoked (B') repetitive firing of mDLX-GFP+ (MGEO-derived) neurons in MGEO-CO assembloid slices at 204 DIV. AP firing was evoked from RMP by injection of 1500 ms pulse currents (20 pA). (**C**) Representative trace of spontaneous excitatory postsynaptic currents (sEPSCs) recorded from an mDLX-GFP+ neuron within an assembloid slice

at 204 DIV (holding potential -70 mV). (**D**) Representative trace of spontaneous inhibitory postsynaptic currents (sIPSCs) recorded from a CAG-tdT+ (CO-derived) neuron in the same slice as (C). (D') sIPSC were recorded at a holding potential of -70 mV in the presence of 6-cyano-7-nitroquinoxaline-2,3-dione (CNQX, 10 μM) and amino-5-phosphonopentanoic acid (APV, 50 - 100 μM). (**E**) Brightfield image of a 6-month MGEO-CO assembloid acutely plated on an MEA plate for recording. (**F**) Representative MEA voltage traces from 3 electrodes taken from 2 representative MGE-CO assembloid recordings shown over 2 s (left) and 5 min (right) windows. (**G**) Cumulative distribution of maximum firing rates between DIV-140 CO-CO (gray) and MGEO-CO (light blue) assembloids. n=3 each from 2 cell lines with 62 putative units/assembloid type. Two-tailed Kolmogorov-Smirnov test. (**H**) Representative raster plots of putative units in MGEO-CO assembloids at different maturation stages: DIV-140 (n=3), DIV-212 (n=4-6), and DIV-235 (n=4-6) from 2 cell lines. (**I-J**) Cumulative distribution of maximum firing rates (I) and burst counts (J) across maturation stages (DIV-140, DIV-212, and DIV-235) using same samples as in H. Two-tailed Kolmogorov-Smirnov test, DIV 140 vs 212: (I) KS=0.5010, **, P=2.3247e-07, (J) KS=0.5062, ***, P=1.6290 $x10^{-7}$. DIV 140 vs 235: (I) KS Stat=0.4597, ***, P=4.1009e-06, (J) KS Stat=0.5123, ***, P=1.5173 $x10^{-7}$. DIV 212 vs 235: (I) KS Stat=0.1350, n.s., P=8.1858e-01, (J) KS=0.1404, n.s., P=0.77593. N=38-62 putative units/3-5 assembloids per timepoint. (**K**) Electrode-matched representative voltage traces from a 5-min recording before (gray, top) and after (black, bottom) application of 10 μM bicuculline. (**L**) Firing rate per burst of putative units. Boxplots display the median, 25th and 75th percentiles (box edges), whiskers extending to the most extreme data points, and individual outliers plotted separately. Two-tailed Mann-Whitney U=113, Pre Bic treatment: N=9-11 putative units/3 MGEO-COs, During Bic treatment: 8-10 putative units/2 MGEO-COs. (**M**) Representative voltage trace with corresponding raster plots of three putative units recorded during a network burst. Red represents a regular-spiking unit (RS1); brown (FS1) and gold (FS2) represent fast-spiking (FS) units. (**N**) Quantification from panel (**M**): histogram distribution of putative FS vs. RS units pooled from n=10 assembloids across ≥2 independent differentiations each from 2 cell lines. (**N'**) representative voltage traces of putative RS and FS units aligned to the trough. The mean trough-normalized waveforms of each unit are overlaid, showing trough to peak (TTP) measurements and non-overlapping RS and FS waveforms. MEA data pooled from 2-4 independent differentiations.

MGEO-CO assembloids display functional integration of interneurons, complex activity and fast-spiking neurons

To provide evidence for functional synapses and examine neuronal activity, we next performed whole-cell patch-clamp and multielectrode array (MEA) recordings from MGEO-CO assembloids. Action potential (AP) firing and spontaneous post-synaptic currents in both excitatory and inhibitory neurons were examined using whole-cell recordings of slices made from 6-month-old assembloids (**Figure 2.8 A-D**). We observed spontaneous AP firing in 50% (9 of 18 cells) of recorded neurons, and an additional 17% (3 of 18 cells) displayed repetitive AP firing upon depolarizing current injection (**Figure 2.8 B, B'**, respectively). We also found that glutamatergic and GABAergic neurons formed functional connections, with recordings of mDLX-

GFP-labeled interneurons displaying spontaneous excitatory post-synaptic currents (sEPSCs; **Figure 2.8 C**) and CAG-tdTomato-labeled, putative excitatory neurons receiving spontaneous inhibitory post-synaptic currents (sIPSCs; **Figure 2.8 D**). sIPSCs were also recorded after co-application of the AMPA and NMDA receptor antagonists CNQX and AVP to isolate GABAergic synapses (**Figure 2.8 D'**).

Most published MEA recordings from brain organoids are conducted with the organoids chronically cultured on the MEA plates, leading to the migration of many neurons out of the organoids onto the surface of the MEA plate (Trujillo et al., 2019). This approach disrupts the 3D neural organoid cytoarchitecture and records activity from both 2D and 3D networks that may not faithfully replicate activity exclusively derived from 3D brain structures. To overcome this limitation, we transiently plated MGEO-CO assembloids grown in suspension onto MEA plates for recordings (**Figure 2.8 E**), before placing them back in suspension culture, allowing for recordings made exclusively from 3D networks as well as subsequent recordings from the same organoid at later timepoints (see **Methods**). Inspection of the raw voltage time series revealed large-amplitude voltage fluctuations, the presence of both single- and multi-unit action potentials, and bursts of action potentials (recordings made at 212 and 235 DIV) (**Figure 2.8 F**). We hypothesized that MGEO-CO assembloids would contain a significant number of MGE-derived high-firing-rate inhibitory neurons, as compared to CO-CO assembloids without interneurons. Consistent with this prediction, 140 DIV CO-CO assembloids exhibited a larger fraction of putative units with low firing rates relative to MGEO-CO assembloids (**Figure 2.8 G**). This finding suggests that some of the MGE-derived interneurons in the MGEO-CO assembloids include fast-spiking interneurons, aligning with the observed increase in high-firing-rate units in MGEO-CO assembloids.

Raster plots of MGEO-CO assembloids recorded at DIV 140, 212, and 235 illustrate the expected emergence of network complexity and synchronicity as a function of organoid maturation (**Figure 2.8 H**). Cumulative distribution analyses of maximum firing rates across different maturation stages revealed that firing rates at DIV 140 are significantly lower compared to those at DIV 212 and 235, while no significant difference was observed between DIV 212 and 235 (**Figure 2.8 I**). Similarly, the cumulative distribution of the number of bursts increased over time, as DIV 140 assembloids exhibited significantly fewer bursts compared to DIV 212 and 235 **(Figure 2.8 J**). No significant difference in number of bursts was observed for MGEO-CO

assembloids between DIV 212 and 235 **(Figure 2.8 J**); Collectively, these data suggest that as MGEO-CO assembloids mature, both firing rates and network bursting activity increase.

To further confirm the presence of functional inhibitory neurons in MGEO-CO assembloids, we applied 10 μM bicuculline, a GABA-A receptor antagonist, to assess the role of GABAergic transmission in regulating network activity. Electrode-matched representative voltage traces from a 5-minute recording before and after bicuculline application showed clear alterations in firing rates with bicuculline exposure (**Figure 2.8 K**). Quantification of this effect (**Figure 2.8 L**) confirms that blocking GABAergic transmission leads to a net increase in firing rates within network bursts. In addition, we classified putative units from extracellular recordings to distinguish between fast-spiking (FS) and regular-spiking (RS) neurons using spike sorting and measurements of trough to peak (TTP) AP duration (**Figure 2.8 M, N, N′**). The majority of putative units in MGEO-CO assembloids were FS units, further supporting the presence of MGE-derived fast-spiking interneurons. These results provide direct evidence that inhibitory neurons in MGEO-CO assembloids are functionally integrated and that FS units are effectively generated in MGEO-CO assembloids.

2.5 Discussion

A critical challenge for studying human cortical development and brain disorders with human cellular models is the inability to generate late developing PV interneurons. These cells arise from the embryonic MGE, and nearly all existing subpallial organoid models are very limited in generating MGE lineages, especially PV. Here we show the development of an MGE-specific subpallial organoid protocol, MGEOs, that robustly and consistently produces MGE lineages closely resembling the embryonic human MGE and gives rise to highly migratory interneuron progenitors that differentiate into PV and SST interneurons. These interneurons integrate with excitatory cortical neurons in assembloids that exhibit complex network activity and show a substantial proportion of fast-spiking neurons.

We designed our small molecule manipulations to optimally pattern toward MGE, but starting with a hPSC monolayer was also advantageous. The even distribution of morphogens across all cells in the monolayer increases culture purity and better replicates the formation of the neural plate in human embryonic development. For multi-rosette organoid models that initiate with hPSC aggregation into embryoid bodies, the optimal timing and concentrations of patterning factor

application may differ. Notably, a recent study described a multi-rosette subpallial organoid protocol with increased MGE specificity and the generation of some PV cortical interneurons in assembloids (Walsh et al., 2025). This group also reported the presence of PV reporter-labeled neurons with fast-spiking properties in their assembloids, although the firing rates were rarely above 60 Hz. Another group enriched for MGE-like pallial interneurons in 2D culture and grafted them into mouse cortex (Bershteyn et al., 2023). They successfully generated a large proportion of ERBB4+/SST cells transcriptomically predicted to be of PV basket cell identity, but detected no PVALB mRNA up to 18 months post transplantation (Bershteyn et al., 2025). In contrast, we observed robust immunoreactivity for PV in MGEOs (with or without fusion to hCOs) by 4 months, along with evidence of basket and axoaxonic subtypes and robust expression of Kv3.1 and a perineuronal net marker, both of which are components of fast-spiking PV interneurons.

By MEA recordings, we identified fast-spiking neurons in assembloids with the top 20% at DIV 235 showing firing rates of 30-160 Hz, and the top 5 FS units above 80 Hz (Figure 6I). The detection of fast-spiking neurons in our assembloids likely reflects the capacity of MGEOs to generate PV cortical interneurons, along with the enrichment of interneurons at the assembloid periphery (see Figure 3E) in close juxtaposition to the MEA electrodes leading to a disproportionate identification of fast-spiking neurons. Our novel MEA recording approach, which allows for established 3D networks to remain intact as they mature rather than reorganizing into 2D structures (Trujillo et al., 2019), also likely contributed. However, we did not have access to a PV reporter line for patch-clamp recordings to definitively show that the fast-spiking neurons are PV interneurons.

Our novel hPSC-derived MGEO model provides a valuable tool to study MGE-derived cortical interneuron development and for modeling of interneuron-related phenotypes in genetic epilepsies and related neurodevelopmental disorders (see Chapter 3 for expression of genes in MGEOs that are commonly implicated in neurodevelopmental disorders). In particular, our protocol offers the unique opportunity to study the intrinsic developmental programs of human PV cortical interneurons and their associated disorders. In addition to disease modeling, MGEOs may also serve as a potential source of MGE interneuron progenitors for therapeutic grafting to treat disorders associated with MGE-derived interneuron dysfunction, including epilepsies, ASD and neurodegenerative disorders.

Limitations of this study

Some cell line variability appeared in the MGEO electrophysiological characterizations, particularly in their maturation timelines, with the fibroblast-derived line (2E) displaying slightly delayed electrophysiological development compared to the embryonic (H9) and blood-derived (79B) lines. These differences highlight the importance of validating hPSC lines and the need to utilize proper isogenic or cell-line-origin matched controls when modeling diseases.. Additionally, while the maturation time of MGEOs is considerably accelerated compared to *in vivo* human developmental timelines, we found that a prolonged maturation time of MGEOs *in vitro* was necessary for them to robustly express PV (~120 days) and to display complex network activity (~200 days). We are currently working on methods to further shorten the maturation period needed for PV expression. Additionally, MGEOs must be individually removed from the thick extracellular matrix manually at 10-12 DIV, limiting large scalability of this method. Further protocol optimizations are therefore needed to identify an efficient way to overcome this rate-limiting protocol step. Lastly, our MEA recordings were performed at a sampling rate of 12.5 kHz, limiting the temporal resolution needed to accurately classify fast spike waveform features (e.g. trough to peak) faithfully. To increase the specificity of cell-type identification in future experiments, incorporating a reporter line that specifically labels PV cortical interneurons would enable selective targeting of these cells. Regardless of these limitations, our findings demonstrate MGEO-CO assembloid network maturation, including increased firing rates, burst dynamics, and the presence of functionally integrated MGEO-derived inhibitory neurons.

Notes on Chapter 2

A modified version of this chapter is in included in a manuscript currently under revision for publication and is available as a preprint under:

Varela, M. C., Walker, M. P., Bok, J., Crespo, E. L., Thenstedt, T., Goldstein, L., Tidball, A. M., Yuan, Y., Isom, L. L., Fu, J., Uhler, M., & Parent, J. M. (2025). Human Medial Ganglionic Eminence Organoids Robustly Generate Parvalbumin Interneurons and Fast-Spiking Neurons and Reveal Migratory Deficits in SLC6A1 Deficient Interneurons. BioRxiv, 2025.07.01.662594. https://doi.org/10.1101/2025.07.01.662594

Contributions: All of the experimental design, data generation, imaging, data analysis, and figure generation in this chapter was conducted by me (unless noted otherwise) with contributions from others as follows: Miranda Walker contributed equally to the morphogen screening experimental design and execution, conducted the RT-qPCR analysis and plot generation in Fig 2.1 E, C, and 2.5 A, contributed images in Fig 2.5 H and 2.7 E, H, J, and generated schematics in Fig 2.1 B, D and 2.8 A, and contributed equally to the schematic in Fig 2.1 A. Jeyoon Bok conducted the preliminary preparation and analysis of the scRNAseq data and generated plots in Figs 2.3 A, B, D, E and 2.6 A-E, G, H while I contributed the analysis and generation of plots in Figs 2.3 C, F, all plots in Fig 2.4, and 2.6 F. I conducted all MEA recordings and Emmanuel Crespo conducted the analysis of the MEA recordings and generated plots in Fig 2.8 F-N′. Yukun Yuan conducted the single-cell electrophysiological recordings and contributed the traces used in Fig 2.8 B-D′. Undergraduate trainees under my supervision, Tyler Thenstedt and Leah Goldstein, assisted with select experimental assays and data analysis.

Chapter 3 *SLC6A1* Haploinsufficiency Alters Cortical Interneuron Migration, Maturation and Subtype Specification in Human Medial Ganglionic Eminence Organoids

3.1 Summary

Haploinsufficiency (HI) of *SLC6A1*, which encodes the GABA transporter GAT1, has been strongly linked to neurodevelopmental disorders characterized by epilepsy and cognitive impairment. While the consequences of *SLC6A1* variants on transporter function and synaptic inhibition have been increasingly characterized, far less is known about how reduced *SLC6A1* expression impacts the developmental trajectory of medial ganglionic eminence (MGE)–derived interneurons. Given the important role of GABA signaling in progenitor proliferation, migration, and subtype specification, we hypothesized that *SLC6A1* HI disrupts key developmental programs within the MGE GABAergic lineage.

In this chapter, we examine how *SLC6A1* HI alters interneuron migration, fate specification, lineage progression, and maturation in human iPSC-derived MGE organoids (MGEOs). Assays of cortical interneuron migration in MGEOs and MGE/Cortical assembloids reveal severe cell autonomous migration defects caused by loss of *SLC6A1*. Through transcriptional profiling and phenotypic analyses, we also identify shifts in interneuron subtype markers and maturation-associated gene expression, revealing that *SLC6A1* HI reshapes developmental trajectories within the GABAergic lineage. Together, these findings demonstrate that GAT1 expression, which is known to be critical for inhibitory neurotransmission, is also required for the proper migration and specification of MGE-derived interneurons during human cortical development.

3.2 Introduction

SLC6A1 pathogenic variants are strongly associated with childhood-onset epilepsies, including myoclonic-atonic epilepsy (MAE, MIM# 616421) and other developmental and epileptic encephalopathies, frequently accompanied by cognitive and behavioral impairments including autism and intellectual disability. While extensive work in rodent models and heterologous expression systems has demonstrated that some pathogenic *SLC6A1* variants impair GABA transport and alter cortical inhibition, these studies have largely focused on synaptic and circuit-level consequences in the mature brain (Guo et al., 2025; Mattison et al., 2018; Mermer, et al., 2021; J. Wang et al., 2020). Whether, and how, *SLC6A1* dysfunction impacts earlier stages of human cortical interneuron development remains an open question.

The protein encoded by *SLC6A1*, GAT1, regulates inhibitory synaptic transmission and network excitability by mediating presynaptic neuronal and astrocytic GABA reuptake. More recently, expression of GAT1 has also been identified in oligodendrocytes and microglia (Fattorini et al., 2017, 2020), suggesting that GAT1 may have broad impacts on multiple cell types. Indeed, evidence suggests that GABA signaling may be a key regulator of neurodevelopmental processes, including progenitor proliferation and fate specification. In the developing forebrain, GABA has been shown to act as a trophic signal that influences cell cycle progression, migratory dynamics, and the timing of interneuron differentiation (Caballero & Tseng, 2016; Fazzari et al., 2020; Inada et al., 2011; Kilb, 2012; LoTurco et al., 1995). These developmental roles raise the possibility that impaired GABA homeostasis resulting from *SLC6A1* mutations could perturb MGE-derived cortical interneuron development long before the establishment of mature inhibitory synapses. However, direct investigation of these processes in humans has been limited by the lack of experimentally accessible models that recapitulate human MGE development while maintaining endogenous regulation of *SLC6A1* expression.

Here, we address this gap by leveraging *SLC6A1* CRISPR gene edited and human patient iPSC-derived single-rosette MGEOs with high endogenous *SLC6A1* expression to examine the developmental impact of GAT1 dysfunction in a human context. We uncover novel abnormalities across multiple stages of interneuron development, including delayed tangential migration, altered maturation, and disrupted interneuron subtype specification, with a bias towards SST lineage over PV lineage. Furthermore, we confirm through transcriptomic analysis that key regulators of MGE lineage specification are altered along with changes in developmental signaling pathway effectors.

Finally, we show that these developmental changes result in network hyperexcitability which is attenuated by pharmacologically-driven rescue of interneuron migration in cortical-MGEO assembloids. These findings reveal a previously unrecognized role for *SLC6A1* in coordinating early human interneuron development and suggest that developmental dysregulation of MGE-derived interneurons contributes fundamentally to disease pathogenesis in *SLC6A1*-associated neurodevelopmental disorders.

3.3 Materials and methods

Human Pluripotent Stem Cell Culture

All human iPSC experiments were conducted with prior approval from the University of Michigan Human Pluripotent Stem Cell Research Oversight (HPSCRO) and Institutional Review Board (IRB) Committees. To ensure the reproducibility of our experiments, iPSC lines derived from both fibroblasts and peripheral blood mononuclear cells, including both male and female lines, were used in all experiments. Human iPSC cultures were maintained in dedicated incubators at 37°C under humidified conditions with 5% CO_2. Prior to initiating organoid differentiation, cells were expanded under feeder-free conditions in mTeSR-1 (STEMCELL Technologies, Cat# 85850) or mTeSR-Plus (STEMCELL Technologies, Cat# 100-0276) on 6-well plates pre-coated with 1:100 Geltrex (Thermo Fisher Scientific, Cat# A1413302). Cultures were passaged at approximately 60–70% confluence using 0.8 mM EDTA. Cell lines were routinely screened for mycoplasma contamination and closely evaluated for typical colony morphology and the absence of spontaneous differentiation. Genomic stability was assessed using single nucleotide polymorphism (SNP) microarray analysis.

Generation of SLC6A1 DEE lines

To establish *SLC6A1* gene-edited iPSC lines, human foreskin fibroblasts were reprogrammed into iPSCs in conjunction with CRISPR/Cas9-mediated genome editing, as previously described (Tidball et al., 2017). Guide RNAs were designed to target exon 7 of *SLC6A1* to introduce frameshift-inducing out-of-frame insertions or deletions (indels). Heterozygous (Het), compound heterozygous knockout (KO), and isogenic control clones were validated by Sanger sequencing and next-generation sequencing.

For generation of the *SLC6A1* rescue line, a PiggyBac transposase system was employed to stably insert a doxycycline (Dox)-inducible, codon-optimized wild-type human *SLC6A1*

construct into a knockout iPSC background (KOi). Induction of GAT1 expression in KOi-derived MGE organoids was confirmed by RT–qPCR following Dox treatment, while parallel cultures maintained without Dox served as negative controls.

Patient-derived iPSC lines were generated from peripheral blood samples obtained with IRB approval and informed consent through the University of Michigan Health System. Peripheral blood mononuclear cells were isolated and processed using the Erythroid Progenitor Reprogramming Kit (STEMCELL Technologies, Cat# 05924) to expand erythroid progenitors, which were subsequently transfected with episomal reprogramming plasmids encoding SOX2 and KLF4 (pCXLE-hSK), L-MYC (pCXLE-hUL), and OCT3/4 (pCXLE-hOCT3/4). Pluripotency of all established iPSC lines was confirmed by RT–qPCR analysis and immunocytochemical staining for canonical pluripotency markers.

MGEO generation

Self-organizing single-rosette MGE organoids (MGEOs) were derived from hPSC monolayers using a modified version of our previously described self-organizing single rosette cortical organoid (SOSR-CO) protocol (Tidball et al., 2023). Briefly, iPSCs were dissociated with Accutase (Innovative Cell Technologies) and seeded onto 1:50 Geltrex-coated 12-well plates at a density of 3–4 × 10^5 cells/mL in mTeSR1 supplemented with Rho-kinase (ROCK) inhibitor (10 μM Y-27632, Tocris, 1254). The ROCK inhibitor was removed the following day, and cultures were fed daily with fresh medium until reaching ~80–100% confluence. Neural induction was initiated by switching to 3N medium (1:1 DMEM/F12 and Neurobasal supplemented with N2 and B27 without vitamin A) containing 2 μM DMH1 (Tocris, 4126), 2 μM XAV939 (Cayman Chemical, 13596), and 10 μM SB431542 (Cayman Chemical, 13031). On day in vitro (DIV) 4, monolayers were briefly incubated (1 min) with L7 hPSC passaging solution (Lonza), mechanically sectioned into uniform squares using a StemPro EZ passage tool, and gently detached by pipetting with pre-warmed differentiation medium. Approximately 200 μL of tissue fragments were transferred into individual wells of a 96-well plate pre-coated with 40 μL of 100% Geltrex (pre-incubated at 37°C for 30 min), yielding ~20–40 organoids per well and up to 16 wells per starting monolayer. Medium was topped off the following day without a full exchange, and half-volume media changes were initiated 48 hours later and performed daily. On day 6, FGF2 (20 ng/mL; Gibco, PHG0261) supplemented with 0.1% human serum albumin was added to enhance survival. By day 10, cultures received a complete medium replacement with 3N containing 100

nM of the forebrain ventralizing factor SAG (Selleckchem, S7779) and FGF2, omitting DMH1, XAV939, and SB431542. Between days 10–12, organoids reaching ~250 μm in diameter were individually transferred using a STRIPPER micropipetter fitted with 275 μm tips into low-attachment U-bottom 96-well plates containing 200 μL of 3N medium lacking vitamin A. Organoids exceeding this size frequently developed multiple rosettes, whereas smaller structures demonstrated reduced viability. Beginning on day 12, half-media changes were performed every other day using 3N supplemented with vitamin A, SAG (100 nM), BDNF (20 ng/mL), and NT3 (20 ng/mL), excluding FGF2. SAG was withdrawn on day 18. After day 35, organoids were maintained in 3N medium with vitamin A alone (without BDNF or NT3), with half-volume changes every other day. As organoids increased in size, they were transferred to low-adhesion 24-well plates to accommodate larger media volumes. From day 90 onward, MGEOs were cultured in BrainPhys medium (STEMCELL Technologies, 05790) supplemented with N2, NeuroCult™ SM1 (STEMCELL Technologies, 05711), BDNF (20 ng/mL), GDNF (20 ng/mL), and ascorbic acid (200 nM). SOSR-COs for assembloid studies were generated as previously described (Tidball et al., 2023).

Cryopreservation, sectioning and immunocytochemistry

Organoids were harvested, rinsed in phosphate-buffered saline (PBS), and fixed in 4% paraformaldehyde (PFA) prepared in PBS at 4°C for 30 minutes (1-month-old organoids) or 60 minutes (older organoids). Following fixation, samples were washed three times for 10 minutes each in PBS and cryoprotected overnight at 4°C in 30% sucrose dissolved in PBS. Organoids were then embedded in O.C.T. compound (Fisher Healthcare, 4585) within cryomolds (Tissue-Tek, 4566), flash-frozen on dry ice, and stored at −80°C. Cryosections (20 μm) were collected onto Superfrost Plus slides (ThermoFisher, 12-550-15) using a Leica CM1850 cryostat. Slides were air-dried at room temperature for at least 2 hours prior to storage at −20°C. For immunofluorescence labeling, sections were rinsed in PBS and permeabilized for 20 minutes at room temperature (RT) in PBS containing 0.2% Triton X-100. Blocking was performed for 1 hour at RT in PBS supplemented with 0.05% Tween-20, 5% normal goat serum, and 1% bovine serum albumin (BSA); normal horse serum was substituted when goat primary antibodies were used. Primary antibodies diluted in blocking buffer were applied overnight at 4°C in a humidified chamber. Sections were subsequently washed three times in PBST (PBS with 0.05% Tween-20) and incubated for 2 hours at RT with Alexa Fluor–conjugated secondary antibodies (1:500). After a

10-minute PBST wash, nuclei were counterstained with bisbenzimide for 5 minutes. Sections were washed three additional times (10 minutes each), mounted using Glycergel (Agilent Dako, C0563), and sealed with clear nail polish. Imaging was performed on an Andor BC43 spinning disk confocal microscope (Oxford Instruments), and image analysis was conducted using Fiji software.

RT–qPCR

Total RNA was isolated from pooled organoids (minimum of four per sample) using the miRNeasy Mini Kit (Qiagen, 217004), including the optional DNase I treatment step. cDNA was synthesized from 100 ng of RNA using the SuperScript™ III First-Strand Synthesis SuperMix kit (Invitrogen, 11752-050). Quantitative PCR reactions were prepared using 2 ng of cDNA template and Power SYBR Green PCR Master Mix (ThermoFisher, 4367659) and run on an Applied Biosystems QuantStudio 3 system (primer sequences are listed in Supplemental Table S1). Relative expression levels were calculated using the 2^−ΔΔCt method, with normalization to the average expression of undifferentiated 2E control iPSCs (n = 3–4 independent experiments). Each sample was analyzed in technical triplicate, and GAPDH served as the endogenous reference gene. For transcripts that were not detected, a Ct value of 40 was assigned for analysis. Data processing was performed in Microsoft Excel, and graphical representations were generated using GraphPad Prism.

Bulk RNA Sequencing and Differential Expression Analysis

Total RNA was isolated from day 21 MGEOs using the RNeasy Kit (Qiagen, Germantown, MD, USA). The MGEOs were solubilized along with the Geltrex hydrogel using Qiazol, and the kit was used according to the manufacturer's recommendations. RNA samples were processed by the University of Michigan Advanced Genomics Core for bulk RNA sequencing. Libraries were generated using a poly(A) enrichment strategy to selectively capture mRNA and subsequent sequencing was performed on an Illumina NovaSeq platform using a shared flow cell configuration. Paired-end sequencing was conducted with 151 bp read lengths on a 300-cycle S4 flow cell with each sample allocated approximately 5% of a flow cell, yielding ~400 million total reads per sequencing run.

Quality Control, Alignment, and Quantification

Raw sequencing reads were processed using a standardized pipeline implemented by the Advanced Genomics Core. Adapter trimming was performed using Cutadapt (v2.3) (Martin, 2011). Read quality was assessed using FastQC (v0.11.8) (Andrews, S. (2010), and potential contamination was evaluated using Fastq Screen (Wingett & Andrews, 2018). Reads were aligned to the human reference genome (GRCh38, ENSEMBL) using the splice-aware aligner STAR (v2.7.8a) (Dobin et al., 2013), with alignment parameters following ENCODE RNA-seq standards. Gene-level expression estimates were generated using RSEM (v1.3.3) (Li & Dewey, 2011).

Differential Expression Analysis

Downstream analyses were performed in RStudio using R (version 4.5.2). Gene-level count matrices generated by RSEM were imported into DESeq2 for normalization and differential expression testing. Genes with counts <10 across samples were filtered prior to analysis. Counts were normalized using the median-of-ratios method, and differential expression was assessed using a negative binomial generalized linear model. P-values were adjusted for multiple comparisons using the Benjamini–Hochberg method, and genes with an adjusted $p < 0.05$ were considered statistically significant. Plots were generated using DESeq2 plotting functions along with other packages within R, or using iDEP (Ge et al., 2018).

Viral Labeling and Generation of Cortical–MGEO Assembloids

To enable visualization of neuronal migration within assembloids, SOSR-COs were transduced with AAV1-CAG-tdTomato (Addgene #59462), while MGEOs were infected with AAV1-mDlx-GFP (Addgene #83900) to selectively label interneuron progenitors and interneurons prior to fusion. For viral transduction, organoids at DIV 46 were transferred to 1.5 mL microcentrifuge tubes and incubated overnight at 37°C with 5% CO_2 in 250 µL of 3N medium containing vitamin A and virus diluted 1:50. The following day, 750 µL of fresh 3N medium with vitamin A was added. After an additional 24 hours, organoids were rinsed with PBS to remove excess viral particles and returned to ultra-low attachment plates in standard culture medium until fusion, typically one week later. To generate cortical–MGEO assembloids, regions of SOSR-COs and MGEOs exhibiting the highest reporter fluorescence were positioned in direct contact along the bottom surface of either 48- or 24-well plates. Plates were angled slightly to maintain sustained contact between the two tissues and left undisturbed for a minimum of 24 hours to promote fusion.

Two-Dimensional Migration Assay of MGEO-Derived Neurons

To assess interneuron migration from three-dimensional MGEOs onto a two-dimensional extracellular matrix substrate, organoids at DIV 21 were individually transferred to wells of a 96-well, thin-bottom, black-walled plate (PerkinElmer, 6055300) pre-coated with 1:50 Geltrex and containing 3N medium supplemented with vitamin A (3N+A). Each organoid was carefully positioned in the center of the well using a pipette tip and allowed to settle prior to imaging.

Time-lapse imaging was performed using either an Incucyte S3 Live Cell Analysis System or an Andor BC43 spinning disk confocal microscope. With the Incucyte platform, multiple 10× phase-contrast images per well were captured every 15 minutes for 48 hours beginning immediately after plating. Confocal imaging on the Andor system was conducted at 5–10-minute intervals for up to 15 hours, starting at least 2 hours after plating. During imaging, cultures were maintained at 37°C with 5% CO_2. At 48 hours post-plating, cultures were fixed in 4% PFA for downstream immunostaining as described above. To pharmacologically inhibit GAT1 function, the selective antagonist NO711 (25 μM) was applied to control (isogenic to *SLC6A1* CRISPR Het and KO lines) MGEO cultures. Drug treatment was maintained throughout the migration assay (DIV 21–25), with fresh compound added during daily half-media changes. At DIV 25, cultures were fixed in 4% PFA and immunostained for DCX and bisbenzimide to quantify migration distances. Imaging was performed on the Andor BC43 microscope, and quantitative analysis was conducted using Fiji software. Quantitative analysis was performed by measuring the average distance of immunostained processes and nuclei from the original organoid boundary. This was completed by manually drawing a boundary around the outermost perimeter of migrated cells and measuring total migratory area. The average migratory radius from the center of the organoid to the perimeter of the migratory area was calculated by taking the square root of the total migratory area divided by π. The average radius of the original organoid was calculated in the same fashion and was subtracted from the average migratory radius leaving only the distance from the outer boundary of the organoid to the perimeter of the migrating cells to be quantified as average cell body migration distance and average process extension distance.

Live Imaging of Assembloids and Quantification of 3D Migration

To evaluate interneuron migration within a 3-D context, virally labeled SOSR-COs and MGEOs were fused at DIV 56 as described above. Time-lapse imaging of GFP-positive migrating interneurons was performed using an Andor BC43 spinning disk confocal microscope, with images acquired every 5 minutes over a 15-hour period. In addition, static confocal images of live

assembloids were collected at multiple intervals ranging from 24 hours to 15 days post-fusion to monitor changes in cell location over time. Quantification was conducted in Fiji by measuring the proportion of mDLX-GFP–positive cell area within the CAG-tdTomato–labeled cortical organoid region. Data were plotted and analyzed using GraphPad Prism.

Multi-Electrode Array (MEA) Recordings

For electrophysiological assessment, assembloids differentiated for 20–34 weeks were individually transferred to wells of a 6-well CytoView MEA plate (Axion Biosystems) coated with poly-L-ornithine (100 µg/mL) and 1:100 Geltrex. Rather than allowing organoids to grow chronically on MEA plates, which can disrupt native 3D architecture, organoids were acutely placed onto electrodes immediately prior to recording. After positioning, excess medium was carefully removed to promote stable electrode contact through surface tension. Three-minute recordings were obtained, after which full medium was replenished, and organoids were gently returned to suspension culture. No acute disruption of activity was observed using this method and recordings were comparable to recordings from organoids chronically plated in the MEA plate. Reproducibility of recordings was validated by repeated plating and recording of the same organoid across multiple wells and time points (data not shown). Recordings were acquired using a Maestro MEA system with AxIS software in Spontaneous Neural Configuration (Axion Biosystems). Signals were sampled at 12.5 kHz and bandpass filtered (200–3000 Hz) using a Butterworth filter for action potential detection. Spikes were identified using a threshold of 5.5 standard deviations above background noise. Single-electrode bursts were defined as at least five spikes with a maximum inter-spike interval of 100 ms. Network bursts were classified as a minimum of 50 spikes occurring within 100 ms intervals across at least 25% of active electrodes. Mean firing rates were calculated within 10-second windows, and synchrony metrics were determined using a 20 ms temporal window.

3.4 Results

Generation of SLC6A1 variant iPSC lines

To model MAE and explore potential effects of *SLC6A1* loss of function on cortical interneuron development, we used CRISPR/Cas9 gene editing to generate loss-of-function variants and also reprogrammed *SLC6A1*-linked MAE patient cells into iPSCs (see Methods). We

performed dual fibroblast reprogramming and *SLC6A1* CRISPR/Cas9 gene editing (Tidball et al., 2017) to create out-of-frame indels in the *SLC6A1* gene, near a known W193* truncation variant linked to MAE with mild autistic features (Carvill et al., 2015). Two heterozygous (Het 1, 2), two compound heterozygous (KO 1, 2), and isogenic control (iCont) lines were generated. For patient-derived iPSCs, we reprogrammed PBMCs from both male and female patients with *SLC6A1*-linked MAE (PT 1, 2) and from an unrelated healthy control (Cont) (**Figure 3.1 A,B**). Together these CRISPR indel and patient variants span various regions of the GAT1 protein including extracellular, intracellular, and transmembrane domains (**Figure 3.1 B**).

Given that GAT1 is mainly expressed in interneurons in the cortex and because hPSC-derived forebrain organoids can recapitulate many of the key milestones in human cortical development including neuronal maturation, migration, and network assembly, we chose to use an MGEO model which we recently developed in our lab (see Chapter 2). We explored the expression of *SLC6A1* in control MGEOs using our previously acquired scRNAseq dataset at 1 month and 3 months (see Chapter 2). We found that *SLC6A1* was highly expressed in the MGEO cortical interneuron clusters at 1 and 3 months and its expression was especially upregulated in our previously identified (see Chapter 2) cortical PV precursor clusters at 3 months (**Figure 3.1 B-E**).

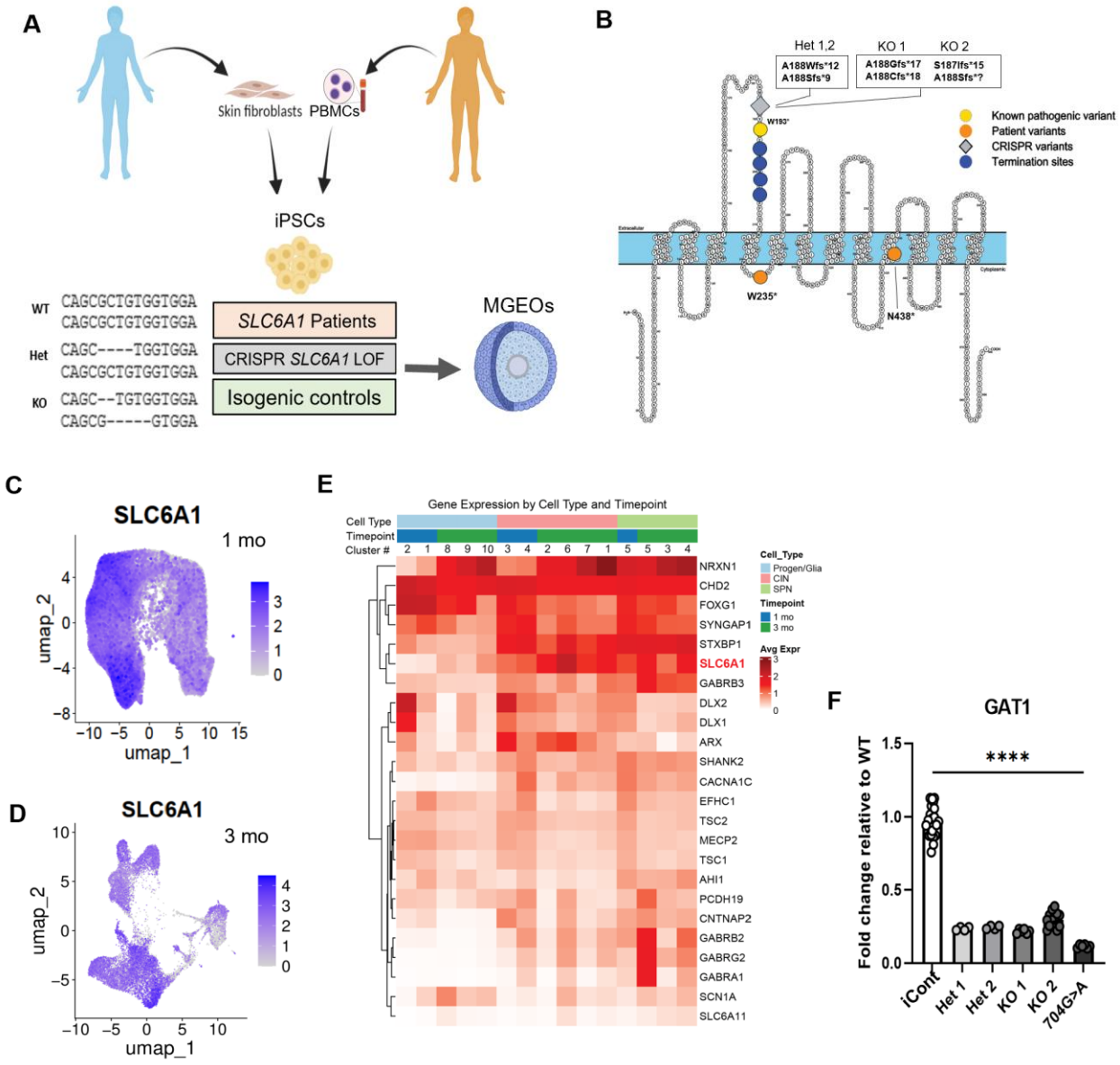

Figure 3.1: Generation and GAT1 CRISPR edited and patient derived iPSCs and validation of GAT1 expression in MGEOs.

(**A**) Schematic depicting the process of generating GAT iPSC lines and deriving single-rosette organoids (**B**) Topography representation of GAT1 protein structure showing location of CRISPR-generated indels, predicted truncation sites, and patient variants. (**C, D**) UMAP plots showing *SLC6A1* expression in 1-month (**C**) and 3-month (**D**) MGEOs. (**E**) scRNAseq heatmap of the expression levels of DEE-related genes in 3-month MGEOs showing high expression of *SLC6A1* in interneuron clusters. (**F**) Analysis of RT-qPCR fold change in GAT1 mRNA expression levels in *SLC6A1* variant lines relative to isogenic control (iCont).

GAT1 mRNA reduction was confirmed in KO, HET and PT lines using RT-qPCR, with GAT1 expression between 5-40% of Cont levels (**Figure 3.1 F**). The KO 2 line, with a predicted termination site occurring within an intronic region in one allele resulting in an unknown definitive termination site due to potential splice variation, (represented as A188Sfs*? in **Figure 3.1 B**), displayed larger variability in GAT1 mRNA expression across samples (**Figure 3.1 F**). This is likely due to differential splicing occurring across samples. Due to inconsistency of GAT1 expression in the KO 2 line, we excluded this line from subsequent experiments.

SLC6A1 LOF results in cortical interneuron cell-autonomous migratory deficits

The migration of MGE- and caudal ganglionic eminence (CGE)-derived interneurons to the cortex parallels that of GAT1 expression during development (Conti et al., 2004). Additionally, ambient GABA levels have been shown to alter cortical interneuron migration through non-synaptic interactions at GABA receptors (Cuzon et al., 2006; Inada et al., 2011; Kilb et al., 2013). To evaluate the effects of *SLC6A1* LOF on cortical interneuron migration, MGEOs from 2 Het lines and 1 line each of PT, KO, CRISPR isogenic control (iCont) and healthy unrelated control (Cont) groups were left embedded in thick extracellular matrix (100% Geltrex; part of the single-rosette MGEO protocol) and both somal migration distance and process extension into the matrix were quantified at DIV 30 (**Figure 3.2 A-D**). We observed a significant reduction in cell migration and process extension from PT-derived, Het, and KO MGEOs compared to iCont and Cont (**Figure 3.2 C, D**). This finding was unexpected as migration deficits have not previously been reported in *SLC6A1* KO mouse models.

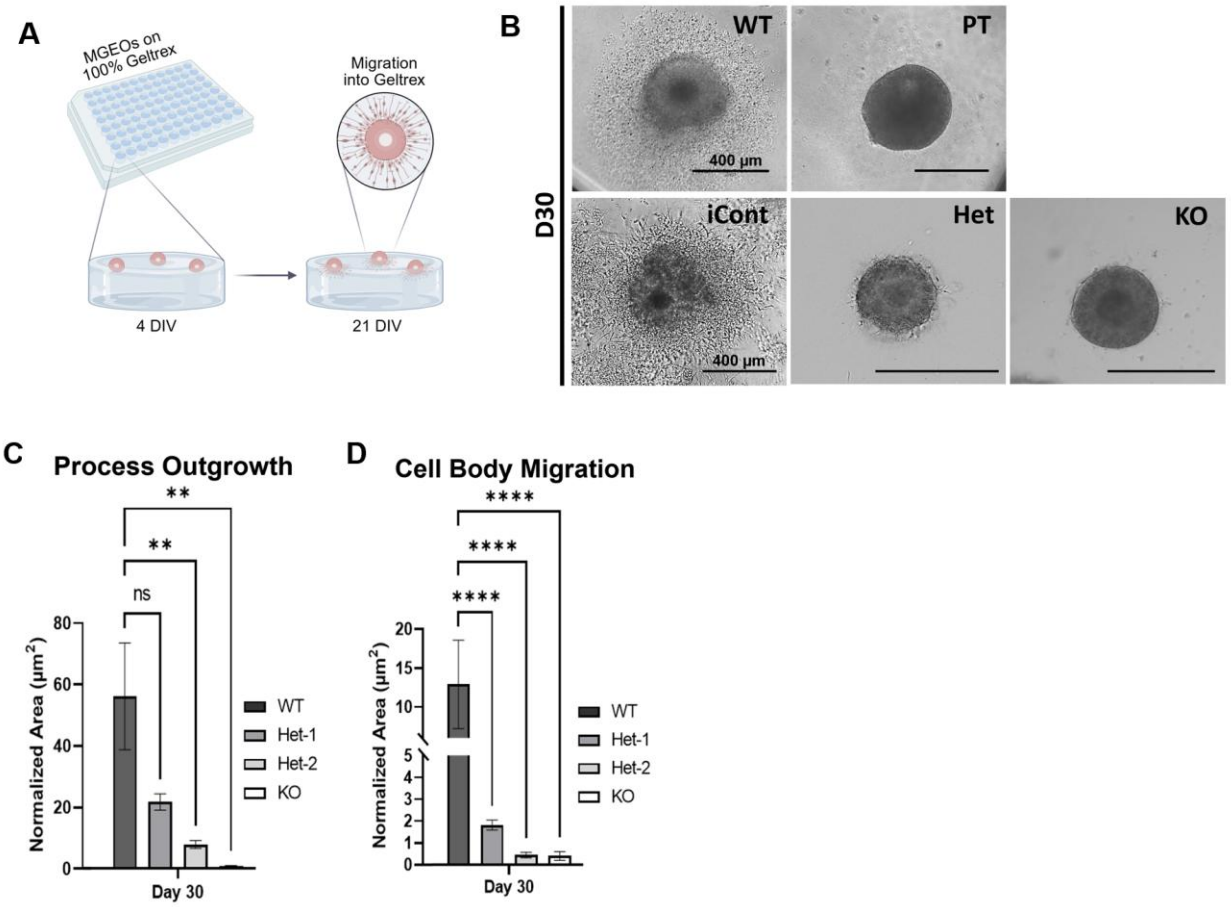

Figure 3.2: Migratory deficits of GAT1 MGEOs on ECM.

(**A**) Schematic representation of MGEO migration assay. (**B**) Brightfield images of cell migration from MGEOs into the surrounding extracellular matrix at day 30 in vitro. (**C, D**) Quantification of MGEO process outgrowth area (**C**) and cell body migration area outside of MGEOs (**D**) in WT, 2 Het and KO groups. ****, pval <0.0001; **, pval <0.0021; ns, non significant

To determine if *SLC6A1* loss was indeed responsible for these migration deficits, we conditionally restored *SLC6A1* expression using PiggyBac transposase to stably integrate a Dox inducible, codon-optimized, wildtype *SLC6A1* cassette into the *SLC6A1* KO line (KOi) (**Fig 3.2 A**). DIV 12 MGEOs embedded on top of thick ECM were exposed to either 0.5 or 1.0 mg/mL Dox in the culture media for either 3 or 9 consecutive days to investigate if *SLC6A1* was important solely for migration initiation (3-day treatment), or if it was required to maintain migration of MGE interneurons (9-day treatment) (**Fig 3.3 B**). Controls included iCont MGEOs with and without Dox, vehicle exposure of KOi MGEOs, and Dox exposure of MGEOs without the overexpression cassette.

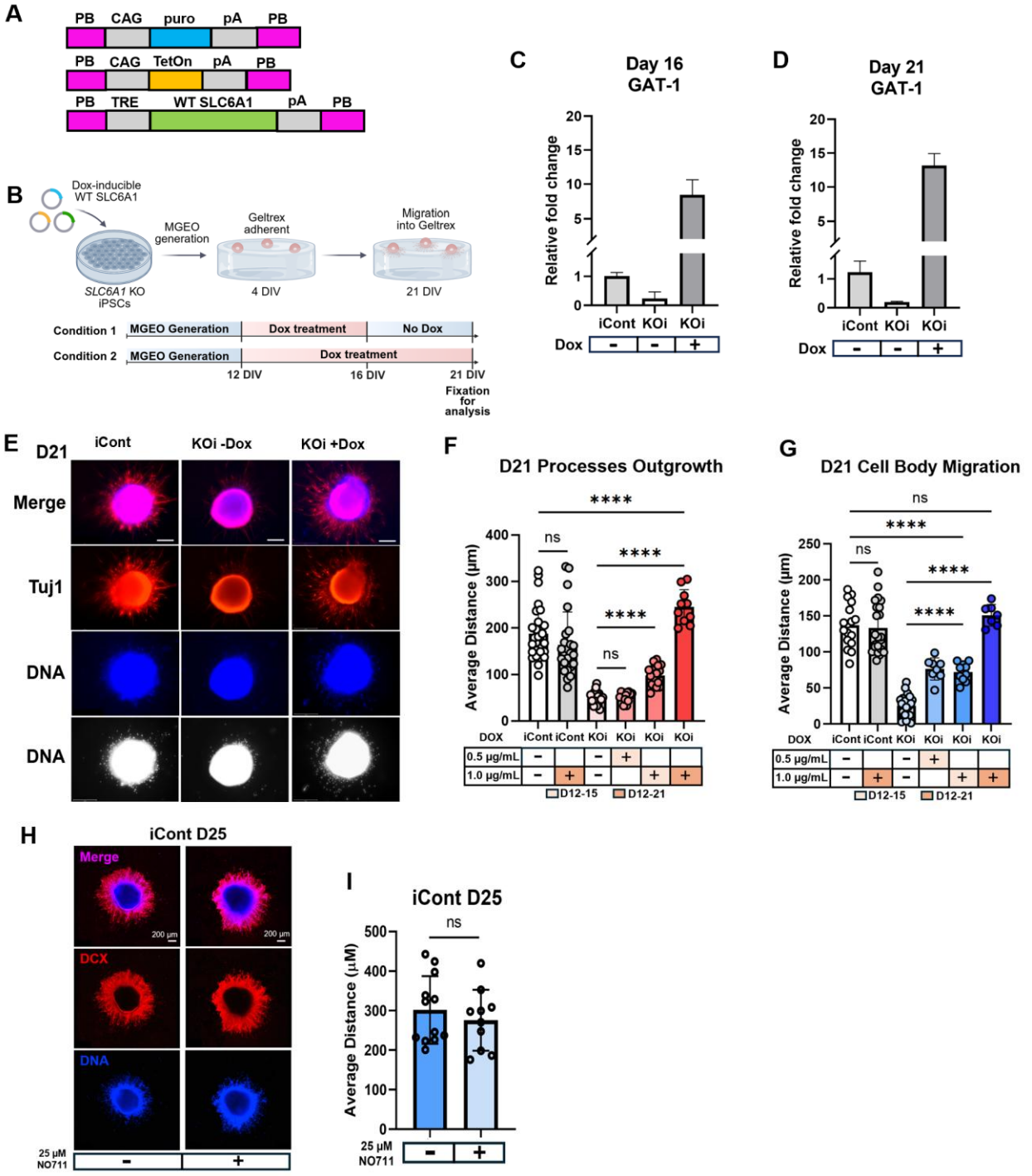

Figure 3.3: Genetic rescue of migratory deficits in GAT1 MGEOs.

(**A, B**) PiggyBac constructs (**A**) and experimental workflow (**B**) for doxycycline (Dox)-inducible *SLC6A1* rescue experiments. (**C, D**) Analysis of GAT1 mRNA expression with (+) or without (-) Dox in DIV 16 (**C**) and DIV 21 (**D**) MGEOs derived from *SLC6A1* Dox inducible KO lines (KOi) and untreated isogenic control (iCont). (**E**) Confocal images showing migrating cells from iCont and KOi DIV 21 MGEOs embedded in ECM and immunolabled for TuJ1 (red) to

identify processes and bisbenzimide labeling (blue) for DNA, which is also pseudocolored white for better visualization of migrated cells. (**F, G**) Quantification of average distance of process outgrowth (**F**) or cell migration (**G**) in iCont and KOi MGEOs without Dox (-) and with two different DOX concentrations (+) for two experimental durations (D12-15) and (D12-21). Each data point represents individual organoids from 3 separate experiments. ****, pval <0.0001; ns, non significant (**H**) Confocal images of doublecortin (DCX)-immunolabeling (red) shows cell migration and process outgrowth from iCont DIV 25 MGEOs 4 days after plating on ECM with (+) or without (-) the addition of the GAT1 blocker NO711. Bisbenzimide DNA labeling in blue. (**I**) Quantification of average cell body migration distance in the presence or absence of the GAT1 blocker NO711. ns, non-significant.

Increases in WT GAT1 mRNA in the KOi MGEOs were confirmed via RT-qPCR at DIV 16 and 21 (**Fig 3.3 C, D**). Migration distance of cell bodies and length of process extension were assessed at DIV 21 after labeling with Hoechst and immunostaining with TuJ1 antibody, respectively (**Fig 3.3 E**). We found that WT *SLC6A1* overexpression in the KOi MGEOs rescued migration and process outgrowth deficits in a Dox dose and duration dependent manner (**Fig 3.3 F-G**). The administration of Dox alone to the iCont MGEOs did not alter migratory behavior, validating that the increase in migration seen in the Dox treated KOi MGEOs was attributed to the induced expression of WT *SLC6A1* and not an artifact of Dox treatment itself (**Fig 3.3 F, G**). We next asked whether inhibiting GAT1 transport activity in control MGEOs would impair interneuron migration. Interestingly, blockade of GAT1 from DIV 12-21 using the GAT1-specific blocker NO711 (also known as NNC-711), at a concentration known to block GAT1 (25 μM), did not inhibit migration from iCont MGEOs at these early timepoints (**Fig 3.3 H, I**). These findings indicate that GAT1 expression is necessary for the initiation and maintenance of migration of MGE-derived interneurons, and that GAT1 may play a non-canonical role in early interneuron migration that is separate from its function as a GABA transporter.

To evaluate the impact of *SLC6A1* loss of function on interneuron migration in a 3-D organoid system, we generated assembloids of mDLX-GFP labeled MGEOs and CAG-TdTom labeled SOSR-COs from iCont, Cont, Het, and PT-derived lines (**Figure 3.4 A**), the latter two groups modeling disease-associated HI. Consistent with our findings above, we observed significantly reduced migration of interneurons into the CO region in all Het and patient groups compared to iCont and Cont (**Figure 3.4 A, B**). Mutant mDLX-GFP+ cells appeared to accumulate at the MGEO-CO junction with very few cells able to cross this boundary. No significant differences were seen between iCont and WT groups.

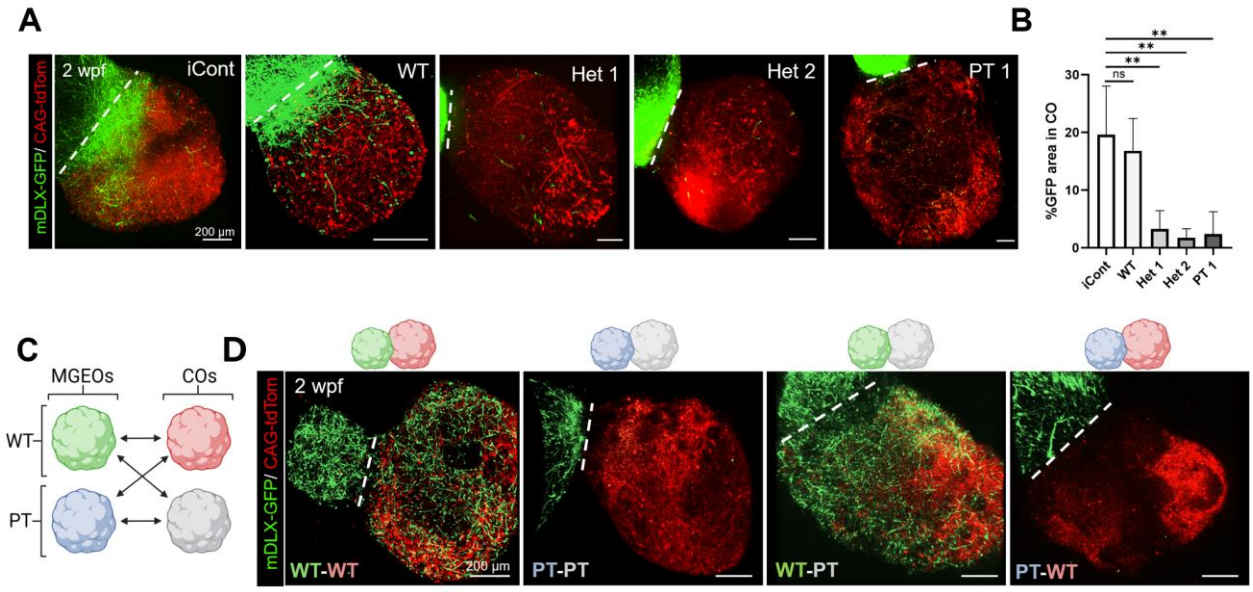

Figure 3.4: SLC6A1 migratory deficits are cell autonomous in MGEO-CO assembloids.

(**A**) Representative live confocal images of MGEO-CO assembloids at 2 weeks post fusion (wpf) and derived from isogenic control (iCont), wildtype (WT), two SLC6A1 heterozygous KO (Het 1, 2) and *SLC6A1* patient (PT1) lines. mDLX-GFP (green) virus labels GABAergic cells originating from the MGEO, and tdTomato (red) labels CO progenitors and putative excitatory neurons. Note decreased MGEO cell migration int COs in HET and PT assembloids. Images are max projections of 150 µm thick assembloid sections. The dashed lines denote the boundary between MGEO and CO. (**B**) Quantification of the average percentage area of mDLX-GFP expression in the CO area ± SD is shown for 6-9 assembloids from 2 separate experimental replicates per cell line for the groups from (**A**). **, p<0,0023; ns, non-significant. (**C**) Schematic representation of assembloid variations in "mix and match" experiments. (**D**) Live confocal images of genotype mixed and matched MGEO-CO assembloids at 2 wpf derived from wildtype (WT) and patient (PT) lines. MGEO migration into assembloids is markedly decreased in assembloids with PT MGEOs, regardless of whether the CO is from the PT or WT, but WT MGEOs show intact migration into PT COs. Images are max projections of 150 µm thick assembloid sections. The dashed lines denote the boundary between MGEO and CO.

We further assessed if the migration deficit reflected cell autonomous or non-cell autonomous effects by creating "mixed and matched" assembloids using Cont or PT COs fused with either Con or PT MGEOs (**Figure 3.4 C**). Defective mDLX-GFP+ cell migration appeared in all conditions containing PT MGEOs, regardless of the CO genotype. A migration deficit was not observed in any condition containing WT MGEOs irrespective of the CO genotype (**Figure 3.4 D)**. Together these findings suggest that GAT1 HI during early development causes a cell-autonomous impairment in MGE cortical interneuron migration, with delays in cortical boundary crossing.

AKT pathway activation rescues migration deficits and network hyperexcitability

Although migratory deficits in neurons resulting from GAT1 reduction has not previously been identified, studies in the field of oncology have identified GAT1 as a modulator of cancer cell migration and invasion (Ji et al., 2021; Y. Zhao et al., 2018). Knockdown of GAT1 in breast cancer cells reduces their migration and metastasis, potentially acting through the PI3K/AKT pathway (Ji et al., 2021). Pan Akt activation in rodents is also known to increase the speed of cortical radial migration (Jossin & Goffinet, 2007) so we questioned if a known AKT pathway activator SC79, which acts downstream of plasma membrane associated pathway regulators, could increase the migration of *SLC6A1* HI interneurons into the cortical organoid, and if so, would the increased number of interneurons in the cortical organoid impact overall network activity.

To answer this question, we generated CO/MGEO assembloids from Cont, iCont, and three *SLC6A1* HI lines (Het 1, Het 2, and PT). Assembloids were given a 1-month untreated period to allow for endogenous migratory behaviors to occur, after which, assembloids were cultured with or without the addition of 10 μM SC79 for 1 month and downstream multielectrode array recordings were acquired from DIV140 until DIV200 (**Figure 3.5 A**). In humans, MGE-derived interneurons continue to migrate until after 2 years of age (Kilb, 2012; Paredes et al., 2016), leaving a potential window of treatment after some migratory deficits have already occurred. The 1-month untreated period prior to drug treatment is designed to assess if treatment after some migration deficit/delay has already occurred will rescue downstream phenotypes.

While short term assessment 2 weeks after fusion showed extremely limited migration of *SLC6A1* HI interneurons as expected (see **Figure 3.4**), longitudinal monitoring of untreated assembloids revealed that a late migratory wave of *SLC6A1* HI mDLX-GFP+ cells, occurring between 2 and 3 months post fusion, was capable of crossing the cortical organoid junction and migrating into the cortical organoid (data not shown); however, the total numbers of GFP+ cells in the cortical organoid region remained greatly reduced compared to controls (**Figure 3.5 B-F′**). In contrast, *SLC6A1* HI assembloids that received SC79 treatment showed a marked increase in GFP+ cells in the cortical region after only 2 weeks of treatment (**Figure 3.5 G-L**).

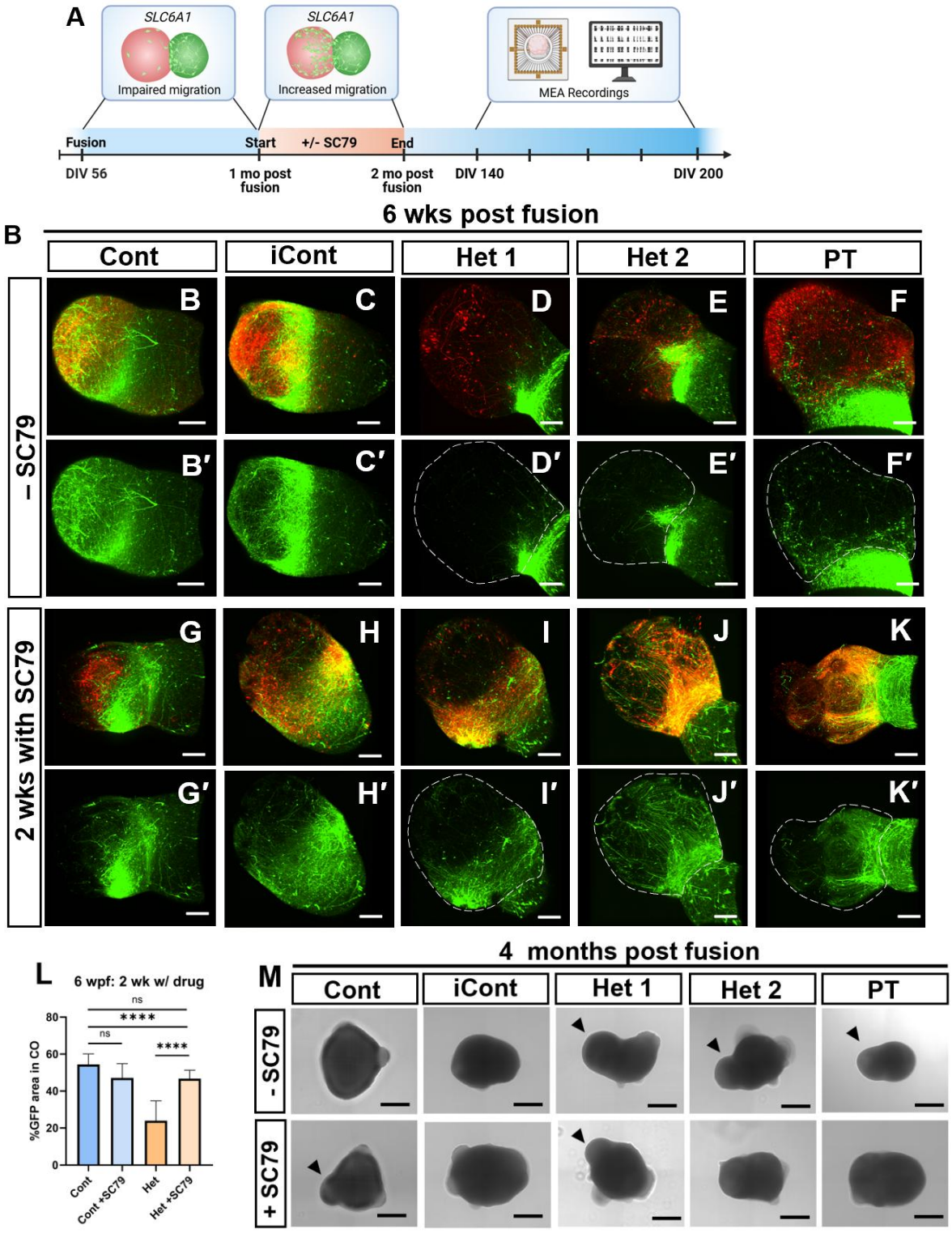

Figure 3.5: Pharmacological rescue of migratory deficits on MGEO-CO assembloids.

(**A**) Schematic of experimental timeline. (**B-K′**) Live confocal images of MGEO-CO assembloids at 6 weeks post fusion (wpf) without (**B-F′**) or with (**G-K′**) AKT activator drug SC79 exposure for 2 weeks. MGEOs and CO assembloids were derived from isogenic control (iCont), control (Cont), two SLC6A1 heterozygous KO (Het 1, 2) and *SLC6A1* patient (PT1) lines. mDLX-GFP (green) virus labels GABAergic cells originating from the MGEO, and tdTomato (red) labels CO progenitors and putative excitatory neurons. (**L**) Quantification of GFP+ area in the CO area after 2 weeks of drug treatment. ****, pval <0.0001; ns, non significant (**M**) Phase contrast images of drug treated and untreated assembloids at 4 months post fusion. Arrows indicate MGEO portion of the assembloid that has not fully merged with the CO.

By 4 months post-fusion, the MGEO region of untreated *SLC6A1* HI assembloid could still clearly be identified in most assembloids (**Figure 3.5 M)**, MGEO region indicated by arrows). In contrast, most SC79 treated *SLC6A1* HI assembloid appeared fully merged by 4 months although a small number retained remnant MGEO regions that had not yet fully merged (**Figure 3.5 M)**, Het 1). While all untreated control MGEOs fully merge with the COs with most reaching this milestone by 2-3 months post-fusion (**Figure 3.5 B-C′, L**), treatment of SC79 in control organoids appeared to slow the migration and merging of some MGEO-CO assembloids (**Figure 3.5 G,G′, L**). While normal or moderately increased Akt activation is necessary to promote the speed of radial migration in rodents, excessive prolonged Akt activation hinders radial migration with neurons remaining stuck in the intermediate zones and unable to enter the cortical plate (Itoh et al., 2016; Jossin & Goffinet, 2007). Our findings suggest that prolonged AKT activation also restricts the migration of tangentially migrating cortical interneurons under control conditions; however, in diseased states where AKT activation is decreased, prolonged AKT activation may ameliorate some migratory deficits.

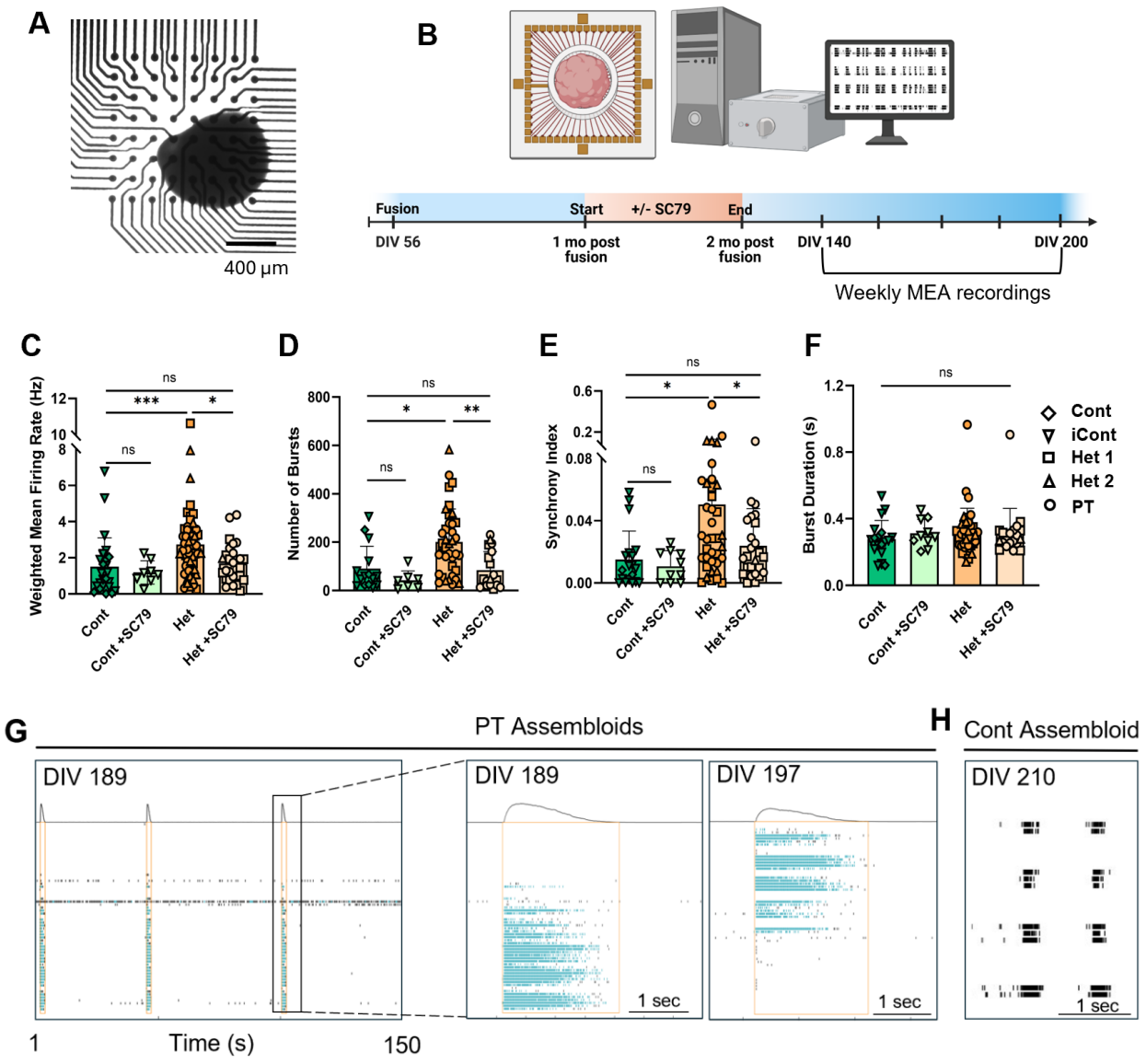

Figure 3.6: Multielectrode array recordings from SC79 treated and untreated assembloids.

(**A**) Phase contrast image of acutely plated assembloid on MEA plate. (**B**) Schematic of experimental timeline. MEA recordings were conducted weekly between 140 DIV to 200 DIV. (**C-F**) Quantification of MEA metrics quantified during 3 minutes of recordings, including weighted mean firing rate (**C**), number of bursts (**D**), synchrony index (**E**), and burst duration (**F**) showing hyperexcitability of Het assembloids which is ameliorated by prior SC79 treatment. (**G**) Representative raster plot and magnified network bursts from two patient-derived assembloids showing occasional aberrant network burst duration of approximately 2 seconds compared to control assembloids (**H**) with typical bust durations lasting less than 1 second. ***, pval <0.001; **, pval <0.002; *, pval <0.033; ns, non significant

To further assess the impact of migration rescue on downstream network activity, MEA recordings were conducted weekly from DIV 140 to DIV 200 on SC79 treated and untreated assembloids from all cell lines (**Figure 3.6 A,B**). Untreated *SLC6A1* HI assembloids displayed increase network excitability with a significant increase in weighted mean firing rates and number of bursts compared to controls. These metrics were corrected to control levels in the *SLC6A1* HI assembloids that received prior SC79 treatment (**Figure 3.6 C,D**). Interestingly, untreated *SLC6A1* HI assembloids displayed earlier network synchrony with a significant increase in their synchrony index compared to controls. This phenomenon was not observed in the SC79 treated *SLC6A1* HI groups (**Figure 3.6 E**). While overall burst duration was not significantly different between groups(**Figure 3.6 F**), some assembloids from the patient-derived line displayed occasional pathological network bursting events with network burst durations far exceeding those of control assembloids (**Figure 3.6 G,H**).

SLC6A1 HI alters MGE GABAergic lineage specification and maturation

With the establishment that deficits in MGE-like interneuron migration contribute to the hyperexcitable phenotype observed in *SLC6A1* HI assembloids, we next asked whether changes in development, maturation, or subtype specification of MGE-derived cortical interneurons may also contribute to aberrant network formation. To address this question, we first conducted bulk RNA sequencing of Cont and KO MGEOs at DIV 21 which coincides with early migration of MGEO-derived interneurons (**Figure 3.7**). Differential gene expression analysis revealed that expression of key MGE lineage markers including LHX6, LHX8, and SOX6 were reduced in KO MGEOs compared to controls (**Figure 3.7 A, D)**. Gene ontology analysis of biological process terms revealed an upregulation of cell adhesion related genes and a down regulation of genes associated with cell migration, neurogenesis, and neuronal differentiation in KOs compared to controls (**Figure 3.7 B, C)**. We further analyzed curated sets of differentially expressed genes associated with MGE lineage, neuronal migration, and synaptic maturation and found that many MGE lineage and migration related genes were downregulated in KO MGEOs compared to control (**Figure 3.7 D, E)**. Interestingly, markers of neuronal maturation including $GABA_A$ receptor gamma subunits and sodium channel *SCN1A* were upregulated while $GABA_A$ receptor beta subunits, generally associated with a more immature state, were downregulated indicating a more mature identity of KO MGEOs compared to control.

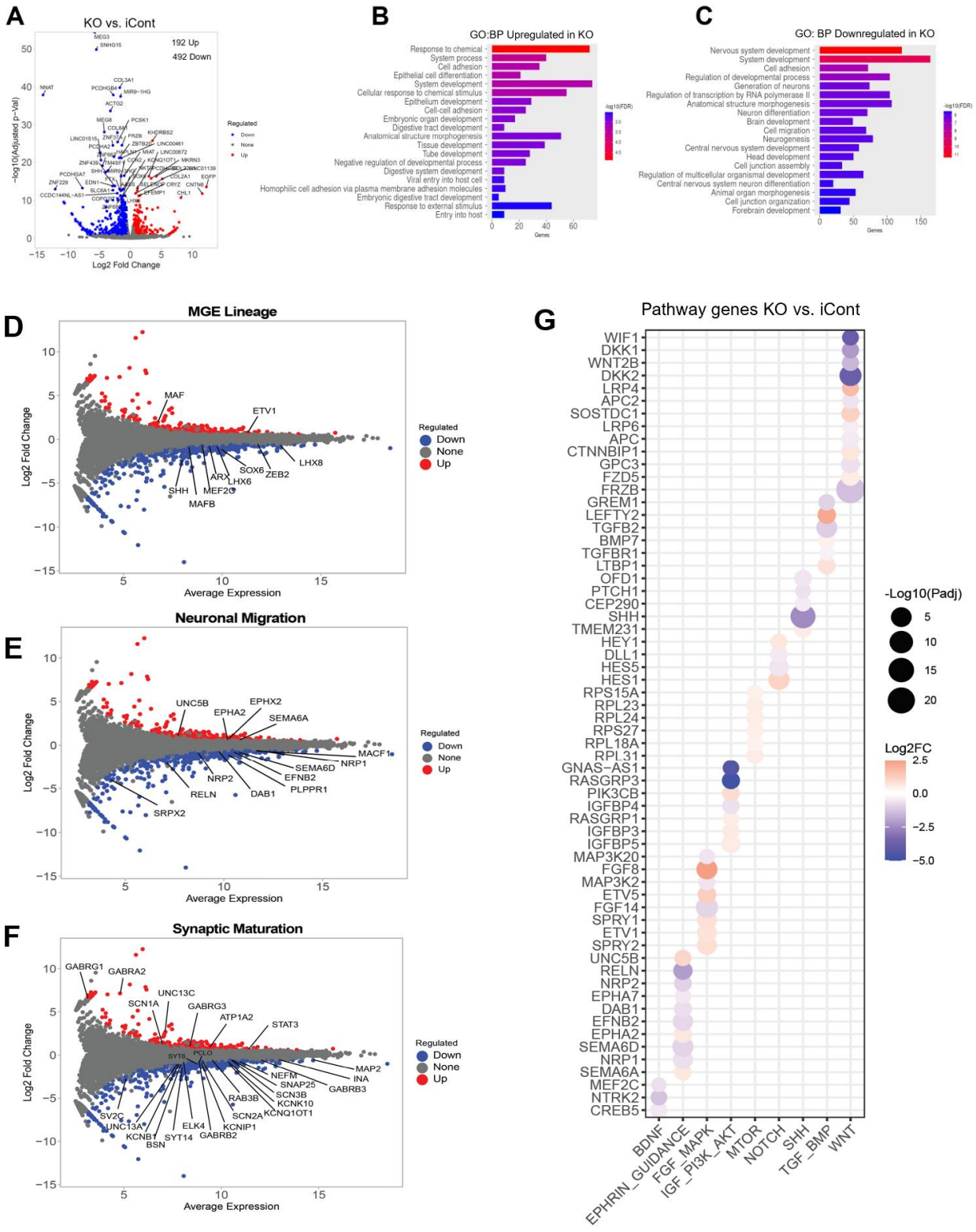

Figure 3.7: Bulk RNAseq analysis of DIV 21 SLC6A1 KO and iCont MGEOs

(A) Volcano plot of the 50 top significant differentially expressed genes in KO vs iCont MGEOs**. (B, C)** Gene ontology analysis for biological process enrichment in KO vs iCont MGEOs

showing terms associated with differentially upregulated genes (**B**) and downregulated genes (**C**). (**D-F**) MA plots of significant differentially expressed genes grouped by their association with MGE lineage (**D**), Neuronal migration (**E**), and synaptic maturation (**F**). (**G**) Bubble plot of significant differentially expressed genes associated with signaling pathways important for MGE neuron specification, migration, and maturation.

Analysis of key signaling pathway related gene revealed that markers indicative of SHH activation, including SHH, and PTCHD1, were reduced in KO compared to WT while WNT pathway inhibitors DKK1 and APC2 were also reduced, indicating that WNT pathway activation is increased while SHH pathway activation is decreased in KO MGEOs despite receiving the same SHH pathway activating morphogens during the differentiation protocol as controls (**Figure 3.7 G)**. These findings suggest that *SLC6A1* loss alters responsiveness to important developmental patterning molecules which alter neuronal lineage specification, migration, and maturation.

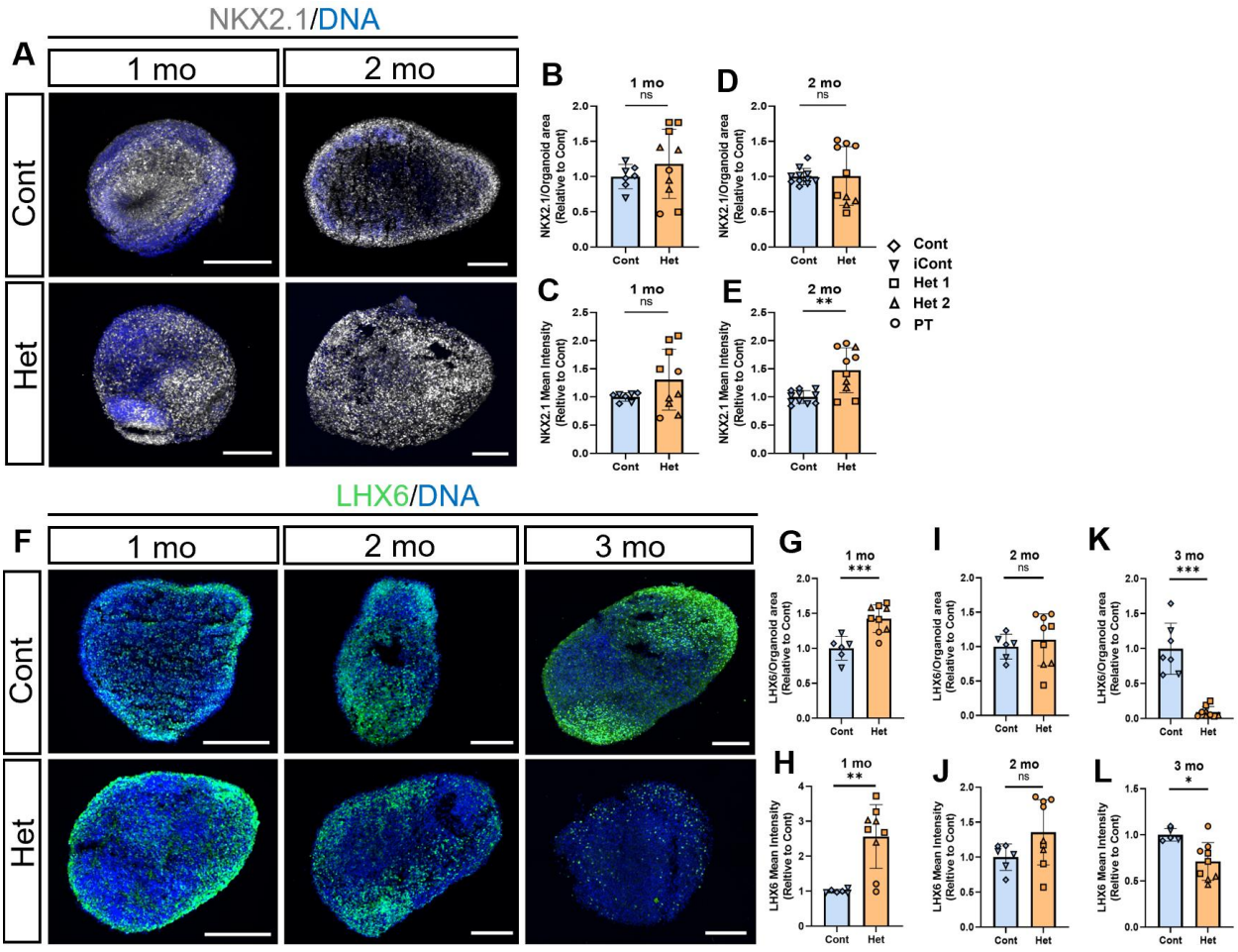

Figure 3.8: Time course of MGE lineage marker expression in control and het MGEOs

(**A**) Representative confocal images of control and het MGEOs immunostained for MGE lineage marker NKX2.1 at 1 month and 2 months in vitro. (**B-E**) Quantification of percent organoid area (**B, D**) and fluorescence intensity (**C, E**) in 1 month and 2 month MGEOs. (**F**) Representative confocal images of control and het MEGEOs immunostained for MGE lineage marker LHX6 at 1, 2, and 3 months in vitro. (**G-L**) Quantification of percent organoid area (**G, I, K**) and fluorescence intensity (**H, J, L**) in 1-, 2-and 3-month MGEOs. All scale bars are 200 μm.

With the insight that early developmental fate specification programs are altered in *SLC6A1* HI, we immunostained MGEOs from *SLC6A1* HI and control lines for markers of MGE lineage commitment, maturation, and GABAergic neuron subtype specification at 1, 2, 3, and 5 months in vitro (**Figure 3.8, 3.9**). We assessed if *SLC6A1* HI MGEOs produce the appropriate MGE lineage progenitors by quantifying the expression of the MGE lineage markers NKX2.1 and LHX6. We found that while *SLC6A1* HI MGEOs produced the same relative amount of NKX2.1+ cells, the expression levels of NKX2.1, quantified by mean fluorescence intensity, was significantly increased in HI MGEOs compared to controls at 2 months (**Figure 3.8 A-D**).

Cortical destined NKX2.1+ MGE populations gradually decrease their expression of NKX2.1 and upregulate the expression of LHX6, while subpallial destined GABAergic neurons that populate the striatum and globus pallidus maintain high levels of NKX2.1 expression throughout maturation. Given the maintenance of high NKX2.1 expression in HI MGEOs, we next evaluated the expression of LHX6. We found that the number of LHX6+ cells was increased at 1 month in mutant MGEOs, consistent with premature differentiation, and unchanged between Hets and controls in 2-month MGEOs; however, a stark decrease of LHX6+ cells was observed in HI MGEOs by 3 months compared to controls, which displayed increased LHX6 expression by 3 months consistent with the upregulation of LHX6 in MGE-derived cortical interneurons (**Figure 3.8 F-L)**. Downregulation of NKX2.1 is required for the initiation of tangential migration of cortical interneurons from the MGE to the cortex and forced overexpression prevents MGE cell migration to the cortex (Du et al., 2008; Nóbrega-Pereira et al., 2008). These findings thus support our previous observation of reduced migration of *SLC6A1* HI interneurons.

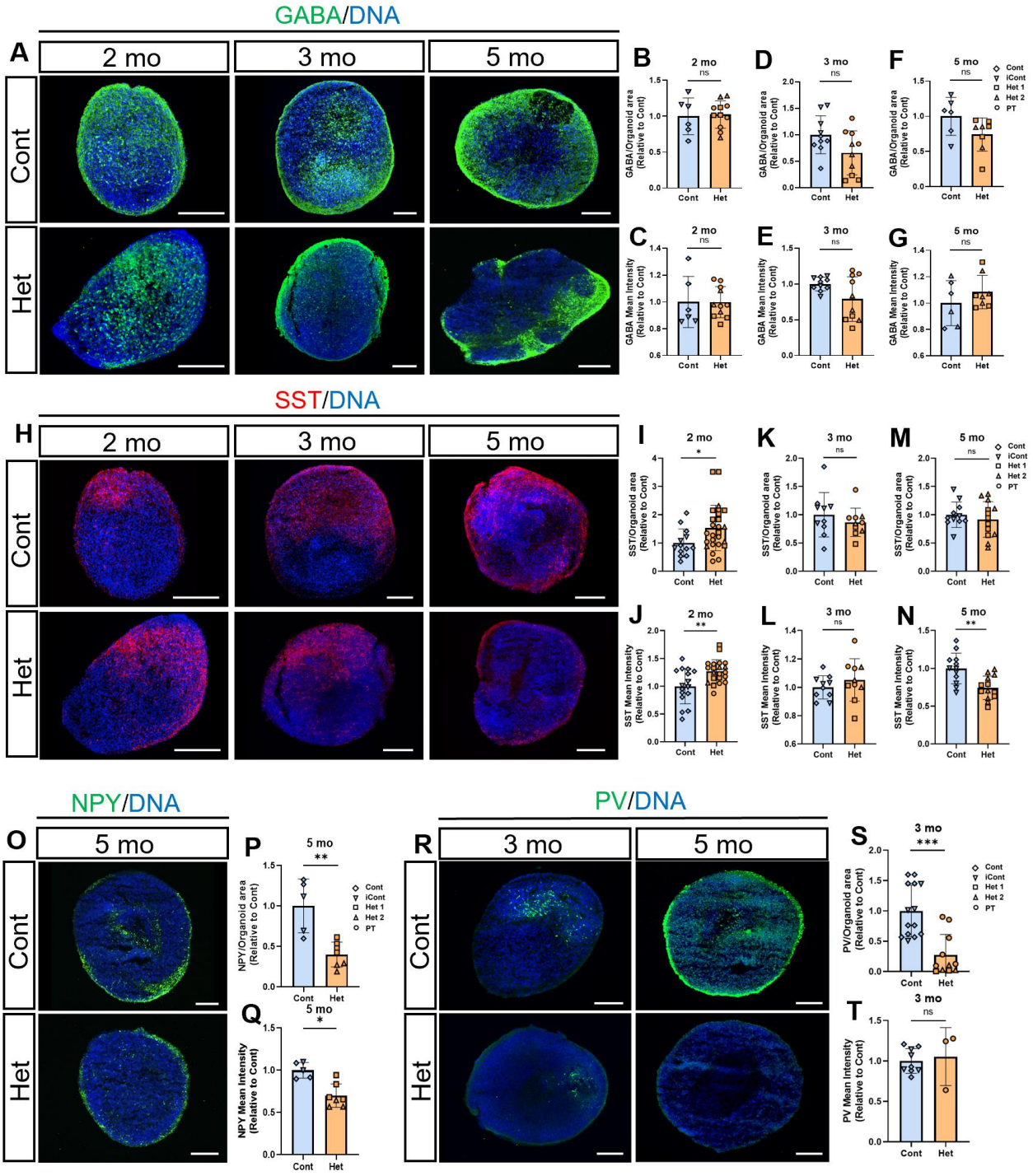

Figure 3.9: Time course of expression of GABAergic neuron subtypes in control and het MGEOs

(**A**) Representative confocal images of control and het MGEOs immunostained for GABA at 2, 3, and 5 months in vitro. (**B-G**) Quantification of percent organoid area (**B, D, F**) and fluorescence intensity (**C, E, G**) in 2-, 3-, and 5-month MGEOs. (**H**) Representative confocal images of control

and het MEGEOs immunostained for MGE neuronal subtype marker SST at 2, 3, and 5 months in vitro. (**I-N**) Quantification of percent organoid area (**I, K, M**) and fluorescence intensity (**J, L, N**) of SST immunoreactivity in 2-, 3-and 5-month MGEOs. (**O**) Representative confocal images of control and het MEGEOs immunostained for MGE neuron subtype marker NPY at 5 months in vitro. Quantification of percent organoid area (**P**) and fluorescence intensity **(Q**) in 5-month MGEOs. (**R**) Representative confocal images of control and het MEGEOs immunostained for MGE neuron subtype marker PV at 3 months in vitro. Quantification of percent organoid area (**S**) and fluorescence intensity **(T**) in 5-month MGEOs. Note: Limited numbers of PV cells were present only in the patient line at 3 months but were no longer present at 5 months. PV cells were not found in any CRISPR edited het lines at either timepoint. For these reasons, PV could not be quantified at 5 months.

To assess interneuron subtype specification and maintenance of subtype identity over time, we immunostained control and HI MGEOs for MGE subtype-specific markers SST, NPY, and PV at 2, 3, and 5 months in vitro (**Figure 3.9**). We additionally assessed the expression of GABA at these same timepoints. Interestingly, we did not observe any significant differences in the % of GABA+ organoid area, nor in immunofluorescence intensity of GABA between HI MGEOs vs controls across all timepoints (**Figure 3.9 A-G**). In assessing MGE interneuron subtypes, we found that SST was significantly increased both in percent of SST+ organoid area and in fluorescence intensity at 2 months in HI MGEOs compared to controls (**Figure 3.9 H-J)**. These differences normalized to control levels at 3 months (**Figure 3.9 H, K, L)**, but mean fluorescence intensity in HI MGEOs significantly decreased at 5 months compared to controls (**Figure 3.9 H, M, N)**. We also found reduced NPY expression at 5 months in HI MGEOs vs controls (**Figure 3.9 O-Q)**. and greatly reduced PV+ cell numbers at all time points with most HI organoids displaying no PV expression (**Figure 3.9 R-T)**. These findings point to shifts in interneuron subtype allocation with an early bias for generating SST+ interneurons at the expense of NPY and PV interneurons. The reduction of all assessed interneuron marker expression at 5 months could suggest a failure to maintain MGE lineage identity or an increased vulnerability of MGE lineages to cell death at later stages of development.

3.5 Discussion

The *SLC6A1* gene has been difficult to study in human model systems due to its limited endogenous expression in existing cerebral organoid and 2D neuronal models, likely reflecting the lack of MGE lineages in these models, particularly PV cortical interneurons. Enrichment of GAT1

in the cortex is found on presynaptic axon terminals of symmetrical synapses on the soma and axon initial segment, characteristic of PV basket and axoaxonic cells (Inda et al., 2007; Melone et al., 2014) which MGEOs readily produce (see Chapter 2). *SLC6A1* variant overexpression models provide insight into effects on transporter function (Mermer, Poliquin, Rigsby, Rastogi, Shen, Romero-Morales, Nwosu, McGrath, et al., 2021; Piniella et al., 2023; J. Wang et al., 2020b) but cannot address the potential role of endogenous GAT1 during early brain development. Animal models also do not fully recapitulate MAE disease phenotypes (Chiu et al., 2005; Cope et al., 2009; Guo et al., 2025). Here we identify a novel MGE interneuron migration deficit in *SLC6A1* mutant MGEOs and assembloids. Migratory phenotypes have not been reported in mouse models of *Slc6a1* developmental and epileptic encephalopathy. However, a recent study of AAV9/h*SLC6A1* gene therapy administered to *Slc6a1* mutant mice at various timepoints from P0 to P28 found that only administration at P0 fully rescued abnormal behavioral and electrophysiological phenotypes in heterozygous and knockout mice, but administration at P5 or beyond did not (Guo et al., 2025). Mouse MGE interneurons complete their migratory journey to the cortex by P7 with the GABA polarity switch occurring by P5. The results of this study point towards the migratory window prior to the GABA polarity switch as the most effective treatment window to halt epileptogenisis.

These findings suggest that events occurring during early brain development underlie the pathogenic phenotypes in *SLC6A1* DEE and highlight the importance of early intervention to treat this disorder. Our results support this idea by identifying that full and prolonged expression of GAT1 throughout the migratory period is required for the proper migration of MGE-derived cortical interneurons. Interestingly, we could not replicate migration defects in WT MGEOs using a highly specific GAT1 blocker, NO711, applied at a concentration established to fully block GABA transport (Davies & Shakesby, 1999; Matthews et al., 2009; Hu & Davies, 1997). This finding suggests that early migration defects do not involve GAT1 transporter dysfunction. Indeed, prior work suggests that GAT1 may not function as a transporter until later developmental timepoints (Conti et al., 2004; Jursky & Nelson, 1996), and one study showed that blockade of GAT1 in E14.5 mouse telencephalic slice co-cultures did not alter the pattern of MGE tangentially migrating cells (Cuzon et al., 2006). While the exact mechanism of how GAT1 regulates early interneuron migration requires further investigation, we show that transient AKT pathway activation in *SLC6A1* assembloids during migratory periods increases interneuron CO boundary crossing, process extension and migration into the cortical region. Furthermore, this increased

interneuron migration resulted in an amelioration of the hyperexcitability phenotype of *SLC6A1*-deficient assembloid activity recorded using an MEA system, suggesting that cortical hyperexcitability linked to *SLC6A1* deficiency results from deficits in interneuron migration (or interneuron subtype specification). Because human MGE-derived cortical interneurons continue to migrate and mature until approximately 2-3 years of age (Nascimento et al., 2023; Paredes et al., 2016; Sanai et al., 2011), they are a plausible target for early treatment interventions. Since AKT pathway activation has broad downstream effects, further work is needed to identify more specific, druggable mediators of the migration rescue for use in clinical applications.

While the migration deficits appear to underlie part of the disease mechanism, we propose that alterations in MGE lineage specification, maturation and subtype specification which stem from altered sensitivity to developmental morphogens could have compounding consequences at later developmental timepoints. In support of this idea, we found broad dysregulation of developmental signaling pathways important for interneuron lineage specification and maintenance, development, maturation, and migration including significant alterations in SHH, WNT, FGF/MAPK, BDNF, PI3K/AKT, MTOR, NOTCH, and TGF/BMP signaling pathways in DIV 21 MGEO compared to controls. A careful balance between SHH and WNT signaling is necessary for the proper specification and maintenance of MGE lineage identity in cortical interneurons. The expression of NKX2.1 and subsequent induction of LHX6 is regulated by SHH and FGF8 signaling, and downregulation of NKX2.1 in cortical-destined MGE interneurons is necessary for their tangential migration to the cortex (Du et al., 2008; Nóbrega-Pereira et al., 2008). Our observed alteration in FGF8 and SHH signaling in KO MGEOs along with maintained high NKX2.1 expression with reduced LHX6 expression at later timepoints in Het MGEOs could also contribute to the migratory deficits of Het and KO MGEOs. PI3K/AKT signaling has been shown to regulate NKX2.1 expression through interactions with FOXO1 (Zhong et al., 2022). However, it remains to be seen if our experiments using the AKT pathway activator, SC79, resulted in normalization or reduction of NKX2.1 expression during the treatment window, and if this contributed to the rapid increase in migration in SC79 treated Het MGEOs.

BMP is also known to regulate cortical GABAergic neuron differentiation (Mabie et al., 1999; Yung et al., 2002) and endogenous BMP signalling influences the migration of GABAergic neurons (Li et al., 1998; Mabie et al., 1999). Bmpr1a/b mutant mice show premature SST expression and a strong increase in SST+ interneurons in the somatosensory cortex at P0.

However, the increased number of SST+ interneurons did not persist by P21. This reduction of SST+ interneurons at later vs. early timepoints was not due to cell death. Additionally, reductions in PV+ interneurons were also observed but no change in overall GABAergic cell numbers were observed (Mukhopadhyay et al., 2009). Our results in MGEOs mirror these findings with an early, transient upregulation of SST expression which did not persist at later timepoints, reduction in PV+ interneurons, and unchanged total GABAergic neuron numbers, suggesting that these phenomena may also be linked to decreased BMP signalling. In support of this hypothesis, LEFTY2, a repressor of BMP signalling, was significantly upregulated in DIV 21 KO MGEOs compared to controls, while other markers of BMP signalling were downregulated, indicating reduced BMP signalling in KO MGEOs.

While the alterations in signalling pathway-related gene expression was striking, our RNAseq analysis was restricted to KO MGEOs which may present with a more severe phenotype. Therefore, the effects of *SLC6A1* HI on developmental signalling pathways may be less severe. All known patient variants are heterozygous indicating that full KO in humans, with severe alterations in signalling pathways, as observed in our study, would result in non-viable progeny. However, a recent mouse study provides evidence that developmental signalling pathways are also altered in heterozygous animals (Liu et al., 2025). BDNF levels in both Het and homozygous knock-in mice carrying the S295L variant were found to be significantly decreased in the hippocampal dentate gyrus at all observed timepoints. Alterations in progenitor dynamics and neurogenesis of dentate gyrus granule cells were also observed (Liu et al., 2025), supporting our finding that *SLC6A1* reduction in early brain development affects neuronal maturation, and fate specification. In accordance with this animal study, we also observed a decrease in the expression of BDNF pathway-related genes in DIV 21 KO MGEOs. Or results, taken together with the findings in animal studies, indicate that changes in signalling dynamics caused by *SLC6A1* reduction affect multiple brain regions and alter the development of both excitatory and inhibitory neurons.

Here we propose that *SLC6A1*-related neurodevelopmental disease may arise from a two-phase mechanism with an early transporter-independent disruption of signaling or altered maturation leading to impaired migration, followed by later network-level consequences that are exacerbated by impaired GABA homeostasis. This reframed model provides potential answers to why some *SLC6A1-related* DEE patients retain normal or near-normal transporter function and

surface protein expression yet still present with symptom of epilepsy or intellectual impairments. More broadly, it suggests that solute carrier proteins traditionally viewed as transporters may exert temporally restricted, non-canonical roles during early corticogenesis that include the regulation of developmental signaling pathways, vastly broadening the scope for identification of potential treatment targets for *SLC6A1* DEEs.

Notes on Chapter 3

Portions of this chapter are included in modified form in a manuscript currently under revision for publication. It is available as a preprint under:

Varela, M. C., Walker, M. P., Bok, J., Crespo, E. L., Thenstedt, T., Goldstein, L., Tidball, A. M., Yuan, Y., Isom, L. L., Fu, J., Uhler, M., & Parent, J. M. (2025). Human Medial Ganglionic Eminence Organoids Robustly Generate Parvalbumin Interneurons and Fast-Spiking Neurons and Reveal Migratory Deficits in SLC6A1 Deficient Interneurons. BioRxiv, 2025.07.01.662594. https://doi.org/10.1101/2025.07.01.662594

Contributions: All experimental conceptualization and execution, data analysis, and figure generation in this chapter was conducted by me. I generated and CRISPR edited all iPSC lines from fibroblasts and patient blood samples as well as control and isogenic control lines with guidance of Andrew Tidball and Sandra Mojica-Perez. Michael Uhler generated the *SLC6A1* Dox inducible rescue vector and clones from my *SLC6A1* KO line and I conducted all clone validation and rescue experiments. All bulk-RNAseq analysis and figure generation was conducted by me. Undergraduate students under my training, Tyler Thenstedt, Leah Goldstein, and Reeya Sannake assisted with select experimental assays and data analysis.

Chapter 4 Dissertation Summary and Future Directions

4.1 Summary of results

Epilepsy, a common and often severe neurological disorder, is characterized by spontaneous recurrent seizures resulting from hyperexcitable neural network activity, yet a fundamental gap remains in understanding how epilepsy-associated gene variants alter early human brain development resulting in this long-term network hyperexcitability. While many epilepsy genes have been studied in the context of resulting electrophysiological changes at the cellular and network level, far less is known about how they influence the development of crucial inhibitory neuron populations that are responsible for establishing the excitation–inhibition balance in the human cortex. In this dissertation, I aimed to elucidate how haploinsufficiency (HI) of *SLC6A1* alters MGE-derived interneuron development in a human context by using a hPSC-derived MGE organoid protocol that we established (described in Chapter 2). This approach enabled the focused interrogation of MGE-specific interneuron development in the context of *SLC6A1* HI. We unexpectedly found that *SLC6A1* variants severely impair MGE-derived cortical interneuron migration, and that AKT pathway activation during migratory relevant timepoints rescued this phenotype. This rescue was also associated with normalization of the subsequent network hyperexcitability phenotype observed in *SLC6A1* deficient organoids. In addition, we found that *SLC6A1* HI alters MGE cortical interneuron lineage specification, maturation, and interneuron subtype composition, including changes in PV, SST, and NPY populations. Together, these findings suggest that *SLC6A1* contributes to epilepsy pathogenesis not only through synaptic mechanisms, but also by perturbing multiple stages of human interneuron development, ultimately compromising inhibitory circuit formation and network stability.

MGE organoid development recapitulates human MGE interneuron development and lineage specification.

The MGE is the primary source of cortical PV+ and SST+ interneurons in the mammalian brain. These cell types are essential for establishing excitation–inhibition balance in the cortex and their disruption has been strongly implicated in epilepsy and other neurodevelopmental disorders. However, many early human forebrain and cortical organoid models have incompletely recapitulated ventral telencephalic patterning, often lacking the specification of PV lineages. In addition, endogenous *SLC6A1* expression has been low or absent in existing subpallial organoid models, restricting their utility for studying developmental consequences of *SLC6A1* HI. These limitations highlight the need for a human organoid model that robustly and specifically generates bona fide MGE progenitors and downstream interneuron lineages. Such a model would enable mechanistic interrogation of genes such as *SLC6A1* within the appropriate developmental context.

Previous studies using 2D directed differentiation protocols and ventralized forebrain organoids have demonstrated that morphogen-based patterning strategies can induce NKX2.1+ progenitors and produce migrating interneuron populations similar to those derived from the human MGE (Bagley et al., 2017; Bershteyn et al., 2023; Birey et al., 2017; Maroof et al., 2013; Nicholas et al., 2013; Xiang et al., 2017). These models have provided key insights into interneuron progenitor proliferation, tangential migration, and early subtype bias, and have revealed human-specific features of interneuron development that are not captured in rodent systems. Nevertheless, challenges remain in achieving high regional specificity, sustained MGE lineage fidelity, and robust generation of later-born interneuron subtypes, particularly PV-lineage cells, at levels sufficient for disease modeling.

The data presented in Chapter 2 of this dissertation describe the development and characterization of an MGE organoid (MGEO) model that is highly specific for MGE-derived lineages and recapitulates transcriptional profiles and key characteristics of human MGE interneuron development. Through optimized patterning and validation strategies, we show that MGEOs robustly generate NKX2.1+ progenitors and postmitotic LHX6+ cortical interneuron lineages, and give rise to downstream interneuron populations, including SST+ and PV+ interneurons. Importantly, we demonstrate that MGEOs endogenously express high levels of *SLC6A1,* providing a human-relevant platform for investigating how *SLC6A1* HI alters MGE

lineage development and specification. While the MGEO model provides insight into MGE interneuron developmental timing and confirms that their lineage specification follows cell-intrinsic programs, it also opens the door for additional avenues of investigation to answer important developmental questions. What molecular mechanisms govern the divergence of SST+ and PV+ interneuron lineages in the human MGE, and how are these processes temporally regulated? What are the transcriptomic signatures that differentiate distinct migratory waves in the human MGE and what is the downstream subtype specification of neuroblasts that comprise each migratory wave?

What are the molecular mechanisms that cause divergence of SST and PV lineages

The majority of SST+ and PV+ cortical interneurons are generated in the MGE and migrate to the cortex where they perform distinct but complementary functions in shaping cortical circuit dynamics. Although both lineages arise from NKX2.1+ progenitors and share early developmental marker expression, they later diverge in their molecular identity, morphology, connectivity, and electrophysiological properties as they progress through embryonic and early postnatal development. Dysfunction of both SST+ and PV+ interneuron subtypes have been identified in epilepsy and other neurodevelopmental disorders. While previous studies have defined key transcription factors and temporal patterning cues involved in interneuron development (Asgarian et al., 2022; Du et al., 2008; Ericson et al., 1995; Flandin et al., 2011; Maroof et al., 2013; Tyson et al., 2015), the molecular mechanisms that drive the divergence of SST and PV lineages in the human MGE remain largely unclear, particularly at the level of progenitor fate competence and early lineage priming.

Seminal work in rodent systems has identified important transcription factors such as LHX6, SOX6, SATB1, and signaling pathways such as SHH which serve as regulators of interneuron maturation and subtype specification. Additional studies have provided evidence to suggest that temporal patterning also contributes to SST versus PV fate bias (Butt et al., 2005; Miyoshi et al., 2007; Tyson et al., 2015). Recent single-cell transcriptomic studies in human fetal tissue have begun to uncover transcriptomic profiles of progenitor populations, yet the dynamic changes in signaling pathways that bias one lineage over the other remain poorly defined. To fully understand how interneuron subtypes emerge in MGEOs, it would be beneficial to follow cells as they transition from early NKX2.1+ progenitors into more defined lineages such as SST and PV

interneurons. To accomplish these processes, one could use a time-resolved single-cell multiomic approach to measure both gene expression and chromatin accessibility using scRNA-seq and scATAC-seq in the same cells. By sampling organoids at several key developmental stages, one could reconstruct lineage trajectories and see how progenitor cells gradually commit to distinct interneuron fates. Combining this dataset with RNA velocity (La Manno et al., 2018) and pseudotime analyses (Trapnell et al., 2014) would allow us to infer the direction of cell-state transitions and identify early transcriptional and epigenetic features that predict whether a progenitor is likely to become an SST- or PV-lineage interneuron.

Once candidate regulators have been identified, their functions could be directly tested using CRISPR interference or activation (CRISPRi/a) (Gilbert et al., 2014). These methods allow for selective dampening or enhancing expression of these genes within MGEOs. Coupling these perturbations with single-cell transcriptomic profiling, for example using Perturb-seq (Dixit et al., 2016), would reveal not only which transcription factors or signaling pathways are necessary or sufficient for SST versus PV fate specification, but also whether lineage divergence is intrinsically coded at the progenitor stage or determined later during postmitotic maturation.

Using the knowledge gained from these experiments, small-molecule modulation of key pathways could be optimized using high-throughput screening platforms to identify conditions that selectively expand PV-primed progenitors while suppressing alternative fates such as SST specification. Downstream validation using single-cell transcriptomics and electrophysiological characterization would confirm lineage purity and functional maturation. Together, these approaches would enable the intentional and scalable production of enriched PV+ interneuron populations, providing powerful tools for disease modeling, cell therapy exploration, and mechanistic studies of PV-specific vulnerability in epilepsy and other neurodevelopmental, neurodegenerative, and psychiatric conditions.

Decoding migratory waves in the human MGE

The tangential migration of interneurons from the MGE to the developing cortex occurs in temporally and molecularly distinct waves that are essential for establishing appropriate cortical circuitry. In rodents, early- and late-born populations of MGE interneurons exhibit differences in migratory behavior, laminar distribution, and eventual subtype identity (Butt et al., 2005; Miyoshi et al., 2007; Valcanis & Tan, 2003; Wichterle et al., 1999; Wonders & Anderson, 2006), suggesting that migration timing and dynamics are tightly coupled to lineage specification. The prolonged

window of neurogenesis and expanded progenitor diversity in human fetal development hints at the possibility that distinct migratory waves from the human MGE may be even more transcriptomically nuanced and may result in unique fate biases. While single-cell studies have begun to define progenitor and postmitotic populations, it is largely unclear what transcriptomic signatures define distinct migratory waves in the human MGE and how the neuroblasts within each wave are primed toward specific downstream interneuron subtypes.

Previous single-cell RNA-seq analyses of human ganglionic eminences have identified transcriptionally distinct progenitor and postmitotic interneuron populations (Keefe et al., 2023; Shi et al., 2021; Z. Zhao et al., 2022), and rodent birthdating experiments have linked temporal origin to SST versus PV fate bias (Valcanis & Tan, 2003; Q. Xu, Cobos, De La Cruz, et al., 2004b). However, the dynamic molecular states of migratory populations in human systems, and the relationship between migratory transcriptional signatures and eventual subtype identity remains poorly defined. To dissect these relationships in MGEOs, dox-inducible CRISPR-Cas9-based lineage recording systems such as iTracer (He et al., 2021) or STICR (Bandler et al., 2021; Delgado et al., 2021) could be used to label neuroblasts during multiple temporally defined migratory waves. These methods integrate a synthetic barcode reporter along with a doxycycline inducible cas9 cassette which can be conditionally activated to create unique "scars" (indels) on the synthetic barcode region. Each cell's scar pattern is subsequently inherited by their progeny. Cas9-mediated edits can then be activated at precise developmental windows corresponding to early, mid, or late migratory populations of interneurons. Single-cell RNA-seq coupled with STICR barcode sequencing would then allow simultaneous recovery of transcriptomic states and lineage identity, enabling reconstruction of the transcriptomic signatures unique to each migratory wave and prediction of downstream subtype specification. Spatial transcriptomic approaches could also be used to preserve positional context, distinguishing ventricular zone progenitors, intermediate progenitors in the outer subventricular zone-like space, and actively migrating interneurons. This strategy would identify gene expression modules, surface markers, and signaling pathways unique to each migratory cohort and generate predictive maps linking early migratory states to downstream subtype trajectories. Concurrent utilization of a PV reporter line and/or SST and PV subtype-specific viral labeling (Furlanis et al., 2025) during these experiments could further focus the transcriptomic characterization down to the subtype level.

Collectively, these experiments would establish a developmental framework linking human MGE migratory dynamics to interneuron subtype allocation. Defining transcriptomic signatures of discrete migratory waves would not only illuminate fundamental principles of human interneuron development but also provide a mechanistic lens through which to interpret disease-associated disruptions. Moreover, the identification of specific cell surface markers would allow for enrichment of specific migratory populations for cell therapy purposes.

SLC6A1 HI alters cortical interneuron migration, maturation, and subtype specification

SLC6A1 encodes GABA transporter 1 (GAT1), a critical regulator of extracellular GABA levels and inhibitory neurotransmission, and pathogenic variants in this gene are strongly associated with developmental and epileptic encephalopathies. While GAT1 has traditionally been studied in the context of synaptic GABA reuptake, its potential roles during early human interneuron development remain poorly understood. Chapter 3 of this dissertation investigated how *SLC6A1* HI alters MGE-derived cortical interneuron development using both CRISPR-edited and patient-derived human MGEOs. Using molecular, cellular, and functional analyses, this chapter defines developmental mechanisms through which *SLC6A1* variants may predispose neural circuits to hyperexcitability.

The data presented in Chapter 3 of this dissertation suggest that *SLC6A1* HI disrupts multiple stages of human MGE interneuron development. We found that all Het and KO CRISPR-edited and patient-derived MGEOs exhibited reduced migration of cortical interneurons, and that this migratory impairment is cell autonomous and not dependent on the genotype of the cortical environment. Furthermore, we found that *SLC6A1* HI organoids show altered MGE lineage marker expression, including a significant increase in the expression levels of NKX2.1 by 2 months and reduced LHX6 expression by 3 months, suggesting disrupted MGE cortical interneuron lineage commitment. Mutant interneurons also displayed signs of accelerated maturation, marked by earlier expression and upregulation of GABA and KCC2 and an upregulation of mature GABA receptor subunit types. Interestingly, the levels of GABA in HI MGEOs normalized after 2 months and were not significantly different from controls through the 5-month timepoint. We then assessed the distribution of interneuron subtypes and found a transient overexpression of SST at 2 months which subsequently fell below control levels by 5 months. NPY and PV expression were also reduced at 5 months, indicating long-term shifts in interneuron subtype composition.

Together, these findings demonstrate that *SLC6A1* HI alters fate commitment, migratory behavior, maturation timing, and interneuron subtype allocation, which could lead to changes in in inhibitory circuit assembly.

An important feature missing from these studies is a precise understanding of GAT1 protein localization and dynamics throughout human cortical development. Commercially available antibodies against GAT1 lack specificity, limiting interpretation of when and where GAT1 functions during progenitor, migratory, and maturation stages. Fluorescent tagging of the GAT1 protein would allow high-resolution spatiotemporal mapping of GAT1 localization in MGEOs and cortico-subpallial assembloids. Such studies would clarify when and where GAT1 protein is expressed, and could help elucidate its function in progenitors, migrating interneurons, synaptic compartments, astrocytes, or specialized subcellular domains such as primary cilia during development. Using iPSC lines with fluorescently tagged GAT1, several outstanding questions could be answered. What is the contribution of astrocytic GAT1 in healthy cortical development and to the pathogenesis of *SLC6A1*-DEEs? How does *SLC6A1* HI influence the development and integration of cortical excitatory neurons, thereby affecting network balance beyond interneuron-autonomous mechanisms? And what is the functional role of GAT1 in primary cilia (Kostyanovskaya et al., 2025; Loukil et al., 2025), and how might altered GAT1 ciliary expression contribute to disease states? Additionally, we were not able to directly assess GAT1 transporter function in these studies leaving open questions regarding the contribution to GABA uptake in the observed phenotypes. When does GAT1 begin to acquire its transport function during human development and how is this timeline altered in *SLC6A1*-DEE? What are the intrinsic or environmental factors that initiate this change? To assess the kinetics of GABA clearance from the extracellular space, genetically encoded, membrane-tethered, GABA sensors such as iGABAsnFR2 (Kolb et al., 2026), which emits a fluorescent signal upon the binding of GABA, could be used in control and *SLC6A1*-mutant MGEOs. Live imaging and quantification of the fluorescence intensity decay time, indicative of extracellular GABA clearance, could be conducted at basal levels and upon stimulation of the network either pharmacologically, electrophysiologically, or ontogenetically at various developmental timepoints in MGEOs alone and in assembloids. Specific pharmacological blockade of GAT2 and GAT3 during these experiments would isolate the uptake mediated by GAT1 alone and could provide clues to the efficiency of GAT1 transporter function as neurons progress through maturation. Addressing these

questions will be essential for fully defining the developmental roles of GAT1 and for understanding how *SLC6A1* variants reshape cortical circuit formation.

What is the contribution of astrocytic GAT1 to the pathogenesis of SLC6A1-DEE?

Astrocytes play a central role in regulating extracellular neurotransmitter homeostasis, synaptic maturation, network stability, and more recently appreciated, neuromodulation (A. B. Chen et al., 2025; Guttenplan et al., 2025; Lefton et al., 2025). GAT1, encoded by *SLC6A1*, is not only expressed in interneurons, but also in astrocytes, to a lesser extent, in the cortex, where it contributes to GABA uptake, GABA degradation, and modulation of tonic inhibition. In contrast, GAT1 in the thalamus is expressed exclusively on astrocytes (De Biasi et al., 1998). Thalamocortical circuits are strongly implicated in absence seizures, a seizure type in myoclonic-atonic epilepsy associated with *SLC6A1* variants, suggesting that astrocytic GAT1 may also play an important role in modulating thalamo-cortical network activity. Most studies of GAT1 have focused on neuronal dysfunction, with only a few rodent and cellular overexpression studies focusing on transporter function/dysfunction in astrocytes (Mermer et al., 2022; Mermer et al., 2021). The contribution of endogenous astrocytic GAT1 to cortical and thalamic network development and its role in disease pathogenesis remains largely undefined. Given the growing appreciation of astrocytes as active regulators of circuit assembly and excitability, it is critical to determine whether astrocytic GAT1 dysfunction contributes to hyperexcitability and/or altered neuron development in *SLC6A1*-DEE.

Previous work in rodent models suggests that astrocytic GAT1 regulates tonic GABA currents and seizure susceptibility (Mermer et al., 2022; Moldavan et al., 2017), while conditional deletion studies have demonstrated that glial GABA transport can influence network excitability (Wagner et al., 2026). However, astrocyte-specific roles of GAT1 during human cortical development have not been examined in a disease-relevant human context. To follow this line of investigation, MGEOs and cortical organoids could be generated from iPSC lines carrying an astrocyte-specific *SLC6A1* knockdown using allele-specific inducible CRISPRi under the astrocyte-specific promoter *ALDH1L1* (Gilbert et al., 2013, 2014; Koh et al., 2017; Nave et al., 2016; Smith et al., 2015). Single-cell RNA-seq and spatial transcriptomics could be used to determine whether astrocytic GAT1 loss alters GABAergic or glutamatergic developmental landscapes. Electrophysiological experiments using multielectrode arrays and patch-clamp

recordings could assess network synchrony and tonic inhibition, respectively. Alternatively, 2D neuron-astrocyte tri-cultures containing wildtype inducible excitatory and inhibitory neurons cultured with patient or CRISPR gene edited transcription factor induced astrocytes, could be used to rapidly assess the impact of astrocytic GAT1 loss at the network or single cell resolution. These experiments would reveal whether astrocytic GAT1 deficiency alone is sufficient to disrupt network balance and whether it can alter interneuron migration and maturation as we observed in our global *SLC6A1* HI model.

To assess circuit-level consequences relevant to thalamocortical networks, thalamic, cortical, and MGE organoids could be fused to generate assembloids that model thalamocortical circuitry. Comparing astrocyte-specific and neuron-specific *SLC6A1* perturbations within these assembloids would clarify cell-autonomous versus non-cell-autonomous contributions to network dysfunction. Together, these experiments would elucidate the developmental and circuit-level role of astrocytic GAT1 and provide mechanistic insight into how glial dysfunction contributes to *SLC6A1*-DEE, potentially revealing astrocyte-targeted therapeutic strategies.

How does SLC6A1 HI affect the development of cortical excitatory neurons?

Cortical circuit assembly depends on the coordinated development of excitatory projection neurons and inhibitory interneurons, with precise timing of neurogenesis, migration, and synaptic maturation required from both cell types to establish balanced networks. Although GAT1 has primarily been studied in the context of inhibitory signaling, GABA itself plays well-established roles during early cortical development, including regulating progenitor proliferation, neuronal migration, dendritic growth, and synaptogenesis (Behar, 2000; Cuzon et al., 2006; Inada et al., 2011; Jursky & Nelson, 1996; LoTurco et al., 1995; Telezhkin et al., 2016). In immature neurons, GABA has a depolarizing effect prior to KCC2 upregulation, which influences calcium signaling and activity-dependent maturation. Given that we observed premature GABA expression and early upregulation of KCC2 in our *SLC6A1*-deficient MGEOS, and that our cortical organoids do contain population of probable LGE-like GABAergic neurons, it is plausible that altered GABA dynamics may not only affect interneurons, but also the development of cortical excitatory neurons. Notwithstanding this possibility, the impact of *SLC6A1* HI on excitatory neuron development, specification, and maturation has not been examined in a human developmental model.

Previous rodent studies have demonstrated that altered GABA signaling can influence cortical layering, dendritic arborization, and synaptic connectivity (Imbrosci & Mittmann, 2011; Oh et al., 2016), and *SLC6A1* knockout in rodents leads to impaired neurogenesis in the dentate gyrus of the hippocampal formation (Liu et al., 2025). However, the specific contribution of GAT1 dysfunction to cortical excitatory lineage development remains unexplored. We have already acquired preliminary data from *SLC6A1* CRISPR edited Het, KO, patient, and control single rosette cortical organoids across developmental timepoints ranging from 1 month to 1 year in vitro and found an increase in the production of TBR2 expressing intermediate progenitors at 5 months in KO COs compared to controls (**Figure 4.1 A, B**).

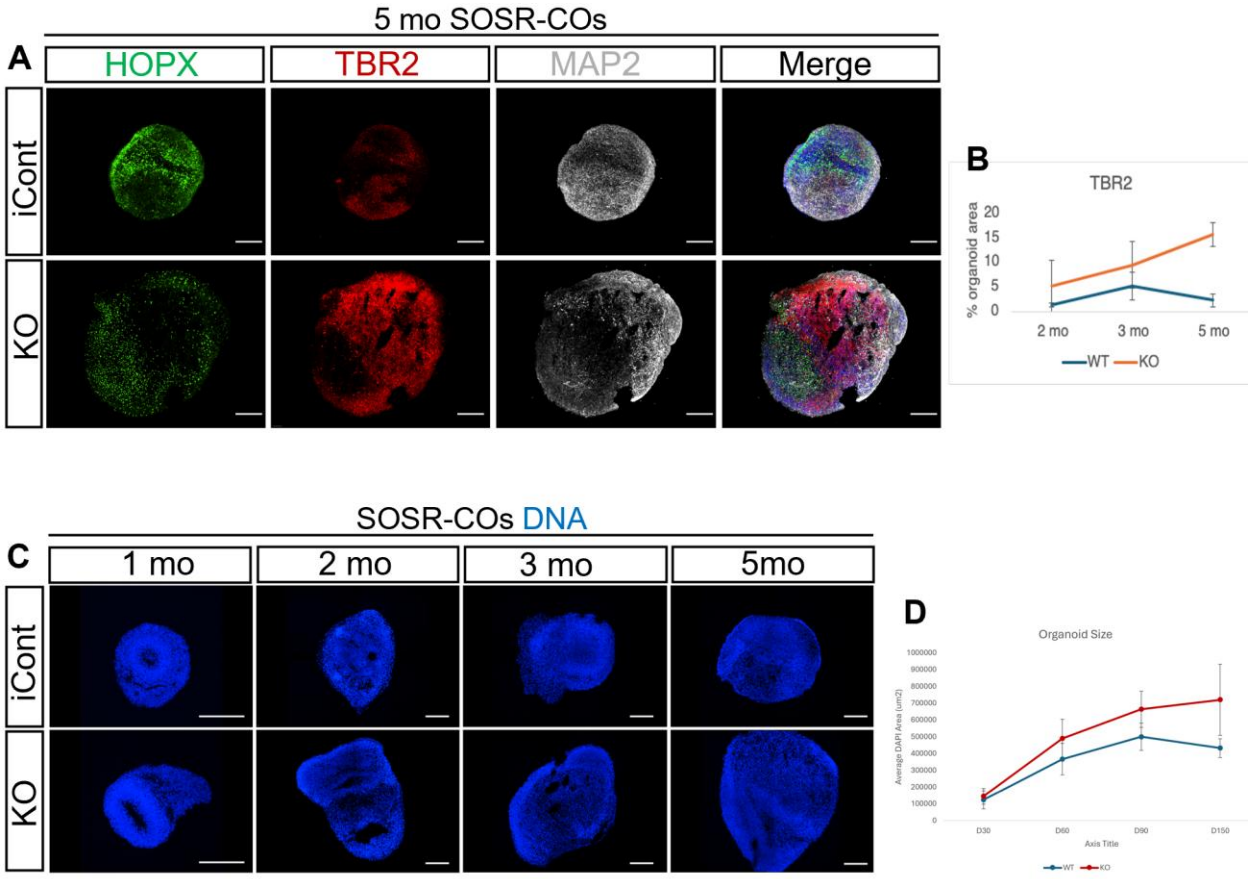

Figure 4.1: SLC6A1 Cortical organoids display increased intermediate progenitor population expansion and increased organoid size.

(**A**) Representative confocal images of immunostained cortical organoids at 5 months in vitro generated from knockout (KO) and isogenic control (iCont) lines. Outer radial glial marker HOPX is shown in green, intermediate progenitor marker TBR2 is shown in red, and neuronal marker

MAP2 is shown in grey. (**B**) Quantification of percent organoid area of TBR2+ cells at 5 months showing an increase in TBR2+ cells in KO COs compared to controls. (**C**) Representative confocal images of KO and iCont bisbenzimide stained cortical organoids from 1- 5 months in vitro. (D) Quantification of KO and iCont organoid size from 1 month to 5 months in vitro using bisbenzimide area as readout for size. KO organoids size increases at a steeper rate than control organoids and display larger size by 5 months in vitro. All scale bars are 200 μm.

In accordance, we also found an increase in organoid size in KO COs compared to controls (**Figure 4.1 C, D**). We then looked at cortical layer-specific markers and found that the number of neurons was increased across deep layer (CTIP2), intermediate layer (SATB2), and superficial layer (CUX1) subsets. Additionally, we observed that upper layer marker, CUX1, expressing cells appeared mislocalized and dispersed throughout the organoid instead of localizing mostly to the superficial zones as they do in control COs (**Figure 4.2 A-D**). Interestingly, we observed strong ectopic expression of somatostatin (SST) in KO COs which is a subtype marker that is not typically expressed in control COs. The expression timeline matched that of increased SST in the MGEOs with significant expression of SST at 2 months followed by a decline in expression at 5 months (**Figure 4.2 E, F)**.

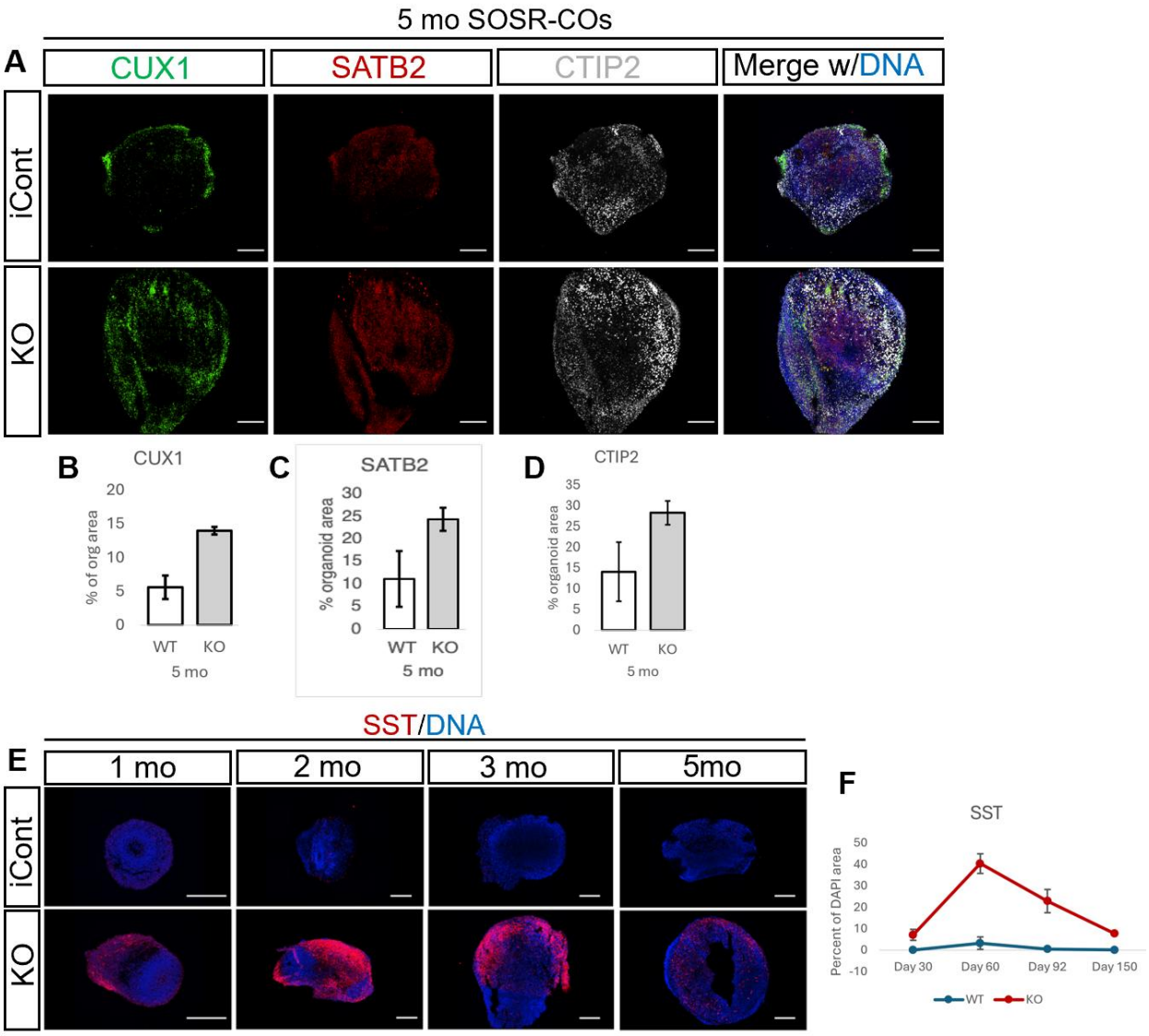

Figure 4.2: Dysregulated numbers and positioning of cortical neurons and ectopic expression of somatostatin in SLC6A1 KO cortical organoids.

(**A**) Representative confocal images of immunostained cortical organoids at 5 months in vitro generated from knockout (KO) and isogenic control (iCont) lines. Upper cortical layer marker CUX1 is shown in green, intermediate cortical layer marker SATB2 is shown in red, and deep cortical layer marker CTIP2 is shown in grey. (**B-D**) Quantification of percent organoid area of CUX1+, SATB2+, and CTIP2+ cells at 5 months showing an increase in all layer markers at 5 months compared to controls. (**E**) Representative confocal images of KO and iCont cortical organoids immunostained for somatostatin (SST) from 1- 5 months in vitro. Ectopic expression of SST is present at all time points in KO cortical organoids with strongest expression at 2 months. SST expression is not seen in control cortical organoids. (F) Quantification of KO and iCont SST expression from 1 month to 5 months in vitro. All scale bars are 200 µm.

These findings suggest that cell division, fate determination, maturation, laminar distribution, and neuronal subtype specification may be altered in COs as a consequence of GAT1 reduction. However, more in-depth transcriptomic analysis is needed to determine the mechanism by which the observed changes in proliferation, neurogenesis, and cortical layer lamination occur. High-resolution spatial transcriptomics methods such as MERFISH (K. H. Chen et al., 2015) , which have recently been optimized for use in 3D tissue (Fang et al., 2024), could be used to precisely map the spatial and temporal progression of excitatory neuron development in GAT1 mutant cortical organoids. By designing a panel of probes targeting key markers of excitatory progenitors, intermediate precursors, mature cortical neurons, and genes associated with synaptic function and activity, one could visualize how these cells emerge, migrate, and mature within the 3D architecture of the organoid. Imaging across multiple developmental stages would allow one to track lineage progression and maturation trajectories at single-cell resolution, providing more insight into how GAT1 loss alters the timing of differentiation, the spatial organization of neuronal layers, or the coordinated expression of activity-dependent genes.

Morphological and synaptic development could be assessed using high-resolution imaging of dendritic arborization, and synapse quantification. Functional maturation could be evaluated via patch-clamp and multielectrode array recordings, while live imaging using genetically encoded calcium indicators could quantify early spontaneous activity patterns and progression of calcium dynamics as the cells mature. Establishing the role of *SLC6A1* in excitatory neuron development will broaden our understanding of how GAT1 dysfunction reshapes cortical circuits, likely revealing that *SLC6A1*-DEE arises from combined inhibitory and excitatory developmental perturbations rather than interneuron-specific defects alone.

What is the function of GAT1 on primary cilia and how is it altered in diseased states?

In recent years, independent studies have found GAT1 localized on the primary cilia of neurons and pluripotent stem cells (Kostyanovskaya et al., 2025; Loukil et al., 2025). Primary cilia are microtubule-based sensory organelles that serve as major signaling hubs during neurodevelopment. They coordinate and regulate signaling pathways including SHH, WNT, and BDNF signaling that influence cell division, progenitor proliferation, polarity, neuronal migration, fate specification, and dorsal/ventral regionalization (Li et al., 2025). Knockout of ciliary protein ARL13B has been shown to result in increased SHH signaling resulting in ventralization of human dorsal forebrain organoids despite receiving dorsal patterning morphogens (Shimada et al., 2024).

These findings suggest that dysfunction of proteins localized to primary cilia can have extreme consequences during human brain development.

Experiments in patient iPSC lines carrying the *SLC6A1* p.S295L mutation showed reduced localization of GAT1 on primary cilia compared to controls (Loukil et al., 2025), suggesting that trafficking of the variant protein to the ciliary membrane is impaired. Ciliary membrane proteins contain a ciliary targeting motif, often located on the c-terminus, which instructs trafficking of the protein to the ciliary membrane (Mazelova et al., 2009). A common c-terminal-located ciliary targeting motif is VXPX where V and P represent valine and proline, respectively, and X represents any other amino acid. These motifs are highly conserved across species, indicating their importance in development (Ward et al., 2011). Upon careful examination of the GAT1 c-terminal amino acid sequence, I identified two consecutive VXPX motifs separated by 3 amino acids (VQPS, residues 571–574, and VRPE residues 578-581) which are plausible candidates for the ciliary targeting region of the GAT1 protein. Interestingly, while the second motif (VRPE) was conserved across most mammalian species including rodents, the first motif was specific to only human and non-human primates (**Figure 4.3**). Previous research has also identified a PDZ-binding motif at the end of the c-terminus (residues 596–599) that is responsible for scaffold anchoring and there is evidence of direct interaction of GAT1 with Actin, Syntaxin 1a, and Syntenin 1 (Imoukhuede et al., 2009; Jahodova et al., 2023; Lin et al., 2024). Additionally, MUPP1, a scaffolding protein for organizing signaling complexes, was found to bind to the GAT1 PDZ binding motif (Baliova et al., 2014). This places GAT1 within signaling complexes in the cilia that may regulate signaling pathways such as SHH and WNT.

		V 571	Q 572	P 573	S 574	E 575	D 576	I 577	V 578	R 579	P 580	E 581	
Human	M	V	Q	P	S	E	D	I	V	R	P	E	N
Chimp	M	V	Q	P	S	E	D	I	V	R	P	E	N
Gorilla	M	V	Q	P	S	E	D	I	V	R	P	E	N
Gibbon	M	V	Q	P	S	E	D	I	V	R	P	E	N
Rhesus	M	V	Q	P	S	E	D	I	V	R	P	E	N
Marmoset	M	V	Q	P	S	E	D	I	V	R	P	E	N
Mouse	M	I	Q	P	S	E	D	I	V	R	P	E	N
Rat	M	I	Q	P	S	E	D	I	V	R	P	E	N
Rabbit	M	I	Q	P	S	E	D	L	G	G	P	E	N
Pig	M	I	Q	P	S	E	D	I	V	R	P	E	N
Dog	M	I	Q	P	S	E	D	I	V	R	P	E	N
Elephant	M	I	Q	P	S	E	D	I	V	R	P	E	N
Chicken	M	I	Q	P	S	E	D	I	S	H	P	E	N

Figure 4.3: Species conservation of VXPX ciliary targeting motifs on the c-terminus of GAT1

Depiction of amino acid sequences from position 571 to 581 on the GAT1 protein. Identified VXPX ciliary targeting motifs are indicated by red boxes. Conservation of amino acids in each sequence are shown in pink. Of note, the valine in the VQPS motif from amino acids 571-574 is only conserved in human and non-human primates suggesting that the function of this motif is important for the development of these species.

Understanding whether GAT1 participates structurally or functionally in ciliary signaling could reveal a previously unrecognized developmental mechanism linking GAT1 to morphogen regulation or responsiveness. Could GAT1 serve a non-canonical function as a receptor-like sensor involved in morphogen signaling platforms? Given that MGE lineage maintenance was altered in our MGEOs and MGE lineage is determined by SHH signaling, linking GAT1 to dysfunctional SHH signaling would be an important first step. To answer this question, we would first need to confirm that SHH pathways are altered in *SLC6A1* HI or knockout MGEOs. Since the SHH pathway activator Smoothened agonist (SAG) is a key morphogen used in our differentiation protocol, one could measure the level of SHH pathway activation by measuring SHH downstream regulators such as GLI1, a readout of SHH activation, or PTCHD1, a negative feedback regulator of the SHH pathway using RT-qPCR or immunostaining for GLI1 protein accumulation. Differences in SHH responsiveness between wild-type and GAT1-deficient cells would indicate whether GAT1 contributes functionally to ciliary signal transduction independently of its transporter role.

To determine whether GAT1 interacts structurally with within the cilium, fluorescently tagged WT and mutants with c-terminal truncated GAT1, tagged at the n-terminus to preserve the C-terminal PDZ-motif and VXPX cilia targeting motif, could be imaged along with ARL13b to test whether GAT1 presence in cilia depends on scaffold interactions at the C-terminus, a region that is lost in many truncating variants. To identify GAT1 interacting partners relevant to SHH signaling, co-immunoprecipitation coupled with mass spectrometry could be performed. A comprehensive list of GAT1-associated factors could then be generated. Direct interactions with known SHH pathway proteins such as SMO and GLI within the ciliary compartment could further be confirmed with a proximity ligation assay using the tagged lines mentioned previously. Association of GAT1 with these proteins upon SAG stimulation, or lack of association due to a c-terminus truncation, could determine if GAT1 forms a complex with these important SHH pathway regulators. Additional experiments using a transport-dead GAT1 that retains intact c-terminus motifs could further provide insight into its transport-independent function. These approaches

would reveal molecular scaffolds or regulatory proteins that link GAT1 to ciliary signaling platforms and provide mechanistic insight into its potential non-canonical function in early human brain development.

4.2 Progressing onward

The work presented in this dissertation provides insight into the developmental consequences of *SLC6A1* HI within a human-relevant context and reveals that the consequences of GAT1 disruption extend beyond impaired GABA uptake to influence interneuron lineage progression, maturation, and subtype maintenance. Our findings strengthen the hypothesis that *SLC6A1*-DEEs may stem from early alterations in progenitor competence and morphogen responsiveness, long before the onset of seizures or overt clinical symptoms. However, the developmental effects we observed are complex and multifactorial, involving dynamic shifts in progenitor identity, altered differentiation, and long-term instability of interneuron subtypes. Moving forward, *SLC6A1* research should be addressed from two complementary perspectives. First, a careful characterization of the mechanisms driving its developmental impact in shaping interneuron specification and circuit assembly in non-diseased and diseased states is still needed. These experiments will inform treatment strategies that could be implicated prior to symptom onset that may be able to prevent or halt the progression of the disorder. Second, it is imperative to continue the avenues of investigation that focus on the canonical role of *SLC6A1* in GABA reuptake and synaptic inhibition to provide more effective treatment options for patients after pathological symptoms have emerged. An integrative and holistic understanding of *SLC6A1*-related pathology ranging from early developmental mis-patterning to later-stage synaptic and network dysfunction will be essential in understanding the intricacies of this disorder and advising effective, broad reaching therapeutic strategies.

One such strategy that has proved to be promising is cell-based therapy. Transplantation of MGE-derived interneurons in animal models has shown efficacy in the treatment of epilepsy and other neurodevelopmental disorders (Bershteyn et al., 2023; Upadhya et al., 2019). Grafted interneurons migrate, mature, and functionally integrate into the host brain to restore inhibitory tone. Human-focused clinical trials using transplantation of neural stem cells, neurons, or neural progenitors derived from human PSCs are now broadly being conducted for the treatment of multiple neurological disorders including Parkinson's disease, amyotrophic lateral sclerosis, and

spinal cord injuries (ClinicalTrials.gov Identifiers: NCT04802733, NCT01730716, NCT01772810). One clinical study using the transplant of GABAergic progenitors to treat temperal lobe epilepsy is currently underway (ClinicalTrials.gov Identifier: NCT05135091). However, the strategies used to generate interneuron progenitors in this trial fail to provide a reliable source of PV interneurons, an important interneuron subtype implicated in many neurological and psychiatric disorders including epilepsy, autism, schizophrenia, and Alzheimer's disease. Here we show that our MGEO model produces robust numbers of cortical PV interneurons that could serve as a platform for scalable PV interneuron production, supporting transplantation approaches across a broad spectrum of circuit-level disorders including *SLC6A1*-DEEs. Xenograft experiments transplanting human MGEO-derived progenitors into animal models will be an important validation of their utility in an in-vivo system.

While our *SLC6A1* results are intriguing and reframe the way we now think of GAT1 function, there are some caveats that should be considered. The *SLC6A1* studies in this dissertation entirely utilize protein-truncating variants to ensure robust loss of protein function. However, the majority of patient variants identified in *SLC6A1* are missense mutations. These missense variants have been shown to exert diverse effects, including severe, partial (see Chapter 1 for variant localization), or no loss of transporter function, altered or normal trafficking, and in rare cases, dominant-negative interactions.

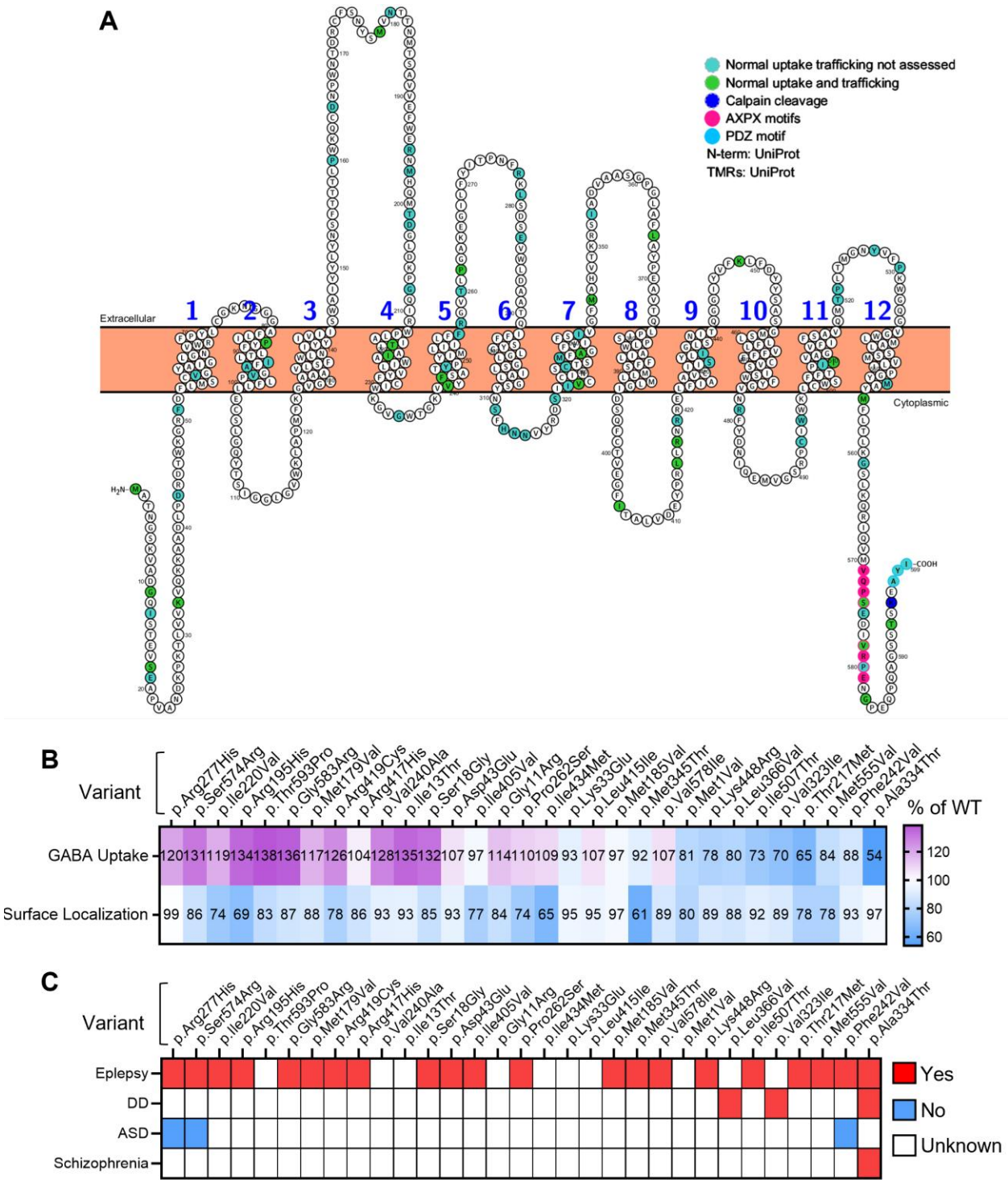

Figure 4.4: Evaluation of patient variants reported in the Silva et al., 2024 dataset with no loss of GAT1 function and their associated clinical diagnoses.

(A) GAT1 protein topography map displaying amino acid locations of patient variants that retain normal transport function and normal trafficking to the membrane (shown in green) and normal

transport function but trafficking not assessed (shown in turquoise). Note that variants are absent from transmembrane domains 3, 6, 8, and 10 which are important for transporter function. The PDZ binding motif at the end of the c-terminus is indicated in light blue and the calpain cleavage site is labeled in dark blue. Proposed ciliary targeting motifs are indicated in pink and variants that fall within these regions contain a pink border. (**B**) Heatmap of GAT1 transport function and surface localization as a percent of wildtype for variants in the Silva et al. dataset that had both typical uptake and typical protein trafficking (green group). A range between 50% of WT to 150% of wildtype was deemed to be within typical function range by the Silva et al. group. Numbers within each box indicate the % of wildtype function for each variate (**C**) Plot depicting the clinical diagnoses for patients with the same set of variants depicted in B. Red boxes indicate a clinical diagnosis of epilepsy while blue boxes indicate that a diagnosis of autism spectrum disorder (ASD) was ruled out. White boxes indicate unknown or data unavailable.

Even more puzzling, approximately 40% of patient variants that were assessed for their effect on transporter function were found to function normally, with a subset also assessed for trafficking and found to have normal trafficking, yet patients still developed epilepsy or developmental delay in the majority of these cases ((**Figure 4.4**), and see (Silva et al., 2024)). It will therefore be important to systematically characterize the developmental and functional consequences of representative missense variants to determine if and how they differ from truncating variants. Furthermore, while human iPSC-derived organoids provide unparalleled access to early human developmental processes, in vivo animal models remain indispensable for capturing long range connectivity, communication pathways between brain regions, and assessing behavioral readouts of experimental perturbations. Combining organoid-based mechanistic insights with conditional knock-in mouse models or humanized transplantation paradigms will be essential to determine how faithfully in vitro phenotypes are recapitulated in model organisms.

The translational relevance of these findings lies largely in the reframing of *SLC6A1*-DEEs as having both developmental and synaptic components to the mechanisms by which loss of function causes diseases. By identifying early alterations in interneuron lineage progression and morphogen responsiveness, our work suggests that therapeutic intervention windows may precede clinical seizure onset. Early modulation of developmental signaling pathways, enhancement of interneuron migration, or stabilization of vulnerable interneuron subtypes could complement later interventions aimed at restoring inhibitory balance through pharmacologic, antisense oligonucleotide, or gene correction approaches. Correcting the associated intellectual disability would likely present even greater challenges. More broadly, these findings expand our concept of transporter functions and open the door for potential non-canonical roles of other DEE related

synaptic proteins to be explored at early developmental timepoints. This perspective may have implications beyond *SLC6A1*, prompting reevaluation of how membrane transporters contribute to morphogen integration, progenitor competence, and circuit assembly across neurodevelopmental disorders.

As utilization of complex and increasingly sophisticated methodologies continues to expand, the pace and scope of new discoveries in neuroscience and developmental biology will only accelerate. However, with increased technological power comes greater ethical responsibility. With the credibility and integrity of science being questioned by the public in recent years, it is now more imperative that ever that we as a community maintain rigorous experimental design, transparent reporting, and thoughtful interpretation of experimental findings. Moving forward, it will be essential for the scientific community to prioritize reproducibility through transparent protocols, appropriate controls, replication across independent lines and model systems, and open sharing of data and analytical pipelines. As our tools grow more precise, so too must our commitment to upholding the rigor and integrity of science. Cooperative collaboration and open communication with each other and the public will be essential for maintaining credibility and translational impact of our work and will ensure that scientific advances remain robust, reliable, and ultimately beneficial to patients and to society.

References

Allaway, K. C., Gabitto, M. I., Wapinski, O., Saldi, G., Wang, C. Y., Bandler, R. C., Wu, S. J., Bonneau, R., & Fishell, G. (2021). Genetic and epigenetic coordination of cortical interneuron development. *Nature*, *597*(7878), 693–697. https://doi.org/10.1038/S41586-021-03933-1

Alzu'bi, A., Lindsay, S., Kerwin, J., Looi, S. J., Khalil, F., & Clowry, G. J. (2017). Distinct cortical and sub-cortical neurogenic domains for GABAergic interneuron precursor transcription factors NKX2.1, OLIG2 and COUP-TFII in early fetal human telencephalon. *Brain Structure and Function*, *222*(5), 2309–2328. https://doi.org/10.1007/S00429-016-1343-5

Amegandjin, C. A., Choudhury, M., Jadhav, V., Carriço, J. N., Quintal, A., Berryer, M., Snapyan, M., Chattopadhyaya, B., Saghatelyan, A., & Di Cristo, G. (2021). Sensitive period for rescuing parvalbumin interneurons connectivity and social behavior deficits caused by TSC1 loss. *Nature Communications*, *12*(1). https://doi.org/10.1038/S41467-021-23939-7

Anderson, S. A., Eisenstat, D. D., Shi, L., & Rubenstein, J. L. R. (1997). Interneuron migration from basal forebrain to neocortex: dependence on Dlx genes. *Science (New York, N.Y.)*, *278*(5337), 474–476. https://doi.org/10.1126/science.278.5337.474

Anderson, S. A., Kaznowski, C. E., Horn, C., Rubenstein, J. L. R., & McConnell, S. K. (2002). Distinct origins of neocortical projection neurons and interneurons in vivo. *Cerebral Cortex (New York, N.Y. : 1991)*, *12*(7), 702–709. https://doi.org/10.1093/CERCOR/12.7.702

Anderson, S. A., Marín, O., Horn, C., Jennings, K., & Rubenstein, J. L. R. (2001). Distinct cortical migrations from the medial and lateral ganglionic eminences. *Development*, *128*(3), 353–363. https://doi.org/10.1242/dev.128.3.353

Andrews, S. (2010) FastQC A Quality Control Tool for High Throughput Sequence Data. - References - Scientific Research Publishing. (n.d.). Retrieved March 22, 2026, from https://www.scirp.org/reference/referencespapers?referenceid=4024153

Antonoudiou, P., Tan, Y. L., Kontou, G., Louise Upton, A., & Mann, E. O. (2020). Parvalbumin and somatostatin interneurons contribute to the generation of hippocampal gamma oscillations. *Journal of Neuroscience*, *40*(40), 7668–7687. https://doi.org/10.1523/JNEUROSCI.0261-20.2020

Asgarian, Z., Oliveira, M. G., Stryjewska, A., Maragkos, I., Rubin, A. N., Magno, L., Pachnis, V., Ghorbani, M., Hiebert, S. W., Denaxa, M., & Kessaris, N. (2022). MTG8 interacts with LHX6 to specify cortical interneuron subtype identity. *Nature Communications 2022 13:1*, *13*(1), 5217-. https://doi.org/10.1038/s41467-022-32898-6

Atamian, A., Birtele, M., Hosseini, N., Nguyen, T., Seth, A., Del Dosso, A., Paul, S., Tedeschi, N., Taylor, R., Coba, M. P., Samarasinghe, R., Lois, C., & Quadrato, G. (2024). Human cerebellar organoids with functional Purkinje cells. *Cell Stem Cell*, *31*(1), 39-51.e6. https://doi.org/10.1016/j.stem.2023.11.013

Avilés, E. C., Wilson, N. H., & Stoeckli, E. T. (2013). Sonic hedgehog and Wnt: Antagonists in morphogenesis but collaborators in axon guidance. *Frontiers in Cellular Neuroscience*, (MAY). https://doi.org/10.3389/FNCEL.2013.00086/FULL

Baer, S., Rebert, M., Burger, P., Mandel, J. L., Villeneuve, N., Gibaud, M., Altuzarra, C., Villega, F., Cances, C., Lacan, L., Nguyen, S., Lesca, G., Isnard, H., Allani-Essid, N., Laugel, V., Coutelle, R., & de Saint Martin, A. (2025). Behavioral, neurodevelopmental profile, and epilepsy trajectory in two series of SLC6A1-NDD: A retrospective study with comprehensive assessment, and a participatory database study. *European Journal of Paediatric Neurology*, *54*, 121–129. https://doi.org/10.1016/j.ejpn.2025.01.003

Bagley, J. A., Reumann, D., Bian, S., Lévi-Strauss, J., & Knoblich, J. A. (2017). Fused cerebral organoids model interactions between brain regions. *Nature Methods 2017 14:7*, *14*(7), 743–751. https://doi.org/10.1038/nmeth.4304

Baldassari, S., Musante, I., Iacomino, M., Zara, F., Salpietro, V., & Scudieri, P. (2020). Brain Organoids as Model Systems for Genetic Neurodevelopmental Disorders. *Frontiers in Cell and Developmental Biology*, *8*. https://doi.org/10.3389/fcell.2020.590119

Baliova, M., Juhasova, A., & Jursky, F. (2014). Using a collection of MUPP1 domains to investigate the similarities of neurotransmitter transporters C-terminal PDZ motifs. *Biochemical and Biophysical Research Communications*, *454*(1), 25–29. https://doi.org/10.1016/j.bbrc.2014.10.011

Bandler, R. C., Vitali, I., Delgado, R. N., Ho, M. C., Dvoretskova, E., Ibarra Molinas, J. S., Frazel, P. W., Mohammadkhani, M., Machold, R., Maedler, S., Liddelow, S. A., Nowakowski, T. J., Fishell, G., & Mayer, C. (2021). Single-cell delineation of lineage and genetic identity in the mouse brain. *Nature*, *601*(7893), 404. https://doi.org/10.1038/s41586-021-04237-0

Baraban, S. C. (2021). A zebrafish-centric approach to antiepileptic drug development. *Disease Models & Mechanisms*, *14*(7). https://doi.org/10.1242/dmm.049080

Bartos, M., Vida, I., Frotscher, M., Meyer, A., Monyer, H., Geiger, J. R. P., Jonas, P., & Heidelberg. (2002). Fast synaptic inhibition promotes synchronized gamma oscillations in hippocampal interneuron networks. *Proceedings of the National Academy of Sciences of the United States of America*, *99*(20), 13222–13227. https://doi.org/10.1073/PNAS.192233099,

Behar, T. N. (2000). GABA Receptor Antagonists Modulate Postmitotic Cell Migration in Slice Cultures of Embryonic Rat Cortex. *Cerebral Cortex*, *10*(9), 899–909. https://doi.org/10.1093/cercor/10.9.899

Behar, T. N., Li, Y. X., Tran, H. T., Ma, W., Dunlap, V., Scott, C., & Barker, J. L. (1996). GABA stimulates chemotaxis and chemokinesis of embryonic cortical neurons via calcium-dependent mechanisms. *Journal of Neuroscience*, *16*(5), 1808–1818. https://doi.org/10.1523/jneurosci.16-05-01808.1996

Ben-Ari, Y. (2002). Excitatory actions of GABA during development: The nature of the nurture. *Nature Reviews Neuroscience*, *3*(9), 728–739. https://doi.org/10.1038/nrn920

Berg, A. T. (2010). Comorbidities in Epilepsies: Overview. *Atlas of Epilepsies*, 1321–1324. https://doi.org/10.1007/978-1-84882-128-6_194

Bershteyn, M., Bröer, S., Parekh, M., Maury, Y., Havlicek, S., Kriks, S., Fuentealba, L., Lee, S., Zhou, R., Subramanyam, G., Sezan, M., Sevilla, E. S., Blankenberger, W., Spatazza, J., Zhou, L., Nethercott, H., Traver, D., Hampel, P., Kim, H., … Nicholas, C. R. (2023). Human pallial MGE-type GABAergic interneuron cell therapy for chronic focal epilepsy. *Cell Stem Cell*, *30*(10), 1331-1350.e11. https://doi.org/10.1016/J.STEM.2023.08.013

Bershteyn, M., & Kriegstein, A. R. (2013). Cerebral organoids in a dish: Progress and prospects. *Cell*, *155*(1), 19. https://doi.org/10.1016/j.cell.2013.09.010

Bershteyn, M., Zhou, H., Fuentealba, L., Chen, C., Subramanyam, G., Cherkowsky, D., Sevilla, E. S., Hampel, P., Salvatierra, J., Sezan, M., Maury, Y., Havlicek, S., Kriks, S., Lee, S., Au, W., Watson, M., Kuzmenko, O., Grimmett, M. E., Vogel, A., … Nicholas, C. R. (2025). Human stem cell-derived GABAergic interneuron development reveals early emergence of subtype diversity and gradual electrochemical maturation. *Neuron*, *113*(19), 3162-3184.e10. https://doi.org/10.1016/j.neuron.2025.06.010

Birey, F., Andersen, J., Makinson, C. D., Islam, S., Wei, W., Huber, N., Fan, H. C., Metzler, K. R. C., Panagiotakos, G., Thom, N., O'Rourke, N. A., Steinmetz, L. M., Bernstein, J. A., Hallmayer, J., Huguenard, J. R., & Pasca, S. P. (2017). Assembly of functionally integrated human forebrain spheroids. *Nature*, *545*(7652), 54–59. https://doi.org/10.1038/nature22330

Boitor-Borza, D., Turcu, F., Farcasanu, S., & Crivii, C. (2021). Early development of human ganglionic eminences assessed in vitro by using 7.04 Tesla micro-MRI – a pilot study. *Medicine and Pharmacy Reports*, *94*(1), 35. https://doi.org/10.15386/mpr-1715

Bragina, L., Marchionni, I., Omrani, A., Cozzi, A., Pellegrini-Giampietro, D. E., Cherubini, E., & Conti, F. (2008). GAT-1 regulates both tonic and phasic GABAA receptor-mediated inhibition in the cerebral cortex. *Journal of Neurochemistry*, *105*(5), 1781–1793. https://doi.org/10.1111/j.1471-4159.2008.05273.x

Briscoe, J., Pierani, A., Jessell, T. M., & Ericson, J. (2000). A homeodomain protein code specifies progenitor cell identity and neuronal fate in the ventral neural tube. *Cell*, *101*(4), 435–445. https://doi.org/10.1016/S0092-8674(00)80853-3

Bröer, S. (2006). The SLC6 orphans are forming a family of amino acid transporters. *Neurochemistry International*, *48*(6–7), 559–567. https://doi.org/10.1016/j.neuint.2005.11.021

Butt, S. J. B., Fuccillo, M., Nery, S., Noctor, S., Kriegstein, A., Corbin, J. G., & Fishell, G. (2005). The temporal and spatial origins of cortical interneurons predict their physiological subtype. *Neuron*, *48*(4), 591–604. https://doi.org/10.1016/j.neuron.2005.09.034

Buzsáki, G., & Chrobak, J. J. (1995). Temporal structure in spatially organized neuronal ensembles: a role for interneuronal networks. *Current Opinion in Neurobiology*, *5*(4), 504–510. https://doi.org/10.1016/0959-4388(95)80012-3

Caballero, A., & Tseng, K. Y. (2016). GABAergic function as a limiting factor for prefrontal maturation during adolescence. *Trends in Neurosciences*, *39*(7), 441. https://doi.org/10.1016/j.tins.2016.04.010

Cardin, J. A. (2018). Inhibitory interneurons regulate temporal precision and correlations in cortical circuits. *Trends in Neurosciences*, *41*(10), 689. https://doi.org/10.1016/j.tins.2018.07.015

Carvill, G. L., McMahon, J. M., Schneider, A., Zemel, M., Myers, C. T., Saykally, J., Nguyen, J., Robbiano, A., Zara, F., Specchio, N., Mecarelli, O., Smith, R. L., Leventer, R. J., Møller, R. S., Nikanorova, M., Dimova, P., Jordanova, A., Petrou, S., Helbig, I., … Mefford, H. C. (2015). Mutations in the GABA transporter SLC6A1 cause epilepsy with myoclonic-atonic seizures. *American Journal of Human Genetics*, *96*(5), 808–815. https://doi.org/10.1016/j.ajhg.2015.02.016

Chen, A. B., Duque, M., Rymbek, A., Dhanasekar, M., Wang, V. M., Mi, X., Tocquer, L., Narayan, S., Marquez Legorreta, E., Eddison, M., Yu, G., Wyart, C., Prober, D. A., Engert, F., & Ahrens, M. B. (2025). Norepinephrine changes behavioral state through astroglial purinergic signaling. *Science (New York, N.Y.)*, *388*(6748), 769–775. https://doi.org/10.1126/science.adq5233

Chen, D., Wang, C., Li, M., She, X., Yuan, Y., Chen, H., Zhang, W., & Zhao, C. (2019). Loss of Foxg1 Impairs the Development of Cortical SST-Interneurons Leading to Abnormal Emotional and Social Behaviors. *Cerebral Cortex*, *29*(8), 3666–3682. https://doi.org/10.1093/cercor/bhz114

Chen, K. H., Boettiger, A. N., Moffitt, J. R., Wang, S., & Zhuang, X. (2015). Spatially resolved, highly multiplexed RNA profiling in single cells. *Science*, *348*(6233). https://doi.org/10.1126/science.aaa6090

Chen, Q., Deister, C. A., Gao, X., Guo, B., Lynn-Jones, T., Chen, N., Wells, M. F., Liu, R., Goard, M. J., Dimidschstein, J., Feng, S., Shi, Y., Liao, W., Lu, Z., Fishell, G., Moore, C. I., & Feng, G. (2020). Dysfunction of cortical GABAergic neurons leads to sensory hyper-reactivity in a Shank3 mouse model of ASD. *Nature Neuroscience*, *23*(4), 520–532. https://doi.org/10.1038/S41593-020-0598-6

Chiang, C., Litingtung, Y., Lee, E., Young, K. E., Corden, J. L., Westphal, H., & Beachy, P. A. (1996). Cyclopia and defective axial patterning in mice lacking Sonic hedgehog gene function. *Nature*, *383*(6599), 407–413. https://doi.org/10.1038/383407a0

Chiu, C. S., Brickley, S., Jensen, K., Southwell, A., Mckinney, S., Cull-Candy, S., Mody, I., & Lester, H. A. (2005). GABA Transporter Deficiency Causes Tremor, Ataxia, Nervousness, and Increased GABA-Induced Tonic Conductance in Cerebellum. *Journal of Neuroscience*, *25*(12), 3234–3245. https://doi.org/10.1523/JNEUROSCI.3364-04.2005

Chung, S.-K., Everett, K. V., Thomas, R. H., Dudley, E., Higgins, A. T., Jones, C. A., Derrick, A. V., Davies, J. S., Pickrell, W. O., Bellows, S. T., Harvey, R. J., Bergin, P. S., Mullins, J. G. L., Scheffer, I. E., Berkovic, S. F., & Rees, M. I. (2025). Pathogenic ultra-rare variants in SLC6A1, SLC6A11, GAD1 and GAD2 are new & recurrent GABAergic loci for GGE syndromes. *MedRxiv*, 2025.04.01.24316792. https://doi.org/10.1101/2025.04.01.24316792

Cong, L., Ran, F. A., Cox, D., Lin, S., Barretto, R., Habib, N., Hsu, P. D., Wu, X., Jiang, W., Marraffini, L. A., & Zhang, F. (2013). Multiplex genome engineering using CRISPR/Cas systems. *Science (New York, N.Y.)*, *339*(6121), 819–823. https://doi.org/10.1126/science.1231143

Conti, F., Melone, M., De Biasi, S., Minelli, A., Brecha, N. C., & Ducati, A. (1998). Neuronal and Glial Localization of GAT-1, a High-Affinity-Aminobutyric Acid Plasma Membrane Transporter, in Human Cerebral Cortex: With a Note on Its Distribution in Monkey Cortex. *Journal of Comparative Neurology*.

Conti, F., Minelli, A., & Melone, M. (2004). GABA transporters in the mammalian cerebral cortex: Localization, development and pathological implications. *Brain Research Reviews*, *45*(3), 196–212. https://doi.org/10.1016/j.brainresrev.2004.03.003

Cope, D. W., Di Giovanni, G., Fyson, S. J., Orbán, G., Errington, A. C., Lrincz, M. L., Gould, T. M., Carter, D. A., & Crunelli, V. (2009a). Enhanced tonic GABA A inhibition in typical absence epilepsy. *Nature Medicine*, *15*(12), 1392–1398. https://doi.org/10.1038/nm.2058

Cuzon Carlson, V. C., & Yeh, H. H. (2011). GABAA receptor subunit profiles of tangentially migrating neurons derived from the medial ganglionic eminence. *Cerebral Cortex (New York, N.Y. : 1991)*, *21*(8), 1792–1802. https://doi.org/10.1093/cercor/bhq247

Cuzon, V. C., Yeh, P. W., Cheng, Q., & Yeh, H. H. (2006). Ambient GABA promotes cortical entry of tangentially migrating cells derived from the medial ganglionic eminence. *Cerebral Cortex (New York, N.Y. : 1991)*, *16*(10), 1377–1388. https://doi.org/10.1093/CERCOR/BHJ084

Davies, J. A., & Shakesby, A. (1999). Blockade of GABA uptake potentiates GABA-induced depolarizations in adult mouse cortical slices. *Neuroscience Letters*, *266*(3), 201–204. https://doi.org/10.1016/S0304-3940(99)00292-X

De Biasi, S., Vitellaro-Zuccarello, L., & Brecha, N. C. (1998). Immunoreactivity for the GABA transporter-1 and GABA transporter-3 is restricted to astrocytes in the rat thalamus. A light

and electron-microscopic immunolocalization. *Neuroscience*, *83*(3), 815–828. https://doi.org/10.1016/S0306-4522(97)00414-4

Delgado, R. N., Allen, D. E., Keefe, M. G., Mancia Leon, W. R., Ziffra, R. S., Crouch, E. E., Alvarez-Buylla, A., & Nowakowski, T. J. (2021). Individual human cortical progenitors can produce excitatory and inhibitory neurons. *Nature 2021 601:7893*, *601*(7893), 397–403. https://doi.org/10.1038/s41586-021-04230-7

Demarque, M., Represa, A., Becq, H. élène, Khalilov, I., Ben-Ari, Y., & Aniksztejn, L. (2002). Paracrine Intercellular Communication by a Ca2+- and SNARE-Independent Release of GABA and Glutamate Prior to Synapse Formation. *Neuron*, *36*(6), 1051–1061. https://doi.org/10.1016/S0896-6273(02)01053-X

Devries, S., Mulder, M., Charron, J. G., Prokop, J. W., & Mark, P. R. (2020). SLC6A1 G443D associated with developmental delay and epilepsy. *Cold Spring Harbor Molecular Case Studies*, *6*(4). https://doi.org/10.1101/MCS.A005371

Dimidschstein, J., Chen, Q., Tremblay, R., Rogers, S. L., Saldi, G. A., Guo, L., Xu, Q., Liu, R., Lu, C., Chu, J., Grimley, J. S., Krostag, A. R., Kaykas, A., Avery, M. C., Rashid, M. S., Baek, M., Jacob, A. L., Smith, G. B., Wilson, D. E., … Fishell, G. (2016). A viral strategy for targeting and manipulating interneurons across vertebrate species. *Nature Neuroscience*, *19*(12), 1743–1749. https://doi.org/10.1038/NN.4430

Dixit, A., Parnas, O., Li, B., Chen, J., Fulco, C. P., Jerby-Arnon, L., Marjanovic, N. D., Dionne, D., Burks, T., Raychowdhury, R., Adamson, B., Norman, T. M., Lander, E. S., Weissman, J. S., Friedman, N., & Regev, A. (2016). Perturb-Seq: Dissecting Molecular Circuits with Scalable Single-Cell RNA Profiling of Pooled Genetic Screens. *Cell*, *167*(7), 1853-1866.e17. https://doi.org/10.1016/j.cell.2016.11.038

Dobin, A., Davis, C. A., Schlesinger, F., Drenkow, J., Zaleski, C., Jha, S., Batut, P., Chaisson, M., & Gingeras, T. R. (2013). STAR: ultrafast universal RNA-seq aligner. *Bioinformatics (Oxford, England)*, *29*(1), 15–21. https://doi.org/10.1093/bioinformatics/bts635

Du, T., Xu, Q., Ocbina, P. J., & Anderson, S. A. (2008a). NKX2.1 specifies cortical interneuron fate by activating Lhx6. *Development*, *135*(8), 1559–1567. https://doi.org/10.1242/DEV.015123

Dzhala, V. I., Kuchibhotla, K. V., Glykys, J. C., Kahle, K. T., Swiercz, W. B., Feng, G., Kuner, T., Augustine, G. J., Bacskai, B. J., & Staley, K. J. (2010). Progressive NKCC1-Dependent Neuronal Chloride Accumulation during Neonatal Seizures. *The Journal of Neuroscience*, *30*(35), 11745. https://doi.org/10.1523/JNEUROSCI.1769-10.2010

Ericson, J., Muhr, J., Placzek, M., Lints, T., Jessel, T. M., & Edlund, T. (1995). Sonic hedgehog induces the differentiation of ventral forebrain neurons: A common signal for ventral patterning within the neural tube. *Cell*, *81*(5), 747–756. https://doi.org/10.1016/0092-8674(95)90536-7

Fang, R., Halpern, A., Rahman, M. M., Huang, Z., Lei, Z., Hell, S. J., Dulac, C., & Zhuang, X. (2024). Three-dimensional single-cell transcriptome imaging of thick tissues. *ELife*, *12*, RP90029. https://doi.org/10.7554/elife.90029

Fattorini, G., Catalano, M., Melone, M., Serpe, C., Bassi, S., Limatola, C., & Conti, F. (2020). Microglial expression of GAT-1 in the cerebral cortex. *Glia*, *68*(3), 646–655. https://doi.org/10.1002/glia.23745

Fattorini, G., Melone, M., Sánchez-Gómez, M. V., Arellano, R. O., Bassi, S., Matute, C., & Conti, F. (2017). GAT-1 mediated GABA uptake in rat oligodendrocytes. *Glia*, *65*(3), 514–522. https://doi.org/10.1002/glia.23108

Favuzzi, E., Marques-Smith, A., Deogracias, R., Winterflood, C. M., Sánchez-Aguilera, A., Mantoan, L., Maeso, P., Fernandes, C., Ewers, H., & Rico, B. (2017). Activity-Dependent Gating of Parvalbumin Interneuron Function by the Perineuronal Net Protein Brevican. *Neuron*, *95*(3), 639-655.e10. https://doi.org/10.1016/J.NEURON.2017.06.028

Fazzari, P., Mortimer, N., Yabut, O., Vogt, D., & Pla, R. (2020). Cortical distribution of GABAergic interneurons is determined by migration time and brain size. *Development (Cambridge)*, *147*(14), dev185033. https://doi.org/10.1242/dev.185033

Feng, Y., Wei, Z. H., Liu, C., Li, G. Y., Qiao, X. Z., Gan, Y. J., Zhang, C. C., & Deng, Y. C. (2022). Genetic variations in GABA metabolism and epilepsy. *Seizure*, *101*, 22–29. https://doi.org/10.1016/j.seizure.2022.07.007

Ferguson, B., Glick, C., & Huguenard, J. R. (2023). Prefrontal PV interneurons facilitate attention and are linked to attentional dysfunction in a mouse model of absence epilepsy. *ELife*, *12*. https://doi.org/10.7554/ELIFE.78349

Fisher, R. S., Acevedo, C., Arzimanoglou, A., Bogacz, A., Cross, J. H., Elger, C. E., Engel, J., Forsgren, L., French, J. A., Glynn, M., Hesdorffer, D. C., Lee, B. I., Mathern, G. W., Moshé, S. L., Perucca, E., Scheffer, I. E., Tomson, T., Watanabe, M., & Wiebe, S. (2014a). ILAE official report: a practical clinical definition of epilepsy. *Epilepsia*, *55*(4), 475–482. https://doi.org/10.1111/epi.12550

Flames, N., Pla, R., Gelman, D. M., Rubenstein, J. L. R., Puelles, L., & Marín, O. (2007). Delineation of multiple subpallial progenitor domains by the combinatorial expression of transcriptional codes. *Soc NeuroscienceN Flames, R Pla, DM Gelman, JLR Rubenstein, L Puelles, O MarínJournal of Neuroscience, 2007•Soc Neuroscience*. https://doi.org/10.1523/JNEUROSCI.2750-07.2007

Flandin, P., Kimura, S., Neuroscience, J. R.-J. of, & 2010, undefined. (2010). The progenitor zone of the ventral medial ganglionic eminence requires Nkx2-1 to generate most of the globus pallidus but few neocortical interneurons. *Soc NeuroscienceP Flandin, S Kimura, JLR RubensteinJournal of Neuroscience, 2010•Soc Neuroscience*, *30*(8), 2812–2823. https://doi.org/10.1523/JNEUROSCI.4228-09.2010

Flandin, P., Zhao, Y., Vogt, D., Jeong, J., Long, J., Potter, G., Westphal, H., & Rubenstein, J. L. R. (2011). Lhx6 and Lhx8 Coordinately Induce Neuronal Expression of Shh that Controls the Generation of Interneuron Progenitors. *Neuron*, *70*(5), 939. https://doi.org/10.1016/J.NEURON.2011.04.020

Fogarty, M., Grist, M., Gelman, D., Marín, O., Pachnis, V., & Kessaris, N. (2007). Spatial genetic patterning of the embryonic neuroepithelium generates GABAergic interneuron diversity in the adult cortex. *Soc NeuroscienceM Fogarty, M Grist, D Gelman, O Marín, V Pachnis, N KessarisJournal of Neuroscience, 2007•Soc Neuroscience*, *27*(41), 10935–10946. https://doi.org/10.1523/JNEUROSCI.1629-07.2007

Fragkouli, A., van Wijk, N. V., Lopes, R., Kessaris, N., & Pachnis, V. (2009). LIM homeodomain transcription factor-dependent specification of bipotential MGE progenitors into cholinergic and GABAergic striatal interneurons. *Development*, *136*(22), 3841–3851. https://doi.org/10.1242/DEV.038083

Furlanis, E., Dai, M., Leyva Garcia, B., Tran, T., Vergara, J., Pereira, A., Gorissen, B. L., Wills, S., Vlachos, A., Hairston, A., Dwivedi, D., Du, S., McMahon, J., Huang, S., Morabito, A., Vazquez, A., Kim, S., Lee, A. T., Chang, E. F., … Wang, Y. (2025a). An enhancer-AAV toolbox to target and manipulate distinct interneuron subtypes. *Neuron*, *113*(10), 1525-1547.e15. https://doi.org/10.1016/J.NEURON.2025.05.002

Gabitto, M. I., Travaglini, K. J., Rachleff, V. M., Kaplan, E. S., Long, B., Ariza, J., Ding, Y., Mahoney, J. T., Dee, N., Goldy, J., Melief, E. J., Agrawal, A., Kana, O., Zhen, X., Barlow, S. T., Brouner, K., Campos, J., Campos, J., Carr, A. J., … Lein, E. S. (2024). Integrated multimodal cell atlas of Alzheimer's disease. *Nature Neuroscience 2024 27:12*, *27*(12), 2366–2383. https://doi.org/10.1038/s41593-024-01774-5

Gao, P., Sultan, K. T., Zhang, X. J., & Shi, S. H. (2013). Lineage-dependent circuit assembly in the neocortex. *Development*, *140*(13), 2645–2655. https://doi.org/10.1242/dev.087668

Ge, S. X., Son, E. W., & Yao, R. (2018). iDEP: an integrated web application for differential expression and pathway analysis of RNA-Seq data. *BMC Bioinformatics*, *19*(1). https://doi.org/10.1186/s12859-018-2486-6

Gertler, T. S., Cherian, S., DeKeyser, J. M., Kearney, J. A., & George, A. L. (2022). KNa1.1 gain-of-function preferentially dampens excitability of murine parvalbumin-positive interneurons. *Neurobiology of Disease*, *168*. https://doi.org/10.1016/J.NBD.2022.105713

Gilbert, L. A., Horlbeck, M. A., Adamson, B., Villalta, J. E., Chen, Y., Whitehead, E. H., Guimaraes, C., Panning, B., Ploegh, H. L., Bassik, M. C., Qi, L. S., Kampmann, M., & Weissman, J. S. (2014). Genome-Scale CRISPR-Mediated Control of Gene Repression and Activation. *Cell*, *159*(3), 647. https://doi.org/10.1016/j.cell.2014.09.029

Gilbert, L. A., Larson, M. H., Morsut, L., Liu, Z., Brar, G. A., Torres, S. E., Stern-Ginossar, N., Brandman, O., Whitehead, E. H., Doudna, J. A., Lim, W. A., Weissman, J. S., & Qi, L. S. (2013). CRISPR-mediated modular RNA-guided regulation of transcription in eukaryotes. *Cell*, *154*(2), 442. https://doi.org/10.1016/j.cell.2013.06.044

Gonzalez-Burgos, G., & Lewis, D. A. (2012). NMDA Receptor Hypofunction, Parvalbumin-Positive Neurons, and Cortical Gamma Oscillations in Schizophrenia. *Schizophrenia Bulletin*, *38*(5), 950. https://doi.org/10.1093/SCHBUL/SBS010

Goodspeed, K., Pérez-Palma, E., Iqbal, S., Cooper, D., Scimemi, A., Johannesen, K. M., Stefanski, A., Demarest, S., Helbig, K. L., Kang, J., Shaffo, F. C., Prentice, B., Brownstein, C. A., Lim, B., Helbig, I., De Los Reyes, E., McKnight, D., Crunelli, V., Campbell, A. J., … Lal, D. (2020). Current knowledge of SLC6A1-related neurodevelopmental disorders. *Brain Communications*, *2*(2), 1–10. https://doi.org/10.1093/braincomms/fcaa170

Guo, W., Rioux, M., Shaffo, F., Hu, Y., Yu, Z., Xing, C., & Gray, S. J. (2025). AAV9/SLC6A1 gene therapy rescues abnormal EEG patterns and cognitive behavioral deficiencies in Slc6a1–/– mice. *The Journal of Clinical Investigation*, *135*(3). https://doi.org/10.1172/JCI182235

Guttenplan, K. A., Maxwell, I., Santos, E., Borchardt, L. A., Manzo, E., Abalde-Atristain, L., Kim, R. D., & Freeman, M. R. (2025). GPCR signaling gates astrocyte responsiveness to neurotransmitters and control of neuronal activity. *Science*, *388*(6748), 763–768. https://doi.org/10.1126/science.adq5729

Hájos, N., Pálhalini, J., Mann, E. O., Nèmeth, B., Paulsen, O., & Freund, T. F. (2004). Spike Timing of Distinct Types of GABAergic Interneuron during Hippocampal Gamma Oscillations In Vitro. *The Journal of Neuroscience*, *24*(41), 9127. https://doi.org/10.1523/JNEUROSCI.2113-04.2004

Hamburger, V., & Hamilton, H. L. (1951). A series of normal stages in the development of the chick embryo. *Journal of Morphology*, *88*(1), 49–92. https://doi.org/10.1002/jmor.1050880104

Hansen, D. V., Lui, J. H., Flandin, P., Yoshikawa, K., Rubenstein, J. L., Alvarez-Buylla, A., & Kriegstein, A. R. (2013). Non-epithelial stem cells and cortical interneuron production in the human ganglionic eminences. *Nature Neuroscience 2013 16:11*, *16*(11), 1576–1587. https://doi.org/10.1038/nn.3541

Hansen, D. V., Lui, J. H., Parker, P. R. L., & Kriegstein, A. R. (2010). Neurogenic radial glia in the outer subventricular zone of human neocortex. *Nature*, *464*(7288), 554–561. https://doi.org/10.1038/nature08845

Härtig, W., Brauer, K., & Brückner, G. (1992). Wisteria floribunda agglutinin-labelled nets surround parvalbumin-containing neurons. *Neuroreport*, *3*(10), 869–872. https://doi.org/10.1097/00001756-199210000-00012

Hawrylycz, M. J., Lein, E. S., Guillozet-Bongaarts, A. L., Shen, E. H., Ng, L., Miller, J. A., Van De Lagemaat, L. N., Smith, K. A., Ebbert, A., Riley, Z. L., Abajian, C., Beckmann, C. F., Bernard, A., Bertagnolli, D., Boe, A. F., Cartagena, P. M., Mallar Chakravarty, M., Chapin, M., Chong, J., … Jones, A. R. (2012). An anatomically comprehensive atlas of the adult human brain transcriptome. *Nature 2012 489:7416*, *489*(7416), 391–399. https://doi.org/10.1038/nature11405

He, Z., Dony, L., Fleck, J. S., Szałata, A., Li, K. X., Slišković, I., Lin, H.-C., Santel, M., Atamian, A., Quadrato, G., Sun, J., Pașca, S. P., Amin, N. D., Kelley, K. W., Bertucci, T., Temple, S., Bowles, K. R., Caporale, N., Villa, E., … Treutlein, B. (2024). An integrated transcriptomic cell atlas of human neural organoids. *Nature 2024 635:8039*, *635*(8039), 690–698. https://doi.org/10.1038/s41586-024-08172-8

He, Z., Maynard, A., Jain, A., Gerber, T., Petri, R., Lin, H. C., Santel, M., Ly, K., Dupré, J. S., Sidow, L., Sanchis Calleja, F., Jansen, S. M. J., Riesenberg, S., Camp, J. G., & Treutlein, B. (2021). Lineage recording in human cerebral organoids. *Nature Methods 2021 19:1*, *19*(1), 90–99. https://doi.org/10.1038/s41592-021-01344-8

Helbig, K. L., Farwell Hagman, K. D., Shinde, D. N., Mroske, C., Powis, Z., Li, S., Tang, S., & Helbig, I. (2016). Diagnostic exome sequencing provides a molecular diagnosis for a significant proportion of patients with epilepsy. *Genetics in Medicine*, *18*(9), 898–905. https://doi.org/10.1038/gim.2015.186

Hildebrand, M. S., Dahl, H. H. M., Damiano, J. A., Smith, R. J. H., Scheffer, I. E., & Berkovic, S. F. (2013). Recent advances in the molecular genetics of epilepsy. *Journal of Medical Genetics*, *50*(5), 271–279. https://doi.org/10.1136/jmedgenet-2012-101448

Hongo, I., Kengaku, M., & Okamoto, H. (1999). FGF signaling and the anterior neural induction in Xenopus. *Developmental Biology*, *216*(2), 561–581. https://doi.org/10.1006/dbio.1999.9515

Hu, X., Zhao, M., Yang, X., Wang, D., & Wu, Q. (2023). Association between the SLC6A11 rs2304725 and GABRG2 rs211037 polymorphisms and drug-resistant epilepsy: a meta-analysis. *Frontiers in Physiology*, *14*, 1191927. https://doi.org/10.3389/fphys.2023.1191927

Huberfeld, G., Wittner, L., Clemenceau, S., Baulac, M., Kaila, K., Miles, R., & Rivera, C. (2007). Perturbed Chloride Homeostasis and GABAergic Signaling in Human Temporal Lobe Epilepsy. *The Journal of Neuroscience*, *27*(37), 9866. https://doi.org/10.1523/JNEUROSCI.2761-07.2007

Imbrosci, B., & Mittmann, T. (2011). Functional Consequences of the Disturbances in the GABA-Mediated Inhibition Induced by Injuriesin the Cerebral Cortex. *Neural Plasticity*, *2011*, 614329. https://doi.org/10.1155/2011/614329

Imoukhuede, P. I., Moss, F. J., Michael, D. J., Chow, R. H., & Lester, H. A. (2009). Ezrin Mediates Tethering of the γ-Aminobutyric Acid Transporter GAT1 to Actin Filaments Via a C-Terminal PDZ-Interacting Domain. *Biophysical Journal*, *96*(7), 2949–2960. https://doi.org/10.1016/j.bpj.2008.11.070

Inada, H., Watanabe, M., Uchida, T., Ishibashi, H., Wake, H., Nemoto, T., Yanagawa, Y., Fukuda, A., & Nabekura, J. (2011). GABA Regulates the Multidirectional Tangential Migration of GABAergic Interneurons in Living Neonatal Mice. *PLoS ONE*, *6*(12), e27048. https://doi.org/10.1371/JOURNAL.PONE.0027048

Inda, M. C., DeFelipe, J., & Muñoz, A. (2007). The distribution of chandelier cell axon terminals that express the GABA plasma membrane transporter GAT-1 in the human neocortex. *Cerebral Cortex (New York, N.Y. : 1991)*, *17*(9), 2060–2071. https://doi.org/10.1093/CERCOR/BHL114

Isaacson, J. S., Solis, J. M., & Nicoll, R. A. (1993). Local and diffuse synaptic actions of GABA in the hippocampus. *Neuron*, *10*(2), 165–175. https://doi.org/10.1016/0896-6273(93)90308-E

Itoh, Y., Higuchi, M., Oishi, K., Kishi, Y., Okazaki, T., Sakai, H., Miyata, T., Nakajima, K., & Gotoh, Y. (2016). PDK1-Akt pathway regulates radial neuronal migration and microtubules in the developing mouse neocortex. *Proceedings of the National Academy of Sciences of the United States of America*, *113*(21), E2955–E2964. https://doi.org/10.1073/pnas.1516321113

Jacobs, J., Kahana, M. J., Ekstrom, A. D., & Fried, I. (2007). Brain oscillations control timing of single-neuron activity in humans. *Journal of Neuroscience*, *27*(14), 3839–3844. https://doi.org/10.1523/JNEUROSCI.4636-06.2007,

Jahodova, I., Baliova, M., & Jursky, F. (2023). PDZ interaction of the GABA transporter GAT1 with the syntenin-1 in Neuro-2a cells. *Neurochemistry International*, *165*, 105522. https://doi.org/10.1016/j.neuint.2023.105522

Jakovcevski, I., Mayer, N., & Zecevic, N. (2010). Multiple Origins of Human Neocortical Interneurons Are Supported by Distinct Expression of Transcription Factors. *Cerebral Cortex (New York, NY)*, *21*(8), 1771. https://doi.org/10.1093/CERCOR/BHQ245

Jensen, K., Chiu, C. S., Sokolova, I., Lester, H. A., & Mody, I. (2003). GABA transporter-1 (GAT1)-deficient mice: Differential tonic activation of GABAA versus GABAB receptors in the hippocampus. *Journal of Neurophysiology*, *90*(4), 2690–2701. https://doi.org/10.1152/jn.00240.2003

Ji, L., Xu, Y., & Tang, N. (2021). Solute carrier family 6 member 1 promoting the proliferation and invasion of breast cancer cells through affecting the phosphorylation of PI3K/Akt signaling pathway. *Acta Anatomica Sinica*, *52*(5), 759–766. https://doi.org/10.16098/J.ISSN.0529-1356.2021.05.013

Jiang, X., Lachance, M., & Rossignol, E. (2016). Involvement of cortical fast-spiking parvalbumin-positive basket cells in epilepsy. *Progress in Brain Research*, *226*, 81–126. https://doi.org/10.1016/BS.PBR.2016.04.012

Jiang, X., Lupien-Meilleur, A., Tazerart, S., Lachance, M., Samarova, E., Araya, R., Lacaille, J. C., & Rossignol, E. (2018). Remodeled cortical inhibition prevents motor seizures in generalized epilepsy. *Annals of Neurology*, *84*(3), 436–451. https://doi.org/10.1002/ANA.25301

Johannesen, K. M., Gardella, E., Linnankivi, T., Courage, C., de Saint Martin, A., Lehesjoki, A. E., Mignot, C., Afenjar, A., Lesca, G., Abi-Warde, M. T., Chelly, J., Piton, A., Merritt, J. L., Rodan, L. H., Tan, W. H., Bird, L. M., Nespeca, M., Gleeson, J. G., Yoo, Y., … Møller, R.

S. (2018). Defining the phenotypic spectrum of SLC6A1 mutations. *Epilepsia*, *59*(2), 389–402. https://doi.org/10.1111/epi.13986

Jossin, Y., & Goffinet, A. M. (2007). Reelin Signals through Phosphatidylinositol 3-Kinase and Akt To Control Cortical Development and through mTor To Regulate Dendritic Growth. *Molecular and Cellular Biology*, *27*(20), 7113. https://doi.org/10.1128/mcb.00928-07

Juarez, P., & Martínez Cerdeño, V. (2022). Parvalbumin and parvalbumin chandelier interneurons in autism and other psychiatric disorders. *Frontiers in Psychiatry*, *13*. https://doi.org/10.3389/FPSYT.2022.913550/FULL

Jursky, F., & Nelson, N. (1996). Developmental expression of GABA transporters GAT1 and GAT4 suggests involvement in brain maturation. *Journal of Neurochemistry*, *67*(2), 857–867. https://doi.org/10.1046/J.1471-4159.1996.67020857.X

Kaczmarek, L. K., & Zhang, Y. (2017). Kv3 Channels: Enablers of Rapid Firing, Neurotransmitter Release, and Neuronal Endurance. *Physiological Reviews*, *97*(4), 1431–1468. https://doi.org/10.1152/PHYSREV.00002.2017

Kadoshima, T., Sakaguchi, H., Nakano, T., Soen, M., Ando, S., Eiraku, M., & Sasai, Y. (2013). Self-organization of axial polarity, inside-out layer pattern, and species-specific progenitor dynamics in human ES cell-derived neocortex. *Proceedings of the National Academy of Sciences of the United States of America*, *110*(50), 20284–20289. https://doi.org/10.1073/pnas.1315710110

Kaneko, K., Currin, C. B., Goff, K. M., Wengert, E. R., Somarowthu, A., Vogels, T. P., & Goldberg, E. M. (2022). Developmentally regulated impairment of parvalbumin interneuron synaptic transmission in an experimental model of Dravet syndrome. *Cell Reports*, *38*(13). https://doi.org/10.1016/j.celrep.2022.110580

Kang, H. J., Kawasawa, Y. I., Cheng, F., Zhu, Y., Xu, X., Li, M., Sousa, A. M. M., Pletikos, M., Meyer, K. A., Sedmak, G., Guennel, T., Shin, Y., Johnson, M. B., Krsnik, Ž., Mayer, S., Fertuzinhos, S., Umlauf, S., Lisgo, S. N., Vortmeyer, A., … Šestan, N. (2011). Spatio-temporal transcriptome of the human brain. *Nature 2011 478:7370*, *478*(7370), 483–489. https://doi.org/10.1038/nature10523

Keefe, F., Monzón-Sandoval, J., Rosser, A. E., Webber, C., & Li, M. (2023). Single-Cell Transcriptomics Reveals Conserved Regulatory Networks in Human and Mouse Interneuron Development. *International Journal of Molecular Sciences*, *24*(9). https://doi.org/10.3390/IJMS24098122

Kékesi, O., Ioja, E., Szabó, Z., Kardos, J., & Héja, L. (2015). Recurrent seizure-like events are associated with coupled astroglial synchronization. *Frontiers in Cellular Neuroscience*, *9*(JUNE), 128954. https://doi.org/10.3389/fncel.2015.00215

Kessaris, N., Fogarty, M., Iannarelli, P., Grist, M., Wegner, M., & Richardson, W. D. (2006). Competing waves of oligodendrocytes in the forebrain and postnatal elimination of an embryonic lineage. *Nature Neuroscience*, *9*(2), 173–179. https://doi.org/10.1038/NN1620

Kilb, W. (2012). Development of the GABAergic system from birth to adolescence. *Neuroscientist*, *18*(6), 613–630. https://doi.org/10.1177/1073858411422114

Kilb, W., Kirischuk, S., & Luhmann, H. J. (2013). Role of tonic GABAergic currents during pre- and early postnatal rodent development. *Frontiers in Neural Circuits*, *7*(SEP), 59343. https://doi.org/10.3389/FNCIR.2013.00139/FULL

Kim, E., Kim, Y., Hong, S., Kim, I., Lee, J., Yoo, J. Y., Kim, J., Yoo, K., Lee, H., Kim, J. H., Choi, J., & Shin, K. (2025). Single rosette-based generation of uniform cortical assembloids recapitulating cellular interactions between neurons and glial cells. *Nature Communications 2025 16:1*, *16*(1), 11362-. https://doi.org/10.1038/s41467-025-66440-1

Koh, W., Park, Y. M., Lee, S. E., & Lee, C. J. (2017). AAV-Mediated Astrocyte-Specific Gene Expression under Human ALDH1L1 Promoter in Mouse Thalamus. *Experimental Neurobiology*, *26*(6), 350. https://doi.org/10.5607/en.2017.26.6.350

Kohtz, J. D., Baker, D. P., Corte, G., & Fishell, G. (1998). Regionalization within the mammalian telencephalon is mediated by changes in responsiveness to Sonic Hedgehog. *Development (Cambridge, England)*, *125*(24), 5079–5089. https://doi.org/10.1242/DEV.125.24.5079

Kolb, I., Hasseman, J. P., Matsumoto, A., Jensen, T. P., Kopach, O., Arthur, B. J., Zhang, Y., Tsang, A., Reep, D., Tsegaye, G., Zheng, J., Patel, R. H., Looger, L. L., Marvin, J. S., Korff, W. L., Rusakov, D. A., Yonehara, K., Team, G. P., & Turner, G. C. (2026). iGABASnFR2: Improved genetically encoded protein sensors of GABA. *ELife*, *14*. https://doi.org/10.7554/eLife.108319.2

Kostyanovskaya, E., Lasser, M. C., Wang, B., Schmidt, J., Bader, E., Buteo, C., Arbelaez, J., Sindledecker, A. R., McCluskey, K. E., Castillo, O., Wang, S., Dea, J., Helde, K. A., Graglia, J. M., Brimble, E., Kastner, D. B., Ehrlich, A. T., State, M. W., Willsey, A. J., & Willsey, H. R. (2025). Convergence of autism proteins at the cilium. *BioRxiv*, 2024.12.05.626924. https://doi.org/10.1101/2024.12.05.626924

La Manno, G., Soldatov, R., Zeisel, A., Braun, E., Hochgerner, H., Petukhov, V., Lidschreiber, K., Kastriti, M. E., Lönnerberg, P., Furlan, A., Fan, J., Borm, L. E., Liu, Z., van Bruggen, D., Guo, J., He, X., Barker, R., Sundström, E., Castelo-Branco, G., … Kharchenko, P. V. (2018). RNA velocity of single cells. *Nature 2018 560:7719*, *560*(7719), 494–498. https://doi.org/10.1038/s41586-018-0414-6

Lancaster, M. A., Renner, M., Martin, C. A., Wenzel, D., Bicknell, L. S., Hurles, M. E., Homfray, T., Penninger, J. M., Jackson, A. P., & Knoblich, J. A. (2013). Cerebral organoids model human brain development and microcephaly. *Nature*, *501*(7467), 373–379. https://doi.org/10.1038/nature12517

Lazarus, M. S., & Josh Huang, Z. (2011). Distinct maturation profiles of perisomatic and dendritic targeting GABAergic interneurons in the mouse primary visual cortex during the critical period of ocular dominance plasticity. *Journal of Neurophysiology*, *106*(2), 775. https://doi.org/10.1152/jn.00729.2010

Lefton, K. B., Wu, Y., Dai, Y., Okuda, T., Zhang, Y., Yen, A., Rurak, G. M., Walsh, S., Manno, R., Myagmar, B. E., Dougherty, J. D., Samineni, V. K., Simpson, P. C., & Papouin, T. (2025). Norepinephrine signals through astrocytes to modulate synapses. *Science*, *388*(6748), 776–783. https://doi.org/10.1126/science.adq5480

Lester, H. A., Mager, S., Quick, M. W., & Corey, J. L. (1994). Permeation properties of neurotransmitter transporters. *Annual Review of Pharmacology and Toxicology*, *34*, 219–249. https://doi.org/10.1146/annurev.pa.34.040194.001251

Lévesque, M., Wang, S., Etter, G., Williams, S., & Avoli, M. (2022). Bilateral optogenetic activation of inhibitory cells favors ictogenesis. *Neurobiology of Disease*, *171*. https://doi.org/10.1016/j.nbd.2022.105794

Lewis, D. A. (2014). Inhibitory neurons in human cortical circuits: substrate for cognitive dysfunction in schizophrenia. *Current Opinion in Neurobiology*, *26*, 22–26. https://doi.org/10.1016/J.CONB.2013.11.003

Li, B., & Dewey, C. N. (2011). RSEM: accurate transcript quantification from RNA-Seq data with or without a reference genome. *BMC Bioinformatics*, *12*. https://doi.org/10.1186/1471-2105-12-323

Li, B., He, Y. Y., & Yang, Z. M. (2025). Primary cilia function as hubs for signal transduction. *Cell & Bioscience*, *15*(1), 163. https://doi.org/10.1186/s13578-025-01471-1

Li, W., Cogswell, C. A., & LoTurco, J. J. (1998). Neuronal Differentiation of Precursors in the Neocortical Ventricular Zone Is Triggered by BMP. *Journal of Neuroscience*, *18*(21), 8853–8862. https://doi.org/10.1523/jneurosci.18-21-08853.1998

Liem, J., Jessell, T. M., & Briscoe, J. (2000). Regulation of the neural patterning activity of sonic hedgehog by secreted BMP inhibitors expressed by notochord and somites. *Development (Cambridge, England)*, *127*(22), 4855–4866. https://doi.org/10.1242/DEV.127.22.4855

Lim, L., Mi, D., Llorca, A., & Marín, O. (2018). Development and Functional Diversification of Cortical Interneurons. *Neuron*, *100*(2), 294–313. https://doi.org/10.1016/J.NEURON.2018.10.009

Lin, Y. H., Wu, F., Li, T. Y., Lin, L., Gao, F., Zhu, L. J., Xu, X. M., Chen, M. Y., Hou, Y. L., Zhang, C. J., Wu, H. Y., Chang, L., Luo, C. X., Qin, Y. J., & Zhu, D. Y. (2024). Disrupting stroke-induced GAT-1-syntaxin1A interaction promotes functional recovery after stroke. *Cell Reports Medicine*, *5*(11). https://doi.org/10.1016/j.xcrm.2024.101789

Liodis, P., Denaxa, M., Grigoriou, M., Akufo-Addo, C., Yanagawa, Y., & Pachnis, V. (2007). Lhx6 activity is required for the normal migration and specification of cortical interneuron subtypes. *Soc NeuroscienceP Liodis, M Denaxa, M Grigoriou, C Akufo-Addo, Y Yanagawa, V PachnisJournal of Neuroscience, 2007•Soc Neuroscience*, *27*(12), 3078–3089. https://doi.org/10.1523/JNEUROSCI.3055-06.2007

Liu, W., Yang, Y., Liu, Y., Ni, B., Zhuang, H., Chen, K., Shi, J., Zhu, C., Wang, H., & Fei, J. (2025). γ-Aminobutyric Acid Transporter Mutation GAT1 (S295L) Substantially Impairs Neurogenesis in Dentate Gyrus. *Brain Sciences*, *15*(4), 393. https://doi.org/10.3390/brainsci15040393

López-Bendito, G., Luján, R., Shigemoto, R., Ganter, P., Paulsen, O., & Molnár, Z. (2003). Blockade of GABA(B) receptors alters the tangential migration of cortical neurons. *Cerebral Cortex (New York, N.Y. : 1991)*, *13*(9), 932–942. https://doi.org/10.1093/cercor/13.9.932

Lopez-Santiago, L. F., Yuan, Y., Wagnon, J. L., Hull, J. M., Frasier, C. R., O'Malley, H. A., Meisler, M. H., & Isom, L. L. (2017). Neuronal hyperexcitability in a mouse model of SCN8A epileptic encephalopathy. *Proceedings of the National Academy of Sciences of the United States of America*, *114*(9), 2383–2388. https://doi.org/10.1073/PNAS.1616821114

LoTurco, J. J., Owens, D. F., Heath, M. J. S., Davis, M. B. E., & Kriegstein, A. R. (1995). GABA and glutamate depolarize cortical progenitor cells and inhibit DNA synthesis. *Neuron*, *15*(6), 1287–1298. https://doi.org/10.1016/0896-6273(95)90008-X

Loukil, A., Ebright, E., Hamdi, K., Menzel, E., Uezu, A., Gao, Y., Soderling, S. H., & Goetz, S. C. (2025). Identification of New Ciliary Signaling Pathways in the Brain and Insights into Neurological Disorders. *Journal of Neuroscience*, *45*(33). https://doi.org/10.1523/JNEUROSCI.0800-24.2025

Lu, J., Tucciarone, J., Lin, Y., & Huang, Z. J. (2014). Input-specific maturation of synaptic dynamics of parvalbumin interneurons in primary visual cortex. *Proceedings of the National Academy of Sciences*, *111*(47), 16895–16900. https://doi.org/10.1073/pnas.1400694111

Lupien-Meilleur, A., Jiang, X., Lachance, M., Taschereau-Dumouchel, V., Gagnon, L., Vanasse, C., Lacaille, J. C., & Rossignol, E. (2021). Reversing frontal disinhibition rescues behavioural deficits in models of CACNA1A-associated neurodevelopment disorders. *Molecular Psychiatry*, *26*(12), 7225–7246. https://doi.org/10.1038/S41380-021-01175-1

Lybrand, Z. R., Goswami, S., Zhu, J., Jarzabek, V., Merlock, N., Aktar, M., Smith, C., Zhang, L., Varma, P., Cho, K. O., Ge, S., & Hsieh, J. (2021). A critical period of neuronal activity results in aberrant neurogenesis rewiring hippocampal circuitry in a mouse model of epilepsy. *Nature Communications 2021 12:1*, *12*(1), 1423-. https://doi.org/10.1038/s41467-021-21649-8

Ma, T., Wang, C., Wang, L., Zhou, X., Tian, M., Zhang, Q., Zhang, Y., Li, J., Liu, Z., Cai, Y., Liu, F., You, Y., Chen, C., Campbell, K., Song, H., Ma, L., Rubenstein, J. L., & Yang, Z. (2013). Subcortical origins of human and monkey neocortical interneurons. *Nature Neuroscience 2013 16:11*, *16*(11), 1588–1597. https://doi.org/10.1038/nn.3536

Mabie, P. C., Mehler, M. F., & Kessler, J. A. (1999). Multiple Roles of Bone Morphogenetic Protein Signaling in the Regulation of Cortical Cell Number and Phenotype. *Journal of Neuroscience*, *19*(16), 7077–7088. https://doi.org/10.1523/jneurosci.19-16-07077.1999

MacAulay, N., Zeuthen, T., & Gether, U. (2002a). Conformational basis for the Li(+)-induced leak current in the rat gamma-aminobutyric acid (GABA) transporter-1. *The Journal of Physiology*, *544*(2), 447–458. https://doi.org/10.1113/jphysiol.2002.022897

MacAulay, N., Zeuthen, T., & Gether, U. (2002b). Conformational basis for the Li+-induced leak current in the rat γ-aminobutyric acid (GABA) transporter-1. *The Journal of Physiology*, *544*(2), 447–458. https://doi.org/10.1113/jphysiol.2002.022897

Macdonald, R. L., Kang, J.-Q., & Gallagher, M. J. (2012). GABAA Receptor Subunit Mutations and Genetic Epilepsies. *Jasper's Basic Mechanisms of the Epilepsies*, 740–749. https://doi.org/10.1093/med/9780199746545.003.0057

Mager, S., Naeve, J., Quick, M., Labarca, C., Davidson, N., & Lester, H. A. (1993a). Steady states, charge movements, and rates for a cloned GABA transporter expressed in Xenopus oocytes. *Neuron*, *10*(2), 177–188. https://doi.org/10.1016/0896-6273(93)90309-F

Mager, S., Naeve, J., Quick, M., Labarca, C., Davidson, N., & Lester, H. A. (1993b). Steady states, charge movements, and rates for a cloned GABA transporter expressed in Xenopus oocytes. *Neuron*, *10*(2), 177–188. https://doi.org/10.1016/0896-6273(93)90309-F

Mann, E. O., & Mody, I. (2009). Control of hippocampal gamma oscillation frequency by tonic inhibition and excitation of interneurons. *Nature Neuroscience*, *13*(2), 205. https://doi.org/10.1038/nn.2464

Marín, O. (2012). Interneuron dysfunction in psychiatric disorders. *Nature Reviews Neuroscience*, *13*(2), 107–120. https://doi.org/10.1038/nrn3155

Marín, O., Anderson, S. A., & Rubenstein, J. L. R. (2000). Origin and molecular specification of striatal interneurons. *Journal of Neuroscience*, *20*(16), 6063–6076. https://doi.org/10.1523/JNEUROSCI.20-16-06063.2000

Maroof, A. M., Keros, S., Tyson, J. A., Ying, S. W., Ganat, Y. M., Merkle, F. T., Liu, B., Goulburn, A., Stanley, E. G., Elefanty, A. G., Widmer, H. R., Eggan, K., Goldstein, P. A., Anderson, S. A., & Studer, L. (2013). Directed differentiation and functional maturation of cortical interneurons from human embryonic stem cells. *Cell Stem Cell*, *12*(5), 559–572. https://doi.org/10.1016/j.stem.2013.04.008

Marshall, G. F., Gonzalez-Sulser, A., & Abbott, C. M. (2021). Modelling epilepsy in the mouse: challenges and solutions. *Disease Models & Mechanisms*, *14*(3), dmm047449. https://doi.org/10.1242/DMM.047449

Martin, M. (2011). Cutadapt removes adapter sequences from high-throughput sequencing reads. *EMBnet.Journal*, *17*(1), 10–12. https://doi.org/10.14806/ej.17.1.200

Martínez-Cerdeño, V., Cunningham, C. L., Camacho, J., Antczak, J. L., Prakash, A. N., Cziep, M. E., Walker, A. I., & Noctor, S. C. (2012). Comparative analysis of the subventricular zone in rat, ferret and macaque: evidence for an outer subventricular zone in rodents. *PloS One*, *7*(1). https://doi.org/10.1371/journal.pone.0030178

Matthews, E., Rahnama-Vaghef, A., & Eskandari, S. (2009). Inhibitors of the γ-Aminobutyric Acid Transporter 1 (GAT1) Do Not Reveal a Channel Mode of Conduction. *Neurochemistry International*, *55*(8), 732. https://doi.org/10.1016/J.NEUINT.2009.07.005

Mattison, K. A., Butler, K. M., Inglis, G. A. S., Dayan, O., Boussidan, H., Bhambhani, V., Philbrook, B., da Silva, C., Alexander, J. J., Kanner, B. I., & Escayg, A. (2018). SLC6A1 variants identified in epilepsy patients reduce γ-aminobutyric acid transport. *Epilepsia*, *59*(9), e135–e141. https://doi.org/10.1111/epi.14531

Mayhew, C. N., & Singhania, R. (2023a). A review of protocols for brain organoids and applications for disease modeling. *STAR Protocols*, *4*(1), 101860. https://doi.org/10.1016/j.xpro.2022.101860

Mayhew, C. N., & Singhania, R. (2023b). A review of protocols for brain organoids and applications for disease modeling. *STAR Protocols*, *4*(1), 101860. https://doi.org/10.1016/j.xpro.2022.101860

Mazelova, J., Astuto-Gribble, L., Inoue, H., Tam, B. M., Schonteich, E., Prekeris, R., Moritz, O. L., Randazzo, P. A., & Deretic, D. (2009). Ciliary targeting motif VxPx directs assembly of a trafficking module through Arf4. *The EMBO Journal*, *28*(3), 183. https://doi.org/10.1038/emboj.2008.267

Meissner, A., Wernig, M., & Jaenisch, R. (2007). Direct reprogramming of genetically unmodified fibroblasts into pluripotent stem cells. *Nature Biotechnology*, *25*(10), 1177–1181. https://doi.org/10.1038/nbt1335

Melone, M., Ciappelloni, S., & Conti, F. (2014). Plasma membrane transporters GAT-1 and GAT-3 contribute to heterogeneity of GABAergic synapses in neocortex. *Frontiers in Neuroanatomy*, *8*(JULY). https://doi.org/10.3389/FNANA.2014.00072

Mermer, F., Poliquin, S., Rigsby, K., Rastogi, A., Shen, W., Romero-Morales, A., Nwosu, G., McGrath, P., Demerast, S., Aoto, J., Bilousova, G., Lal, D., Gama, V., & Kang, J. Q. (2021). Common molecular mechanisms of SLC6A1 variant-mediated neurodevelopmental disorders in astrocytes and neurons. *Brain*, *144*(8), 2499. https://doi.org/10.1093/BRAIN/AWAB207

Mermer, F., Poliquin, S., Zhou, S., Wang, X., Ding, Y., Yin, F., Shen, W., Wang, J., Rigsby, K., Xu, D., Mack, T., Nwosu, G., Flamm, C., Stein, M., & Kang, J. Q. (2022). Astrocytic GABA transporter 1 deficit in novel SLC6A1 variants mediated epilepsy: Connected from protein destabilization to seizures in mice and humans. *Neurobiology of Disease*, *172*, 105810. https://doi.org/10.1016/j.nbd.2022.105810

Minelli, A., Brecha, N. C., Karschin, C., DeBiasi, S., & Conti, F. (1995). GAT-1, a high-affinity GABA plasma membrane transporter, is localized to neurons and astroglia in the cerebral cortex. *The Journal of Neuroscience : The Official Journal of the Society for Neuroscience*, *15*(11), 7734–7746. https://doi.org/10.1523/JNEUROSCI.15-11-07734.1995

Minelli, A., DeBiasi, S., Brecha, N. C., Zuccarello, L. V., & Conti, F. (1996). GAT-3, a High-Affinity GABA Plasma Membrane Transporter, Is Localized to Astrocytic Processes, and It

Is Not Confined to the Vicinity of GABAergic Synapses in the Cerebral Cortex. *Journal of Neuroscience*, *16*(19), 6255–6264. https://doi.org/10.1523/jneurosci.16-19-06255.1996

Minocha, S., Valloton, D., Ypsilanti, A. R., Fiumelli, H., Allen, E. A., Yanagawa, Y., Marin, O., Chédotal, A., Hornung, J. P., & Lebrand, C. (2015). Nkx2.1-derived astrocytes and neurons together with Slit2 are indispensable for anterior commissure formation. *Nature Communications*, *6*. https://doi.org/10.1038/NCOMMS7887

Miralles, R. M., Boscia, A. R., Kittur, S., Hanflink, J. C., Panchal, P. S., Yorek, M. S., Deutsch, T. C. J., Reever, C. M., Vundela, S. R., Wengert, E. R., & Patel, M. K. (2024). Parvalbumin interneuron impairment causes synaptic transmission deficits and seizures in SCN8A developmental and epileptic encephalopathy. *JCI Insight*, *9*(20). https://doi.org/10.1172/jci.insight.181005

Miri, M. L., Vinck, M., Pant, R., & Cardin, J. A. (2018). Altered hippocampal interneuron activity precedes ictal onset. *ELife*, *7*, e40750. https://doi.org/10.7554/eLife.40750

Miyoshi, G., Butt, S. J. B., Takebayashi, H., & Fishell, G. (2007). Physiologically Distinct Temporal Cohorts of Cortical Interneurons Arise from Telencephalic Olig2-Expressing Precursors. *Journal of Neuroscience*, *27*(29), 7786–7798. https://doi.org/10.1523/JNEUROSCI.1807-07.2007

Mo, Z., & Zecevic, N. (2008). Is Pax6 critical for neurogenesis in the human fetal brain? *Cerebral Cortex (New York, N.Y. : 1991)*, *18*(6), 1455–1465. https://doi.org/10.1093/CERCOR/BHM181

Mohammadi, N. A., Ahring, P. K., Yu Liao, V. W., Chua, H. C., Ortiz de la Rosa, S., Johannesen, K. M., Michaeli-Yossef, Y., Vincent-Devulder, A., Meridda, C., Bruel, A. L., Rossi, A., Patel, C., Klepper, J., Bonanni, P., Minghetti, S., Trivisano, M., Specchio, N., Amor, D., Auvin, S., … Møller, R. S. (2024). Distinct neurodevelopmental and epileptic phenotypes associated with gain- and loss-of-function GABRB2 variants. *EBioMedicine*, *106*, 105236. https://doi.org/10.1016/j.ebiom.2024.105236

Moldavan, M., Cravetchi, O., & Allen, C. N. (2017). GABA transporters regulate tonic and synaptic GABAA receptor-mediated currents in the suprachiasmatic nucleus neurons. *Https://Doi.Org/10.1152/Jn.00194.2017*, *118*(6), 3092–3106. https://doi.org/10.1152/jn.00194.2017

Muguruma, K., Nishiyama, A., Kawakami, H., Hashimoto, K., & Sasai, Y. (2015). Self-organization of polarized cerebellar tissue in 3D culture of human pluripotent stem cells. *Cell Reports*, *10*(4), 537–550. https://doi.org/10.1016/j.celrep.2014.12.051

Mukhopadhyay, A., McGuire, T., Peng, C. Y., & Kessler, J. A. (2009). Differential effects of BMP signaling on parvalbumin and somatostatin interneuron differentiation. *Development (Cambridge, England)*, *136*(15), 2633. https://doi.org/10.1242/dev.034439

Munguba, H., Nikouei, K., Hochgerner, H., Oberst, P., Kouznetsova, A., Ryge, J., Muñoz-Manchado, A. B., Close, J., Batista-Brito, R., Linnarsson, S., & Hjerling-Leffler, J. (2023).

Transcriptional maintenance of cortical somatostatin interneuron subtype identity during migration. *Neuron*, *111*(22), 3590-3603.e5. https://doi.org/10.1016/J.NEURON.2023.07.018

Muñoz, A., Méndez, P., Defelipe, J., & Alvarez-Leefmans, F. J. (2007). Cation-chloride cotransporters and GABA-ergic innervation in the human epileptic hippocampus. *Epilepsia*, *48*(4), 663–673. https://doi.org/10.1111/j.1528-1167.2007.00986.x

Nadarajah, B., Alifragis, P., Wong, R. O. L., & Parnavelas, J. G. (2003). Neuronal migration in the developing cerebral cortex: Observations based on real-time imaging. *Cerebral Cortex*, *13*(6), 607–611. https://doi.org/10.1093/CERCOR/13.6.607

Nascimento, M. A., Biagiotti, S., Herranz-Pérez, V., Santiago, S., Bueno, R., Ye, C. J., Abel, T. J., Zhang, Z., Rubio-Moll, J. S., Kriegstein, A. R., Yang, Z., Garcia-Verdugo, J. M., Huang, E. J., Alvarez-Buylla, A., & Sorrells, S. F. (2023). Protracted neuronal recruitment in the temporal lobes of young children. *Nature 2023 626:8001*, *626*(8001), 1056–1065. https://doi.org/10.1038/s41586-023-06981-x

Nave, K. A., Winchenbach, J., Düking, T., Berghoff, S. A., Stumpf, S. K., Hülsmann, S., & Saher, G. (2016). Inducible targeting of CNS astrocytes in Aldh1l1-CreERT2 BAC transgenic mice. *F1000Research*, *5*, 2934. https://doi.org/10.12688/f1000research.10509.1

Neves, G., Shah, M. M., Liodis, P., Achimastou, A., Denaxa, M., Roalfe, G., Sesay, A., Walker, M. C., & Pachnis, V. (2013). The LIM homeodomain protein Lhx6 regulates maturation of interneurons and network excitability in the mammalian cortex. *Cerebral Cortex (New York, N.Y. : 1991)*, *23*(8), 1811–1823. https://doi.org/10.1093/CERCOR/BHS159

Nicholas, C. R., Chen, J., Tang, Y., Southwell, D. G., Chalmers, N., Vogt, D., Arnold, C. M., Chen, Y. J. J., Stanley, E. G., Elefanty, A. G., Sasai, Y., Alvarez-Buylla, A., Rubenstein, J. L. R., & Kriegstein, A. R. (2013). Functional maturation of hPSC-derived forebrain interneurons requires an extended timeline and mimics human neural development. *Cell Stem Cell*, *12*(5), 573–586. https://doi.org/10.1016/j.stem.2013.04.005

Nieto-Estévez, V., & Hsieh, J. (2020). Human Brain Organoid Models of Developmental Epilepsies. *Epilepsy Currents*, *20*(5), 282–290. https://doi.org/10.1177/1535759720949254

Niu, W., Deng, L., Mojica-Perez, S. P., Tidball, A. M., Sudyk, R., Stokes, K., & Parent, J. M. (2024). Abnormal cell sorting and altered early neurogenesis in a human cortical organoid model of Protocadherin-19 clustering epilepsy. *Frontiers in Cellular Neuroscience*, *18*. https://doi.org/10.3389/FNCEL.2024.1339345/FULL

Nóbrega-Pereira, S., Gelman, D., Bartolini, G., Pla, R., Pierani, A., & Marín, O. (2010). Origin and molecular specification of globus pallidus neurons. *Soc NeuroscienceS Nóbrega-Pereira, D Gelman, G Bartolini, R Pla, A Pierani, O MarínJournal of Neuroscience, 2010•Soc Neuroscience*, *30*(8), 2824–2834. https://doi.org/10.1523/JNEUROSCI.4023-09.2010

Nóbrega-Pereira, S., Kessaris, N., Du, T., Kimura, S., Anderson, S. A., & Marín, O. (2008). Postmitotic Nkx2-1 controls the migration of telencephalic interneurons by direct repression of guidance receptors. *Neuron*, *59*(5), 733. https://doi.org/10.1016/j.neuron.2008.07.024

Nomura, T. (2021). Interneuron dysfunction and inhibitory deficits in autism and fragile X syndrome. *Cells*, *10*(10). https://doi.org/10.3390/CELLS10102610

Oh, W. C., Lutzu, S., Castillo, P. E., & Kwon, H. B. (2016). De novo synaptogenesis induced by GABA in the developing mouse cortex. *Science*, *353*(6303), 1037–1040. https://doi.org/10.1126/science.aaf5206

Okita, K., Yamakawa, T., Matsumura, Y., Sato, Y., Amano, N., Watanabe, A., Goshima, N., & Yamanaka, S. (2013). An efficient nonviral method to generate integration-free human-induced pluripotent stem cells from cord blood and peripheral blood cells. *Stem Cells (Dayton, Ohio)*, *31*(3), 458–466. https://doi.org/10.1002/stem.1293

Pai, E. L. L., Chen, J., Darbandi, S. F., Cho, F. S., Chen, J., Lindtner, S., Chu, J. S., Paz, J. T., Vogt, D., Paredes, M. F., & Rubenstein, J. L. R. (2020). Maf and mafb control mouse pallial interneuron fate and maturation through neuropsychiatric disease gene regulation. *ELife*, *9*. https://doi.org/10.7554/ELIFE.54903

Paredes, M. F., James, D., Gil-Perotin, S., Kim, H., Cotter, J. A., Ng, C., Sandoval, K., Rowitch, D. H., Xu, D., McQuillen, P. S., Garcia-Verdugo, J. M., Huang, E. J., & Alvarez-Buylla, A. (2016). Extensive migration of young neurons into the infant human frontal lobe. *Science*, *354*(6308). https://doi.org/10.1126/science.aaf7073

Pasca, A. M., Sloan, S. A., Clarke, L. E., Tian, Y., Makinson, C. D., Huber, N., Kim, C. H., Park, J. Y., O'Rourke, N. A., Nguyen, K. D., Smith, S. J., Huguenard, J. R., Geschwind, D. H., Barres, B. A., & Pasca, S. P. (2015). Functional cortical neurons and astrocytes from human pluripotent stem cells in 3D culture. *Nature Methods*, *12*(7), 671–678. https://doi.org/10.1038/nmeth.3415

Pavon, N., Sun, Y., & Pak, C. H. (2024). Cell type specification and diversity in subpallial organoids. *Frontiers in Genetics*, *15*, 1440583. https://doi.org/10.3389/fgene.2024.1440583

Piniella, D., Canseco, A., Vidal, S., Xiol, C., Díaz de Bustamante, A., Martí-Carrera, I., Armstrong, J., Bastolla, U., & Zafra, F. (2023). Experimental and Bioinformatic Insights into the Effects of Epileptogenic Variants on the Function and Trafficking of the GABA Transporter GAT-1. *International Journal of Molecular Sciences*, *24*(2), 955. https://doi.org/10.3390/IJMS24020955/S1

Pla, R., Borrell, V., Flames, N., Neuroscience, O. M.-J. of, & 2006, undefined. (2006). Layer acquisition by cortical GABAergic interneurons is independent of Reelin signaling. *Soc NeuroscienceR Pla, V Borrell, N Flames, O MarínJournal of Neuroscience, 2006•Soc Neuroscience*. https://doi.org/10.1523/JNEUROSCI.0245-06.2006

Powell, E. M., Campbell, D. B., Stanwood, G. D., Davis, C., Noebels, J. L., & Levitt, P. (2003). Genetic disruption of cortical interneuron development causes region- and GABA cell type-specific deficits, epilepsy, and behavioral dysfunction. *The Journal of Neuroscience : The Official Journal of the Society for Neuroscience*, *23*(2), 622–631. https://doi.org/10.1523/jneurosci.23-02-00622.2003

Qi Hu, R., & Davies, J. A. (1997). Tiagabine hydrochloride, an inhibitor of γ-aminobutyric acid (GABA) uptake, induces cortical depolarizations in vitro. *Brain Research*, *753*(2), 260–268. https://doi.org/10.1016/S0006-8993(97)00013-9

Qian, X., Nguyen, H. N., Song, M. M., Hadiono, C., Ogden, S. C., Hammack, C., Yao, B., Hamersky, G. R., Jacob, F., Zhong, C., Yoon, K. J., Jeang, W., Lin, L., Li, Y., Thakor, J., Berg, D. A., Zhang, C., Kang, E., Chickering, M., … Ming, G. L. (2016). Brain-Region-Specific Organoids Using Mini-bioreactors for Modeling ZIKV Exposure. *Cell*, *165*(5), 1238–1254. https://doi.org/10.1016/j.cell.2016.04.032

Rakic, P. (1972). Mode of cell migration to the superficial layers of fetal monkey neocortex. *Journal of Comparative Neurology*, *145*(1), 61–83. https://doi.org/10.1002/cne.901450105

Rakić, S., Kanatani, S., Hunt, D., Faux, C., Cariboni, A., Chiara, F., Khan, S., Wansbury, O., Howard, B., Nakajima, K., Nikolić, M., & Parnavelas, J. G. (2015). Cdk5 phosphorylation of ErbB4 is required for tangential migration of cortical interneurons. *Cerebral Cortex*, *25*(4), 991–1003. https://doi.org/10.1093/CERCOR/BHT290

Ran, F. A., Hsu, P. D., Wright, J., Agarwala, V., Scott, D. A., & Zhang, F. (2013). Genome engineering using the CRISPR-Cas9 system. *Nature Protocols*, *8*(11), 2281–2308. https://doi.org/10.1038/nprot.2013.143

Rao, J., He, Z., Loskarn, S., Bender, A., Jo, Y., Lückel, J., Curcio, M., Cubela, I., Camp, J. G., Treutlein, B., & Lutolf, M. P. (2025). Unified Generation of Regionalized Neural Organoids from Single-Lumen Neuroepithelium. *BioRxiv*, 2025.11.18.689013. https://doi.org/10.1101/2025.11.18.689013

Rauch, A., Wieczorek, D., Graf, E., Wieland, T., Endele, S., Schwarzmayr, T., Albrecht, B., Bartholdi, D., Beygo, J., Di Donato, N., Dufke, A., Cremer, K., Hempel, M., Horn, D., Hoyer, J., Joset, P., Röpke, A., Moog, U., Riess, A., … Strom, T. M. (2012). Range of genetic mutations associated with severe non-syndromic sporadic intellectual disability: An exome sequencing study. *The Lancet*, *380*(9854), 1674–1682. https://doi.org/10.1016/S0140-6736(12)61480-9

Reilly, C., Atkinson, P., Das, K. B., Chin, R. F. M. C., Aylett, S. E., Burch, V., Gillberg, C., Scott, R. C., & Neville, B. G. R. (2014). Neurobehavioral Comorbidities in Children With Active Epilepsy: A Population-Based Study. *Pediatrics*, *133*(6), e1586–e1593. https://doi.org/10.1542/peds.2013-3787

Risso, S., DeFelice, L. J., & Blakely, R. D. (1996). Sodium-dependent GABA-induced currents in GAT1-transfected HeLa cells. *Journal of Physiology*, *490*(3), 691–702. https://doi.org/10.1113/jphysiol.1996.sp021178

Roberts, B., Haupt, A., Tucker, A., Grancharova, T., Arakaki, J., Fuqua, M. A., Nelson, A., Hookway, C., Ludmann, S. A., Mueller, I. A., Yang, R., Horwitz, R., Rafelski, S. M., & Gunawardane, R. N. (2017). Systematic gene tagging using CRISPR/Cas9 in human stem cells to illuminate cell organization. *Molecular Biology of the Cell*, *28*(21), 2854–2874. https://doi.org/10.1091/mbc.E17-03-0209

Rossignol, E., Kruglikov, I., Van Den Maagdenberg, A. M. J. M., Rudy, B., & Fishell, G. (2013). CaV2.1 ablation in cortical interneurons selectively impairs fast-spiking basket cells and causes generalized seizures. *Annals of Neurology*, *74*(2), 209–222. https://doi.org/10.1002/ANA.23913

Rudy, B., Fishell, G., Lee, S. H., & Hjerling-Leffler, J. (2011). Three groups of interneurons account for nearly 100% of neocortical GABAergic neurons. *Developmental Neurobiology*, *71*(1), 45–61. https://doi.org/10.1002/dneu.20853

Ryner, R. F., Derera, I. D., Armbruster, M., Kansara, A., Sommer, M. E., Pirone, A., Noubary, F., Jacob, M., & Dulla, C. G. (2023). Cortical Parvalbumin-positive interneuron development and function are altered in the APC conditional knockout mouse model of infantile and epileptic spasms. *Soc NeuroscienceRF Ryner, ID Derera, M Armbruster, A Kansara, ME Sommer, A Pirone, F Noubary, M JacobJournal of Neuroscience, 2023•Soc Neuroscience*, *43*(8), 1422–1440. https://doi.org/10.1523/JNEUROSCI.0572-22.2022

Sakaguchi, H., Kadoshima, T., Soen, M., Narii, N., Ishida, Y., Ohgushi, M., Takahashi, J., Eiraku, M., & Sasai, Y. (2015). Generation of functional hippocampal neurons from self-organizing human embryonic stem cell-derived dorsomedial telencephalic tissue. *Nature Communications 2015 6:1*, *6*(1), 8896-. https://doi.org/10.1038/ncomms9896

Samarasinghe, R. A., Miranda, O. A., Buth, J. E., Mitchell, S., Ferando, I., Watanabe, M., Allison, T. F., Kurdian, A., Fotion, N. N., Gandal, M. J., Golshani, P., Plath, K., Lowry, W. E., Parent, J. M., Mody, I., & Novitch, B. G. (2021). Identification of neural oscillations and epileptiform changes in human brain organoids. *Nature Neuroscience*, *24*(10), 1488–1500. https://doi.org/10.1038/s41593-021-00906-5

Sanai, N., Nguyen, T., Ihrie, R. A., Mirzadeh, Z., Tsai, H. H., Wong, M., Gupta, N., Berger, M. S., Huang, E., Garcia-Verdugo, J. M., Rowitch, D. H., & Alvarez-Buylla, A. (2011). Corridors of migrating neurons in the human brain and their decline during infancy. *Nature 2011 478:7369*, *478*(7369), 382–386. https://doi.org/10.1038/nature10487

Sanders, S. J., Murtha, M. T., Gupta, A. R., Murdoch, J. D., Raubeson, M. J., Willsey, A. J., Ercan-Sencicek, A. G., Di Lullo, N. M., Parikshak, N. N., Stein, J. L., Walker, M. F., Ober, G. T., Teran, N. A., Song, Y., El-Fishawy, P., Murtha, R. C., Choi, M., Overton, J. D., Bjornson, R. D., … State, M. W. (2012). De novo mutations revealed by whole-exome sequencing are strongly associated with autism. *Nature 2012 485:7397*, *485*(7397), 237–241. https://doi.org/10.1038/nature10945

Scheffer, I. E., French, J., Hirsch, E., Jain, S., Mathern, G. W., Moshé, S. L., Perucca, E., Tomson, T., Wiebe, S., Zhang, Y. H., & Zuberi, S. M. (2016). Classification of the epilepsies: New concepts for discussion and debate—Special report of the ILAE Classification Task Force of the Commission for Classification and Terminology. *Epilepsia Open*, *1*(1–2), 37. https://doi.org/10.1002/epi4.5

Schevon, C. A., Weiss, S. A., McKhann, G., Goodman, R. R., Yuste, R., Emerson, R. G., & Trevelyan, A. J. (2012). Evidence of an inhibitory restraint of seizure activity in humans. *Nature Communications*, *3*, 1060. https://doi.org/10.1038/ncomms2056

Scimemi, A. (2014). Structure,function,and plasticity of GABA transporters. *Frontiers in Cellular Neuroscience*, *8*(JUN), 97471. https://doi.org/10.3389/fncel.2014.00161

Shen, M., Guo, Y., Dong, Q., Gao, Y., Stockton, M. E., Li, M., Kannan, S., Korabelnikov, T., Schoeller, K. A., Sirois, C. L., Zhou, C., Le, J., Wang, D., Chang, Q., Sun, Q. Q., & Zhao, X. (2021). FXR1 regulation of parvalbumin interneurons in the prefrontal cortex is critical for schizophrenia-like behaviors. *Molecular Psychiatry*, *26*(11), 6845–6867. https://doi.org/10.1038/S41380-021-01096-Z

Shepard, T. H., Brent, R. L., Friedman, J. M., Jones, K. L., Miller, R. K., Moore, C. A., & Polifka, J. E. (2002). The two sites of fusion of the neural folds and the two neuropores in the human embryo. *Teratology*, *65*(4), 162–170. https://doi.org/10.1002/tera.10007

Shi, Y., Wang, M., Mi, D., Lu, T., Wang, B., Dong, H., Zhong, S., Chen, Y., Sun, L., Zhou, X., Ma, Q., Liu, Z., Wang, W., Zhang, J., Wu, Q., Marín, O., & Wang, X. (2021). Mouse and human share conserved transcriptional programs for interneuron development. *Science*, *374*(6573). https://doi.org/10.1126/SCIENCE.ABJ6641

Shimada, I. S., Goto, A., Hashimoto, Y., Takase, H., Itoh, M., & Kato, Y. (2024). Spatial ciliary signaling regulates the dorsal/ventral regionalization of human brain organoids. *BioRxiv*, 2024.07.18.604098. https://doi.org/10.1101/2024.07.18.604098

Shimamura, K., & Rubenstein, J. L. R. (1997). Inductive interactions direct early regionalization of the mouse forebrain. *Development (Cambridge, England)*, *124*(14), 2709–2718. https://doi.org/10.1242/dev.124.14.2709

Silva, D. B., Trinidad, M., Ljungdahl, A., Revalde, J. L., Berguig, G. Y., Wallace, W., Patrick, C. S., Bomba, L., Arkin, M., Dong, S., Estrada, K., Hutchinson, K., LeBowitz, J. H., Schlessinger, A., Johannesen, K. M., Møller, R. S., Giacomini, K. M., Froelich, S., Sanders, S. J., & Wuster, A. (2024). Haploinsufficiency underlies the neurodevelopmental consequences of SLC6A1 variants. *American Journal of Human Genetics*, *111*(6), 1222–1238. https://doi.org/10.1016/j.ajhg.2024.04.021

Sloan, S. A., Andersen, J., Paşca, A. M., Birey, F., & Paşca, S. P. (2018). Generation and assembly of human brain region–specific three-dimensional cultures. *Nature Protocols 2018 13:9*, *13*(9), 2062–2085. https://doi.org/10.1038/s41596-018-0032-7

Smith, A. L., Jung, E. M., Jeon, B. T., & Kim, W. Y. (2020). Arid1b haploinsufficiency in parvalbumin- or somatostatin-expressing interneurons leads to distinct ASD-like and ID-like behavior. *Scientific Reports*, *10*(1). https://doi.org/10.1038/S41598-020-64066-5

Smith, C., Abalde-Atristain, L., He, C., Brodsky, B. R., Braunstein, E. M., Chaudhari, P., Jang, Y. Y., Cheng, L., & Ye, Z. (2015). Efficient and allele-specific genome editing of disease loci in human iPSCs. *Molecular Therapy*, *23*(3), 570–577. https://doi.org/10.1038/mt.2014.226

Sohal, V. S., & Rubenstein, J. L. R. (2019). Excitation-inhibition balance as a framework for investigating mechanisms in neuropsychiatric disorders. *Molecular Psychiatry*, *24*(9), 1248–1257. https://doi.org/10.1038/S41380-019-0426-0

Sohal, V. S., Zhang, F., Yizhar, O., & Deisseroth, K. (2009). Parvalbumin neurons and gamma rhythms enhance cortical circuit performance. *Nature*, *459*(7247), 698–702. https://doi.org/10.1038/NATURE07991;KWRD=SCIENCE

Stefanski, A., Pérez-Palma, E., Brünger, T., Montanucci, L., Gati, C., Klöckner, C., Johannesen, K. M., Goodspeed, K., MacNee, M., Deng, A. T., Aledo-Serrano, Á., Borovikov, A., Kava, M., Bouman, A. M., Hajianpour, M. J., Pal, D. K., Engelen, M., Hagebeuk, E. E. O., Shinawi, M., … Lal, D. (2023). SLC6A1 variant pathogenicity, molecular function and phenotype: a genetic and clinical analysis. *Brain*, *146*(12), 5198. https://doi.org/10.1093/brain/awad292

Stoeckli, E. T. (2009). Morphogens and Neural Development. *Encyclopedia of Neuroscience*, 2397–2401. https://doi.org/10.1007/978-3-540-29678-2_3562

Stumm, R. K., Zhou, C., Ara, T., Lazarini, F., Dubois-Dalcq, M., Nagasawa, T., Höllt, V., & Schulz, S. (2003). CXCR4 regulates interneuron migration in the developing neocortex. *Journal of Neuroscience*, *23*(12), 5123–5130. https://doi.org/10.1523/JNEUROSCI.23-12-05123.2003

Su, Z., Lu, J., Shi, Y., Qi, B., & Guo, Z. (2025). Global, regional, and national children and adolescent epilepsy burden, 1990–2021: an analysis based on the global burden of disease study 2021. *Annals of Medicine*, *57*(1), 2534087. https://doi.org/10.1080/07853890.2025.2534087

Subramanian, D., Eisenberg, C., Huang, A., Baek, J., Naveed, H., Komatireddy, S., Shiflett, M. W., Tran, T. S., & Santhakumar, V. (2025). Dysregulation of neuropilin-2 expression in inhibitory neurons impairs hippocampal circuit development and enhances risk for autism-related behaviors and seizures. *Molecular Psychiatry*, *30*(7), 2799–2809. https://doi.org/10.1038/s41380-024-02839-4

Sun, A. X., Yuan, Q., Fukuda, M., Yu, W., Yan, H., Lim, G. G. Y., Nai, M. H., D'Agostino, G. A., Tran, H. D., Itahana, Y., Wang, D., Lokman, H., Itahana, K., Lim, S. W. L., Tang, J., Chang, Y. Y., Zhang, M., Cook, S. A., Rackham, O. J. L., … Je, H. S. (2019). Potassium channel dysfunction in human neuronal models of Angelman syndrome. *Science (New York, N.Y.)*, *366*(6472), 1486–1492. https://doi.org/10.1126/science.aav5386

Sussel, L., Marin, O., Kimura, S., & Rubenstein, J. L. R. (1999a). Loss of Nkx2.1 homeobox gene function results in a ventral to dorsal molecular respecification within the basal telencephalon: evidence for a transformation of the pallidum into the striatum. *Development (Cambridge, England)*, *126*(15), 3359–3370. https://doi.org/10.1242/dev.126.15.3359

Takahashi, K., Tanabe, K., Ohnuki, M., Narita, M., Ichisaka, T., Tomoda, K., & Yamanaka, S. (2007). Induction of Pluripotent Stem Cells from Adult Human Fibroblasts by Defined Factors. *Cell*, *131*(5), 861–872. https://doi.org/10.1016/j.cell.2007.11.019

Takahashi, K., & Yamanaka, S. (2006). Induction of Pluripotent Stem Cells from Mouse Embryonic and Adult Fibroblast Cultures by Defined Factors. *Cell*, *126*(4), 663–676. https://doi.org/10.1016/j.cell.2006.07.024

Takla, T. N., Luo, J., Sudyk, R., Huang, J., Walker, J. C., Vora, N. L., Sexton, J. Z., Parent, J. M., & Tidball, A. M. (2023). A Shared Pathogenic Mechanism for Valproic Acid and SHROOM3 Knockout in a Brain Organoid Model of Neural Tube Defects. *Cells*, *12*(13). https://doi.org/10.3390/CELLS12131697,

Telezhkin, V., Schnell, C., Yarova, P., Yung, S., Cope, E., Hughes, A., Thompson, B. A., Sanders, P., Geater, C., Hancock, J. M., Joy, S., Badder, L., Connor-Robson, N., Comella, A., Straccia, M., Bombau, G., Brown, J. T., Canals, J. M., Randall, A. D., … Kemp, P. J. (2016). Forced cell cycle exit and modulation of GABAA, CREB, and GSK3β signaling promote functional maturation of induced pluripotent stem cell-derived neurons. *American Journal of Physiology - Cell Physiology*, *310*(7), C520–C541. https://doi.org/10.1152/ajpcell.00166.2015

Thijs, R. D., Surges, R., O'Brien, T. J., & Sander, J. W. (2019). Epilepsy in adults. *The Lancet*, *393*(10172), 689–701. https://doi.org/10.1016/S0140-6736(18)32596-0

Thomas, R. H., & Berkovic, S. F. (2014). The hidden genetics of epilepsy—a clinically important new paradigm. *Nature Reviews Neurology 2014 10:5*, *10*(5), 283–292. https://doi.org/10.1038/nrneurol.2014.62

Thomson, J. A. (1998). Embryonic stem cell lines derived from human blastocysts. *Science*, *282*(5391), 1145–1147. https://doi.org/10.1126/SCIENCE.282.5391.1145,

Tian, G. F., Azmi, H., Takano, T., Xu, Q., Peng, W., Lin, J., Oberheim, N. A., Lou, N., Wang, X., Zielke, H. R., Kang, J., & Nedergaard, M. (2005). An astrocytic basis of epilepsy. *Nature Medicine*, *11*(9), 973. https://doi.org/10.1038/nm1277

Tidball, A. M., Dang, L. T., Glenn, T. W., Kilbane, E. G., Klarr, D. J., Margolis, J. L., Uhler, M. D., & Parent, J. M. (2017). Rapid Generation of Human Genetic Loss-of-Function iPSC Lines by Simultaneous Reprogramming and Gene Editing. *Stem Cell Reports*, *9*(3), 725–731. https://doi.org/10.1016/J.STEMCR.2017.07.003

Tidball, A. M., Lopez-Santiago, L. F., Yuan, Y., Glenn, T. W., Margolis, J. L., Clayton Walker, J., Kilbane, E. G., Miller, C. A., Martina Bebin, E., Scott Perry, M., Isom, L. L., & Parent, J. M. (2020). Variant-specific changes in persistent or resurgent sodium current in SCN8A-related epilepsy patient-derived neurons. *Brain*, *143*(10), 3025–3040. https://doi.org/10.1093/BRAIN/AWAA247

Tidball, A. M., Niu, W., Ma, Q., Takla, T. N., Walker, J. C., Margolis, J. L., Mojica-Perez, S. P., Sudyk, R., Deng, L., Moore, S. J., Chopra, R., Shakkottai, V. G., Murphy, G. G., Yuan, Y., Isom, L. L., Li, J. Z., & Parent, J. M. (2023). Deriving early single-rosette brain organoids from human pluripotent stem cells. *Stem Cell Reports*, *18*(12), 2498–2514. https://doi.org/10.1016/J.STEMCR.2023.10.020

Toudji, I., Toumi, A., Chamberland, É., & Rossignol, E. (2023). Interneuron odyssey: molecular mechanisms of tangential migration. *Frontiers in Neural Circuits*, *17*. https://doi.org/10.3389/FNCIR.2023.1256455/FULL

Trapnell, C., Cacchiarelli, D., Grimsby, J., Pokharel, P., Li, S., Morse, M., Lennon, N. J., Livak, K. J., Mikkelsen, T. S., & Rinn, J. L. (2014). The dynamics and regulators of cell fate decisions are revealed by pseudotemporal ordering of single cells. *Nature Biotechnology*, *32*(4), 381–386. https://doi.org/10.1038/nbt.2859

Trevelyan, A. J., Sussillo, D., & Yuste, R. (2007). Feedforward Inhibition Contributes to the Control of Epileptiform Propagation Speed. *The Journal of Neuroscience*, *27*(13), 3383. https://doi.org/10.1523/JNEUROSCI.0145-07.2007

Trujillo, C. A., Gao, R., Negraes, P. D., Gu, J., Buchanan, J., Preissl, S., Wang, A., Wu, W., Haddad, G. G., Chaim, I. A., Domissy, A., Vandenberghe, M., Devor, A., Yeo, G. W., Voytek, B., & Muotri, A. R. (2019). Complex oscillatory waves emerging from cortical organoids model early human brain network development. *Cell Stem Cell*, *25*(4), 558. https://doi.org/10.1016/J.STEM.2019.08.002

Tuncdemir, S. N., Wamsley, B., Stam, F. J., Osakada, F., Goulding, M., Callaway, E. M., Rudy, B., & Fishell, G. (2016). Early Somatostatin Interneuron Connectivity Mediates the Maturation of Deep Layer Cortical Circuits. *Neuron*, *89*(3), 521–535. https://doi.org/10.1016/j.neuron.2015.11.020

Tyson, J. A., Goldberg, E. M., Maroof, A. M., Xu, Q., Petros, T. J., & Anderson, S. A. (2015). Duration of culture and sonic hedgehog signaling differentially specify PV versus SST cortical interneuron fates from embryonic stem cells. *Development (Cambridge)*, *142*(7), 1267–1278. https://doi.org/10.1242/DEV.111526/VIDEO-1

Upadhya, D., Hattiangady, B., Castro, O. W., Shuai, B., Kodali, M., Attaluri, S., Bates, A., Dong, Y., Zhang, S. C., Prockop, D. J., & Shetty, A. K. (2019). Human induced pluripotent stem cell-derived MGE cell grafting after status epilepticus attenuates chronic epilepsy and comorbidities via synaptic integration. *Proceedings of the National Academy of Sciences of the United States of America*, *116*(1), 287–296. https://doi.org/10.1073/pnas.1814185115

Valcanis, H., & Tan, S. S. (2003). Layer specification of transplanted interneurons in developing mouse neocortex. *The Journal of Neuroscience : The Official Journal of the Society for Neuroscience*, *23*(12), 5113–5122. https://doi.org/10.1523/jneurosci.23-12-05113.2003

Valiente, M., migration, F. M.-C. adhesion &, & 2009, undefined. (2009). Migration of cortical interneurons relies on branched leading process dynamics. *Taylor & FrancisM Valiente, FJ MartiniCell Adhesion & Migration, 2009•Taylor & Francis*, *3*(3), 278–280. https://doi.org/10.4161/cam.3.3.8832

Vanhatalo, S., Matias Palva, J., Andersson, S., Rivera, C., Voipio, J., & Kaila, K. (2005). Slow endogenous activity transients and developmental expression of K +-Cl- cotransporter 2 in the immature human cortex. *European Journal of Neuroscience*, *22*(11), 2799–2804. https://doi.org/10.1111/j.1460-9568.2005.04459.x

Vogt, D., Cho, K. K. A., Shelton, S. M., Paul, A., Huang, Z. J., Sohal, V. S., & Rubenstein, J. L. R. (2018). Mouse Cntnap2 and Human CNTNAP2 ASD Alleles Cell Autonomously Regulate

PV + Cortical Interneurons. *Cerebral Cortex*, *28*(11), 3868–3879. https://doi.org/10.1093/CERCOR/BHX248

Vogt, D., Hunt, R. F., Mandal, S., Sandberg, M., Silberberg, S. N., Nagasawa, T., Yang, Z., Baraban, S. C., & Rubenstein, J. L. R. (2014). Lhx6 directly regulates Arx and CXCR7 to determine cortical interneuron fate and laminar position. *Neuron*, *82*(2), 350–364. https://doi.org/10.1016/J.NEURON.2014.02.030

Wagner, V. A., Thapa, R., Norman, A. O., Varallo, A., Wimberly, J., Rais, M., Gerasymchuk, D., Piepponen, T. P., Razak, K. A., Castren, M. L., & Ethell, I. M. (2026). Astrocytic GABA controls fidelity of temporal cortical processing in Fragile X Syndrome. *Neurobiology of Disease*, *219*(22), 107233. https://doi.org/10.1016/j.nbd.2025.107233

Walsh, R. M., Crabtree, G. W., Kalpana, K., Jubierre, L., Koo, S. Y., Ciceri, G., Gogos, J. A., Kruglikov, I., & Studer, L. (2025). Forebrain assembloids support the development of fast-spiking human PVALB+ cortical interneurons and uncover schizophrenia-associated defects. *Neuron*, *113*(19), 3185-3203.e7. https://doi.org/10.1016/j.neuron.2025.06.017

Wang, J., Poliquin, S., Mermer, F., Eissman, J., Delpire, E., Wang, J., Shen, W., Cai, K., Li, B. M., Li, Z. Y., Xu, D., Nwosu, G., Flamm, C., Liao, W. P., Shi, Y. W., & Kang, J. Q. (2020). Endoplasmic reticulum retention and degradation of a mutation in SLC6A1 associated with epilepsy and autism. *Molecular Brain*, *13*(1), 1–15. https://doi.org/10.1186/s13041-020-00612-6

Wang, Y., Chiola, S., Yang, G., Russell, C., Armstrong, C. J., Wu, Y., Spampanato, J., Tarboton, P., Ullah, H. M. A., Edgar, N. U., Chang, A. N., Harmin, D. A., Bocchi, V. D., Vezzoli, E., Besusso, D., Cui, J., Cattaneo, E., Kubanek, J., & Shcheglovitov, A. (2022). Modeling human telencephalic development and autism-associated SHANK3 deficiency using organoids generated from single neural rosettes. *Nature Communications 2022 13:1*, *13*(1), 5688-. https://doi.org/10.1038/s41467-022-33364-z

Wang, Y., Li, G., Stanco, A., Long, J. E., Crawford, D., Potter, G. B., Pleasure, S. J., Behrens, T., & Rubenstein, J. L. R. (2011). CXCR4 and CXCR7 Have Distinct Functions in Regulating Interneuron Migration. *Neuron*, *69*(1), 61–76. https://doi.org/10.1016/j.neuron.2010.12.005

Ward, H. H., Brown-Glaberman, U., Wang, J., Morita, Y., Alper, S. L., Bedrick, E. J., Gattone, V. H., Deretic, D., & Wandinger-Ness, A. (2011). A conserved signal and GTPase complex are required for the ciliary transport of polycystin-1. *Molecular Biology of the Cell*, *22*(18), 3289. https://doi.org/10.1091/mbc.E11-01-0082

Watanabe, M., Buth, J. E., Vishlaghi, N., de la Torre-Ubieta, L., Taxidis, J., Khakh, B. S., Coppola, G., Pearson, C. A., Yamauchi, K., Gong, D., Dai, X., Damoiseaux, R., Aliyari, R., Liebscher, S., Schenke-Layland, K., Caneda, C., Huang, E. J., Zhang, Y., Cheng, G., … Novitch, B. G. (2017). Self-Organized Cerebral Organoids with Human-Specific Features Predict Effective Drugs to Combat Zika Virus Infection. *Cell Reports*, *21*(2), 517–532. https://doi.org/10.1016/j.celrep.2017.09.047

Wengert, E. R., Miralles, R. M., Wedgwood, K. C. A., Wagley, P. K., Strohm, S. M., Panchal, P. S., Idrissi, A. M., Wenker, I. C., Thompson, J. A., Gaykema, R. P., & Patel, M. K. (2021). Somatostatin-Positive Interneurons Contribute to Seizures in SCN8A Epileptic Encephalopathy. *The Journal of Neuroscience : The Official Journal of the Society for Neuroscience*, *41*(44), 9257–9273. https://doi.org/10.1523/JNEUROSCI.0718-21.2021

Wichterle, H., Garcia-Verdugo, J. M., Herrera, D. G., & Alvarez-Buylla, A. (1999). Young neurons from medial ganglionic eminence disperse in adult and embryonic brain. *Nature Neuroscience 1999 2:5*, *2*(5), 461–466. https://doi.org/10.1038/8131

Wingett, S. W., & Andrews, S. (2018). FastQ Screen: A tool for multi-genome mapping and quality control. *F1000Research*, *7*, 1338. https://doi.org/10.12688/f1000research.15931.2

Wonders, C. P., & Anderson, S. A. (2006). The origin and specification of cortical interneurons. *Nature Reviews Neuroscience 2006 7:9*, *7*(9), 687–696. https://doi.org/10.1038/nrn1954

Wu, S. J., Sevier, E., Dwivedi, D., Saldi, G. A., Hairston, A., Yu, S., Abbott, L., Choi, D. H., Sherer, M., Qiu, Y., Shinde, A., Lenahan, M., Rizzo, D., Xu, Q., Barrera, I., Kumar, V., Marrero, G., Prönneke, A., Huang, S., … Fishell, G. (2023). Cortical somatostatin interneuron subtypes form cell-type-specific circuits. *Neuron*, *111*(17), 2675-2692.e9. https://doi.org/10.1016/J.NEURON.2023.05.032/ASSET/6CFA747C-FE1C-4984-9320-AED19E7E55C3/MAIN.ASSETS/GR6.JPG

Xiang, Y., Tanaka, Y., Patterson, B., Kang, Y. J., Govindaiah, G., Roselaar, N., Cakir, B., Kim, K. Y., Lombroso, A. P., Hwang, S. M., Zhong, M., Stanley, E. G., Elefanty, A. G., Naegele, J. R., Lee, S. H., Weissman, S. M., & Park, I. H. (2017). Fusion of regionally-specified hPSC-derived organoids models human brain development and interneuron migration. *Cell Stem Cell*, *21*(3), 383. https://doi.org/10.1016/j.stem.2017.07.007

Xu, K., Qian, W., Xu, W., Yang, W., Yang, Y., Song, Y., Li, Y., Yuan, Z., Zhang, S., Zhao, F., Wei, W., & He, W. (2025). Global, regional, and national epidemiology of childhood epilepsy from 1990 to 2021: a systematic study based on the GBD 2021. *Seizure: European Journal of Epilepsy*, *131*(7), 351–360. https://doi.org/10.1016/j.seizure.2025.08.001

Xu, Q., Cobos, I., De La Cruz, E. D., Rubenstein, J. L., & Anderson, S. A. (2004). Origins of Cortical Interneuron Subtypes. *The Journal of Neuroscience*, *24*(11), 2612. https://doi.org/10.1523/JNEUROSCI.5667-03.2004

Xu, Q., Tam, M., & Anderson, S. A. (2008). Fate mapping Nkx2.1-lineage cells in the mouse telencephalon. *Journal of Comparative Neurology*, *506*(1), 16–29. https://doi.org/10.1002/CNE.21529

Xue, X., Kim, Y. S., Ponce-Arias, A. I., O'Laughlin, R., Yan, R. Z., Kobayashi, N., Tshuva, R. Y., Tsai, Y. H., Sun, S., Zheng, Y., Liu, Y., Wong, F. C. K., Surani, A., Spence, J. R., Song, H., Ming, G. L., Reiner, O., & Fu, J. (2024). A patterned human neural tube model using microfluidic gradients. *Nature*, *628*(8007), 391–399. https://doi.org/10.1038/S41586-024-07204-7

Yamashita, A., Singh, S. K., Kawate, T., Jin, Y., & Gouaux, E. (2005). Crystal structure of a bacterial homologue of Na+/Cl--dependent neurotransmitter transporters. *Nature 2005 437:7056*, *437*(7056), 215–223. https://doi.org/10.1038/nature03978

Yu, D., Jain, S., Wangzhou, A., Zhu, B., Shao, W., Coley-O'Rourke, E. J., De Florencio, S., Kim, J. Y., Choi, J. J. Y., Paredes, M. F., Nowakowski, T. J., Huang, E. J., & Piao, X. (2025). Microglia regulate GABAergic neurogenesis in prenatal human brain through IGF1. *Nature 2025 646:8085*, *646*(8085), 676–686. https://doi.org/10.1038/s41586-025-09362-8

Yu, Y. H., Park, D. K., Yoo, D. Y., & Kim, D. S. (2020). Altered expression of parvalbumin immunoreactivity in rat main olfactory bulb following pilocarpine-induced status epilepticus. *BMB Reports*, *53*(4), 234–239. https://doi.org/10.5483/BMBREP.2020.53.4.002

Yu, Y., Zeng, Z., Xie, D., Chen, R., Sha, Y., Huang, S., Cai, W., Chen, W., Li, W., Ke, R., & Sun, T. (2021). Interneuron origin and molecular diversity in the human fetal brain. *Nature Neuroscience*, *24*(12), 1745–1756. https://doi.org/10.1038/S41593-021-00940-3

Yuan, Y., Lopez-Santiago, L., Denomme, N., Chen, C., O'Malley, H. A., Hodges, S. L., Ji, S., Han, Z., Christiansen, A., & Isom, L. L. (2024). Antisense oligonucleotides restore excitability, GABA signalling and sodium current density in a Dravet syndrome model. *Brain*, *147*(4), 1231–1246. https://doi.org/10.1093/BRAIN/AWAD349

Yuan, Y., O'Malley, H. A., Smaldino, M. A., Bouza, A. A., Hull, J. M., & Isom, L. L. (2019). Delayed maturation of GABAergic signaling in the Scn1a and Scn1b mouse models of Dravet Syndrome. *Scientific Reports*, *9*(1). https://doi.org/10.1038/S41598-019-42191-0

Yung, S. Y., Gokhan, S., Jurcsak, J., Molero, A. E., Abrajano, J. J., & Mehler, M. F. (2002). Differential modulation of BMP signaling promotes the elaboration of cerebral cortical GABAergic neurons or oligodendrocytes from a common sonic hedgehog-responsive ventral forebrain progenitor species. *Proceedings of the National Academy of Sciences of the United States of America*, *99*(25), 16273–16278. https://doi.org/10.1073/pnas.232586699

Zhang, C., Xie, Z., & Wang, N. (2025). Single-cell RNA sequencing of adult primate neocortex reveals the regulatory dynamics of neural plasticity. *American Journal of Translational Research*, *17*(4), 2562. https://doi.org/10.62347/ZEOR5569

Zhao, Y., Flandin, P., Long, J. E., Dela Cuesta, M., Westphal, H., & Rubenstein, J. L. R. (2008). Distinct molecular pathways of development of telencephalic interneuron subtypes revealed through analysis of Lhx6 mutants. *Journal of Comparative Neurology*, *510*(1), 79–99. https://doi.org/10.1002/CNE.21772

Zhao, Y., Marín, O., Hermesz, E., Powell, A., Flames, N., Palkovits, M., Rubenstein, J. L. R., & Westphal, H. (2003). The LIM-homeobox gene Lhx8 is required for the development of many cholinergic neurons in the mouse forebrain. *Proceedings of the National Academy of Sciences of the United States of America*, *100*(15), 9005–9010. https://doi.org/10.1073/PNAS.1537759100

Zhao, Y., Zhou, X., He, Y., & Liao, C. (2018). SLC6A1-miR133a-CDX2 loop regulates SK-OV-3 ovarian cancer cell proliferation, migration and invasion. *Oncology Letters*, *16*(4), 4977–4983. https://doi.org/10.3892/OL.2018.9273/ABSTRACT

Zhao, Z., Zhang, D., Yang, F., Xu, M., Zhao, S., Pan, T., Liu, C., Liu, Y., Wu, Q., Tu, Q., Zhou, P., Li, R., Kang, J., Zhu, L., Gao, F., Wang, Y., & Xu, Z. (2022). Evolutionarily conservative and non-conservative regulatory networks during primate interneuron development revealed by single-cell RNA and ATAC sequencing. *Cell Research 2022 32:5*, *32*(5), 425–436. https://doi.org/10.1038/s41422-022-00635-9

Zhong, Q., Liu, Y., Correa, M. R., Marconett, C. N., Minoo, P., Li, C., Ann, D. K., Zhou, B., & Borok, Z. (2022). FOXO1 Couples KGF and PI-3K/AKT Signaling to NKX2.1-Regulated Differentiation of Alveolar Epithelial Cells. *Cells*, *11*(7), 1122. https://doi.org/10.3390/cells11071122

Zhou, T., Benda, C., Duzinger, S., Huang, Y., Li, X., Li, Y., Guo, X., Cao, G., Chen, S., Hao, L., Chan, Y. C., Ng, K. M., Ho, J. C., Wieser, M., Wu, J., Redl, H., Tse, H. F., Grillari, J., Grillari-Voglauer, R., … Esteban, M. A. (2011). Generation of induced pluripotent stem cells from urine. *Journal of the American Society of Nephrology : JASN*, *22*(7), 1221–1228. https://doi.org/10.1681/ASN.2011010106